DOCTOR OF PHILOSOPHY

Geophysical/sedimentological studies of a Quaternary tidal delta system

Solangi, Sarfraz Hussain

Award date:
1992

Awarding institution:
Bangor University

GEOPHYSICAL/SEDIMENTOLOGICAL STUDIES OF A QUATERNARY TIDAL DELTA SYSTEM.

By

Sarfraz Hussain Solangi B.Sc., M.Sc.

A thesis submitted to the University of Wales for the degree of Doctor of Philosophy

School of Ocean Sciences
University of Wales
Bangor
Gwynedd.

January, 1992.

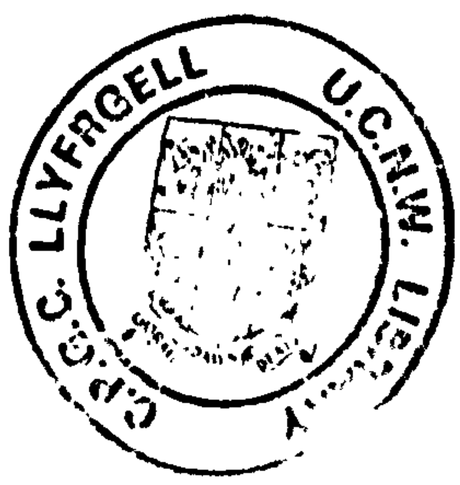

Bangor University Marine Sciences Digitising Project

Solangi, Sarfranz Hussain. Geophysical/sedimentological studies of a quaternary tidal delta system. (1992:S8)

Third Party material to be excluded from digitalization:

Appendix I, 2 pages
Appendix III, 2 pages
Appendix IV, 2 pages
Appendix V, 1 page
Appendix VII, 1 page
Appendix VIII, 2 pages

Please return thesis to:

Chiara Luis, Technical Services
Main Library
Bangor University
College Road
Bangor
Gwynedd LL57 2DG

Bangor University Marine Sciences Digitising Project

Solangi, Sarfranz Hussain. Geophysical/sedimentological studies of a quaternary tidal delta system. (1992:S8)

Third Party material to be excluded from digitalization:

Appendix I, 2 pages
Appendix III, 2 pages
Appendix IV, 2 pages
Appendix V, 1 page
Appendix VII, 1 page
Appendix VIII, 2 pages

Please return thesis to:

Chiara Luis, Technical Services
Main Library
Bangor University
College Road
Bangor
Gwynedd LL57 2DG

Satellite image of the study area.

LANDSAT 22July1984 (3,2,1)

Abstract

An attempt has been made to define the Quaternary development of a tidal delta system and the surrounding area of the Menai Strait and Caernarfon Bay. The morphologies and processes of a tidal inlet and its associated flood and ebb-tidal deltas are described and a model of sediment transport pathways prevailing in the study area has been proposed.

Seismic stratigraphic evidence suggests that the Quaternary deposits in Caernarfon Bay are primarily composed of three depositional sequences i.e. glacial, postglacial, and recent. The oldest sequence i.e. glacial sequence, lies unconformably on bedrock. The bedrock topography was successfully defined using a sparker seismic system and the results suggest that the bedrock surface is very uneven in nature and that there are two NE-SW trending valley features which can be linked to the Berw and Dinorwic faults. However, their typical U-shaped form may be attributed to erosion during the late Devensian ice advance. Various types of progradational reflection patterns within the postglacial sequence suggest a rapid rise in sea level after c. 9000 years B.P.

It appears that the completion of the present morpho-hydrodynamic system most probably took place c. 5000 years B.P. The newly evolved morpholgy and flood and ebb tidal currents resulted in the accumulation of thick deposits of recent sediments in and outside the inlet i.e. flood and ebb-tidal deltas. A comparison of these tidal deltas with standard models suggest that whilst the flood-tidal delta shows hardly any resemblance to the standard model, the ebb-tidal delta is strikingly consistent in morphology and processes with the standard model.

A model of the sediment transport pathways, proposed on the basis of comprehensive studies of bedform characteristics, grain size distribution trends, and to some extent on the basis of sediment transport calculations, suggests that there is a net sediment transport towards the southwest through the Menai Strait. The study of temporal variations in the characteristics of bedforms within the Menai Strait during a neap/spring tidal cycle suggest that the bedforms are ebb-oriented during most of the tidal states. A partial flood orientation occurs only during high spring tide. The extensive occurrence of sand ribbons with superimposed small scale megaripples (1-2m in wavelength) in the deeper parts of the Caernarfon Bay suggest a relatively lesser net sediment transport northeastwards which turns towards the north as it approaches the ebb-tidal delta body.

In the memory of my

FATHER

Who had great enthusiasm for the furthering of education

Acknowledgements

I owe a large debt of gratitude to many colleagues who provided help in the School and in the field, sometimes in very unpleasant weather conditions. In particular I thank Miss Ruth Watkins, P. Larcombe, R. Bates, Nabeel, Shahid Amjad, Asghar, Shams Tunio, and Ian McDermott. I am also indebted to Mr. Saeed Soomro for invaluable companionship and discussions, in particular during the final stages of the thesis.

I am also grateful to all members of the technical staff for their help in the laboratory and in the field. In particular I thank John Moore, Allan Nield, Geraint williams, Gwyn Jones, and Frank Dewes.

I would also like to extend my appreciation to the Captains and crew of the Cadnant, Lewis Morris, and UCNW research vessel Prince Madog. Special thanks also goes to Caernarfon Harbour Trust for kindly lending the Cadnant boat.

Thanks are also due to Dr Dave Bowers and Dr Toby Sherwin for their assistance in understanding the complex tidal current patterns prevailing in the Menai Strait and Caernarfon Bay areas; to Dr John Matthews for introducing me to the colourful field of satellite images; to Dr. Sarah Jones for her invaluable help in grain size analyses and computing.

I am greatly indebted to Dr Jim Bennell for his unlimited help and expert advice throughout the research project, in particular in the acquisition and processing of various geophysical data. Thanks are also due to Dei Hws for important discussions on the seismic stratigraphy of the Caernarfon Bay.

I highly acknowledge the inspiration and moral support provided by Dr Lal B. Bozdar (Professor University of Sindh, Pakistan) throughout my acquaintance with him, first as a student and then as a colleague. Living away for the last five years has not made any difference, I have always found his kindness beside me. Much appreciation also goes to Dr. Salma Bozdar for her invaluable help at a critical time. More than anything, I have always valued and will continue to value, their friendship.

It would be highly unjust if I did not acknowledge the invaluable efforts and expertise of the British doctors, surgeons, and nurses of Gwynedd Hospital (Bangor), Broadgreen Hospital (Liverpool), and Saint Guys and Thomas Hospital (London), who, after two major operations and 18 months of continuous treatment put me back on the track of a healthier life.

I would like to extend my thanks to Professor Denzil Taylor Smith for not only providing the facilities at the School of Ocean Sciences, but also for providing much needed moral encouragement (keep smiling Sarfraz) throughout the study time.

I am grateful to Dr. James Scourse for his guidance and help particularly during the initial stages of my work, and for reading some parts of my thesis, particularly the discussion of the Quaternary sedimentation in the Caernarfon Bay and Menai Strait.

I am greatly indebted to Dr. Colin Jago for providing encouragement and guidance on all the aspects of my thesis. I highly acknowledge his efforts and constructive criticism in the reading and preparation of the final manuscript of the thesis.

Special thanks goes to my supervisor Dr Angela Davis, who, 5 years ago, introduced me to the field of oceanography and since then has had to dig into the depths of patience to keep encouraging and supporting me throughout ups and downs which I had to face in academic and personal matters. I would like to thank her for having the vision and confidence that I would get through those unfortunate times and finish my thesis.

I must say special thank-you to my mother, brothers and many other friends (back home) for keeping me nearer to them by sending messages of love and kindness throughout the study time.

The immeasurable love and support of someone special has seen me through all the times - good and bad - and she has never failed me. Well done Mumtaz. I must also apppreciate the good behaviour and patience of our children, Aftab, Saima, Mehtab, Asma, Yasmeen, and Ishfaq.

Finally I acknowledge the funding and study leave granted by the Ministry of Science and Technology, Pakistan, and University of Sindh, Pakistan, respectively.

CONTENTS

CHAPTER 4
MORPHOLOGIC AND BEDFORM STUDIES

CHAPTER 5
GRAIN SIZE ANALYSIS: INTERPRETATION AND SIGNIFICANCE OF SEABED SEDIMENT DISTRIBUTION

CHAPTER 6

SEDIMENT TRANSPORT

CHAPTER 7

DISCUSSION

CHAPTER 1

GENERAL INTRODUCTION

In the last (late Devensian)) glaciation, the growth of ice sheets removed sufficient water from the oceans to produce a eustatic lowering of over 100m (Fairbridge, 1961). As the temperature rose at the end of the late Devensian, the ice sheets started to melt giving way to a widespread melt water erosion which resulted in deepening of the many areas which served as melt water channels. As the ice thinned, the melt water continuously flowed into the neighbouring seas and/or oceans. This phenomenon resulted in the deposition of fluvio-glacial sediments in many parts and also resulted in the worldwide rise of sea level. Such a rise in sea level, during the early and middle Holocene period, submerged some of the overdeepened melt water channels and other low lying coastal areas around the world (Embleton (1964), Shennan et al (1983), Park et al (1991)).

Within this project, the Quaternary history of an area of the Menai Strait and Caernarfon Bay has been investigated in this general context. The study area is related to a complex morpho-hydrodynamic system and its formation is thought to have been a direct result of the above mentioned phenomena. The Menai Strait is a long narrow channel which flows between Caernarfon Bay (in the SW) and Beaumaris Bay (in the NE). The exact location of the study area is shown in Fig: 1.1. On the southwestern side, the Strait forms a narrow inlet (about 250-300m wide) through which strong flood and ebb tidal currents (of up to 250cm/s velocity) flow twice a day. Under the influence of the local morphology, these strong tidal currents control the formation of large tidal sand deposits in and outside the inlet.

Hayes (1969) suggested the terms, flood and ebb-tidal deltas for the sand bodies in and outside an inlet. On the basis of his

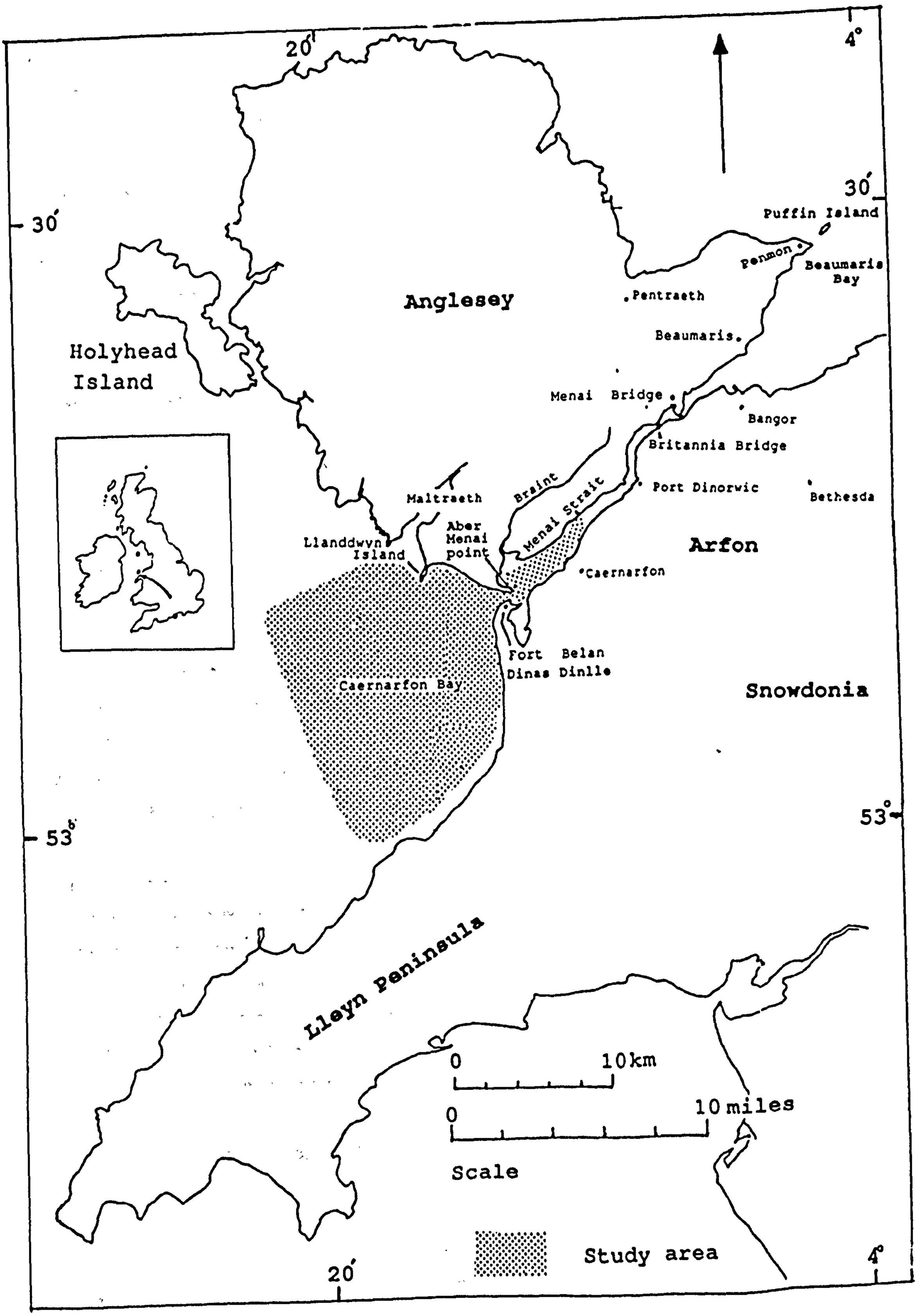

Fig: 1.1 Location map of the study area.

extensive studies of tidal inlet systems along the USA coast, Hayes (1980) put forward standard model of flood and ebb-tidal delta formation and morphology. He reported that these types of tidal deltas are formed around tidal inlets associated primarily with barrier islands or rivers. By contrast, the tidal inlet system in the Menai Strait studied here is associated with the flow of tidal waters through an extended inlet constrained by coastal barriers on both sides. In this way it differs from the basic model of the tidal inlet system proposed by Hayes (1980).

The purpose of the research reported in this thesis was;

1) to study the late Quaternary history of the Menai Strait and Caernarfon Bay regions;
2) to find out when and how the present hydrodynamic regime became established;
3) to study in detail the resulting tidal deltas on either side of the inlet and, by examining the role of the complex local morphology on the development of these deltas, to compare them with the standard models of flood and ebb-tidal deltas suggested by Hayes (1980);
4) to determine the net sediment transport pathways prevailing in the study area.

In order to achieve the above aims, various types of field techniques were employed over a period of three years to survey the study area. The details of each technique and the associated results will be discussed in the coming chapters. However, in order to introduce the reader to the nature and type of the work to be discussed and to give an early idea about the layout of the thesis a synopsis of each chapter is given below.

Following on from this introduction, *CHAPTER 2* reviews the setting and late Quaternary history of the study area. This commences with a description of the general setting, followed by a detailed section on the solid geology of the study area and surroundings. The implications of late Devensian glaciation and

deglaciation processes are also thoroughly covered in this chapter. A detailed section is devoted to a review of the existing hypotheses on the origin of the Menai Strait.

CHAPTER 3 describes the field techniques and the results of extensive seismic surveys employed to study the thickness of the Quaternary cover and the nature of the individual sub-bottom layers and their internal reflection patterns in the Menai Strait and surrounding area of Caernarfon Bay. The results obtained by using three different marine seismic sources i.e. pinger, boomer, and sparker, designed to examine different subsurface features are described and discussed individually, and then the data for specific areas compared with each other in terms of the resolution and penetration. Finally a detailed section is given over to the stratigraphic analysis of the seismic data in order to define various sequences deposited during the Quaternary period.

CHAPTER 4 examines in detail the morphology of the tidal inlet system and of its associated bedforms. This chapter begins with the description of the various processes related to the tidal inlet systems and bedforms found in shallow water environments such as the Menai Strait and Caernarfon Bay. Following on from this, the tidal flow patterns prevailing in the study area are reviewed and the results of the tidal current measurements obtained during the current project are discussed. A section is also included on the geomorphology of the tidal inlet system and associated sand bodies in the study area. This section describes and compares various morphologic features of the flood and ebb-tidal deltas with special reference to the standard models of flood and ebb-tidal deltas suggested by Hayes (1980). The next two sections in chapter 4 deal with the bathymetric and bedform studies undertaken in the current project. The results are obtained from comprehensive side-scan sonar and echo-sounding data collected over a three year period. Various types of bedform features, such as megaripples, sand waves, and sand ribbons, are discussed not only in terms of their

occurrence and morphologic characteristics, but also in terms of temporal variations over neap/spring tidal cycles.

CHAPTER 5 deals exclusively with the study of the seabed grain size distributions. It describes in detail the results obtained from the analysis of 240 bottom sediment samples collected from the study area. This chapter commences with a review of the literature regarding the importance of the grain size analysis and its applicability in morphologic and hydrodynamic studies of areas similar to the one under examination. There then follows a review of the various techniques used for sampling and preparation of the sediment samples. Various laboratory techniques used for the analysis of gravel, sand, and silt and clay-sized fractions are then described and discussed. A number of small sections are also devoted to describe various grain size parameters and their significance, before the detailed results of the grain size analysis are presented.

CHAPTER 6 deals with sediment transport in the area with special reference to sand movement around the tidal inlet. This chapter begins with a review and discussion of various techniques used for the determination of sediment transport and various other important aspects such as sediment transport equations and threshold velocity used for the calculation of sediment transport rate and direction. Following on from this, the next section presents the results of sediment transport calculations carried out during the present study.

CHAPTER 7 brings the various results (presented in the previous chapters) together and discusses their implications. The order of presentation is designed to explain the various phenomena occurring during the late Quaternary period and in present times in the study area. A model of the sediment transport pathways in the study area is also presented and is comprehensively discussed in the light of bedform and grain size studies, and sediment transport calculation results.

CHAPTER 8 concludes the thesis and presents a list of key points drawn from the overall study. Some suggestions for future work are also included at this stage.

CHAPTER 2

SETTING AND GEOLOGICAL BACKGROUND

2.1 General setting.

The most prominent feature of the study area and the feature which led to the choice of the present study area is the Menai Strait. It is a long, narrow stretch of water which separates the Isle of Anglesey from mainland Wales (Fig: 1.1). The Strait runs from Fort Belan to Puffin island, a length of some 28km, and opens out into Beaumaris Bay to the northeast and into Caernarfon Bay to the southwest. The Menai Strait is just one of a series of depressions that cut across Arfon and the Isle of Anglesey. A similar parallel depression runs from Malltraeth to Pentraeth but in this case it lies above sea level (Greenly, 1919). The average width of the Menai Strait between Bangor and Fort Belan is about 800m. The narrowest part of the Strait occurs between the Britannia and Menai bridges (the Swellies). The average water depth along the Strait varies from 1 to 2m at low water spring tide (Boitier, 1982).

For this project the study area covers the southwest end of the Menai Strait (extending from just off Port Dinorwic) and out into Caernarfon Bay. Southward from Port Dinorwic the Strait gradually broadens out and adjacent to Caernarfon Town large sand banks are present (known locally as the Traeth Gwyllt). Being flat topped banks, they undergo a relatively quick submergence in the later stages of the flood tide. During low tide the sand banks are exposed to the prevailing southwesterly wind whose strength is shown by the large wind blown sand dunes of Newborough Warren and Belan, and the large sand spit which forms Aber Menai point. At Aber Menai point, the Menai Strait forms a narrow channel (Fort Belan inlet) which opens into Caernarfon Bay. At the mouth and further offshore of the inlet, large sand deposits form north-south trending sand banks which are exposed to a considerable height during low tide, and the

associated shallow water depth and shoaling outside the Belan inlet inhibit navigation from a southwesterly direction to all but small boats.

2.2 Solid geology.

The solid geology of the Menai Strait and Caernarfon region is related to the pattern of sedimentation and structural deformation along the northwest region of Wales. Much about the geology of Anglesey is covered in the works of Edward Greenly (1919) in his comprehensively written two volume Geological Survey Memoir and solid and drift geological maps. The principal papers published since are by Shackleton (1969), Maltman (1975), and Barber and Max (1979) on the Precambrian, Bates (1968, 1972, 1974) on the Ordovician, and Allen (1965) on the Carboniferous.

Anglesey contains a fascinating variety of solid rock types and geological structures, ranging in age from Precambrian to Carboniferous (Fig: 2.1). The Precambrian rocks are quite scattered and are exposed at various localities. The major group of Precambrian rocks in Anglesey has been given the name 'Mona complex' and contains various types of metamorphic and igneous rocks such as gneisses, tectonic breccias (Gwna melange) and Granite (Coedana). On mainland North Wales the Precambrian rocks form surface exposures in the Lleyn Peninsula and in two small areas i.e. between Bangor-Caernarfon and Bethesda-Penygroes.

On Anglesey, small isolated exposures of Cambrian rocks have been recorded at a few localities and are represented by the Trefdraeth conglomerate and the Careg-onen and Coch-y-miei beds. All these beds are unfossiliferous and are lithologically dissimilar to those on the mainland, where Cambrian rocks are represented by Llanbedr slate, grit, conglomerate and mudstones.

The Ordovician rocks in Anglesey rest directly on the Mona complex (unconformably) and are again quite scattered with a wide variety of rock types eg. basal conglomerate, breccias and

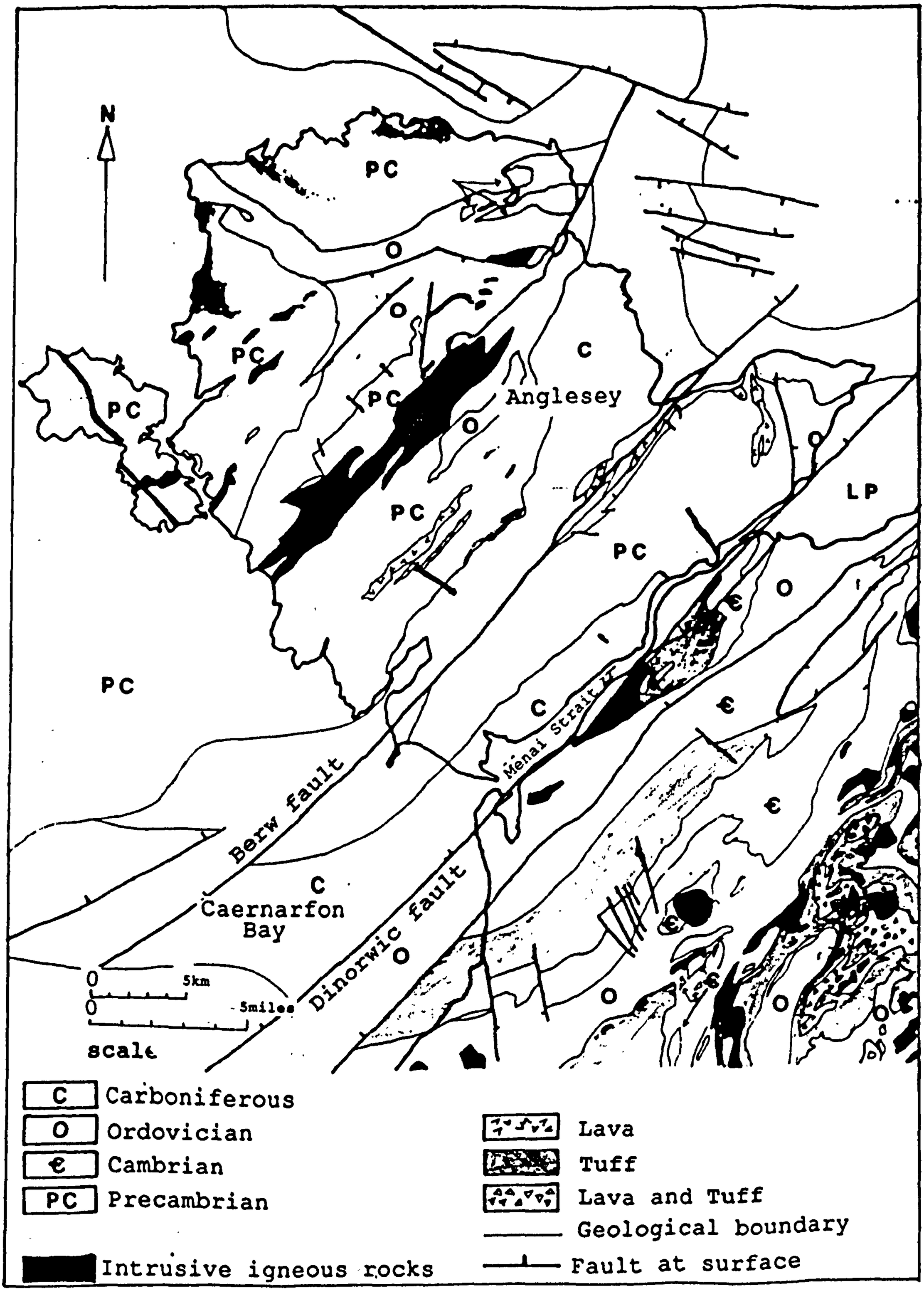

Fig: 2.1 Solid geology of the study area and surroundings.

sandstones. The deposits are related to two transgressions of Arenig and Caradoc age. On the mainland the Ordovician rocks extend northeastward to Conwy and Penmaenmawr, and westward to Caernarfon Bay and the Lleyn Peninsula. The Ordovician rocks of this area are characterized by layers of lava and volcanic ash interbedded with mudstones and slates.

The Caledonian orogeny produced much of the tectonic deformation in the area, resulting in folding, faulting and thrusting of variable intensity. As a result of the Caledonian orogeny, deposition of Carboniferous rocks in Anglesey was largely controlled by the underlying Caledonian structures; thus sediments were deposited in narrow gulfs trending northeast to southwest. The Caledonian earth movements caused a characteristic NE-SW direction of deformation. However, later Hercynian earth movements further emphasized this trend, and it is this which largely contributed towards the present day outcrop pattern on Anglesey. Two parallel downfolds may be recognized, one forms the floor of the Malltraeth depression and the other in part underlies the Menai Strait. Associated with these are major strike faults, the Berw fault along the southern edge of the Malltraeth syncline, and the Dinorwic fault flanking the Menai Strait.

Carboniferous rocks form the third extensive rock system and are well exposed at various places on the island. The Carboniferous rocks are mainly composed of fossiliferous limestone and red brown sandstone with some mudstone. Excellent outcrops of Carboniferous rocks are present on the northeast coast of the island, in the Penmon area, and along the border of the Menai Strait on the Caernarfon side. Carboniferous rocks mark the upper limit of the solid rock deposits on Anglesey, since no Mesozoic rocks are reported from the island. However some igneous activity resulted in intrusions (reported from several localities on the island and Snowdonia area), suggesting that the uplift of Snowdonia occurred after intrusion of dykes. Marine geological research in the Irish sea suggests that

Anglesey may well have been a land mass during the Mesozoic and Tertiary times, and along with the adjacent more major landmass, may have contributed to the supply of sediments to the Irish sea basin (Bates and Davies, 1981).

2.3 Glacial history.

The last widespread glaciation which affected northwest Wales and other parts of the United Kingdom occurred during the Devensian stage of the Pleistocene period. Jehu (1909) identified two different ice sources affecting North Wales and later Greenly (1919) reached similar conclusions from studies of erratics and contrasting till lithologies in the area. One source is linked with a large ice sheet spread over Scandinavia, the North Sea and Scotland. The coalescing and dispersion of the ice sheets from the Scottish highlands and Lake District caused the formation of a large body of ice in the northern section of the Irish Sea (the Irish Sea ice). This flowed down the Irish Sea depression and impinged on North Wales.

The second ice sheet (the Welsh ice) developed locally in the Snowdonia region of North Wales. There has been much controversy concerning the boundary between the Welsh and Irish Sea ice. Mapping of the boundary between the two ice masses is very complicated, since it was continually changing with time due to oscillations of the ice bodies. Greenly (1919) first mapped the zone of contact between the two ice bodies as more or less coinciding with the present day Menai Strait. He supported his idea with the evidence that there is a lack of Anglesey deposits and erratics on the mainland and a corresponding absence of Snowdonian material on Anglesey. On the same basis Saunders (1968) also suggested that the local Welsh ice may have deflected on the intervening lowland area before it even reached the Menai Strait. Bowen (1977) also came to a similar conclusion. He states that, the Menai Strait is thought to form a complex zone between the Aber Ogwen and Seiont (pre-glacial river valleys), where there was once contact between the two

opposing ice bodies.

On the basis of a study of erratics and till fabrics Greenly (1919) concluded that, on Anglesey, except in a few areas showing local variations due to topography, the general direction of Irish Sea ice movement had been from the NE towards the SW. In contrast the Snowdonian ice initially flowed north and north-westwards. This was then deflected southwards, by the Irish Sea advance, in the vicinity of the Menai Strait (Saunders, 1968). Within the literature there appears to have been a disagreement over the number of ice advances associated with the two sources. However, most of the workers agreed that there were essentially two main ice advances in the area. Jehu (1909), whilst working on the Lleyn Peninsula, recognized a tripartite sequence which appears to be repeated over much of North Wales. On the basis of this three layer sequence;

upper boulder clay,
intermediate sand and gravel,
lower boulder clay,

he concluded that there had been two ice advances, the lower and upper boulder clays representing first and second ice advances respectively. The intermediate sand and gravels were postulated to be outwash deposits, characteristic of a period of temporary ice retreat. Greenly (1919) identified a similar three layer sequence in Anglesey and supported the idea of two ice advances in the area.

2.4 The origin of the Menai Strait.

As stated previously, the Menai Strait is one of a series of parallel depressions which cut across Anglesey and the Arfon mainland. These depressions coincide with faults and abrupt lithological changes and were overdeepened due to the erosion associated with the glaciation of the last ice sheet. The last widespread deglaciation caused a worldwide eustatic sea level

rise and, as a result, many low lying areas were inundated by the sea. The uniqueness of the Menai Strait lies in the fact that, unlike other depressions in the area, it was completely flooded during the Holocene sea level rise (another 13m rise in sea level would flood the Bangor-Dinorwic depression and, similarly a rise of 30m by the sea would unite Malltraeth with Red Wharf Bay (Embleton, 1964)).

The origin of the Menai Strait has always been a very controversial subject. However, it is generally agreed that, originally, parts of it had been pre-glacial river valleys. Ramsay (1860) noticed that the trend of the Menai Strait coincided with his postulated ice movement direction of NE-SW. He concluded that the Menai Strait had been overdeepened due to erosion during the last glaciation. Edward (1905) suggested that an ice dammed lake may have been an important factor in the evolution of the Strait and he believed that there had been two watersheds which were cut back due to water entering the Strait to the east and west. Though the initial work was done by Ramsay and Edward, the most quoted hypotheses on the origin of the Menai Strait are those by Greenly (1919) and Embleton (1964).

On the basis of sounding studies in the Menai Strait, Greenly divided the Strait into three areas: the eastern and the western reaches, with the third and shallowest area forming the middle reach. Greenly's theory of the origin of the Menai Strait is illustrated in Fig: 2.2. He suggested that the eastern and western reaches had been independent pre-glacial river valleys, and the middle reach was also predetermined in pre-glacial times. Both river valleys had a NE-SW trend and were separated by a watershed composed of resistant Gwna green schist. The river valley on the western side was once joined with the Bangor-Port Dinorwic depression and ran along the Dinorwic fault into Caernarfon Bay. The eastern reaches were formed from a river valley that ran in the opposite direction, along the edge of the Mona complex and out into Beaumaris Bay. Though the two rivers followed the general structural trend of NE-SW, they had

tributaries with 90 degree confluences (the Cadnant and the Braint). The presence of boulder clay on the floor of the tributaries date their formation as pre-glacial. It is the lower reaches of the Braint which now form the middle reaches of the Strait. It is believed that during the last glaciation there was deepening of the eastern reaches by the Irish Sea ice movement. Greenly argues that at the later stage the Irish Sea ice retreated and decayed, whilst the Welsh ice started to expand from the main valley glaciers (the Ogwen and the Llanberis valleys). He suggested that the Welsh ice advanced far enough to block the flow of the eastern reaches towards the Conwy area. With the eastern reaches blocked by Welsh ice and the presence of the higher ground on the Llanfair and Vaynol side, meltwater continued to accumulate and resulted in the formation of an ice dammed lake. The evidence for this lake is a series of laminated clays described in the Bangor area (Greenly, 1941). Continuous accumulation of meltwater forced the lake to overflow towards the southwest, where it was diverted to join the course of the river Braint which flowed out towards the western reaches and into Caernarfon Bay. Erosion and deepening continued until the eastern reaches had been drained to the watershed, and the middle reaches were formed. After deglaciation the Menai Strait remained as a dry valley until the subsequent rise in sea level drowned the valley and resulted in the formation of the present day Menai Strait.

Greenly's theory remained unchallenged, for decades until Embleton (1964) put forward a new interpretation. Embleton agreed with some of the basic ideas forwarded by Greenly eg. the formation of the pre-glacial river valleys, but he rejected the idea of an ice dammed lake and an advancing local glacier during an overall glacial retreat. To support his new interpretation Embleton put forward evidence of the Irish sea ice esker and moraine deposits found at Penrhyn and around the mouth of the river Ogwen. He argued that any readvance of a local glacier from the Ogwen valley would have removed the above evidence. Embleton also argued that the present day Braint river is too

small for its lower reaches to have once been the middle reaches of the Strait.

Embleton (1964) believed that, either in the pre-glacial or in the last interglacial, there were two parallel rivers (Cadnant and Braint), both flowing southwestwards. Later, the Cadnant changed its course and flowed northeast towards Beaumaris (Fig: 2.3). He postulated that the formation of the Menai Strait occurred during the downwasting of the last Irish Sea ice sheet, and pre-glacial river capture was responsible for determining the route of the Menai Strait. During deglaciation, as the ice thinned, parts of Anglesey and Arfon became ice free, and the resulting topography and ice sheet slope directed the meltwaters southwestwards. Initially the meltwaters flowed through the Pentraeth-Malltraeth and Bangor-Port Dinorwic depressions. At later stages these were abandoned when the watersheds had been lowered to 13m. The Braint river was overdeepened by the flow of meltwaters and, when the ice was no longer continuous between the eastern and western reaches, the meltwater was forced to cut a divide between them forming the middle reaches. Once the Strait was formed it remained as a dry valley until it was submerged during the Flandrian (6000-7000 years ago) sea level rise.

From both the hypotheses it can be concluded that it is generally agreed that parts of the Menai Strait were originally pre-glacial river valleys which were further deepened by erosion associated with the last deglaciation, and a subsequent rise in sea level submerged the depression, thus establishing the present day outcrop pattern. However, the controversy over the melt water flow pattern of the Irish Sea ice and Welsh ice remains.

Since its formation, the Menai Strait has been modified by various processes including tidal currents and wave action. These processes result in extensive erosion in some areas eg. Penmon area, and in accumulation of sand deposits in other areas eg. the Lavan sands, Traeth Gwyllt sand banks (opposite

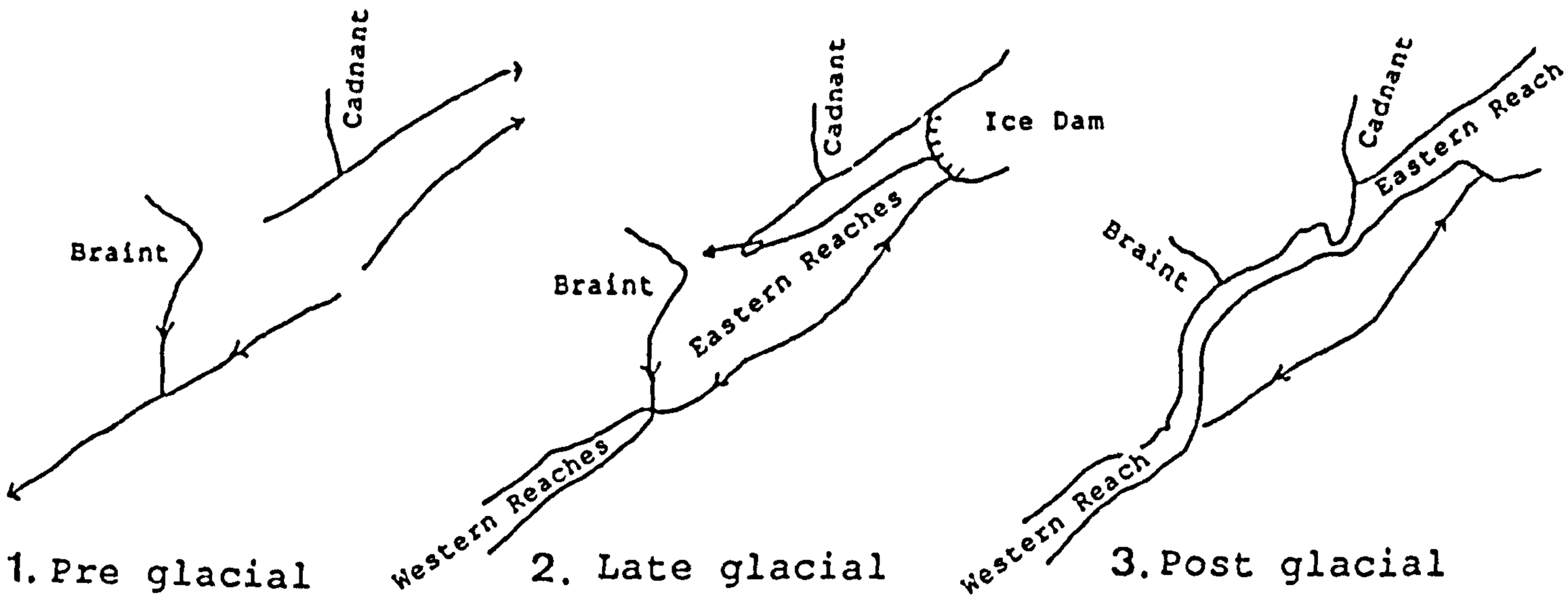

1. Pre glacial 2. Late glacial 3. Post glacial

Fig: 2.2 Greenly's hypothesis for the stages in the formation of the Menai Strait.

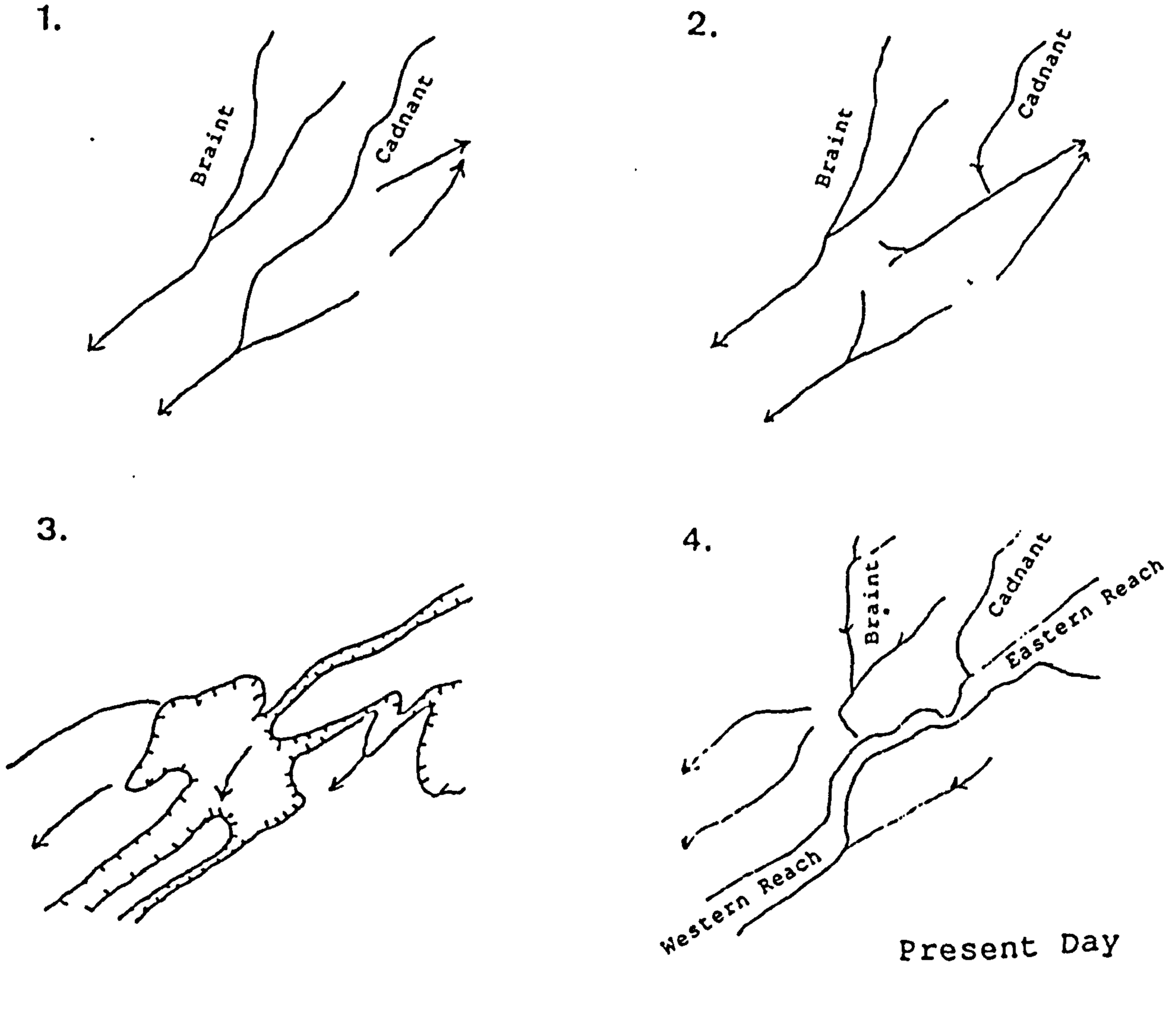

Escaping meltwaters
Ice Margins

Fig: 2.3 Embleton's hypothesis for the Stages in the formation of the Menai Strait.

Caernarfon Town), and in Caernarfon Bay. In the coming chapters, an attempt will be made to study the late Quaternary development of Menai Strait. Its role in the deposition of thick sediment deposits in the southwest end of the Menai Strait and in the Caernarfon Bay will also be examined.

CHAPTER 3

SUB-BOTTOM STUDIES IN CAERNARFON BAY

3.1 Introduction.

Over the years, studies undertaken by various scientists eg. Emerson and Phipps (1968), Van Weering (1975), Vittori et al (1981), Carlson (1989), have revealed that seismic surveys of the sub-bottom sedimentary layers under the sea can provide valuable information about the bedrock depth and Quaternary history of any particular area.

Continuous reflection profiling (CRP) provides one possible means for studying the structure and thickness of the sedimentary layers in areas such as the deep oceans, continental shelf, shallow seas, harbours, estuaries, lakes and rivers (Emerson and Phipps, 1968). The validity of continuous reflection profiling methods for surveying shallow water areas is testified by many workers: Knot and Hersey (1956), Moore and Shumway (1959), Leenhardt (1967), Blundell et al (1969, 1971), Kummer and Creager (1971), Van Weering (1973).

After a study of the above mentioned literature it was concluded that continuous reflection profiling should be able to be successfully applied to solving a number of problems in the area chosen for the current study. That is, within Caernarfon Bay the late Quaternary sedimentary deposits are of a suitable thickness to allow internal reflection information to be obtained by CRP, and the prevailing water depth should not preclude its use.

Within this project the major aim of the CRP exercise was to acquire knowledge about the configuration and the geometry of the recent sedimentary cover and distribution of the glacial and postglacial deposits. This combined with other results obtained by various methods (to be discussed in the later chapters) would provide a better understanding of modern and past sedimentary

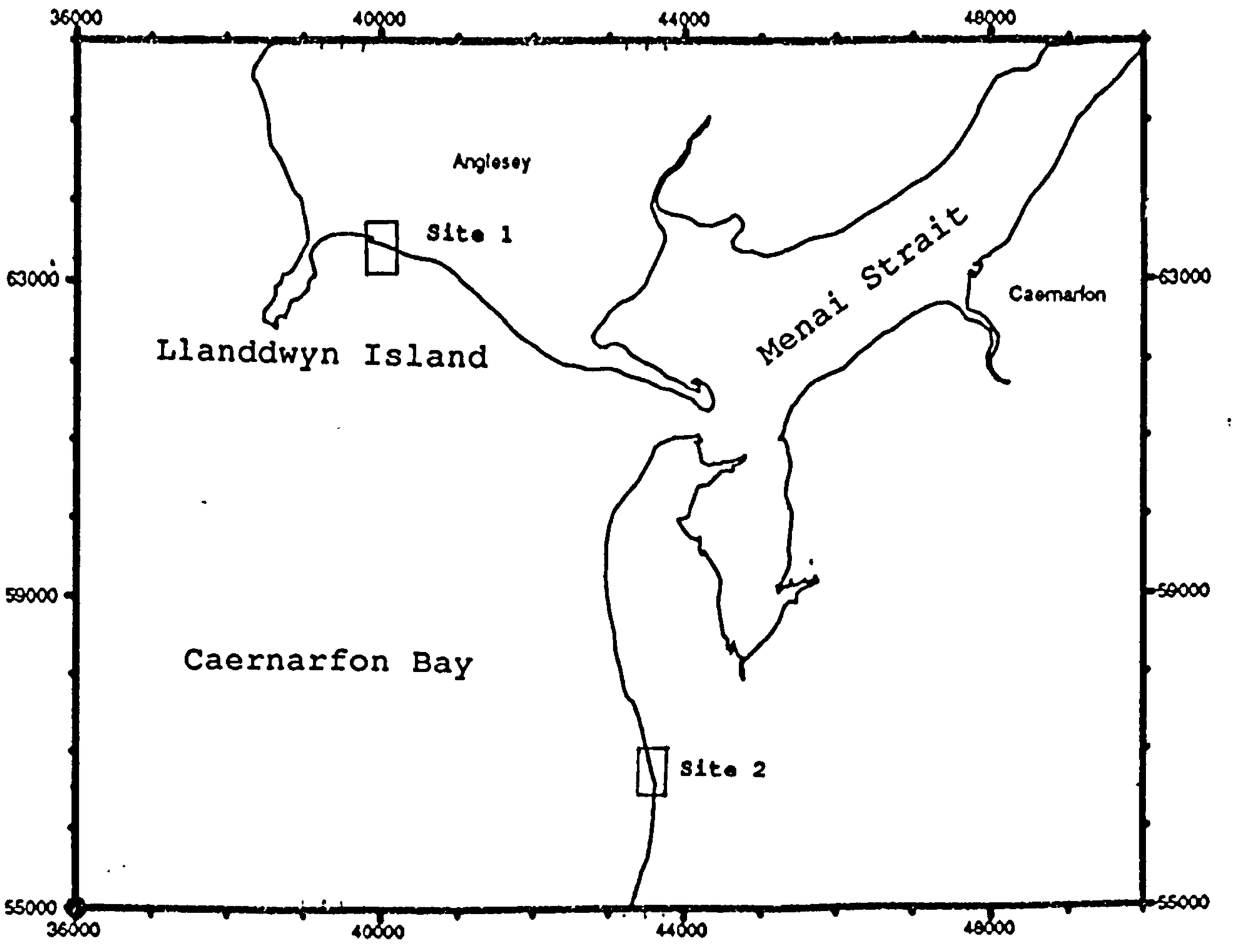

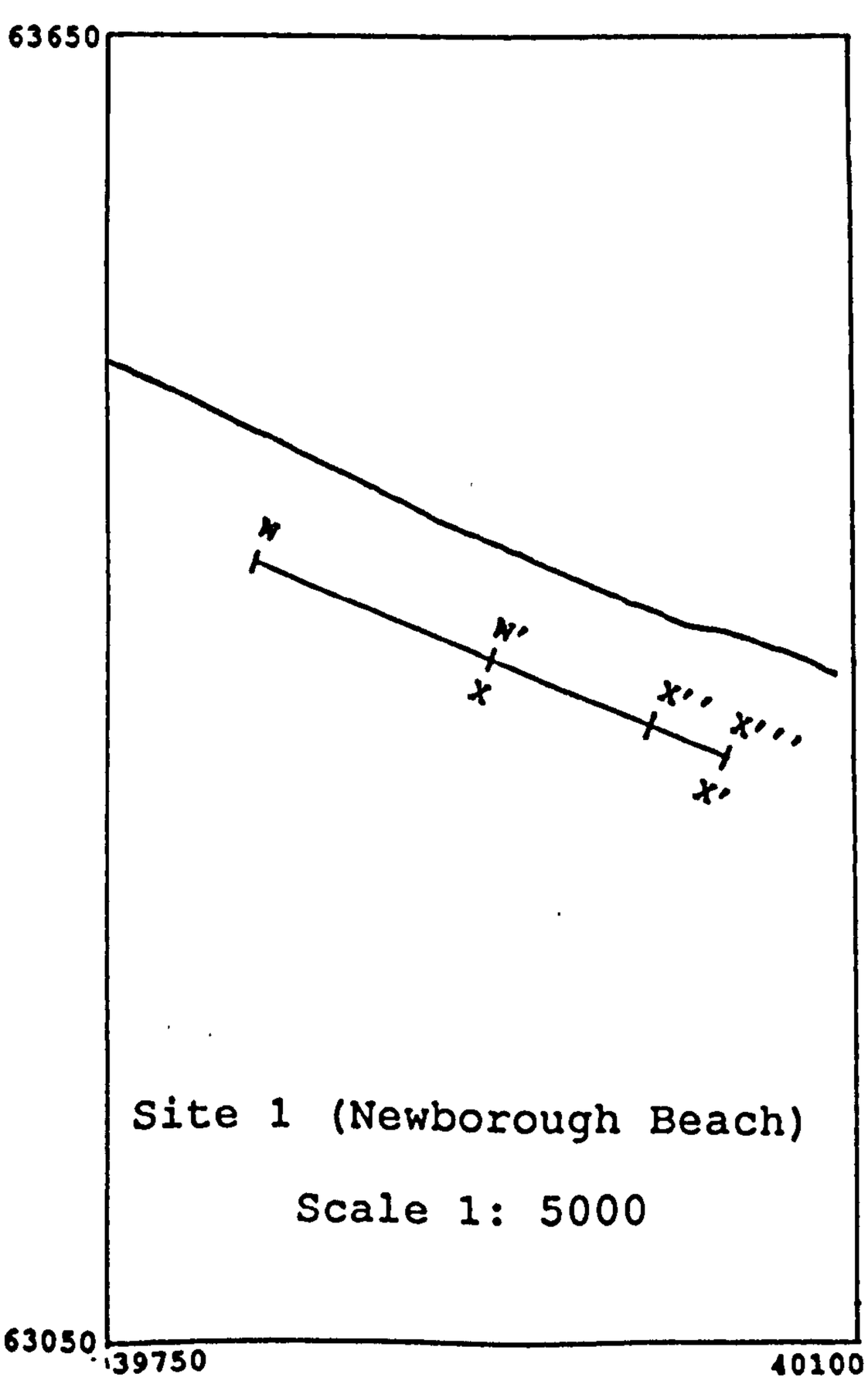

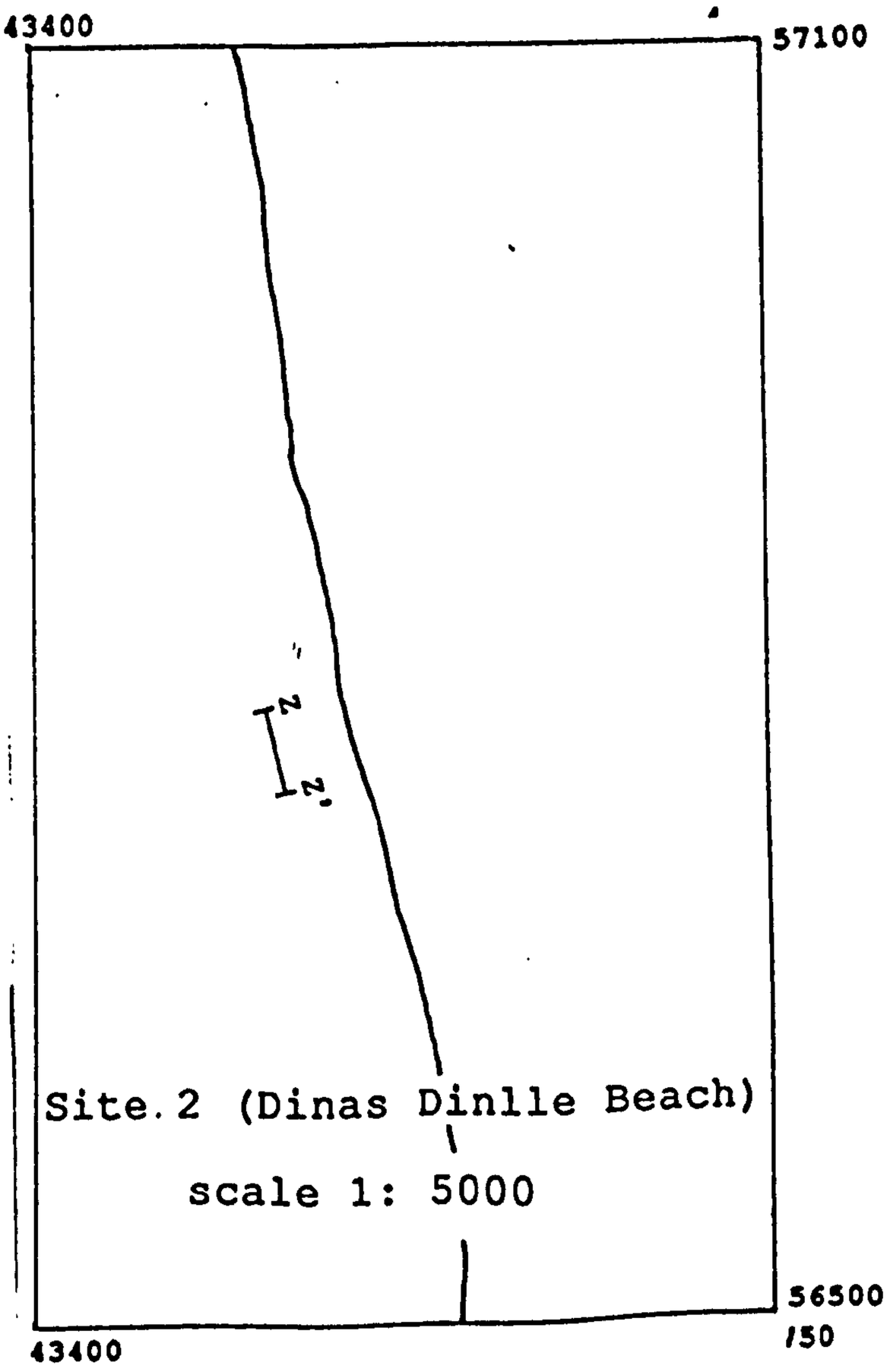

Fig: 3.1 Location map of land seismic lines.

depositional environments with special reference to the Quaternary tidal delta system of Caernarfon Bay and the Menai Strait.

Although the main emphasis was given to continuous marine reflection profiling, some land seismic measurements were also carried out at two coastal sites: the beaches of Newborough and Dinas Dinlle. The prime aim of this additional exercise was to acquire some information about the seismic velocity of the sub-bottom sediments which could then be used to convert travel times to depth for the marine profiles. Furthermore, it was felt that the information about the nature and thickness of the layers at these two points would prove helpful when carrying out a geological interpretation of the total offshore data.

3.2 Land seismics.

To obtain the required data two refraction and two reflection lines were shot at the Newborough and Dinas Dinlle sites.

3.2.1 Position fixing.

The layout of each line was determined using compass bearings. The end points were tied in by taking bearings of a few fixed landmarks which allowed the lines to be plotted onto the site map (Fig:3.1).

3.2.2 Field equipment.

An ABEM Terraloc seismograph coupled to a 12 take-out geophone cable was used for the land seismic work at both the sites. The Terraloc allows various parameters such as spread details, record number, record length, delay time, channel gain, etc. to be entered into the header information of the system memory before a seismic record is produced. Other features of the Terraloc include independent stacking of each signal, frequency filtering and individual channel gain adjustment. It also has a

facility to allow records to be stored on magnetic tape as well as providing a hard copy record (via a portable printer unit). Compressional waves were generated using a vertical impact between a sledge hammer and a metal plate on the ground surface. Timing of the first arrival was initiated using a trigger geophone buried in the surface sediment near the metal plate. Geosource Sensor SM-4 geophones of natural frequency 10Hz were used to detect the signals.

Instrument specification sheets for all the above can be found in appendix I.

3.2.3 Site 1 (Newborough beach).

Refraction survey.

To avoid the disturbances and noise interference produced as a result of the human activity on the beach, an area north of the car park entrance was selected for the seismic survey. The location of the survey lines is shown in Fig: 3.1. Two profiles WW′ and XX′ were shot in a roughly northwest to southeast direction (290 degrees magnetic) using a geophone interval of 10m. This geophone interval was chosen with the expectancy that the thickness of the unconsolidated sediments would be in a depth range of a few metres. Shots were taken at both ends of each line with the source offset 10m from the first geophone.

Interpretation of refraction data.

The refraction records were initially analyzed by picking first arrival times using the ABEM Terraloc's inbuilt viewing facility in combination with variable trace records and digital time readout. Time-distance graphs were plotted for each profile. Each straight line portion of the graph is taken to represent an individual refractor (excluding the initial slope which relates to the direct wave).

There are various interpretational methods which can be applied to seismic refraction data such as: the plus minus method

(Hagedoorn, 1959), critical distance method, and intercept time method (Wyrobek, 1956). Since the plus minus method can only be applied if there is sufficient overlap of refraction branches for any individual refractor on the time-distance graph, it did not appear suited to interpretation of the data at hand. Thus the simple intercept time method was chosen to obtain depths and velocities for each site.

Once the individual refractors were distinguished for each line, a least squares best fit was used to put a straight line through each set of points. The gradients of these lines were used to calculate the apparent velocities of the layers. Knowing the intercept times and apparent velocities for each refractor for reverse shot spreads, the thickness of each layer was calculated.

Results

Profile WW′ and XX′: Time-distance graphs and profiles obtained from end to end refraction lines WW′ and XX′ are shown in Fig: 3.2. Each value of velocity shown on the cross section represents the average velocity obtained from normal and reverse data along a line. For both the profiles, the interpreted sections are sufficiently consistent for continuous layer boundaries to be drawn.

Layer 1: This layer has an average seismic velocity of 1620 and 1615 m/s in the profiles WW′ and XX′ respectively. This relatively low velocity probably represents surficial beach sand.

From the seismic data the thickness of the first layer appears to vary from 13m at the start of profile WW′ to 19m at the end of the XX′ profile suggesting that the refractor is dipping slightly towards the south (although 3D information would be needed to confirm this).

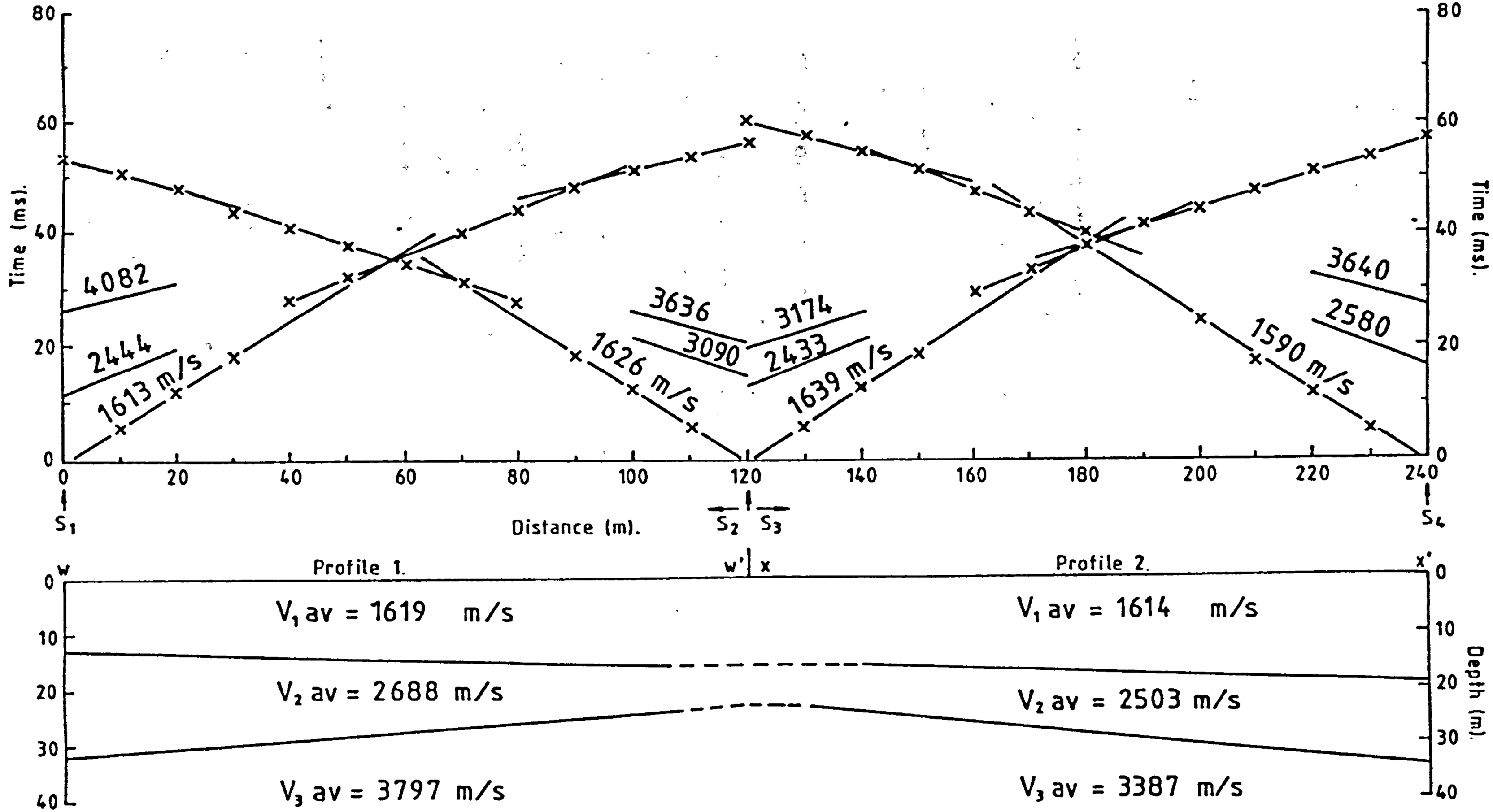

Fig: 3.2 Time-distance graph and interpreted cross section for profiles WW′ and XX′ (for location see Fig: 3.1).

Layer 2: Layer 2 displays an average seismic velocity of 2688 and 2503 m/s for the profiles WW′ and XX′ respectively. Its apparent thickness at the extreme ends of the combined profiles is greater than in the central portion, suggesting a ridge structure forming the surface of the basal layer. The layer 2 velocities suggest that it might be comprised of weathered rock.

Layer 3: The average velocities of 3797 and 3387 m/s for layer 3 for profiles WW′ and XX′ can be attributed to bedrock.

Reflection survey.

A single reflection profile X′′X′′′ was shot over the end portion of the XX′ refraction line. Its location is shown in Fig: 3.1. A 36m geophone spread was laid with a geophone interval of 3m and shots were made at both ends of the line with an offset of 3m.

Interpretation of reflection data.

Full details of the methods commonly used for the interpretation of the above type of reflection records are given in Telford et al (1976). Initially data were analyzed for reflection events. The reflection times were plotted on a time-distance graph to check for the hyperbolic effect. Given correct identification, when T^2 is plotted against X^2 a straight line of slope $1/V^2$ and intercept time To^2 is produced. Thus the slope gives the velocity, and depth can be determined from the intercept time where $2H = VTo$, V is the velocity of the layer and To is the intercept time.

Results

Profile X′′X′′′: The time distance graph for this profile is shown in Fig: 3.3. The data plot indicates a two layer case with very little variation in layer velocities. A comparison of coincident refraction and reflection lines shows good agreement for the first interface.

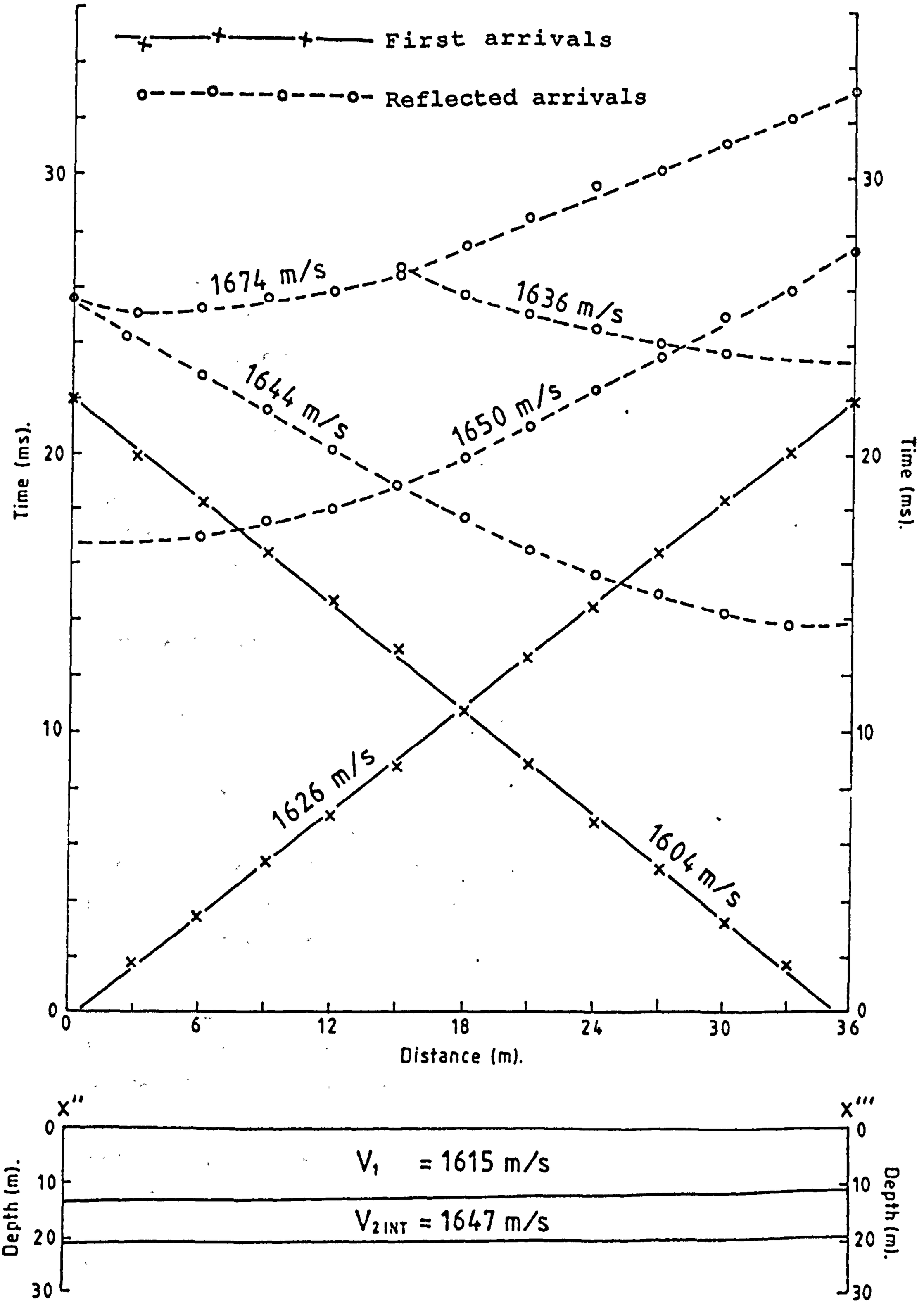

Fig: 3.3 Time distance graph and interpreted section for profile X'' X''' (for location see Fig: 3.1).

Layer 1 has an average seismic velocity of 1615 m/s. The predicted thickness at the two ends is 13 and 11m.

Layer 2 has an interval velocity of 1647 m/s and appears to vary in thickness along the line by approx. 1m i.e. from 7 to 8m.

The velocity variations being only minor, meant that no significant deductions can be made as to internal layer composition. However, the velocity of the first layer does appear to match that obtained for the first layer by refraction shooting. The velocities of layer 2 as predicted by the reflection method, show an increase with depth which may be attributed to either increasing saturation of the sediments or it may be an effect of increasing compaction with depth, or a combination of both factors.

3.3.4 Site 2 (Dinas Dinlle beach).

Unfortunately, due to tidal and weather constraints it was not possible to carry out a full refraction and reflection survey within the time allowed for the initial beach measurements at Dinas Dinlle. Subsequent interpretation of the data collected as part of the reflection survey did however yield sufficient information on refracted events to preclude the need for a further independent survey.

Reflection survey

The chosen site for the reflection survey was just opposite the Marine Hotel. One reflection profile (ZZ′) was shot with a geophone interval of 3m (12 geophones) and a source offset of 3m. Shots were fired at both ends of the spread to provide end to end coverage.

Results

Profile ZZ′: Although the data quality was poor, some reflectors were picked out and the travel times plotted. However, the

accuracy of these results is questionable and this should be borne in mind in the final assessment. The time-distance graph for this profile is shown in Fig: 3.4. While two reflectors can be distinguished when shooting in one direction, only one reflector is evident when shooting in the reverse direction.

Layer 1 has an average seismic velocity of 1668 m/s and variable thickness of between 3 and 1m.

From the single data set an average seismic velocity of 1894 m/s and thickness of approx. 20m was calculated for *layer* 2.

The velocity of layer 1 is representative of a typical beach sand and the velocity of layer 2 might be indicative of a boulder clay layer.

The above geological interpretation is based on the coastal exposures of Quaternary sediments at Dinas Dinlle and is supported by Campbell (1990). He suggests that the red to purple Irish Sea till (exposed at Dinas Dinlle) probably extends beneath the modern beach in the vicinity of the survey area.

Refraction Data

The time-distance plot of the refracted first arrivals obtained at this site (Fig: 3.4) also indicates two layers with a velocity of 1668 and 1894 m/s for the first and second layers respectively. The velocity of the first layer appears to be in full agreement with the expected value for beach sand, while the second layer velocity also fits well with the reflection results. It therefore seems reasonable to conclude that the interface is one between beach sand and till.

In order to summarise the results it can be said that the land seismic survey conducted at the two sites provides valuable information about the probable seismic velocities of the glacial and postglacial sediments present in the offshore areas of Caernarfon Bay. The land seismic results at both the sites

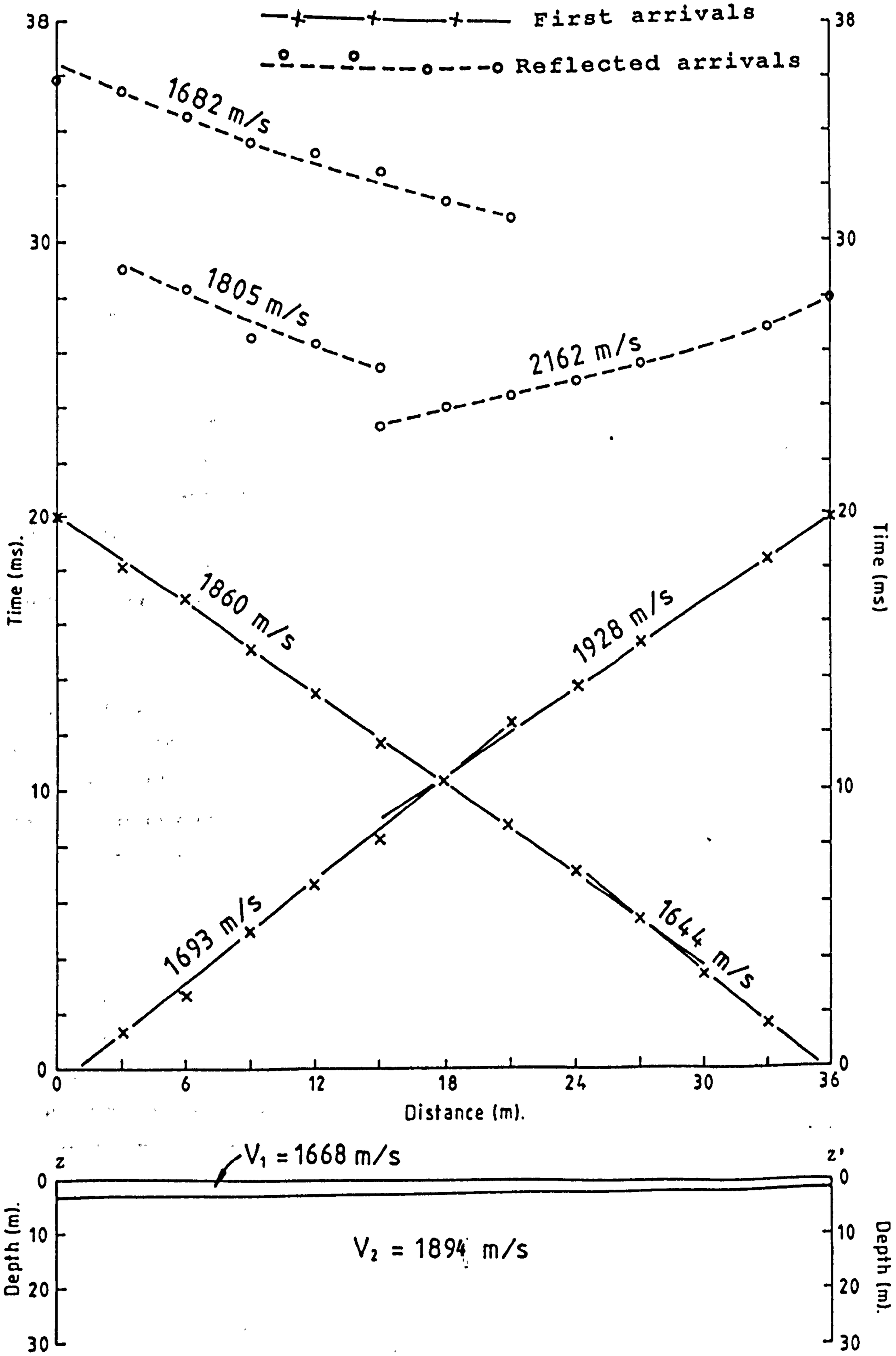

Fig: 3.4 Time-distance graph and interpreted section for profile ZZ′ (for location see Fig: 3.1).

indicate an average velocity of about 1650 m/s for the surficial unconsolidated sediments. The layer 2 velocity of about 1890 m/s obtained from the Dinas Dinlle site indicates the presence of glacial till which lies beneath the surficial sediment cover.

3.3 Continuous reflection profiling (CRP).

The hardware for marine continuous reflection profiling primarily consists of a sound source and towed hydrophone receiver (except, in the case of a pinger system where the same transducer serves as source and receiver), the instrumentation to drive the source, and a recorder for received signal display. The source sends out sound pulses at regular intervals; the hydrophone receives signals reflected from the sea floor and sub-bottom layers.

The reflection of the seismic wave at a boundary is a function of the difference in acoustic impedances (Z) of the two media; the specific acoustic impedance of any particular medium depends on the propagation velocity, V, of the seismic wave and density ρ of the medium:

$$Z = V \cdot \rho$$

The strength of the reflection depends on the impedance difference, i.e. the bigger the difference, the stronger the reflection, and this can be expressed in terms of the reflection coefficient R. In the case of normal incidence on an interface between two layers with impedances Z1 and Z2, the reflection coefficient is given by:

$$R = \frac{Z2 - Z1}{Z2 + Z1}$$

In practical terms, the reflected sound signals, once received by the hydrophone, are translated into electrical signals by the

hydrophone and fed ultimately to a graphic recorder. A continuous record of the sub-bottom profile is produced by firing the source at a fixed repetition rate. For further details on marine reflection surveying see Trabant (1984).

3.3.1 Survey details.

Because of the widely varying field conditions within the chosen survey area and particularly with relation to water depth (often very shallow), the presence of sub-tidal and inter-tidal sand bars, and strong tidal currents at certain places, it was not possible to get full coverage of the entire area with the seismic reflection profiling system. However, where conditions permitted, every effort was made to obtain seismic sub-bottom information. To achieve this, various types of boats and seismic sources (pinger, boomer, and sparker) were used, each being suited for use in that particular part of the area.

Initially (in July 1987), a relatively shallow part of Caernarfon Bay (west of the north and south sand bars) was surveyed using a pinger sub-bottom profiler (nearshore measurements). For this survey a boat (the Cadnant) which was specifically designed for work in shallow waters was kindly lent by the Caernarfon Harbour trust.

Subsequently (in July 87 and July 88) the UCNW research vessel Prince Madog was used to survey further offshore in the area of relatively deep water. For work on the Prince Madog the pinger and boomer were used simultaneously (in July, 87), and later (July, 88) a sparker was used to provide supplementary data and more particularly a greater penetration depth.

3.3.2 Pinger sub-bottom profiling.

Survey 1 (nearshore measurements).

For the initial pinger survey in the shallow water area, the measurements were planned to coincide with high water spring

tide. The final track chart for this area is shown in Fig: 3.5.

Survey 2 (offshore measurements).

The main tracks for survey 2 on the Prince Madog were run approximately in a NW-SE direction, parallel to the lines surveyed previously. In addition to these lines, a few intersecting lines were also run in an attempt to get better coverage and perhaps attempt to define the structures in 3D. The track chart of survey 2 is shown in Fig: 3.5.

Field equipment :

The O.R.E. Inc. Model 140 pinger system used in this survey is specially designed for small boat operations at low speed. The source/receiver transducer consists of an array of 4 elements, which are mounted on a plate at the end of a vertical gimballed staff. The staff is supported by a mounting pad which can be fastened to the deck of the boat and the transducer is mounted over the side. The above assembly ensures that the transducer beam will remain directed towards the seabed despite any motion of the vessel. The staff can be raised and lowered to adjust the transducer depth in accordance with the waterline.

Equipment specifications can be found in appendix II.

3.3.3 Boomer (Uniboom) sub-bottom profiling.

About 81km of Uniboom profiles were run in roughly NW-SE and E-W directions. The aim was to keep the NW-SE lines at an interval of about 1km, but due to the tidal currents and prevailing weather conditions, it was not possible to keep a constant distance between the lines. For the E-W trending lines an interval of about 1.5km was chosen. The location of the completed Uniboom traverses is shown in Fig: 3.6.

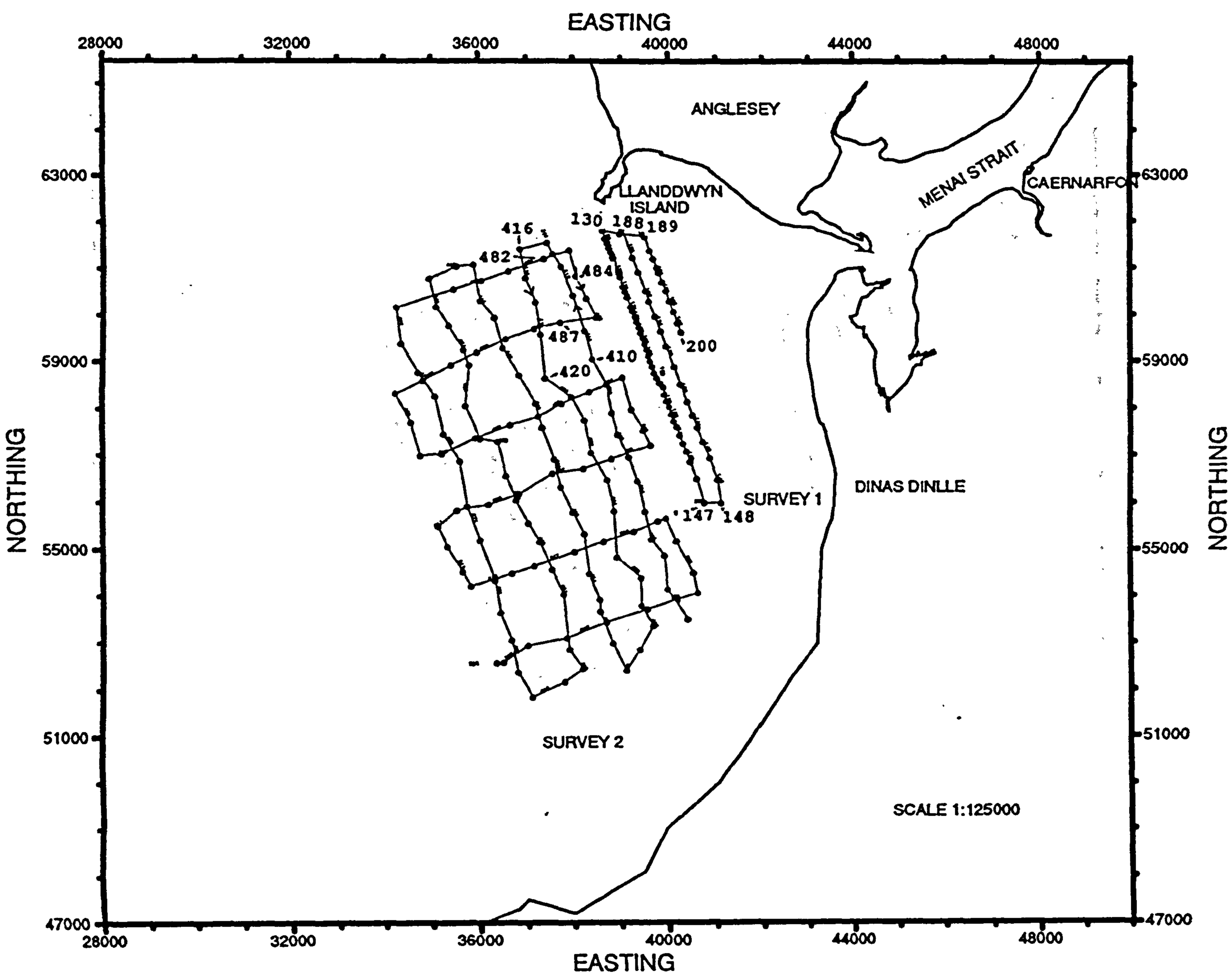

Fig: 3.5 Track chart for pinger sub-bottom profiling (Survey 1 and 2).

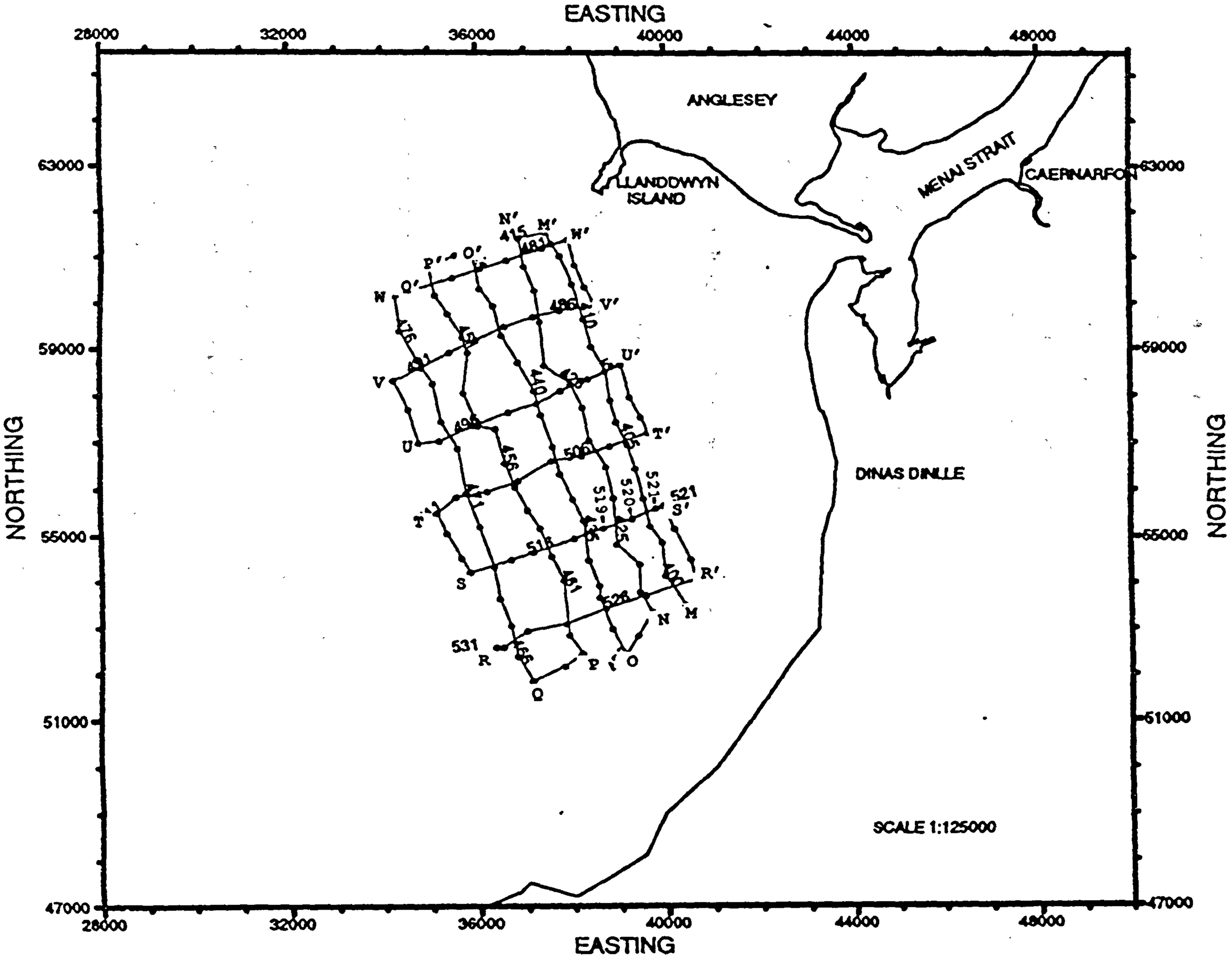

Fig: 3.6 Track chart for boomer sub-bottom profiling.

Field equipment:

An EG&G Model 230 Uniboom system consisting of a sound source, energy supply, hydrophone, band pass filter and a marine graphic recorder was used for this survey. It is a surface towed device which is capable of working in shallow waters such as harbours, rivers etc. It uses a separate source and receiver and is designed to provide a high resolution seismic profile of a narrow section of the sub-bottom (mid point between source and hydrophone) directly beneath the track of the survey vessel.

The frequency and power of the Uniboom are such that it can penetrate to a depth of more than 50m depending upon the bottom and sub-bottom sediments.

Equipment specifications are given in appendix III.

3.3.4 Sparker sub-bottom profiling.

In all, about 187km of sparker profiles were collected with roughly NW-SE and E-W trending traverse lines. As previously, NW-SE lines were run with a gap of about 1km, and E-W lines were run with a gap of about 1.5km. The tracks covered are shown in Fig: 3.7.

Field equipment:

An EG&G model 267A sparker array seismic system was used. It consists of a three electrode sparker array, triggered capacitor bank, power supply, hydrophone and marine graphic recorder. The sparker array generates an acoustic pressure pulse by discharging a short duration electrical pulse between an electrode and a grounded frame (spaced several inches apart in the sea water). The rapid discharge of electrical energy between the electrode and the frame quickly heats and vaporizes the sea water, generating a rapidly expanding plasma bubble. The rapid expansion of the bubble generates an acoustic pulse capable of

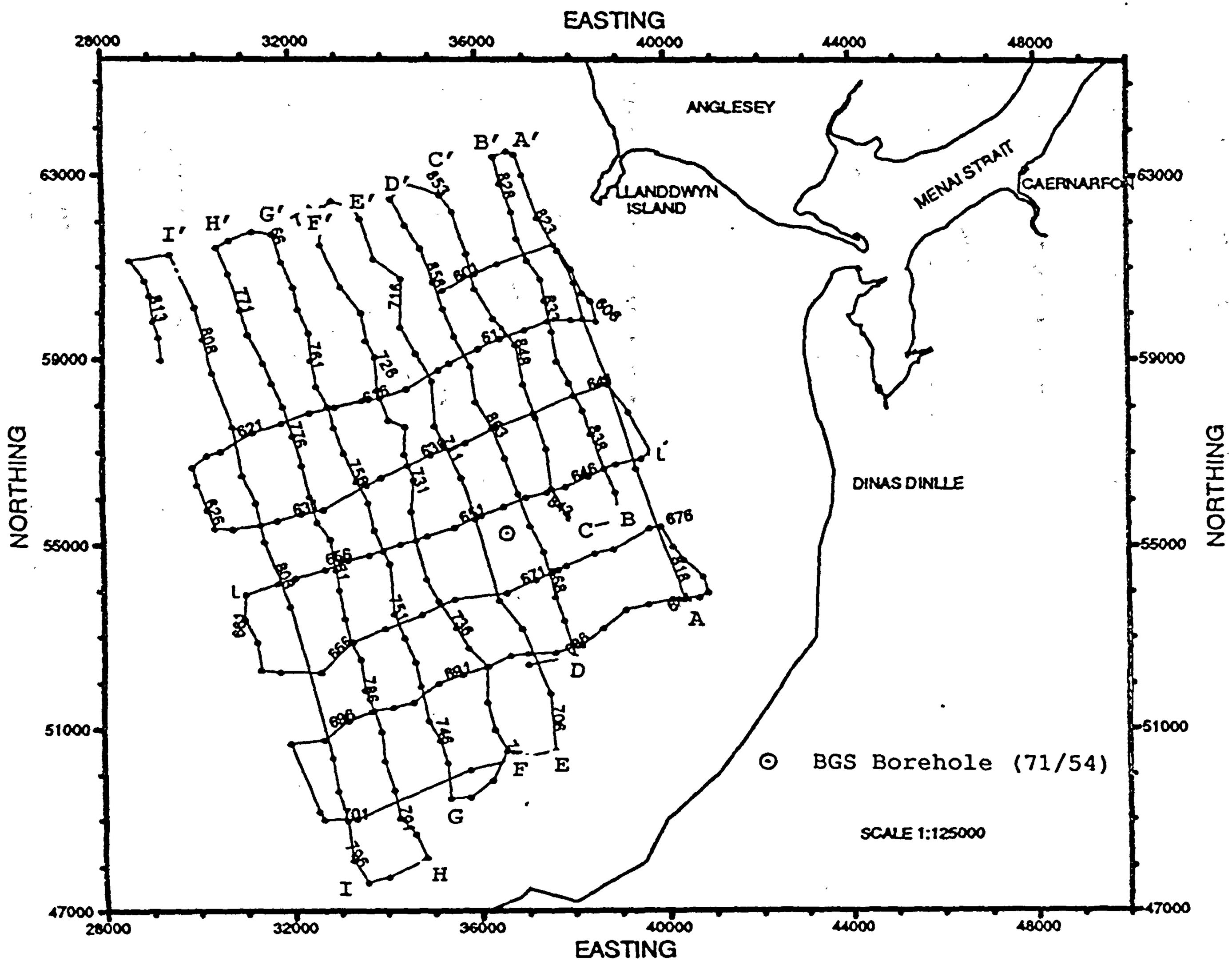

Fig: 3.7 Track chart for sparker sub-bottom profiling. .

penetrating up to 1000m into the sub-bottom layers, with a resolution of 2m or less, dependent on operating power, frequency and bottom materials. Thus this system was employed to get better sub-bottom penetration.

Equipment specifications are given in appendix IV.

3.3.5 Position fixing.

Two different types of position fixing systems were used for the offshore seismic surveys. these are listed and described below:

Type of survey	Position fixing system
Pinger (survey 1)	Decca trisponder system.
Pinger (survey 2)	Decca navigation system.
Uniboom	"
Sparker	"

Decca Trisponder system.

A Decca trisponder system consists of a main (master) mobile station situated on the survey vessel, two or more shore based stations (slaves) with known, fixed National Grid positions, and a digital distance measuring unit. The position of the survey vessel is determined by interrogating the land based slave trisponders using high frequency radio signals. The time taken by a signal from master - slave - master is translated into ranges and displayed by the distance measuring unit.

Knowing the positions of the land based stations and the horizontal ranges between each of the land based and mobile stations, the position of the boat can easily be plotted onto the chart. For automatic conversion and plotting of the ranges the system can be interfaced to a computer and a plotter. The major advantage of this interface system is the continuous display facility i.e. boat's position on the screen, which helps the boat's navigator maintain straight tracks under favourable

conditions. A few traverses were covered with this system and the advantage of the system was clearly evidenced by the straight track lines and regular fix intervals (pinger nearshore measurements, Fig: 3.5).

The accuracy obtainable with the trisponder system is dictated by standard two range pattern geometry (due to logistical problems only two slave stations were used for this particular survey). The best accuracy will be obtained at the point where the range circles intersect at right angles to each other. An accuracy of approx. 3m in horizontal range can be expected with the trisponder system.

Decca navigation system.

A Decca navigation system is permanently installed on the Prince Madog. It is a radio position fixing system which is available for use onland, in the air, and at sea. This system utilizes fixed transmitting stations at known locations to provide hyperbolic lines of position. The receiver delivers position lines as numerical "decometer" readings which are recorded and subsequently plotted on a hyperbolic lattice chart. The intersection of two and more such lines gives the location of the onboard unit, in latitude and longitude.

In this particular survey the fixes were recorded approximately every five minutes and also at the start and end of each line. The latitude and longitude data were subsequently converted into National Grid coordinates to bring it in line with rest of the data.

3.3.6 Interpretation method.

Continuous seismic profiling provides a means of determining the sub-bottom structures on a seismic record which, together with other independent knowledge, helps in the geologic interpretation (Hersey, 1960).

Determining the sub-bottom geology from the seismic records, while apparently straight-forward, can quite often be complicated by the interference of primary reflectors with other unwanted signals (noise) such as the direct arrival, multiple reflections (Fig: 3.8), side echoes, and point source reflection. Therefore, interpretation of seismic records requires great care and expertise to differentiate between primary events and noise.

Recognition of seismic events is based on the following characteristics: coherence, amplitude standout and character (Fig: 3.9 after Sheriff and Geldart, 1982). Coherence is determined by the similarity in appearance from trace to trace, and is the most important factor in recognizing a seismic event. Amplitude standout refers to an increase of amplitude due to the arrival of coherent energy, while character involves the distinctive appearance of the waveform.

Initially, and with the above in mind, the most significant reflectors were picked out. Following on from this, minor reflectors and internal reflection configurations were identified and used in the final analysis.

Seismic velocity.

The inferred depth of any reflector on a seismic record is dependent on the seismic velocity used in the interpretation. The importance of using the closest possible value to the natural velocity of the layers can not be over stressed. Various methods have been used to obtain this information.

Blundell et al (1971) carried out a combined seismic refraction and marine profiling survey over the South Irish Sea and Nymphe Bank and calculated an average velocity of 1800 m/s for the sediments above the basement reflector (bedrock). Hamilton and Bachman (1982) conducted laboratory measurements on various

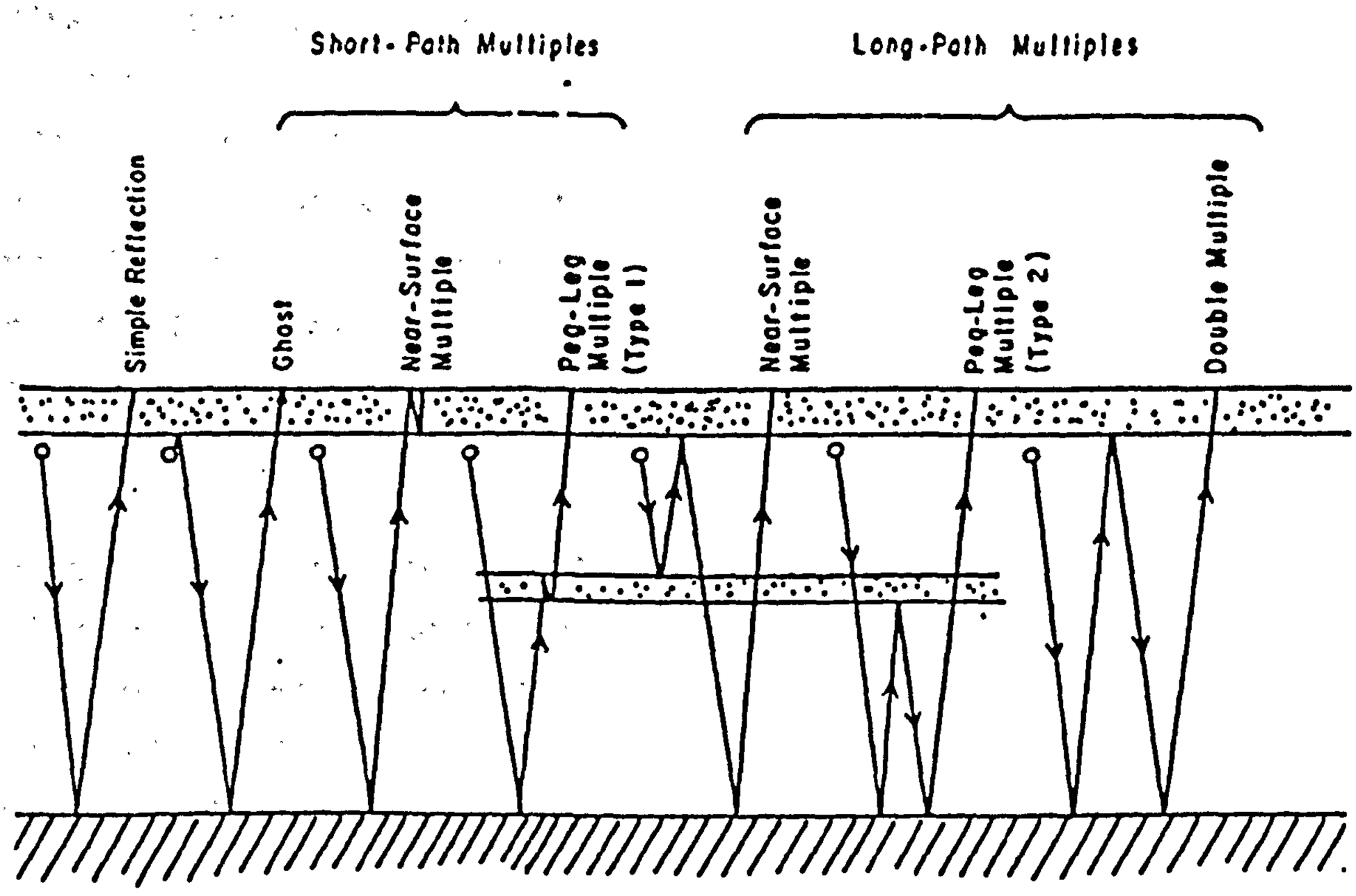

Fig: 3.8 Types of multiples (after Sheriff and Geldart, 1982).

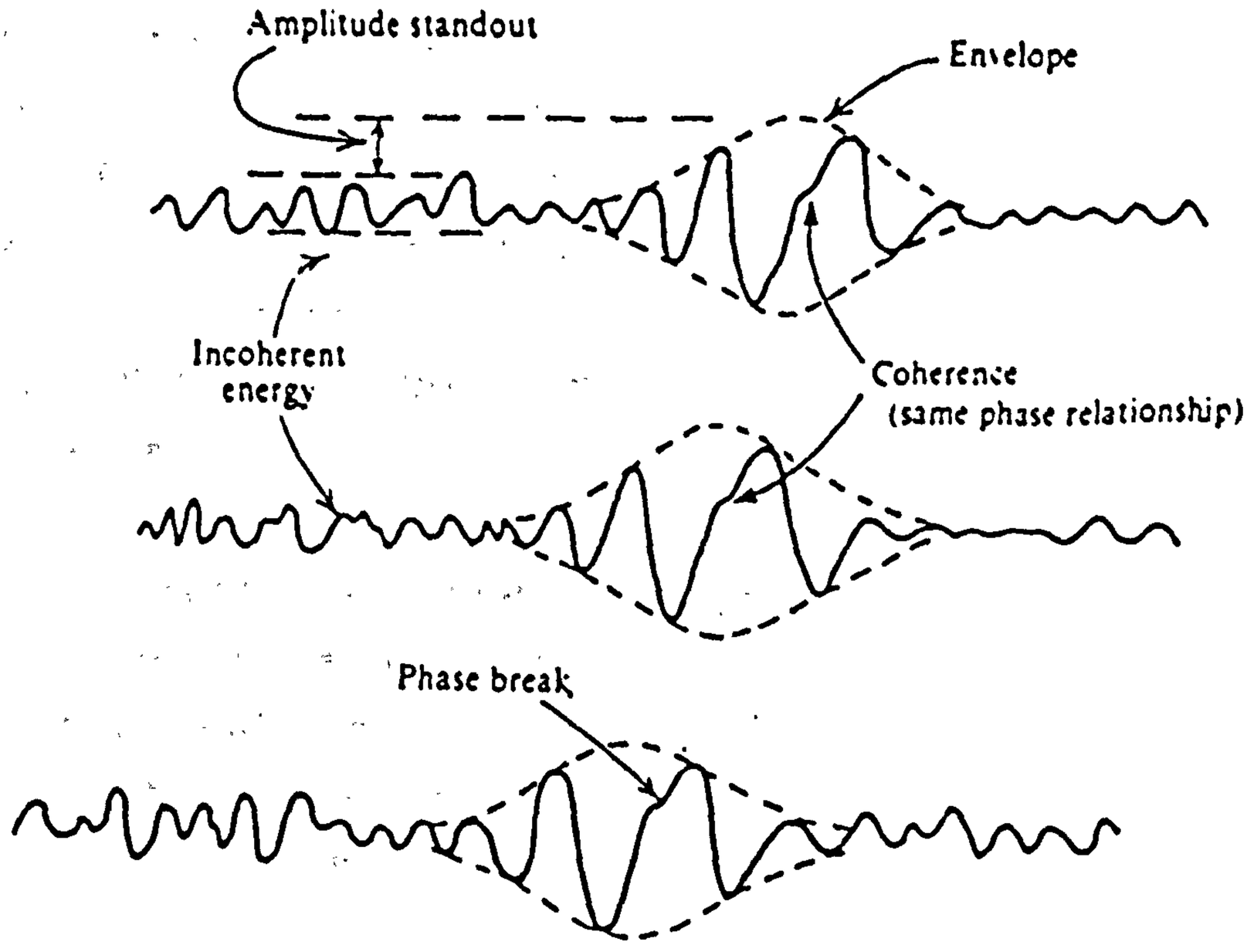

Fig:3.9 Characteristics of seismic events (after Sheriff and Geldart, 1982).

sediment samples recovered from one area and concluded that, from the mean grain size value, a prediction of an average seismic velocity could be made to an accuracy of ± 2% based on empirical relations. Larcombe, (1991 personal communication) carried out some seismic profiling in Mawddach estuary and Barmouth Bay, where he used an average seismic velocity of 1710 m/s for the glacial and recent sediments, calculated on the basis of the mean grain size value of surficial sediments.

For the Caernarfon Bay/Menai Strait area, from an initial analysis of the surficial sediment data (to be discussed in later chapters) it was concluded that the mean grain size of the surficial sediments most probably ranges between medium to coarse sand and using a method similar to Hamilton and Bachman this gives an average velocity of 1700 m/s.

However, land seismic surveys carried out during the current project at the two coastal sites probably provide the best velocity estimate. These suggest that the sediments above bedrock are layered with two distinct materials being present. This in fact also appears to be the case for most of the offshore study area (see sparker results) and thus two velocities should clearly be assigned to the sediments overlying basement i.e. the first layer which has a seismic velocity of around 1650 m/s at the two sites is believed to be representative of the unconsolidated surficial sands, and the second layer (identified at Dinas Dinlle site) is most probably the Irish Sea till (boulder clay) with an average velocity of about 1890 m/s.

While in most of the sparker sections two layers are identifiable, in some sections the boundary between the two is indistinct, and is totally absent in others. In the final situation the use of two velocities would therefore be inappropriate for this data set in some instances.

Taking all the above into consideration and with reference to

all available literature for the area (and required accuracy of the interpretation), it was decided to convert the seismic sections into depth sections using a single velocity of 1750 m/s for all sediments above the bedrock, this being meant to be representative of the two materials. Thus the depth to various reflectors was calculated by reading the corresponding reflection time from the seismic records and making any geometric corrections (where appropriate).

Reflection time.

The time required for the seismic wave to travel from the source to receiver via a reflection at some point is called the reflection time. At normal incidence (eg. in the case of the pinger system) the reflection time would be,

$$To = \frac{2\,H}{V}$$

where To is for the reflection time (two way travel time), H denotes the depth to the reflector, and V denotes the velocity of the seismic wave.

In the case of non-normal incidence (eg. for the boomer and sparker systems), the total reflection time (T) also depends on the distance between the source and the receiver, called the offset (X), and can be written as:

$$T = \frac{2\sqrt{(H^2 + (X/2)^2)}}{V}$$

$$\Rightarrow T^2 = To^2 + \frac{x^2}{V^2}$$

For convenience and to speed up interpretation, depth correction scales were constructed appropriate to the sweep time and the particular geometry used.

3.3.7 Borehole data.

A single borehole (No. 71/54) in the area, drilled by the British Geological Survey and located between the lines P-Q and S-T (for location see Fig: 3.7) revealed that the boundary between recent sediments and boulder clay at that location is at a depth of 11.5m below seabed. The borehole section is illustrated in Fig: 3.10. In this the boulder clay forms two layers (with a total boulder clay thickness of 12m) which are separated by an intermediate bed of sand and gravel. The borehole data also show that the bedrock is at a depth of 26m.

3.3.8 Comparison of the seismic systems.

Since three different seismic systems: pinger, boomer, and sparker were used for the current study, a brief comparison of the three regarding their resolution and penetration will be given. Prior to this, some points relating to vertical resolution and penetration will be discussed.

Vertical Resolution.

In reflection seismics vertical resolution refers to the minimum separation between two interfaces such that they can be called two separate reflectors. The resolution of the recorded sub-bottom profiles is largely frequency dependent. According to Raleigh two reflecting interfaces can be distinguished if their separation is larger than about a quarter of the dominant wavelength of the seismic signal (Trabant, 1984). However, practically it should be regarded as 1/3 to 1/2 of the wavelength at best (Dobrin, 1976).

In addition to frequency and recording technique, the

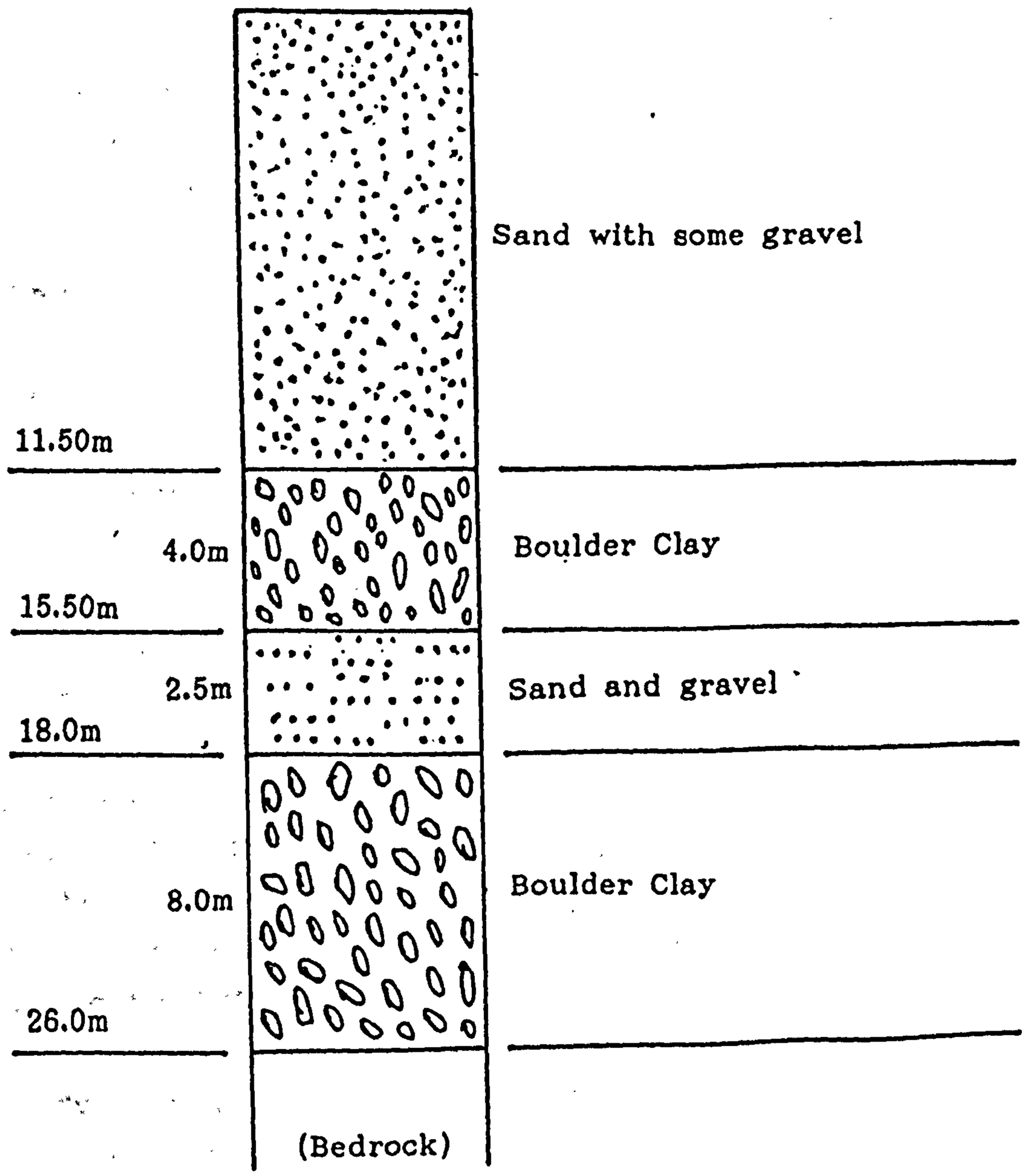

Fig: 3.10 Geological section based on borehole (71/54) data drilled by the British Geological Survey (for location see Fig: 3.7).

composition, physical properties and microfabric of sub-bottom sediments are also important factors which will affect the final recorded resolution.

Penetration.

Penetration range of any seismic system is dependent upon a number of factors including operational frequency, source energy and sediment composition. Higher frequency signals suffer greater absorption losses in the seabed and result in less penetration. Higher peak power and lower frequencies are needed for greater sub-bottom penetration (Edgerton, 1963).

Pinger system.

The penetration and resolution obtained by the pinger system, often called a 'mud probe', in addition to the operational frequency and power, is significantly influenced by the sea bottom composition (Leenhardt, 1963). Optimum penetration is obtained where the bottom material is soft (mud) and hence the pinger system gives good information on mud layering and thickness (Leenhardt, 1963, 1967).

Pinger system has frequency spectrum of 1-12kHz. For the purpose of this study a 3.5kHz (fixed frequency) pinger system was used throughout the survey. Overall a maximum penetration of 8m below seabed surface was obtained. At 3.5kHz frequency and sub-bottom sediment velocity 1750 m/s a vertical resolution of 17 to 25cm (1/2 to 1/3 of the wavelength) was expected. However, in the present study the minimum recorded thickness of the surficial layer was in fact in the range of 0.5 to 1m.

In summary, the pinger system's operational parameters, such as frequency and energy, make it suitable for sedimentological studies, especially for the mapping of the surficial sediments (Leenhardt, 1967). Another advantage of using a pinger system is its portable design, which makes it possible to carry out a CRP

exercise on small boats in shallow water areas, which would otherwise be inaccessible to such a type of survey.

A further factor which should be discussed at this stage is the effect of multiple reflections. In shallow water operations sea bottom multiples are usually a source of concern. However during the current study the penetration at most of the places appeared to be less than the water depth and as such, multiples were not a problem. In fact in some records the sub-bottom reflectors were more clearly displayed by the multiple reflection than the primary one. This is especially true for the surficial sediment layer, because in a few places it was too thin to be differentiated from the sea bottom reflection and the double time effect of multiple reflection made it easier to identify the internal layering (Fig: 3.11a).

Boomer.

The boomer system was operated at a power of 300 joules. During the current study a maximum penetration of more than 15m was obtained using this system. The boomer system's operational frequency spectrum of 400 to 1400Hz and pulse length of 0.2ms allows a high resolution seismic record to be obtained.

The boomer record shown in Fig: 3.11b clearly exhibits the better penetration obtained with the system as opposed to the equivalent pinger record (Fig: 3.11a). Between the fix Nos. 519 and 521, the record shows a channel infill sequence in which the boomer system has successfully mapped the prevailing internal pattern with a vertical resolution of 1.5m approx. between the interfaces.

In certain places, where water depth was shallow, the sea bottom multiples greatly masked the primary reflections and influenced the interpretation since nothing could be seen beyond the multiples.

Sparker.

The sparker array is a low frequency sound source utilized for deeper penetration sub-bottom profiling. The operational energy level and frequency of the system available for the current study (EG&G Model 267A) could be varied between 500 to 8000 joules and 100 to 1000Hz respectively. However, for the current study a power input of 500 joules seemed most appropriate. A comparison of a sparker record (Fig: 3.11c) with an equivalent boomer record shows the higher penetration and characteristically lower resolution with some deeper reflectors clearly being discernible on the sparker record even after the sea bottom multiple.

Conclusions.

The visual comparison of the three systems regarding their penetration and resolution is clearly demonstrated in Fig: 3.11, in which seismic records together with the interpreted sections for roughly the same survey track are illustrated.

It is evident from the above discussion of the three systems that each system is designed to be suitable for one particular purpose and the priority between the penetration and resolution has to be made according to the requirements of the survey.

In shallow water areas such as Caernarfon Bay the pinger would be expected to provide valuable information about the surficial sediments, the boomer to provide further information on the recent sediment layers and glacial and postglacial sediments, and the sparker to define the topography of the bedrock. Ultimately, by combining all seismic information from the three systems a comprehensive geological/sedimentological interpretat-ion should become feasible.

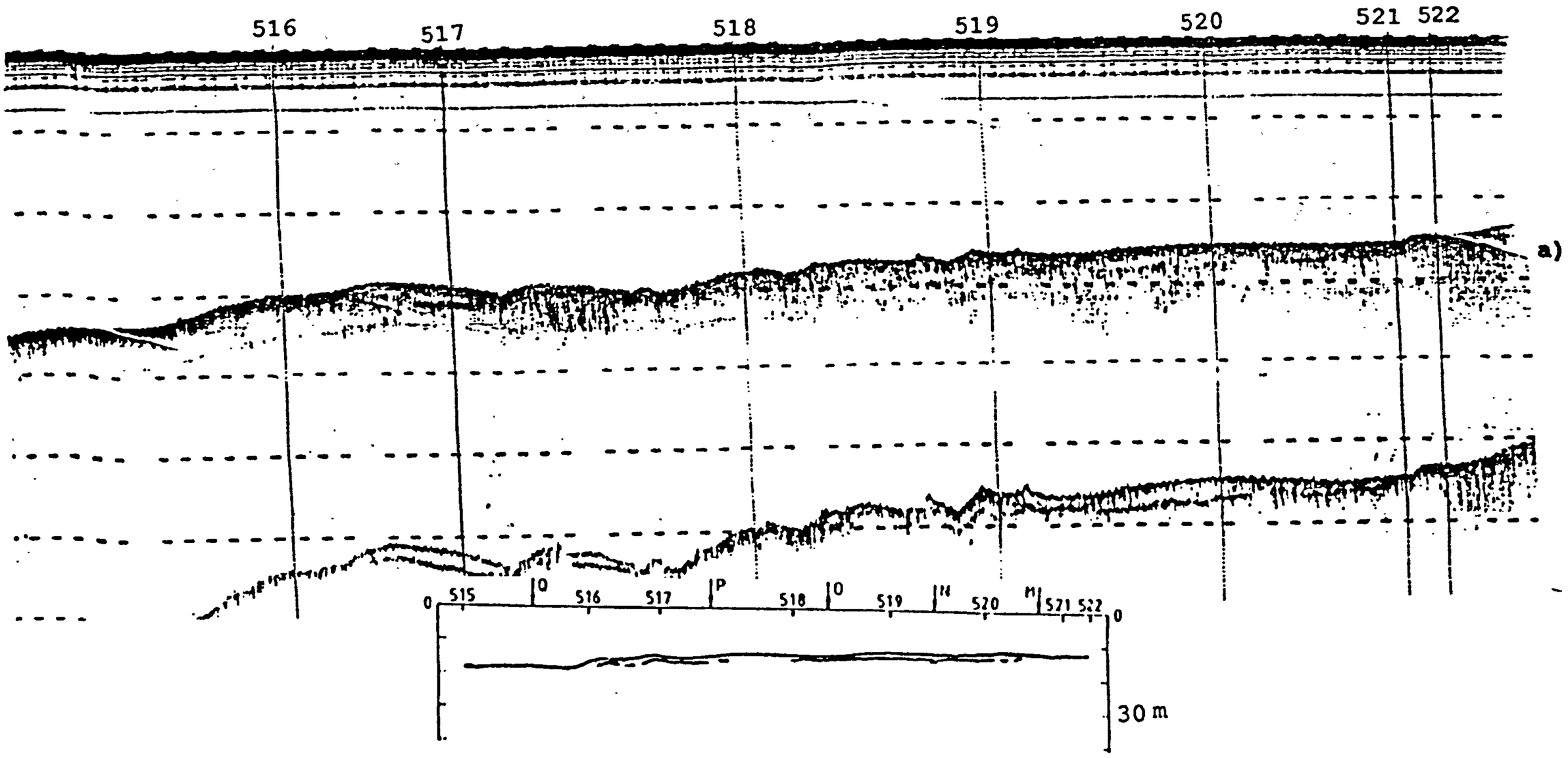

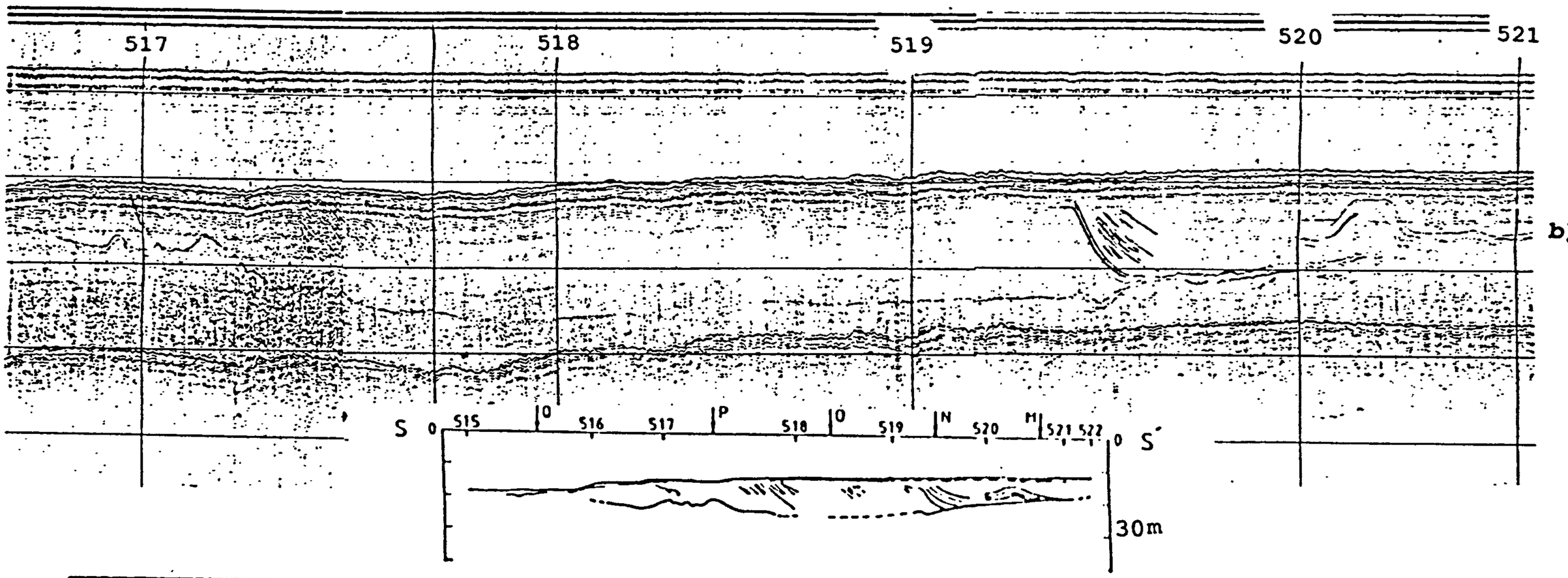

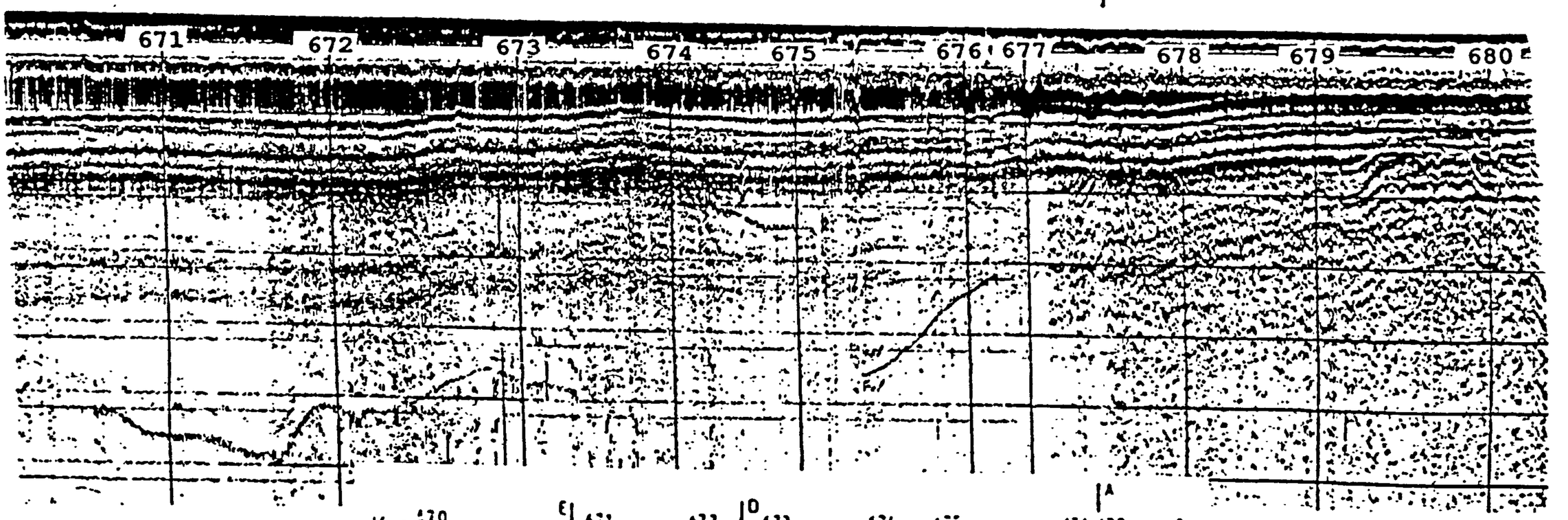

Fig: 3.11 Interpreted sections and seismic records from pinger (a), boomer (b), and Sparker (c) data.

3.3.9 Sub-bottom interpretation.

Pinger

The maximum penetration obtained with this system in the survey area was about 8m, this being achieved in a relatively restricted zone which is characterized by the thickest cover of surficial sediments. In some locations the pinger records reveal layering within the surficial sediment cover. An example of this kind can be seen in the interpreted sections presented in Fig: 3.12.

In the following section a summary interpretation of all pinger profiles will be given as an introduction to the overall geological appraisal for the site.

Fix No. 130 - 200.

These profiles were run in a NW-SE direction, about 4.5km off Fort Belan inlet in Caernarfon Bay. The interpreted sections are shown in Fig: 3.12. These sections show that the thickness of the surficial sediments is greatest in the northwestern half of the area, reaching up to 8m. Three reflecting horizons within the upper unconsolidated surficial sediment layer have been identified in part of the area (Fig: 3.12), indicating internal layering within the top sediment cover. The greater thickness of the surficial sediments at the northern end of the section, is probably a function of the effect of the main channel, which runs through that area. It suggests that considerable amounts of sediment are transported by the main channel and are deposited in that area.

Between fix No.195 & 196 there is a 3m deep, 300m wide depression cut into the layer of surficial sediments which probably represents a distributry channel. A similar feature can be seen 300m south of the above, buried at a depth of 2m below seabed (which deepens to 8m), and perhaps suggests that the latter is a remnant channel. The northward displacement of the

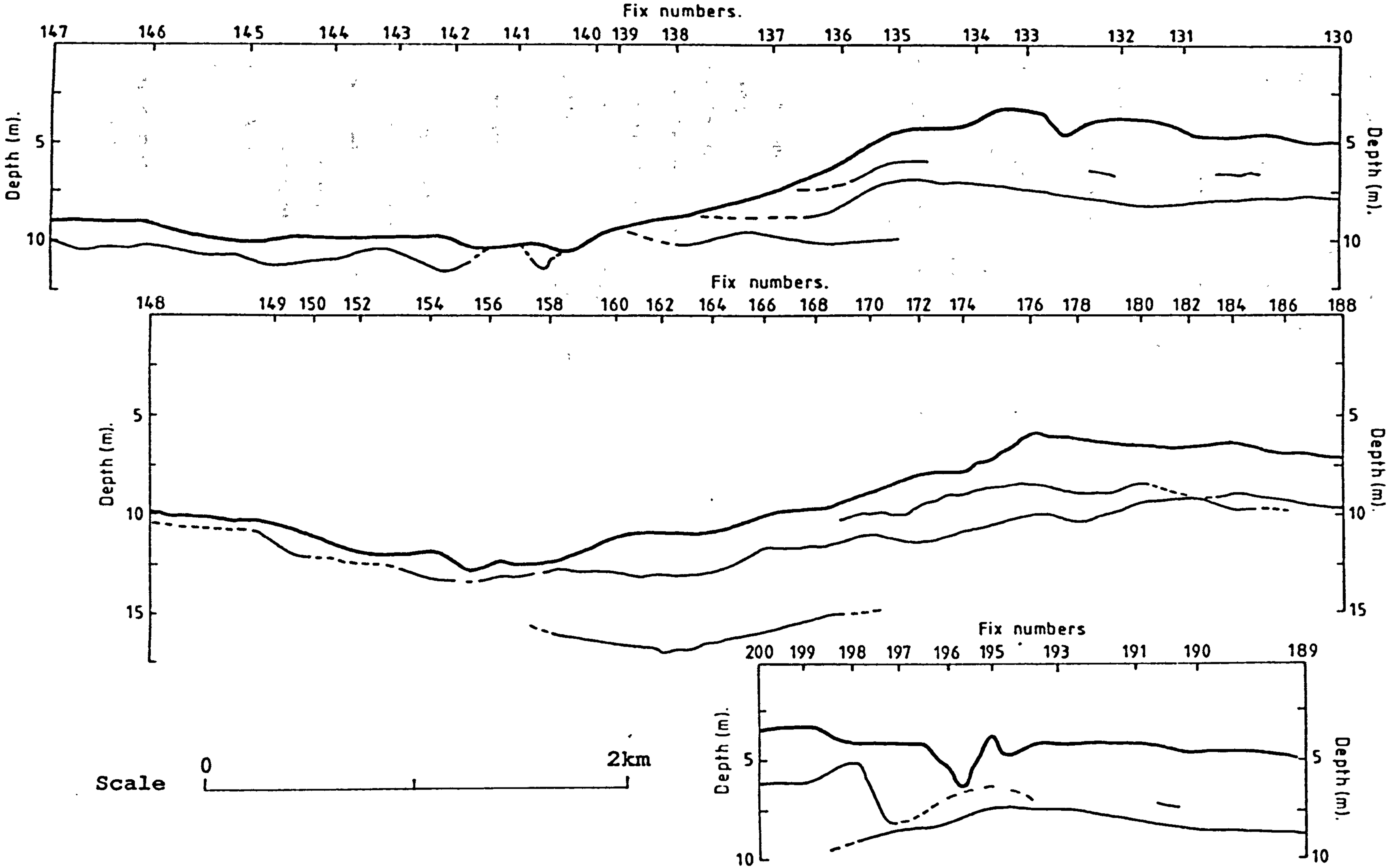

Fig: 3.12 Interpreted sections of pinger sub-bottom profiles (fix No. 130-200) (for location see Fig: 3.5).

present channel, relative to the buried feature, may be evidence that the channel system has been shifting northwards with time and might therefore be responsible for the thickening of the surficial sediment cover in the same direction.

Fix No. 400 - 531.

The records for this part of the survey area were very disappointing since very little penetration was achieved. The maximum penetration obtained was about 3.5m.

Except in two places, (i.e. between fix No. 481 - 484 and at fix No. 419) a single reflector, with depth ranging between 0.5 to 3.5m can be identified. This is again very discontinuous and patchy in nature but is clearly visible in the section displayed in Fig: 3.13.

The interpreted pinger records (described previously) suggested that most of the penetration obtained with this system is restricted to the inshore areas of surficial unconsolidated sediment accumulation with very little penetration being obtained further offshore. This effect probably is due to thinning of the recent unconsolidated sediments as one moves further offshore, and probably indicates that the surficial sediment activity is mostly confined to the nearshore area.

Boomer

The maximum penetration obtained with the boomer system was slightly greater than 15m. A single major reflecting horizon can be identified in most of the sections (see Fig: 3.14). The first layer displays additional irregular minor reflectors, channel fill sequences and numerous small internal structures. The thickness of this layer also correlates very well with that predicted from sparker sections.

In general the thickness of the layer, identified on the boomer records is very variable in the area surveyed. The maximum

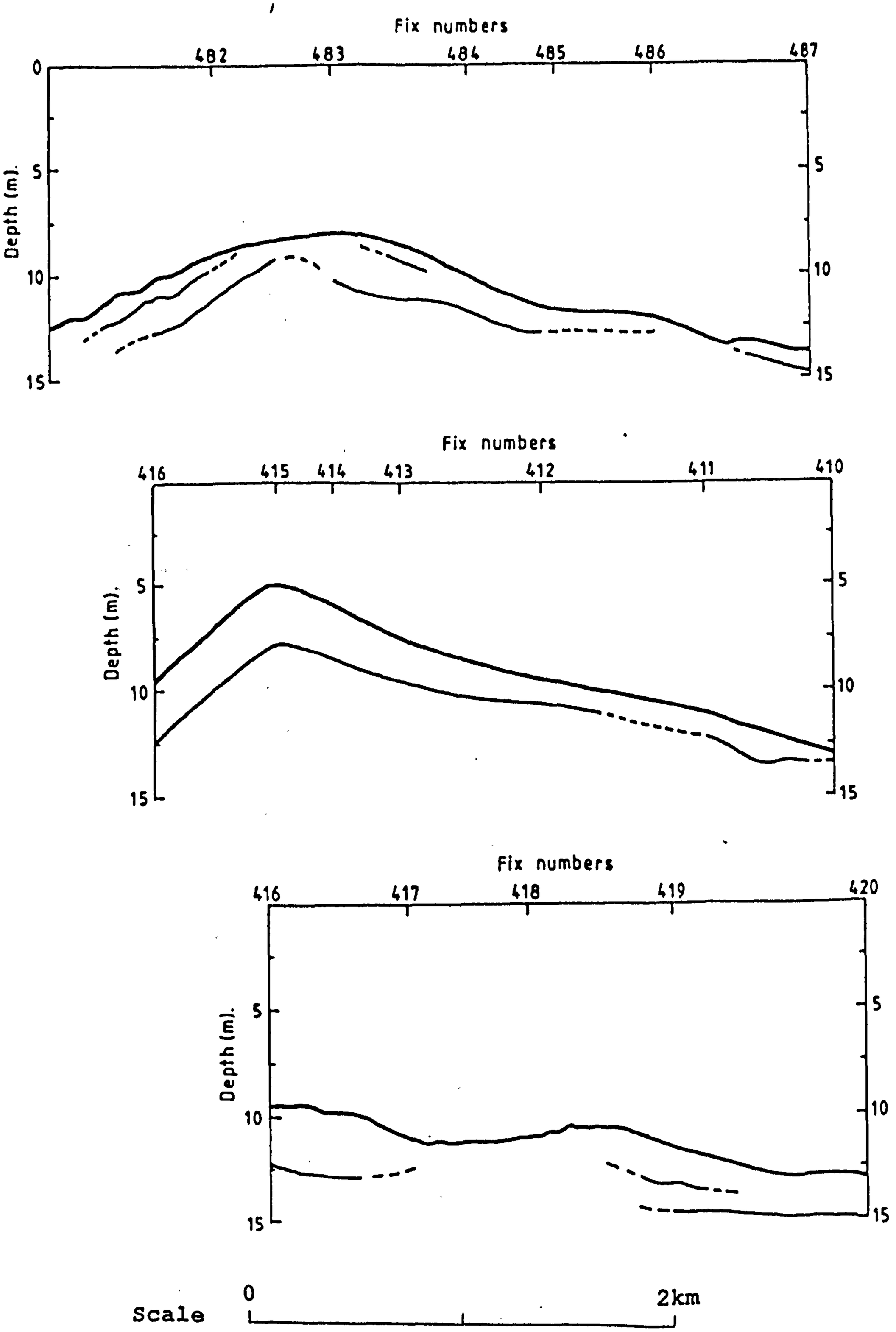

Fig: 3.13 Sample interpreted sections from pinger sub-bottom profiling (for location see Fig: 3.5).

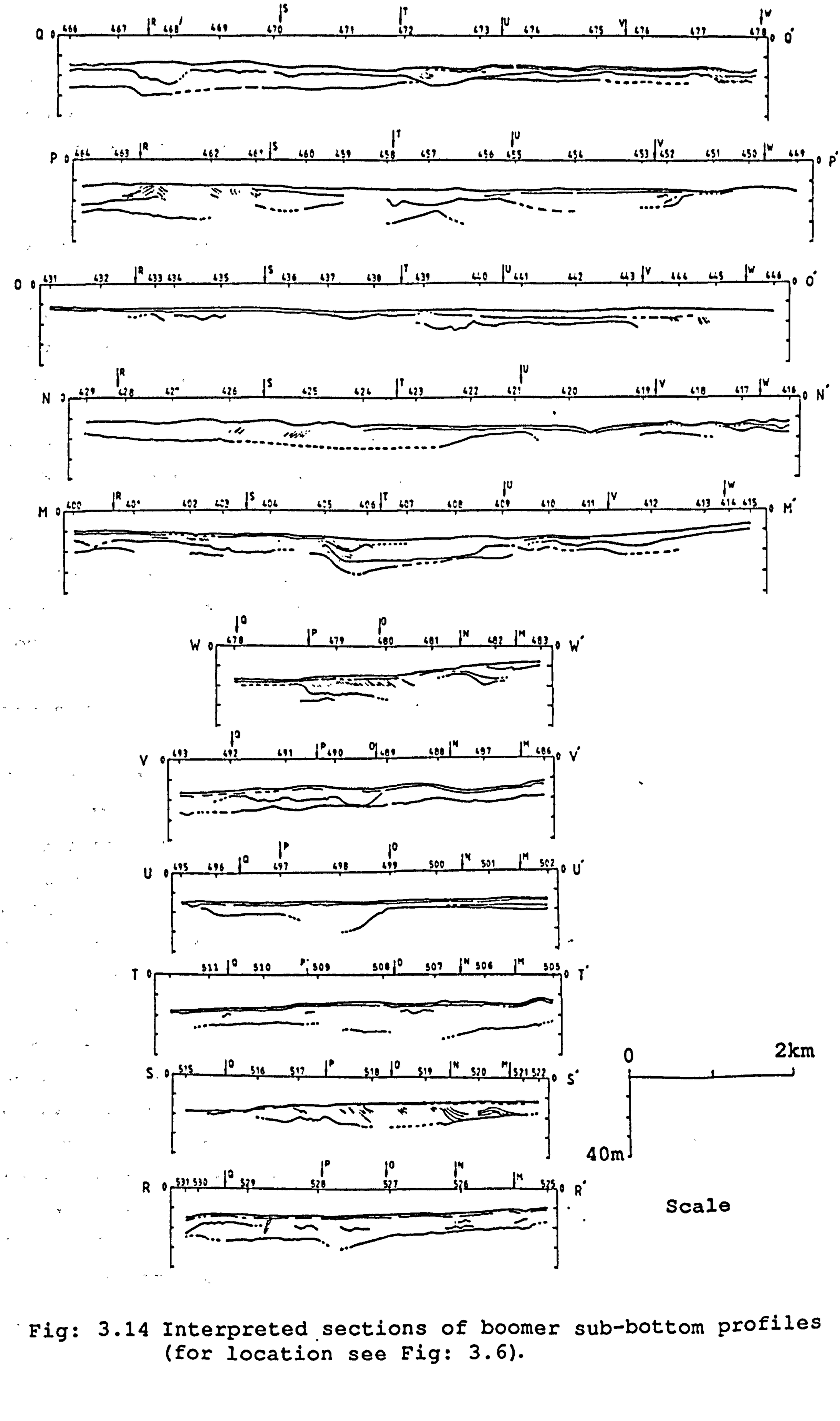

Fig: 3.14 Interpreted sections of boomer sub-bottom profiles (for location see Fig: 3.6).

thickness of more than 15m occurs in the middle section of the intersecting lines R, T, U, where there was probably a channel or depression present before the deposition of over lying sediment layer.

The boomer sections also show a thin, top layer of recent surficial sediment, which ranges in thickness between 0.5 to 3.5m. It correlates well with the top layer recognized on the pinger records (for fix No.s 400-531). Though this top layer has a regular appearance on a few profiles (T and U), it is very discontinuous over most of the area, which probably reflects the patchy nature of the layer or possibly instrumental limitation. Within the surficial sediment layer, channel fill sequences have been identified on a number of sections such as SS′, WW′ and MM′. At this stage it is difficult to establish any firm conclusion regarding the nature of the depositional environments under which the above mentioned channel fill sequences were deposited.

Sparker.

The maximum penetration depth achieved with the sparker in the area surveyed was 98m below O.D. Fig: 3.15 is a diagrammatic representation of the interpreted sparker records. Except in section GG′ where three reflectors can be distinguished, two major reflecting horizons are identified in most of the sections. In section GG′ a channel fill structure has been identified within layer 1. The thickness and the presence of channel fill structures within layer 1 suggest that it can be correlated with layer 1 identified by boomer method. This layer appears to be continuous throughout the area, except in a few places where the deeper reflector rises to interrupt it. The intermediate reflector identified in section GG′ only, probably represents an intermediate layer and its apparent absence in other seismic sections suggests either that this layer may be laterally discontinuous or might possibly be present in other parts of the area, but beyond the resolution range of the

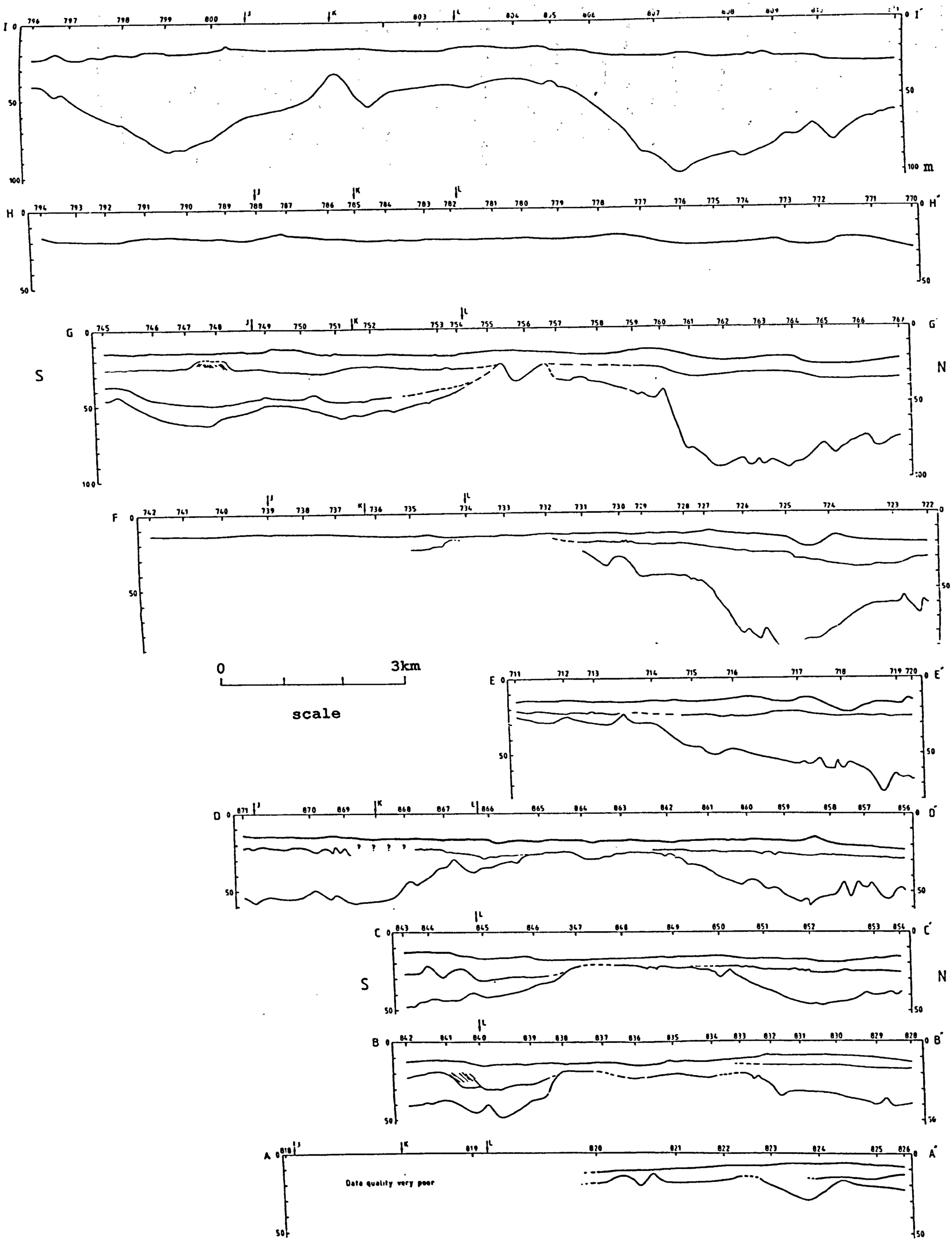

Fig: 3.15 Interpreted sections of sparker sub-bottom profiles (for location see Fig: 3.7).

system. To avoid confusion, the layers between the first sub-bottom reflector and deepest reflector will be treated as a single unit (as shown in the seismic sections Fig: 3.15).

The second major reflecting horizon identified throughout the survey area is most probably the acoustic basement which varies in depth between -14 to -98m below O.D. This interpretation is based upon the borehole data which confirmed the presence of Mesozoic rock at a depth of -26m below sea bed (for location of the borehole rèfer to Fig: 3.7).

The basement boundary is very uneven in nature and exhibits two valley structures separated by a ridge. These features can be traced on all the N-S trending sections and hence they probably represent a double branching valley (the term used by Blundell et al (1969) for a similar type of feature in Cardigan Bay). To illustrate these features, profiles BB′ and LL′ together with the raw seismic records have been included as Fig: 3.16.

3.4 Seismic stratigraphy.

3.4.1 Introduction.

Having interpreted the various seismic records for major reflection/structural boundaries it became evident that further information might be available within the seismic data which could be of stratigraphic significance and hence aid the overall interpretation of the geological history of the area eg. to infer past sedimentary depositional environments responsible for the deposition of the Quaternary sequences in Caernarfon Bay. Before presenting findings of such an interpretation it is at this point necessary to introduce the various concepts involved in seismic stratigraphy.

Seismic stratigraphy offers a practical geological-stratigraphical interpretation tool for seismic data (Vail et al, 1977). The study of the unique patterns of seismic

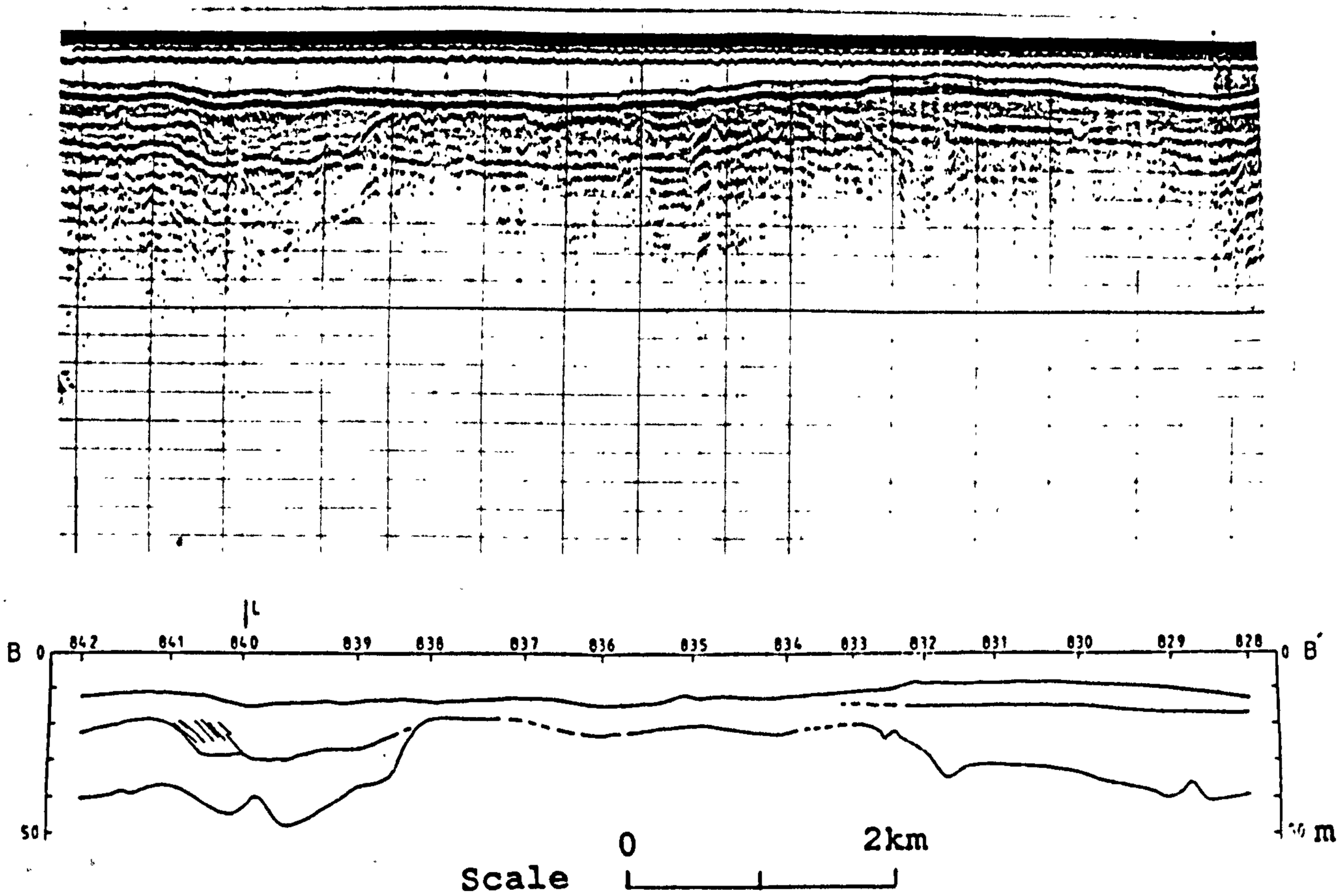

Fig: 3.16 Interpreted sparker sections BB′ (top) and LL′ (bottom) together with raw seismic records.
(for location see fig: 3.7)

reflections allows the direct application of geologic concepts based on physical stratigraphy, leading to a possible interpretation of depositional environments, geologic time correlations, post depositional structural deformation, etc (Vail et al, 1977). Working out the geologic history is one of the key objectives of seismic stratigraphy (Sheriff, 1980).

Chin et al (1988) applied a seismic stratigraphic approach to study the late Quaternary history of southern central Monterey Bay, California. An angular unconformity and various seismic reflection patterns such as progradational, etc. were identified and on the basis of those, a stratigraphic analysis was carried out. Salge and Wong (1988) carried out similar studies in the Skagerrak (northern North Sea). Their seismic stratigraphic studies revealed that erosional truncation at the top of the Mesozoic depositional sequence could be used to define the extent of the Norwegian channel.

The basic approach used in seismic stratigraphic analysis involves three steps: (i) seismic sequence analysis, (ii) seismic facies analysis, from which inferences on (iii) sea level change (Vail et al, 1977) can be made. Various concepts related to the present study are briefly described below.

3.4.2 Seismic sequence analysis.

A seismic sequence is a time-stratigraphical unit, composed of a set of genetically related (by depositional processes and environment) facies, which are bounded at top and base by unconformities. It is equivalent to a depositional sequence (Mitchum et al, 1977), as used in descriptions of sedimentary deposits, the only difference being that a seismic sequence is identified using seismic evidence.

A depositional sequence is defined by the physical relations of the strata at the upper and lower unconformities and their correlative conformities (Fig: 3.17). If the strata above and

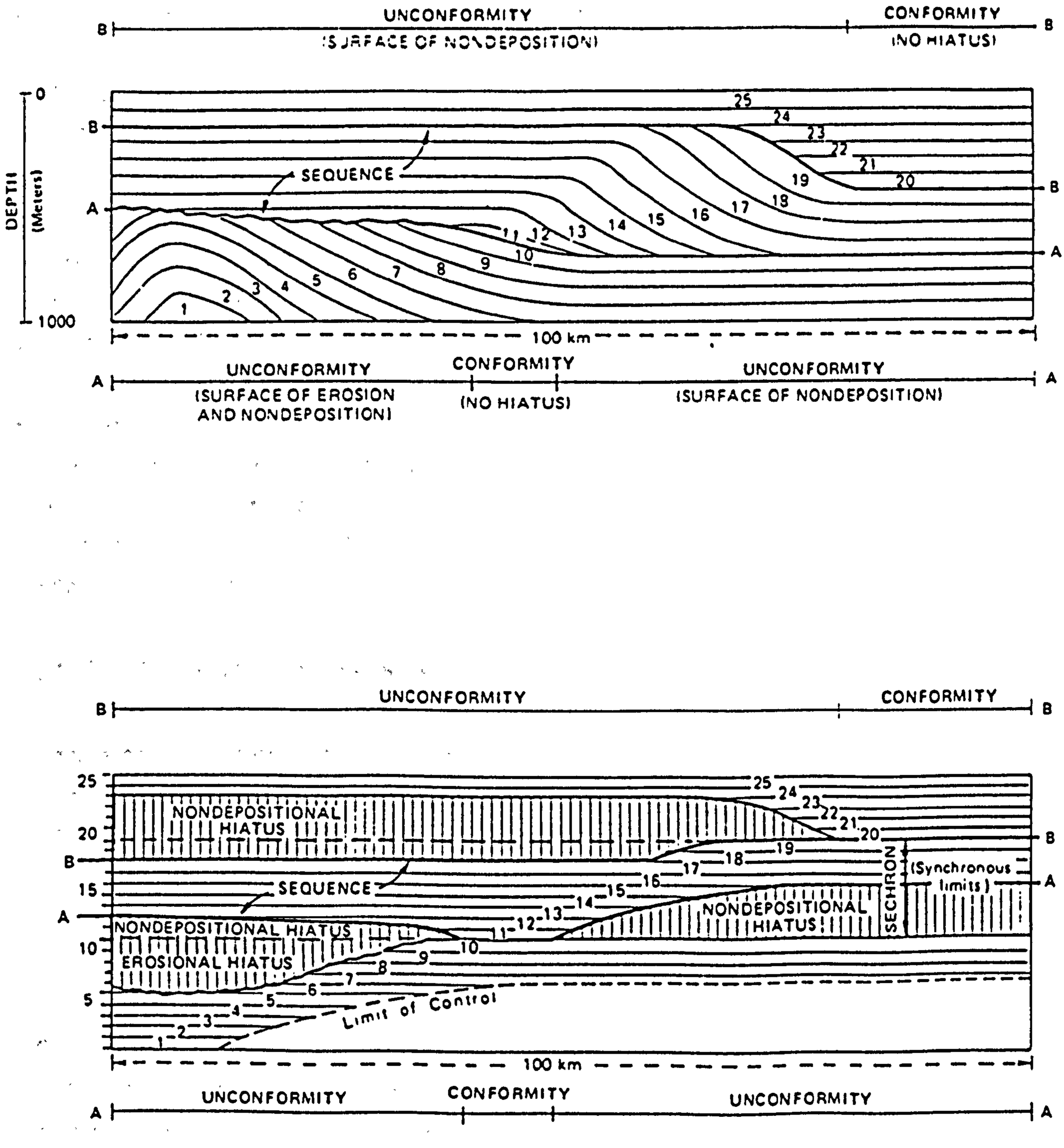

Fig: 3.17 Depositional sequences and types of boundaries (after Mitchum et al, 1977).

below a surface are concordant (i.e. essentially parallel to it), then there is no physical evidence for unconformity. If the strata are discordant (i.e. they terminate against the surface), then there is physical evidence for unconformity (Mitchum et al, 1977). Both concordance and discordance may be seen at the upper or lower boundary of a depositional sequence. Two types of discordance can be distinguished: lapout and truncation. Lapout is the lateral termination of a stratum at its original depositional limit. Truncation is the lateral termination of a stratum as a result of being cut off from its original depositional limit. Lapout may occur at both the upper (toplap) and lower (baselap) boundary, while truncation only occurs at the upper boundary. Baselap can further be classified in two types: onlap and downlap. Various other types of configuration such as toplap and erosional truncation (Fig: 3.18) can be identified. For further details on the above reference should be made to Mitchum et al (1977).

3.4.2 Seismic facies analysis.

A seismic facies is defined on the basis of seismic reflections within a given sequence, characterized by parameters like reflection configuration and continuity (Mitchum et al, 1977).

Major groups of geometrical configuration include parallel, sub parallel, divergent, prograding and chaotic patterns (Fig: 3.19). Parallel and sub parallel patterns suggest uniform rates of deposition on a uniformly subsiding shelf or stable basin setting; Divergent patterns indicate lateral variation in depositional rate or progressive tilting of the depositional surface.

Prograding patterns generally form through the progressive lateral development of gently sloping depositional surfaces called clinoforms. Differences in clinoform patterns are largely due to variations in rate of deposition and water depth (accommodation). Various types of progradational facies such as,

UPPER BOUNDARY

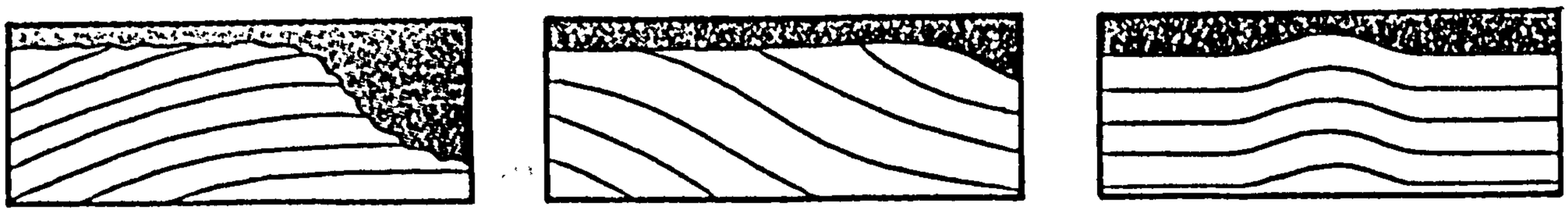

1.EROSIONAL TRUNCATION

2.TOPLAP

3.CONCORDANCE

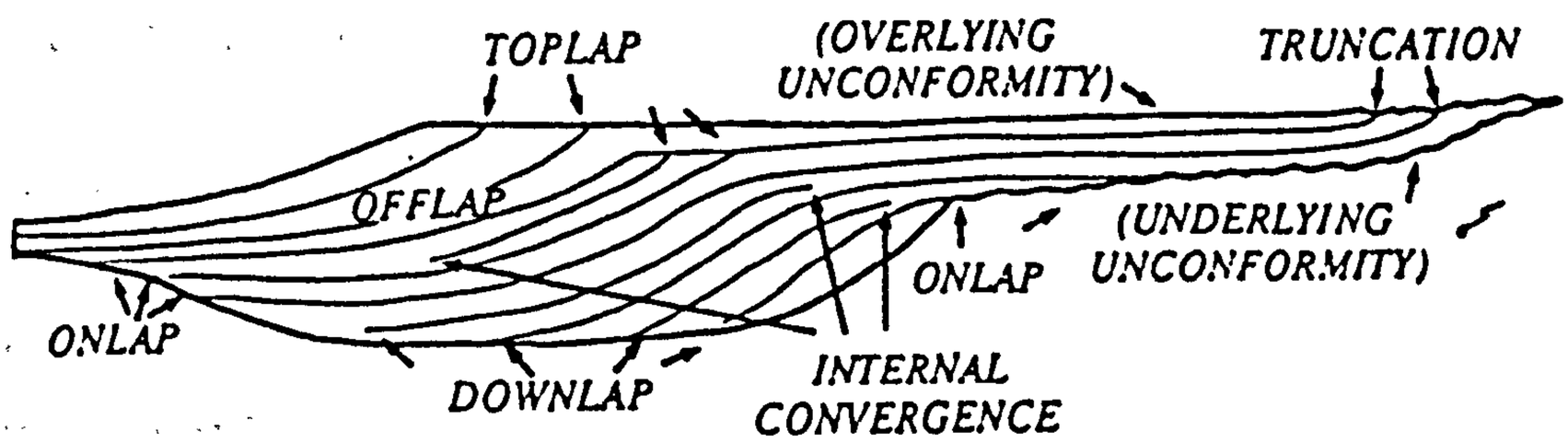

LOWER BOUNDARY

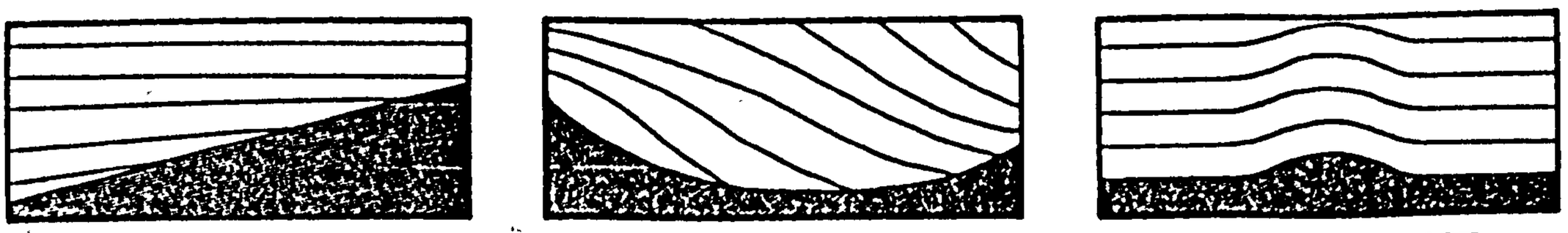

1.ONLAP

2.DOWNLAP

3.CONCORDANCE

BASELAP

Fig:3.18 Relations of strata to boundaries of depositional sequences (after Mitchum et al 1977).

sigmoid, oblique (tangential and parallel), complex sigmoid oblique, shingled, hummocky (Fig: 3.19) can be identified seismically (Mitchum et al, 1977).

Chaotic patterns indicate deposition in a variable, relatively high energy setting, or post depositional deformation of initially continuous strata.

Reflection free areas suggest homogeneous, non stratified or steep dipping geologic units (Mitchum et al, 1977)

Sedimentological implications.

To summarize so far, clearly if such features can be identified on a seismic record then useful information on the depositional environment can be obtained. The application of seismic stratigraphy to sedimentary basin analysis has resulted in a new way to subdivide, correlate and map sedimentary rocks (Vail, 1987). Vail further reports that the identification of stratal patterns within a depositional sequence on seismic sections offers an accurate prediction method of depositional environments.

3.5 A Seismic Stratigraphic interpretation for Caernarfon Bay.

The seismic stratigraphic interpretation for the study area will be based on results from seismic profiling and information from a solitary borehole (see Fig: 3.10). Three distinct seismic sequences (i.e. seismic sequence I, II, and III) within the present study area can be identified (Fig: 3.20). The oldest seismic sequence (III) identified in the study area lies unconformably on the acoustic basement.

3.5.1 Acoustic basement - basal sequence boundary.

The acoustic basement is characterized by a strong reflection

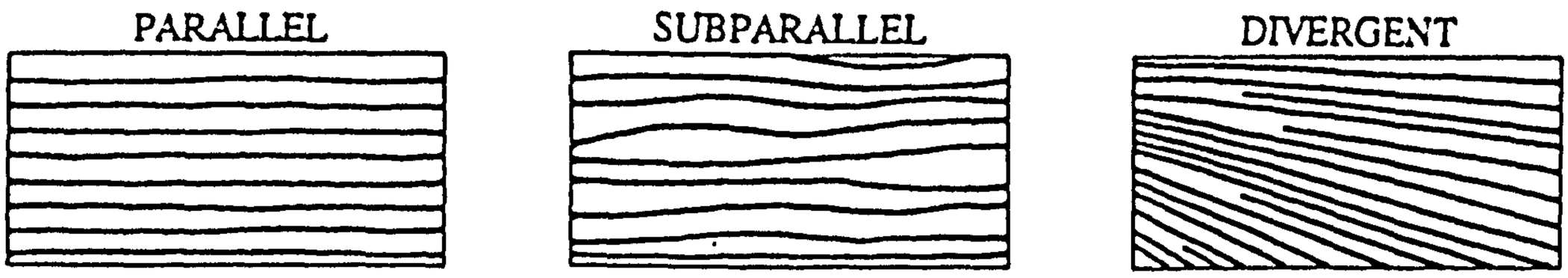

Fig: 3.19 Different types of reflection configurations (after Mitchum et al 1977).

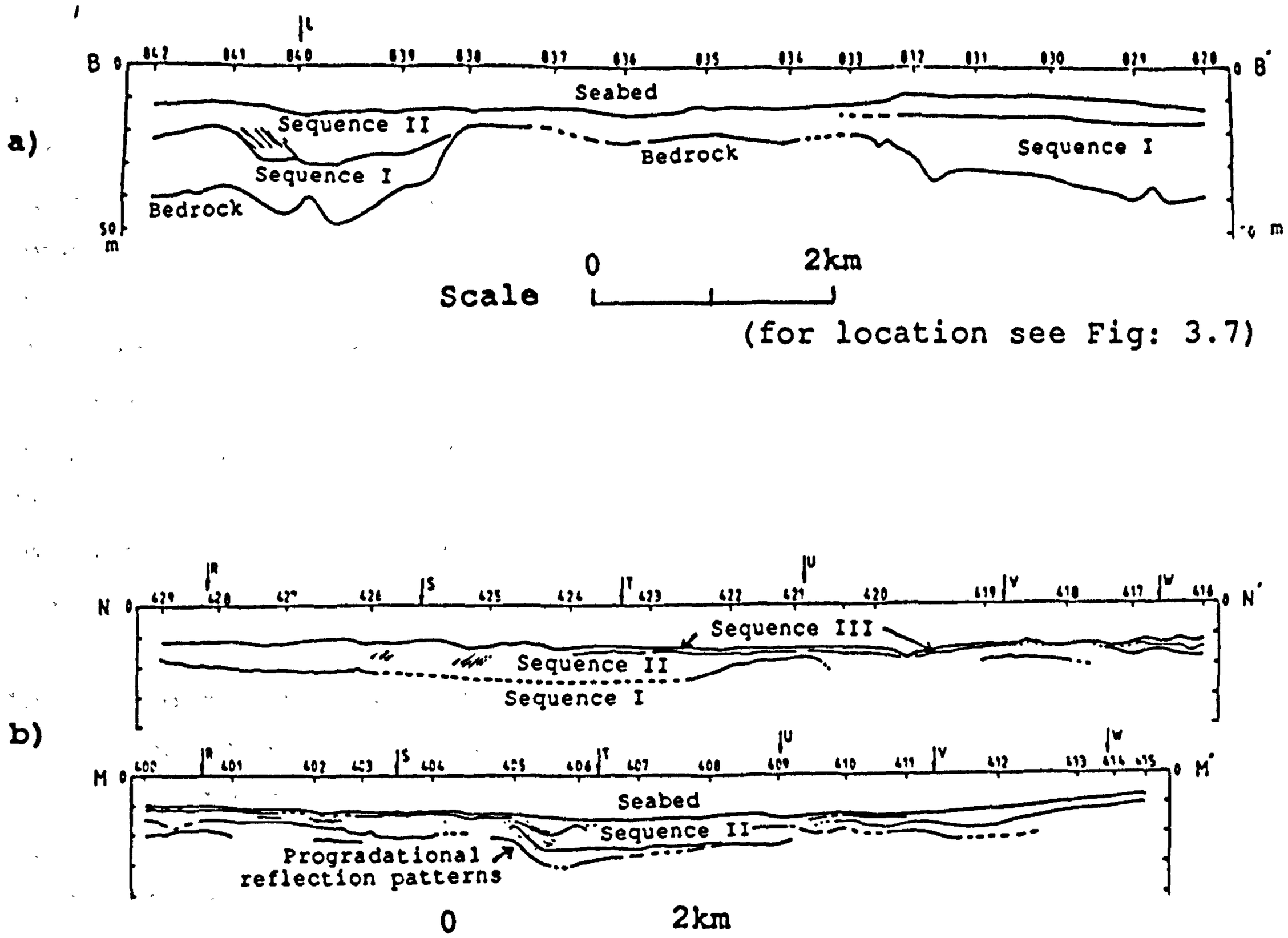

Fig: 3.20 Interpreted seismic sections from **a)** sparker, **b)** boomer, and **c)** pinger sub-bottom profiling.

and is continuous throughout the survey area (Fig: 3.15). On the basis of borehole data and seismic characteristics, it can be said with confidence that the prominent discordance between the lowest reflector and the overlying sequence marks the boundary (unconformity) between bedrock (consisting of seaward extension of onshore Mesozoic sequences) and Quaternary deposits. The bedrock is irregular in relief and the uneven surface is probably the result of differential erosion. From the seismic data, a contour map of the bedrock depth relative to O.D. (ordnance datum, Newlyn) was produced (Fig: 3.21) which suggests that the bedrock occurs at a depth of between -14 and -98m O.D.

As mentioned earlier, the seismic sections show an overdeepening of the bedrock at both ends of the N-S trending profiles, with a central separating ridge i.e. a double branching valley system. It appears that before the last glaciation the area was exposed to subaerial erosion. At the onset of glaciation the area was then further subjected to subglacial erosion, which was, perhaps, mainly responsible for the overdeepening of the bedrock.

On the basis of the general trend of the two valley structures (Fig: 3.21), their origin can also possibly be linked to the two faults, Dinorwic and Berw, which run through the same area. There is a strong possibility that these two faults may have played a major role in determining the course for erosional agencies, which resulted in the overdeepening of the bedrock.

The high bedrock relief to the southwest of Llanddwyn Island, which appears as a ridge structure on the sparker seismic sections, probably represents the resistant Monian Precambrian rocks.

The maximum depth of -98m O.D for the bedrock surface closely ties with the global eustatic sea level curve of Jelgersma (1966), which shows a sea level of -75m at ~ 13000 years B.P. Since maximum lowering of Pleistocene sea level was ~ 100-120m

Fig: 3.21 Depth to the bedrock in Caernarfon Bay
(Below O.D.).

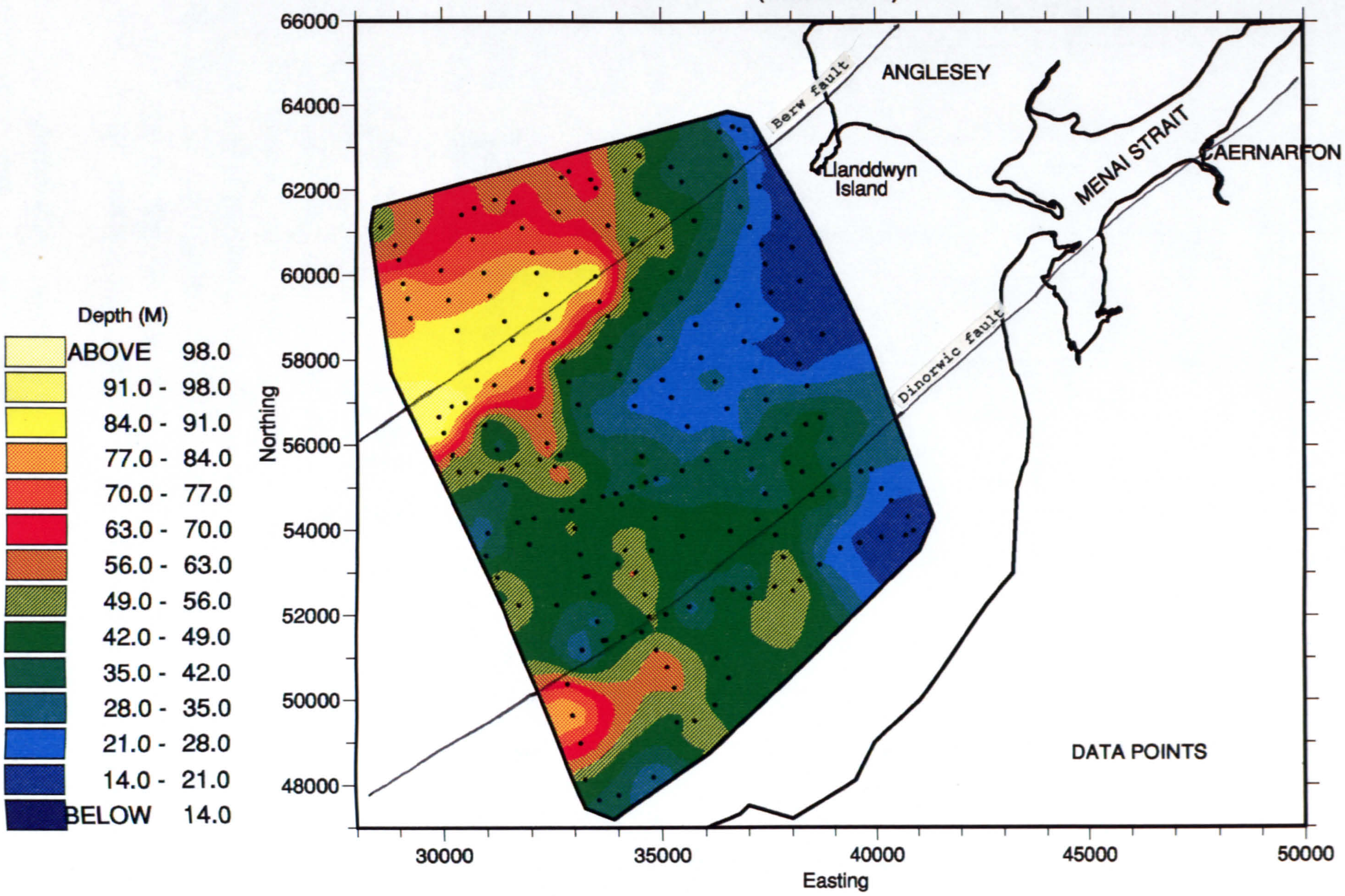

below present sea level, the bedrock depth of -75m in the Mawddach estuary (Larcombe, 1991), -91m in the Dyfi estuary (Blundell et al, 1969), and -98m O.D in Caernarfon Bay shows consistency with the global sea level curve.

3.5.2 Seismic sequence I.

Seismic sequence I (Fig: 3.20) is bounded by bedrock at the base, and by seismic sequence II at its upper surface. The boundaries above and below seismic sequence I are such that it may be differentiated as a separate stratigraphic unit. For example, the onlap of sequence I on the bedrock (in the middle of the N-S trending sparker sections) suggests that sequence I had been cut off from its original depositional limit by erosional action. This suggests an unconformity between sequence I and II. Sequence I (except sparker section GG′) is predominantly reflection free throughout the survey area.

On the basis of the general geological setting of the Quaternary sediments in the surrounding areas (Synge (1964), Helm (1971), borehole data, and geophysical surveys in Cardigan and Tremadoc Bays (Al-Sheikh (1969), Blundell et al (1971)) it can be suggested that seismic sequence I identified in the sparker seismic sections (Fig: 3.15) represents the glacial sequence in Caernarfon Bay.

The borehole (71/54) data suggest that glacial sequence should be composed of three different subunits: upper boulder clay, sand and gravel, and lower boulder clay, all deposited during the Devensian ice age. Clearly these divisions do not have seismic significance as they do not show up on the sparker records. It is useful however, to use the seismic data to draw up an isopach map of the thickness of the glacial sequence (Fig: 3.22) as an aid to the interpretation of the geological history.

It is generally believed that deposition of the glacial sediments was largely controlled by the prevailing bedrock

Fig: 3.22 Isopach map of the thickness of the glacial sediments in Caernarfon Bay.

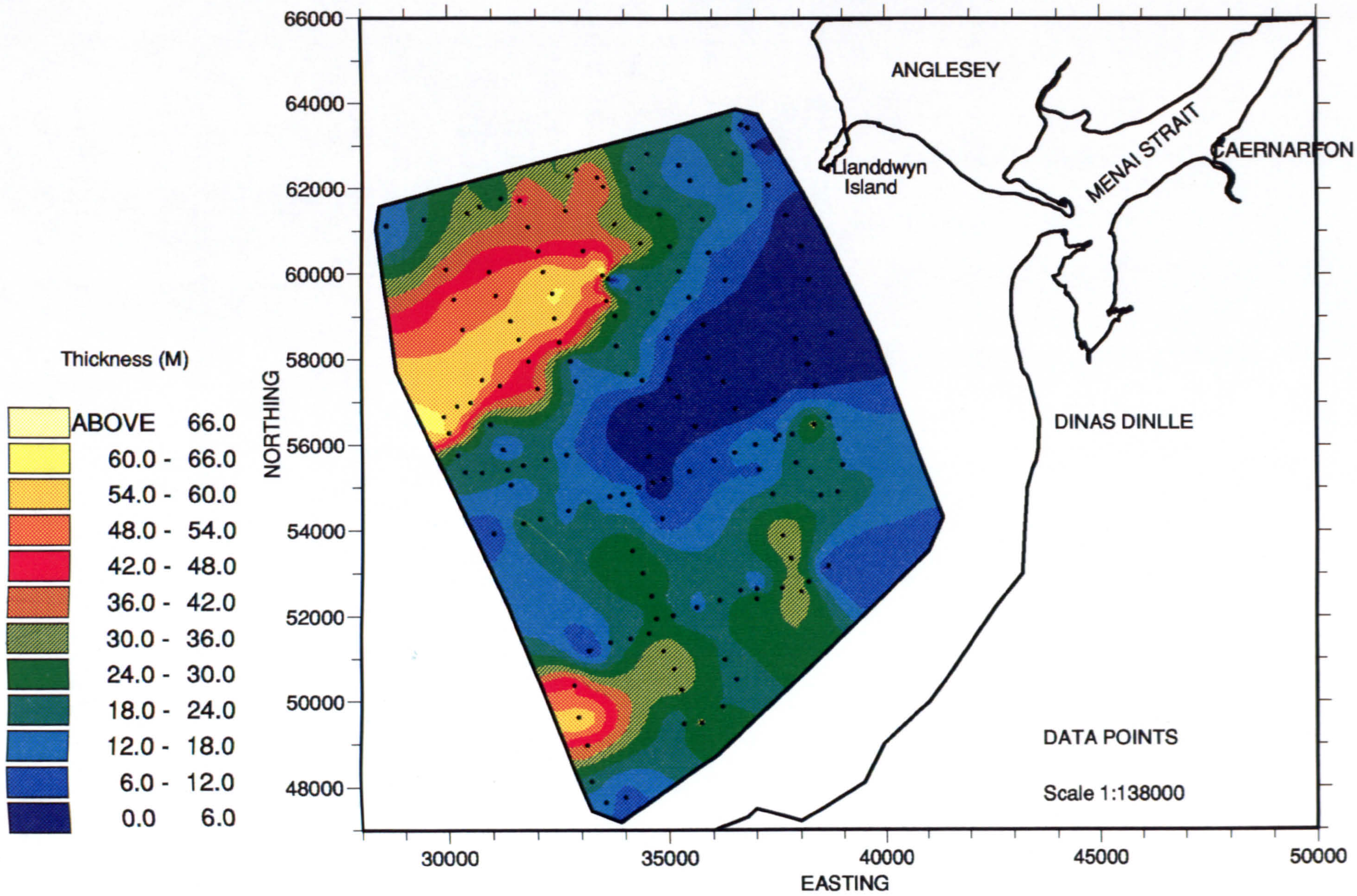

configuration. Thick accumulations of glacial sediments have occurred in the over deepened valley structures, as discussed previously. The thickness of the glacial sequence above the bedrock ridge (i.e. in the middle portion of some of the N-S trending sparker sections) reaches to zero. To explain the absence of glacial sediments above the middle portions of the seismic sections, two explanations can be sought. One is that perhaps the glacial sediments were not deposited in that area. Secondly and most probably the sediments in that area were relatively thinner and were later eroded.

3.5.3 Seismic sequence II.

The presence of internal reflection patterns within seismic sequence II (Fig: 3.14 and 3.20) clearly distinguishes it from seismic sequence I and strongly suggests that seismic sequence II was deposited in a different sedimentary environment. It ranges in thickness between 3m and more than 15m (Fig: 3.23). Though the sparker section BB′ (Fig: 3.15) gives some indication of internal reflection patterns within seismic sequence II, the detailed stratigraphy of this sequence was more closely resolved using high resolution boomer system (Fig: 3.14). Different types of progradational reflection patterns can clearly be seen in boomer seismic sections SS′, WW′, and MM′ (Fig: 3.14). Most of the progradational reflection patterns terminate as toplap at the upper sequence and downlap at the lower boundary indicating lateral outbuilding of the channel infill. An example of this kind is shown in the raw boomer seismic record (Fig: 3.24) which exhibits oblique progradational facies filling a remnant channel. Similar types of progradational facies, identified by Salge and Wong (1988) from the Skagerrak area (northeastern North Sea), are thought to indicate high energy fluvio-glacial and/or fluvial conditions.

On the basis of the above criteria and the borehole information it may be suggested that seismic sequence II represents sediments which were deposited during postglacial times. The

Fig: 3.23 Isopach map of the thickness of the postglacial sediments in Caernarfon Bay.

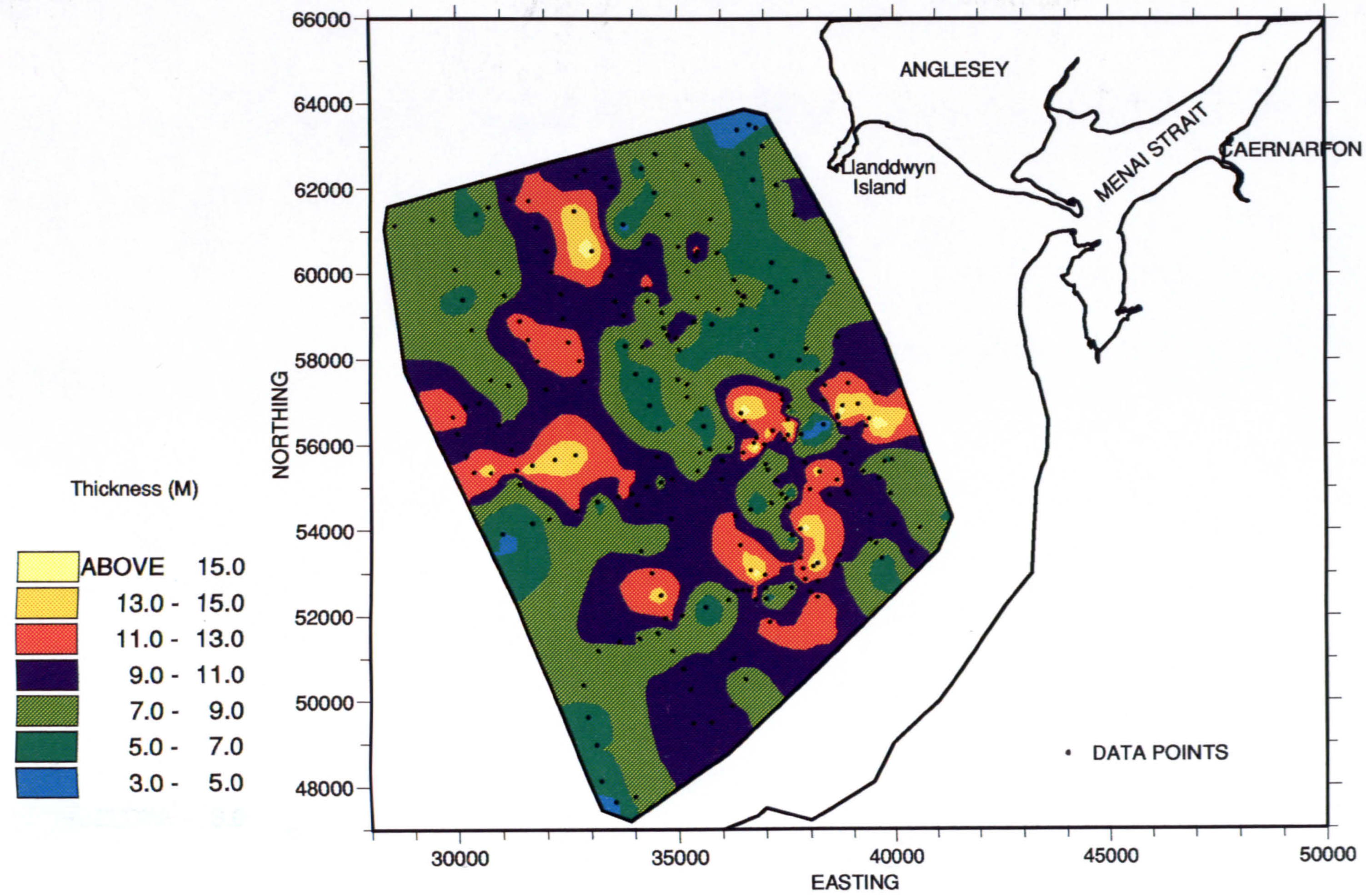

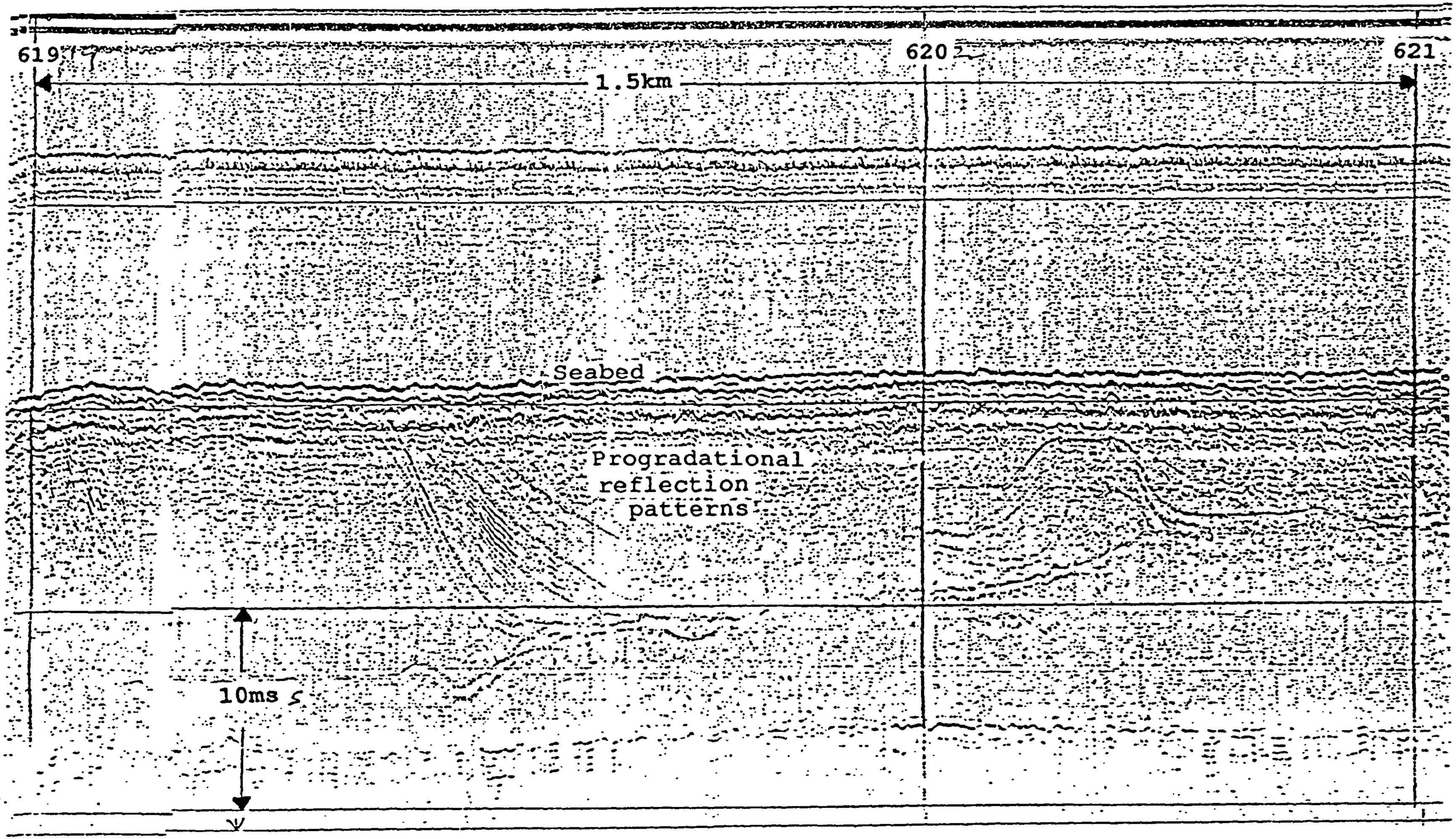

Fig: 3.24 Boomer seismic record showing progradational reflection patterns (for location see Fig: 3.6).

greatest thickness of postglacial sediments occurs in relatively deeper areas (shown by reddish and yellowish colour in Fig: 3.23), which probably originated under the action of fluvio-glacial erosion. According to Jelgersma (1979), at the onset of the Holocene about half of the ice disappeared and eustatic sea level was at 60 to 70m below present level. As such, Caernarfon Bay and the Menai Strait area must have been above sea level. The area under study was therefore subjected to subaerial erosion and may have constituted a favourable outlet for the glacial rivers discussed by Greenly (1919), and Embleton (1964).

The isopach map of the thickness of the postglacial sediments reveals that the overdeepened areas lying on top of the glacial sequence (discussed above) show a pattern which probably indicates a palaeochannel system which was subsequently infilled (in postglacial times). It may be speculated that the northward and eastward extremes of the channel system were perhaps linked to the fluvial discharge from the Menai Strait and Malltraeth depressions.

Most eustatic sea level curves (Fairbridge (1961), Jelgersma (1979)) indicate a rapid rise in sea level during the early stages of the Holocene. This continuous and rapid sea level rise probably eventually flooded Caernarfon bay, resulting in infill. A number of channel fill patterns identified within the postglacial sequence, which are characterized by different types of progradational reflection patterns, strongly support the above interpretation.

On the basis of the above mentioned internal reflection patterns some general conclusions regarding the postglacial sedimentary depositional environment can be drawn. During the Holocene period, when the sea reached a sufficient level to flood Caernarfon Bay, and a particular sedimentary regime was established, sediment accumulation started. The prevailing reflection patterns within the postglacial sequence reflect a

high energy depositional environment and rapid sea level rise. This process continued up to 6000 years B.P., when the eustatic sea level rise came to a halt (Jelgersma, 1979).

3.5.4 Seismic sequence III.

Seismic sequence III represents the youngest sediment layer i.e. the top unconsolidated sediments which ranges in thickness from 0.5 to 8m within the present study area. Sequence III rarely exhibits internal layering (Fig: 3.13 and 3.20) and where it does it is characterized by the subparallel to parallel internal reflectors which indicate a uniform rate of deposition. Henceforth the superficial unconsolidated sediments will be referred to as the recent sediments.

The recent sediments in deeper parts of Caernarfon Bay are characteristically of 0.5 to 3.5m thick. In contrast, in the vicinity of Belan inlet (i.e. in and outside the inlet), the thick deposits of recent sediments (up to 8m) occur in the form of sub-tidal and inter-tidal sand banks. The difference in the thickness of recent sediments between the deeper and shallow (nearshore) parts of Caernarfon Bay indicates a differential rate of deposition i.e. the sediments in the nearshore areas are being deposited relatively quickly.

Much of the thick recent sand deposits within Caernarfon Bay itself are restricted within a closed body of water, extending from the outer most limit of the Llanddwyn Island peninsula to Dinas Dinlle beach. Here it must be pointed out that the thickness of the recent sediments in that area may well be more than 8m but it was perhaps beyond the penetration of the pinger system in this particular case.

A detailed study of the recent sediment deposits and associated bedform patterns will be included in the next chapter, where a full account of the side-scan sonar and bathymetric survey data will be given.

3.6 Conclusions.

In conclusion the following points can be made:

1) The sparker seismic profiling method successfully mapped the boundary between the Quaternary deposits and Mesozoic bedrock.
2) A double branching valley system, formed as a result of overdeepening of the bedrock, shows strong links with the NE and SW trending Dinorwic and Berw faults which lie roughly underneath the Menai Strait and Malltraeth depression respectively.
3) It appears that the overdeepening of the Menai Strait and some parts of Caernarfon Bay occurred as a result of the subglacial and postglacial erosion.
4) The thickness of the glacial deposits in Caernarfon Bay ranges between 0 and 68m. The deposition of glacial sediments was largely controlled by the prevailing bedrock topography where the maximum thickness of glacial sediments occurred in the above mentioned overdeepened parts of the double branching valley system.
5) The thickness of the glacial sediments decreases towards the coast.
6) During the postglacial period the area under study was subjected to subaerial erosion and constituted a favourable outlet for the glacial rivers discussed by Greenly (1919) and Embleton (1964). As a result a channel was incised into the glacial sediments and was later filled with postglacial sediments.
7) The prevailing internal reflection patterns within the channel infill sequence indicate a high energy depositional environment in the area with a relatively high sediment supply.
8) The recent sediments in the area are characterized by thick deposits of sand (up to 8m) present in the form of sub-tidal and inter-tidal sand banks. The layering

observed within the sediments of the outer limits of the tidal sand body in Caernarfon Bay indicates the active nature of the sediments.

CHAPTER 4

MORPHOLOGIC AND BEDFORM STUDIES

4.1 Introduction and objectives.

The bedform distribution and coastal morphology of sand accumulated areas (such as the Menai Strait and Caernarfon Bay) are determined by the interaction of a number of process variables, including: tidal range, tidal currents, wave conditions, and meteorological conditions' (Morton et al 1973). Of these, variations in tidal range have the broadest effect in determining large scale differences in the morphologies of sand accumulations (Hayes, 1980).

The most important features related to tidal shorelines include: barrier islands, tidal inlets, tidal deltas, and recurved spits (Hayes, 1980). The area currently under study is noticeably a tide dominated one and exhibits similar features to those mentioned above. Hence it is appropriate to include a summarised description of these features in the early part of this chapter (sections 4.1.1 and 4.1.2).

The objectives of the current study were to;

1) Carry out geomorphologic investigations of the Belan tidal inlet and its associated sand bodies, with special reference to the standard models of flood and ebb-tidal deltas, given by Hayes (1980).
2) Construct an up to-date bathymetric chart of the seabed topography to define the extent and shape of the recent sand body and related tidal channels.
3) Define various types of bedform patterns and relate the observations of changing size, shape, and orientation of the bedforms to the varying tidal current activity.
4) Draw some preliminary conclusions regarding the dominant

current patterns and their relation to the net sediment transport in the area.

All the above was to be carried out bearing in mind the ultimate objectives in the overall context of this thesis: To understand the prevailing hydrodynamic processes and their role in the development of the tidal delta system in the study area.

4.1.1 Tidal inlets.

Tidal inlets are usually formed between barrier islands. These are influenced twice a day by the flood and ebb tidal currents. A large amount of water has to flow through these inlets over short periods of time, which results in a so-called jet effect. This leads to the formation of deep hollows in the narrowest parts of the inlet trunks which are occasionally excavated to depths considerably greater than the adjoining sea floor (Hayes, 1980).

Tidal inlets are characterised by large sand bodies, deposited by the tidal currents and to a lesser extent by waves, present on either side of the inlet. The primary associated sand deposits are tidal deltas: flood-tidal delta and ebb-tidal delta, and a recurved spit.

Flood-tidal delta.

The sediment accumulation formed on the landward side of an inlet by flood tidal currents represents a flood-tidal delta. Oertel (1972) named these deposits the 'interior shoal'. The morphology and bedforms of flood-tidal deltas have been described by several workers (eg. Hayes (1969), Hine (1975), Boothroyd and Hubbard (1975)). Hayes (1980) suggested a standard model of flood-tidal delta (Fig: 4.1a) which consists of following units:

a) Flood ramp. A seaward dipping surface dominated by

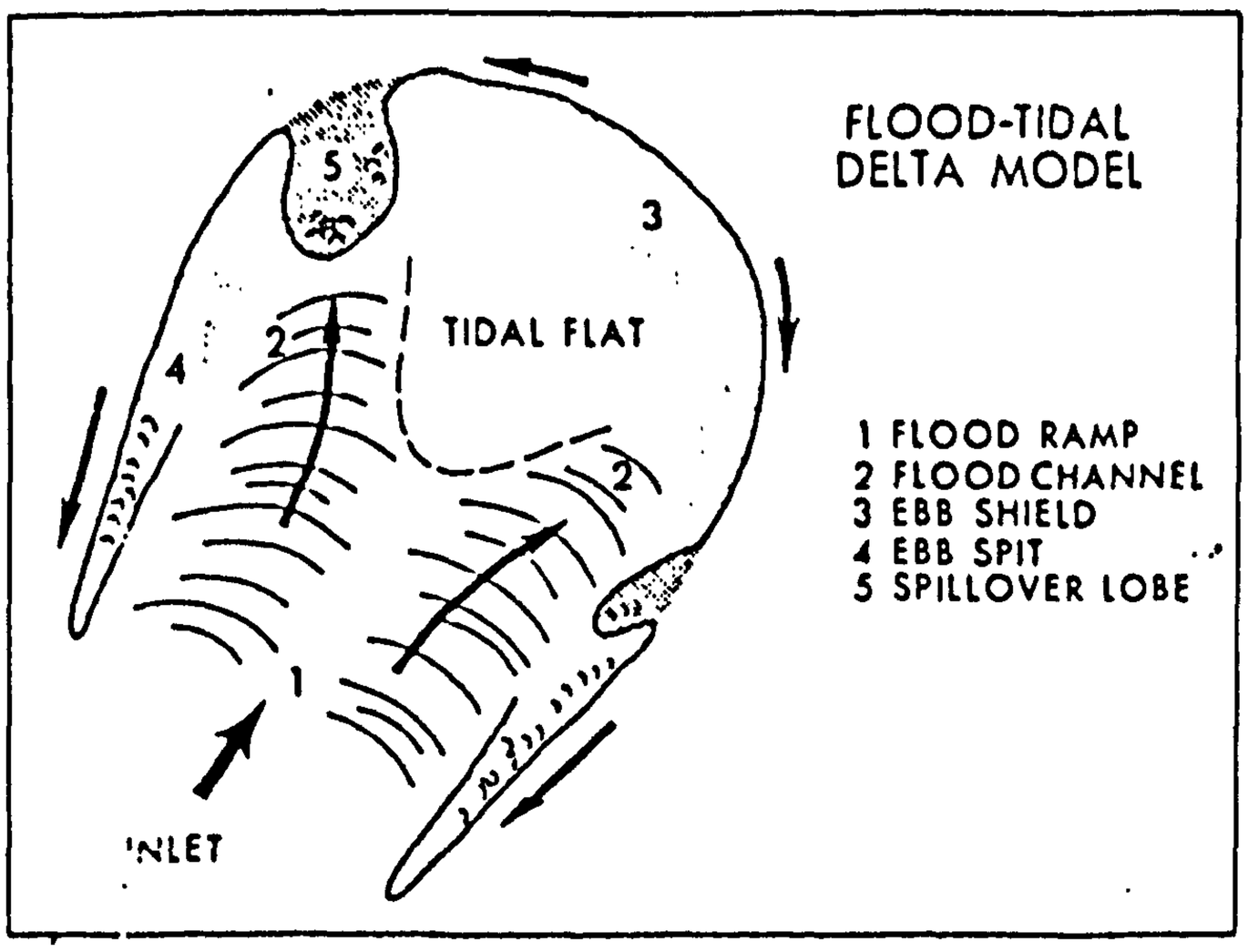

Fig: 4.1a. Model of morphology of flood-tidal deltas. Arrows indicate dominant direction of tidal currents (Hayes, 1980).

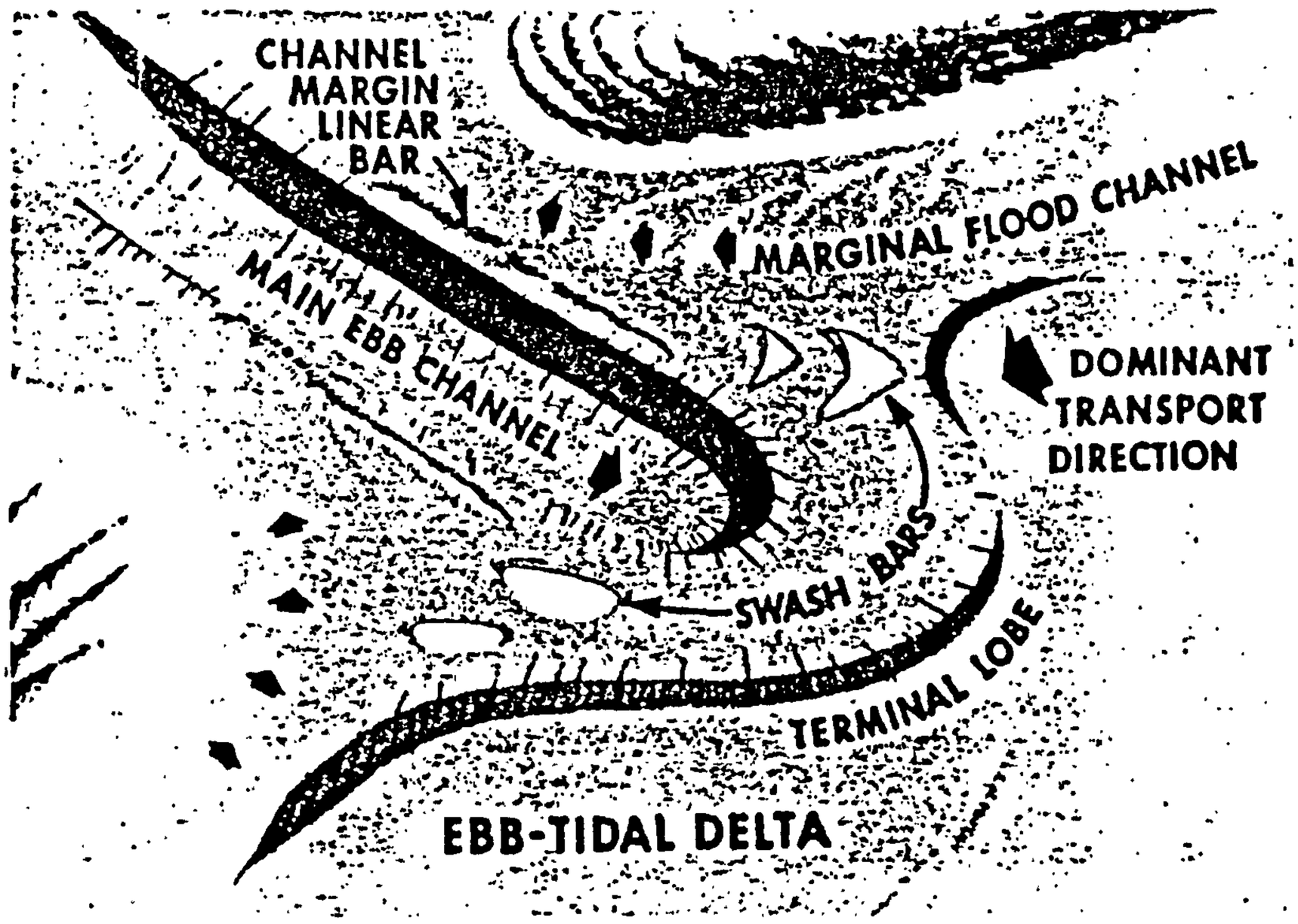

Fig: 4.1b Model of morphology of ebb-tidal deltas. Arrows indicate dominant direction of tidal currents (Hayes, 1980).

flood-tidal currents with major sediment movement accomplished by the migration of sandwaves landward, up the ramp.

b) **Flood channels.** Channels dominated by flood currents that bifurcate off the ramp.

c) **Ebb shields.** Topographically high rims or margins around the tidal-delta that protect portions of it from modification by ebb currents.

d) **Ebb spits.** Spits formed by ebb-tidal currents, with some interaction with flood currents.

e) **Spillover lobes.** Lingoid bar like features formed mainly as a result of ebb tide current flow over low areas of the ebb shield.

Generally speaking, the flood-tidal deltas are dominated by landward-oriented bedforms. Most of the smaller bedforms on the tidal delta, ripples and megaripples, change their orientation with the change in tide (Hayes, 1980).

Ebb-tidal delta.

The discharge of a tidal stream into the sea is morphodynamically comparable to the discharge of a major river. As a result of that high velocity, ebb currents transport major amounts of sediment out through the tidal inlet. At the inlet mouth this sediment load is quickly deposited as the current velocity rapidly decreases. The sand accumulation created in this way is called an ebb-tidal delta (Van Veen, 1950).

Studies of numerous ebb-tidal deltas on the east coast of the USA (eg. Finely (1975, 1978), Hubbard (1975, 1977), FitzGerald (1977), Humphries (1977), Numedal et al (1977)) indicate that the morphology of these sand bodies is similar from place to place. Therefore, Hayes (1980) suggested a standard model of an ebb-tidal delta (Fig: 4.1b) with the following main components;

a) **Main ebb channel.** It usually shows slight to strong dominance

of ebb-tidal currents over flood tidal currents. Its direction is not necessarily normal to the coast.

b) **Channel margin linear bars.** Levee like features that flank the main channel and are built by the interaction of the ebb tidal currents and waves.

c) **The terminal lobe.** Located at the distal end of the ebb channel, where the ebb jet diminishes to allow substantial deposition of sand.

d) **Swash platforms.** Sand sheets deposited mainly by wave action between the main ebb channel and adjacent barrier islands.

e) **Swash bars.** Form and migrate across the swash platforms by the action of wave generated currents from breaking waves (King, 1972).

f) **Marginal flood channels.** May occur between the Swash platforms and both the updrift and downdrift barriers; dominated by flood tidal currents.

The overall morphology of an ebb-tidal delta is a function of the interaction of tidal currents and waves. Of prime importance is a phenomenon called time-velocity asymmetry (this means that maximum ebb and flood tidal currents do not occur at mid tide) of tidal currents as described by Postma (1967).

Recurved spit.

The barrier beach on the updrift side of most tidal inlets between barrier islands is a recurved spit. As the inlet migrates it leaves behind it a series of curving beach ridges separated by marshy swales. This process is, principally one of lateral sedimentation, whereby a vertical sequence of differing sedimentary facies is preserved by lateral migration of sedimentary environments (Hayes, 1980).

A sequence of primary sedimentary structures is preserved due to the migration of the beach ridges of a recurved spit. Three principal bedding types predominate:

a) High angle, shoreward dipping, planar crossbedding formed by migration of the ridge slip face.
b) Flat beds deposited by berm-top overwash (slight shoreward dipping).
c) Small to medium scale trough cross bedding formed by ripples and megaripples in the runnel.

These conclusions were made by Hayes (1980) on inspection of recurved spits in various regions of the USA.

The other features of prime importance associated with the inter-tidal and sub-tidal areas of flood and ebb-tidal deltas and surrounding coastal areas are various types of bedforms which are discussed below.

4.1.2 Bedforms.

Bedforms are those solid shapes into which non-cohesive sediment particles, transported by a fluid, become fashioned on the bed of the flow, through dynamic interaction between the fluids and the particles in transport (Allen, 1965). There is a sequence of bedforms that occurs in sandy sediments in areas of progressively changing flow velocity (Dyer, 1986). Detailed studies undertaken by Boothroyd and Hubbard (1975) indicate that bedform type in tidal depositional areas is governed by;

a) Maximum ebb and flood velocity.
b) Velocity asymmetry, and
c) Velocity duration.

On the basis of their occurrence and general shape, relative to direction of flow, bedforms can be classified as longitudinal

(furrows and sand ribbons), oblique (sand ridges), and transverse (ripples, megaripples and sand waves).

Longitudinal bedforms.

Furrows

Furrows were first described by Dyer (1970) in the estuarine muds of Southampton water, where the furrows have thickness of 0.5 to 1m, and are up to 4Km long. They are generally about 10 to 25m apart and extended from water depths 1m below low water mark to the bottom of the channel. Furrows represent a high mean tidal current velocity, with currents reaching up to 150cm/s (Dyer, 1970).

Sand ribbons

These are narrow bands of mobile sand aligned with the current flow. Sand ribbons are often only a few centimetres thick (i.e. internal thickness), but can be up to 15km long and 200m wide (Dyer, 1986). They are essentially straight, although locally they may be slightly sinuous and generally have a length/width ratio of 40. The actual direction of the sand transport could be found from the small scale structures (ripples and megaripples) associated with ribbons (Klein, 1970). Sand ribbons are formed where peak surface mean spring currents attain about 100cm/s (Kenyon, 1970).

Oblique bedforms.

Sand ridges

A sand ridge is a composite, flow oblique (or parallel) linear accumulation of sand, formed by the superposition and migration of sand wave or megaripple fields. Sand ridges have a linear to sinuous crest line and have a length/width ratio usually greater than 40. They have elevations ranging from 1 - 30m, widths ranging from 700 - 8000m and can be up to 60 km long (Amos and King, 1984).

Transverse bedforms.

The literature related to transverse bedforms suffers from an immense confusion regarding nomenclature and classification of such bedforms. Various authors have used different terms for the same features (Dyer, 1985). Some examples are those of Gilbert (1914), Allen (1968), Klein (1970), Boothroyd and Hubbard (1975), Dalrymple et al (1978). The most common types of transverse bedforms found in tidal areas are various types of ripples, which occur in a wide variety of sizes and shapes.

Davies (1964) classified the transverse bedforms on the basis of wavelength or spacing.

Bedform terminology	Wavelength
Ripples	up to 50cm
Megaripples	50cm to 5m
Sand waves	>5m

Hayes (1969) gave slightly different spacing sizes, although the terminology remained the same.

Ripples	up to 60cm
Megaripples	60cm to 6m
Sand waves	>6m

Dalrymple et al (1978) carried out bedform studies in the Bay of Fundy, Canada. On the basis of morphological and grain size analysis they differentiated 4 types of bedforms: ripples, type 1 megaripples, type 2 megaripples, and sand waves.

Dalrymple et al (1978) suggested the following definitions for the above bedforms.

Ripples

Ripples are the smallest bedform type with heights and wavelengths of less than 0.05m and 0.3m respectively. Ripples

most commonly occur superimposed on the larger bedforms, but they frequently occur on their own. They usually originate in sands with a mean grain size value of 0.184mm and where current speeds average a maximum mean value of 60cm/s.

Megaripples

These are analogous to the dunes of most other authors (eg. Simons and Richardson (1961), Allen (1968) Southard (1971)). All megaripples are characterised by a lee face that occurs at the angle of repose of the sediment during active migration. Apart from this typical feature, they show a wide variation in their detailed morphology. Two types of megaripples, type 1 and type 2, which are analogous to 2-D and 3-D megaripples of Amos and King (1984), can be distinguished:

Type 1

These are simple in appearance, and are characterised by straight to smoothly sinuous lee faces that lack irregularities and consequently have good lateral continuity. The wavelengths (0.1 - 25m) of these megaripples are long relative to the heights (0.1 - 0.5m) and that gives them a typically flat profile with wavelength/height ratios generally greater than 20. Type 1 megaripples have mean grain size values of 0.328mm and are formed at an average maximum mean current speed of 68cm/s.

Type 2

These are complex in appearance and are generally sinuous to lunate in plan. The troughs contains well-developed scour pits. As a result bedform height varies considerably over a short distance along the crestline. Type 2 megaripples have steep profiles, and on average they are higher (0.05 - 0.7m) and shorter (0.05 - 14m) than type 1. These megaripples are formed under a relatively higher average maximum mean current speed (100cm/s) and in sands of relatively smaller mean grain size value (0.272mm).

Sand waves

Sand waves are the largest of the transverse bedforms. Most sand waves are asymmetrical, but their lee faces commonly have inclinations of 10 - 20°. Sand waves display many similarities to type 1 megaripples. They are straight to smoothly sinuous in plan; the height remains uniform along a particular bedform, and they have wavelength/height ratios rarely less than 20. Virtually all sand waves have superimposed ripples or megaripples on their stoss sides and that is one of the main criterion which differentiates the sand waves from type 1 megaripples.

Sand waves can have wavelengths of 5 - 215m and their height may vary between 0.15 to 3.4m. Sand waves occur in sands with mean grain size range between 0.369 - 0.507mm and under moderate flow conditions, with average maximum mean speed up to 95cm/s.

Since bedforms are produced by currents in many aqueous environments, they are of great interest to engineers and geologists. The importance of the bedforms was first recognised by Sorby (1852, 1857, 1859, 1908) in England. On the basis of various experiments he related bedforms to states of flow. Later, Gilbert's (1914) classical work on the relationship between bedforms and flow states led to many more experiments as well as to bedform studies in modern sediments (eg. Caston (1965), Belderson and Stride (1966), Kenyon and Stride (1970), Terwindt (1971), Hine (1975), Boothroyd and Hubbard (1975), Dalrymple et al (1978), Zarillo (1982), Harris and Collins (1985), Sha (1989).

Caston (1965) conducted an echo-sounding survey of Tremadoc Bay, Wales, which revealed an occurrence of asymmetrical sand waves in the southwest corner of the Bay. He used the asymmetry and orientation of the sand waves to determine the direction of mass water and sediment movement.

Werner and Newton (1975) carried out a side-scan sonar survey in

Langeland belt (Baltic sea) to study the large bedforms of that region. They demonstrated that the bedform morphology and orientation allows detailed reconstruction of the current paths and indicate the areas of domination of inflow conditions.

Boothroyd and Hubbard (1975) used bedform orientation to infer direction and magnitude of sand movement in the Gulf of Maine, USA. In a similar type of study Harris (1982) determined the sediment transport paths in various estuaries in the UK.

Harris and Collins (1985) used side-scan sonar techniques to study the bedforms in the Bristol Channel and Severn estuary, U.K. They suggested that sand wave orientations indicated localised bed load divergencies which form part of a larger transport system. A similar technique was also used by Knebel (1989) to study the modern sedimentary environments in a large tidal estuary, Delaware Bay, USA. His study reveals that the orientation of sand waves and sand ribbons indicates that the bottom movement may be towards either the northwest or southeast along the trends of the tidal channel. The direction of the net sediment transport towards the head of the Bay (northwest) was determined on the basis of sand wave asymmetry.

From the above mentioned studies and other available literature on bedform studies, it can be concluded that the importance of bedform studies is multifold. The orientation and asymmetry of bedforms helps to determine the recent bed sediment transport. In addition, the internal sedimentary structures of bedforms within the geological record are very important for palaeogeographic reconstruction (Kohsiek and Terwindt, 1981). A study of bedforms also helps in the reconstruction of hydrodynamic parameters eg. palaeocurrents from the study of preserved sedimentary structures (Boersma and Terwindt, 1981).

4.2 Oceanographic setting of the study area.

4.2.1 Tides

The tides of the Menai Strait and Caernarfon Bay are predominantly semi-diurnal. The mean spring and neap tidal ranges at Caernarfon are approximately 4.7 and 2.2m respectively.

A classification of coasts, on the basis of high spring tidal range, by Davies (1964) identifies three categories;

Micro-tidal coast	less than 2m
Meso-tidal coast	2 to 4m
Macro-tidal coast	> 4m

According to Davies' classification (1964) Caernarfon Bay coast falls in the category of macrotidal.

4.2.2 Characteristics of tidal flow

The pattern of the tidal currents in the study area is dominated by the characteristics of the tidal flow through the Menai Strait. Harvey (1968) reported the first observations of the flow of water through the Menai Strait made during 1956. Using three floats with vanes, the measurements were made over a distance of 275m in the vicinity of position D (Fig: 4.2) during a period of 10 hours. The mean maximum velocity of three floats at any time during northeasterly and southwesterly flow was about 80cm/s and 150cm/s respectively.

On a later date, a float with a vane 1m below the surface was released at position G (Fig: 4.2) at the start of the southwesterly tidal flow and was followed during the complete semi-diurnal tidal period. At the end of an ebb tide it had reached position A and during the subsequent flood tide moved from position A to position F. Its net movement was therefore

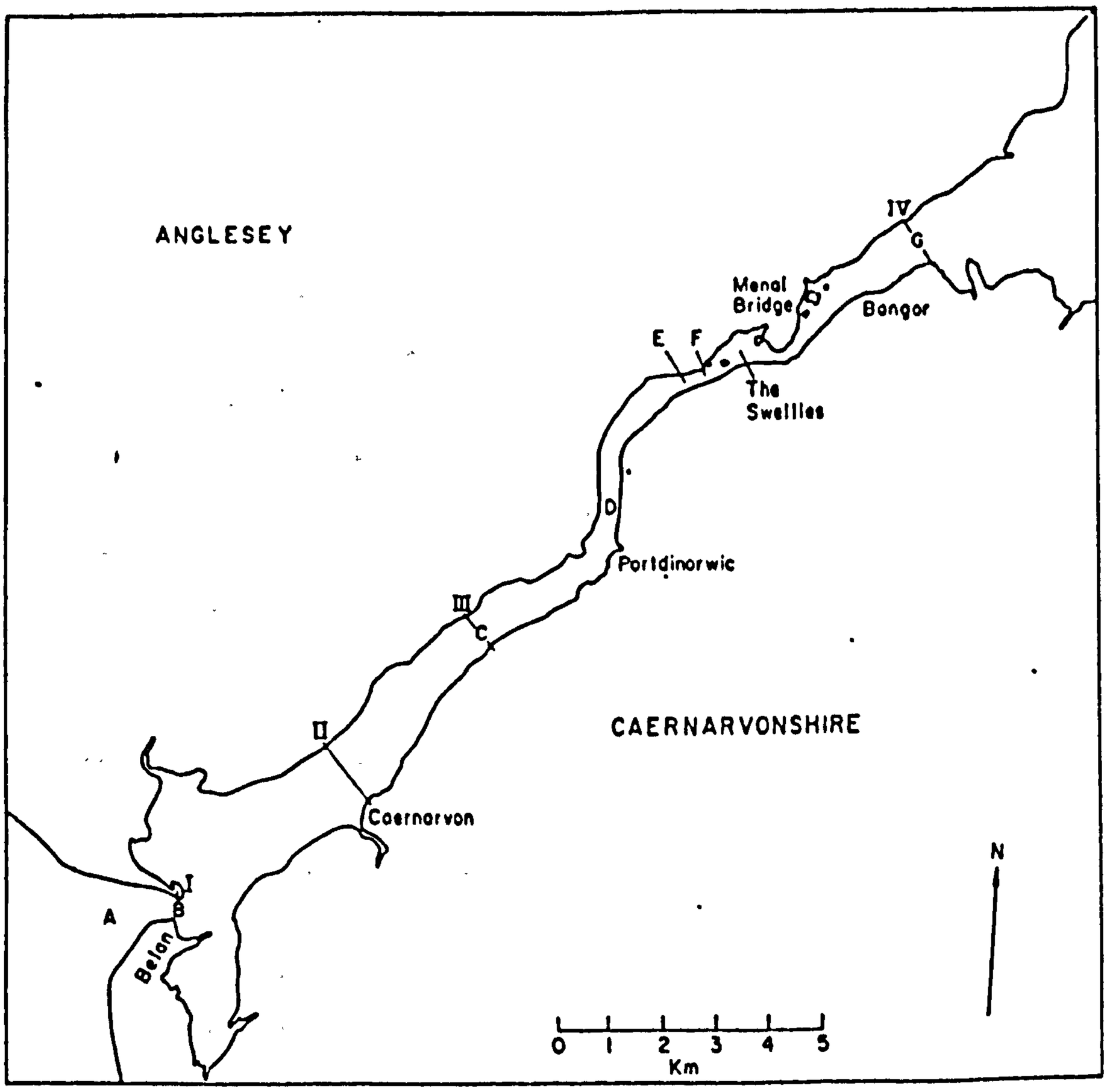

Fig: 4.2 The Menai Strait showing positions and sections referred to in the text section 4.2 (after Harvey, 1968).

4.8km in 12.5 hours, corresponding to a mean velocity of 11cm/s towards the southwest.

During a spring tidal cycle, in April 1961, a recording current meter was first used at position E for a period of 25hours by British Insulated Callenders Construction Co LTD. Maximum velocities of 80cm/s and 120cm/s were recorded in northeasterly and southwesterly directions respectively.

On the basis of a study of Woodhead seabed drifters released at positions B, C, and G, and direct current measurements taken at the cross sections I, II, III, IV (Fig: 4.2), Harvey (1968) also suggested the occurrence of a southwesterly residual flow of water with an average velocity of 15cm/s through the Menai Strait. The residual flow of water from Beaumaris Bay into Caernarfon Bay through the Strait was also indicated by biological investigations carried out by Jones and Haq (1963).

Forbes (1969) reports current measurements taken using direct reading current meters. He found that the duration of the current flow to the southwest is longer than to the northeast.

Sherwin (1985) reports that the maximum spring tidal current velocity occurs at the Fort Belan inlet, where the velocity reaches up to 250cm/s. The diagram in Fig: 4.3 demonstrates the direction and velocity of the flood and ebb tidal currents, during one complete spring tidal cycle, from Fort Belan inlet to Puffin island. It may be noted here that the duration of the ebb currents at Belan inlet is higher than the flood currents and this supports the various claims for a southwesterly residual flow of water through the Menai Strait.

4.2.3 Tidal current measurements.

During this project tidal current measurements were taken at three stations; one inside the Menai Strait (C1) and other two out side the Belan inlet in Caernarfon Bay (C2 and C3). For

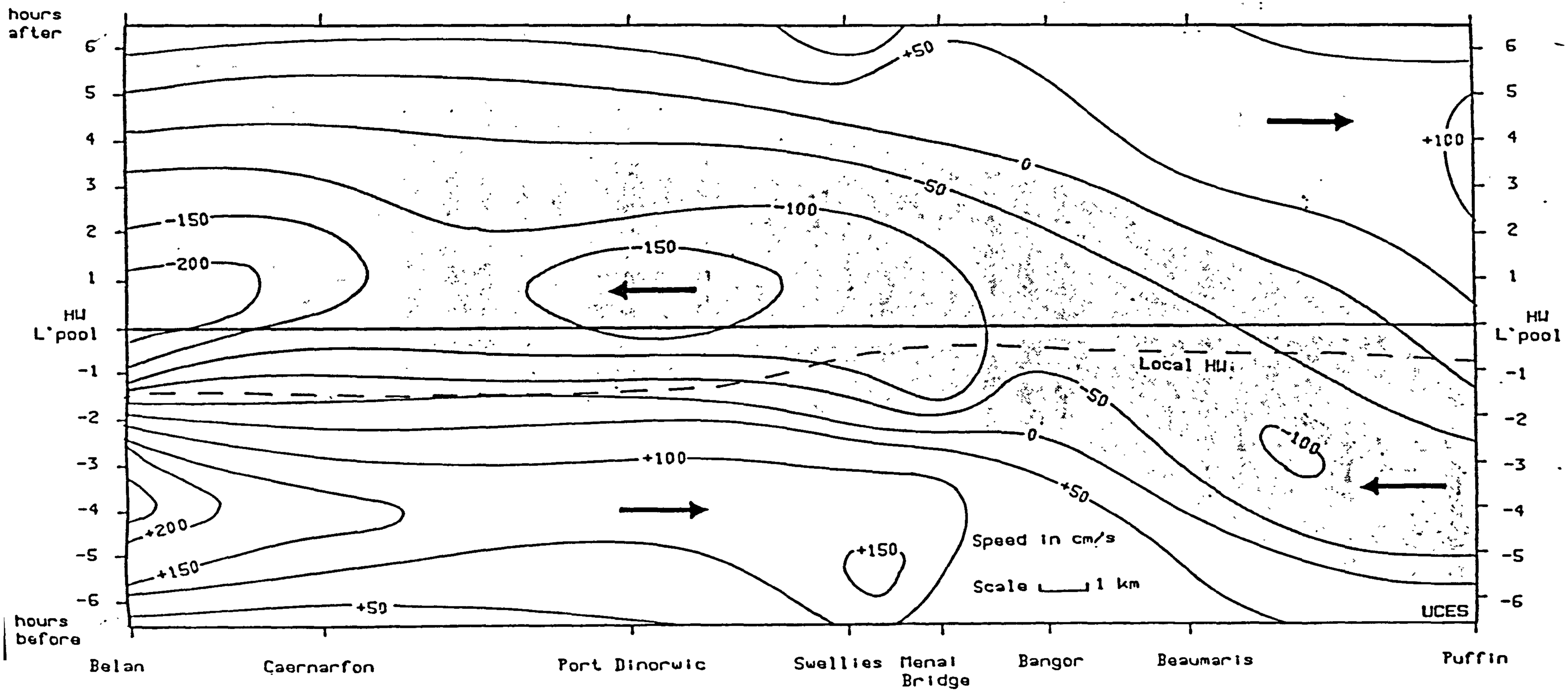

Fig: 4.3 Direction and velocity of mean spring tidal currents in the Menai Strait (from Puffin island to Belan inlet (after Sherwin, 1985).

location of these stations refer to Fig: 4.4. InterOcean systems, Inc model S4 current meter #00670920 was used at all three stations (equipment specifications can be found in appendix V). At each station continuous measurements were recorded over a period of about two weeks. The S4 current meter is computer controlled, small and has a spherical shape. Before deploying the S4 current meter, it has to be programmed, according to specific requirements (such as length of recording time and reading interval), by connecting it to a micro computer. Once programmed it can be left in the water over the required period of time.

The S4 measures current by creating a magnetic field and sensing the voltage induced by the movement of water through the field. An inbuilt micro processor acquires instrument orientation from a fluxgate compass and computes earth referenced current components in north and east coordinates. These current vectors are then recorded immediately or integrated over a pre set length of time (in the case of the present study, 5 minutes) and recorded. All the data is recorded in solid state memory from where it can be retrieved via an appropriate micro-computer.

The S4 is intended primarily for mounting to fixed stations (offshore oil installations, etc), or tautline moorings. However, in the current study the S4 current meter was attached to a purpose built iron frame. The frame was constructed in a way that allowed the current meter to measure current velocity and direction at height of 100cm above sea bed. At each station the current data was recorded for about 15 days and at the end of this period the current meter was brought back to the laboratory for data retrieval and further initialization of the system for the use at the next station. Initially it was intended to deploy the current meter within the nearest possible vicinity of the main channel (in and outside the Strait); however, considering the fact that the strong tidal currents in these areas would not allow the frame to remain trouble free on the sea bed, it seemed impracticable. As such, the current meter

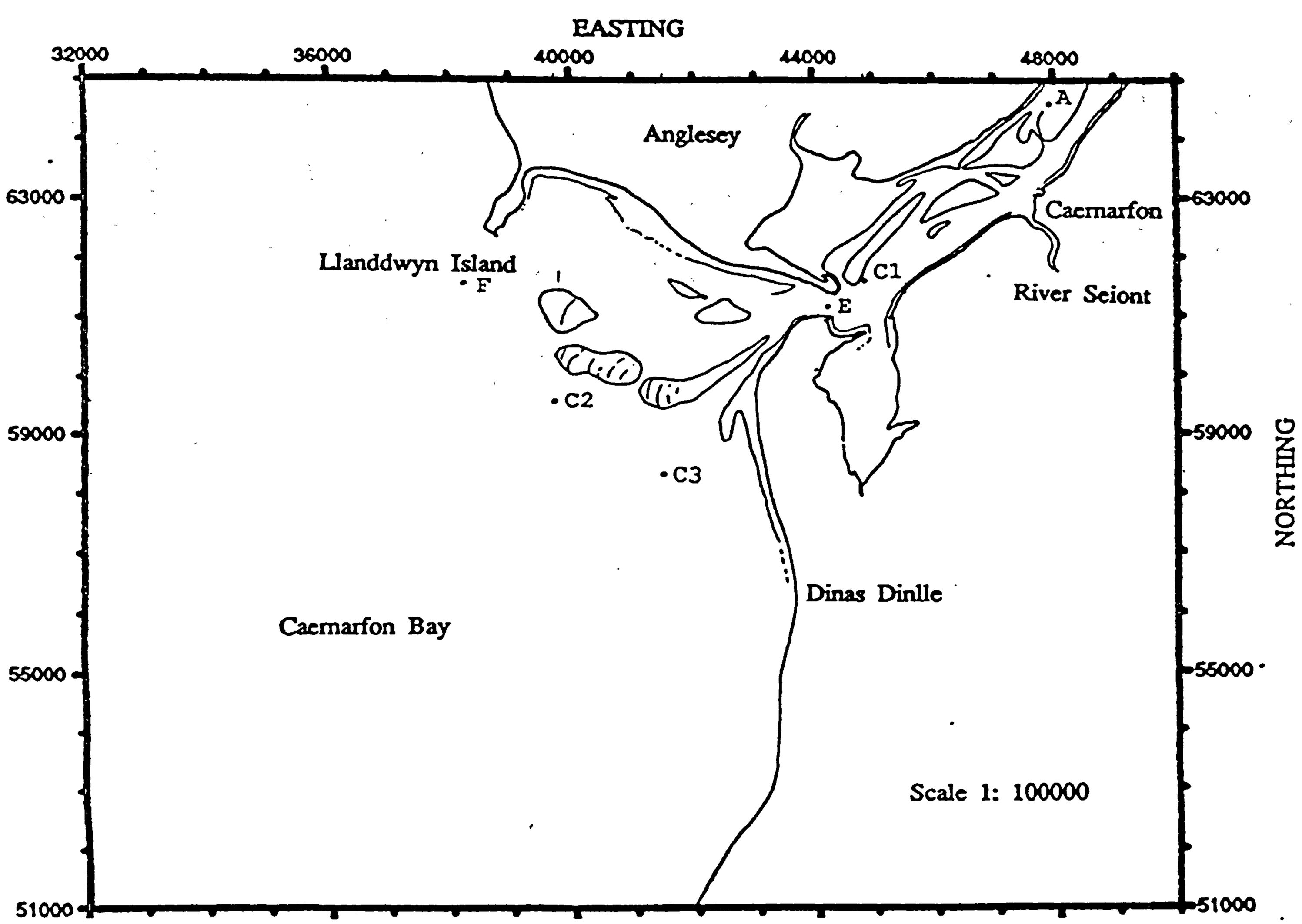

Fig: 4.4 Location map of the current meter stations C1, C2, and C3.
Station A (VGU measurements by Nyandvi (1988)).
Station E and F (from National Hydrographic chart).

was deployed in relatively sheltered areas except in the case of station C1. These doubts were proved true when station C1 data was analysed which suggest that during spring flood tidal currents (when current velocities reached about 130cm/s) the frame had started to tilt and was finally completely overturned. This occurred during five consecutive flood tides. The good thing was that at the start of the subsequent ebb tide the frame returned to its normal position and fortunately did not affect the ebb tide data. The results of the acquired data at all these stations are presented below.

Station C1.

The current measurements at this station were recorded over a period of two weeks i.e. from 21/11/88 to 5/12/88. The S4 current meter was deployed on the seabed just inside the Belan inlet slightly off the main channel. At this station the highest and lowest current velocities of 163cm/s and 66cm/s occurred during spring and neap tides respectively.

Due to some instrumental factors perhaps the s4 current meter failed to record the data properly for about 3 days in total. In all, 24 complete tidal cycles were recorded successfully except during the flood tides of the tidal cycle Nos. 2-6 when because of strong tidal currents, the S4 tilted up to 90 degrees during the later stages of each flood tide. Since it was clearly detected that the data recorded during the above periods was defective it seemed advisable to reject that data. Therefore it was decided to replace the incorrect data with extrapolated values. Considering the fact that the extrapolation of the incorrect part of flood tides 2-6 was carried out on the basis of the data acquired for remaining 19 complete tidal cycles, it may be said that the extrapolated values may not be far from real values. However, the current meter results obtained from this station must be treated with caution.

The variations of current velocity over a period of 24 tidal

cycles at this station are presented in Table No. 4.1 and are shown in Fig: 4.5a. It may be noted here that the strongest tidal currents predominantly occurred during flood tide, and the velocities generally tend to decrease in a regular pattern from spring tide to neap tide. The diagram also suggests that as the current velocity decreases towards neap tide the difference between the maximum velocities of flood and ebb for each tidal cycle also decreases. The highest and lowest maximum flood tidal current velocities recorded at this station are 163cm/s and 77cm/s respectively. It appears that flood tide dominates as far as the current velocities are concerned, However, the diagram of variations in the durations of the flood and ebb tides during 24 tidal cycles (Fig: 4.5b) suggest that the ebb tides generally flow for longer periods than the flood tides. The maximum ebb durations of about 7 hours were recorded during tidal cycle Nos. 2-6. Owing to the fact that the current meter was tilted during the flood tides of the same tidal cycle (2-6), these ebb durations can not be confirmed confidently. Nevertheless, leaving these five tides aside, it is still the case that the duration of the ebb tide is considerably longer than the flood tide. The data also suggest that the ebb tides tend to increase in duration towards neap and spring tides whereas flood and ebb durations reach to an almost equal level for one or two tidal cycles in between the neap and spring tides.

In order to look further into the details of the tidal currents during a typical spring and neap tidal cycle, two data sets, one representing a spring tide and the other a neap tide, were selected from this station (see Fig: 4.6). The figure also clearly demonstrates that the ebb duration is greater than the flood. It also reveals that the strongest flood velocities in the flood direction occur during late stages of the flood tide while during the ebb tide the currents attain higher velocities relatively quickly, suggesting velocity asymmetry in the tidal cycle. While spring and neap tidal currents shown in Fig: 4.5 look identical to each other as far as their direction is concerned, the velocities during spring tide are very high. This

Table No. 4.1

Maximum current velocity and duration of flood and ebb tides at station C1.
Current velocity in cm/s. Duration of flood and ebb in hours

Tide No.	Flood Tide		Ebb Tide	
	Velocity	Duration	Velocity	Duration
1	151	6.00	122	6.50
2	152	5.17	122	7.16
3	163 S	5.08	134 S	7.16
4	160 S	5.00	132 S	7.16
5	157	5.17	130	7.00
6	150	5.00	127	7.16
7	135	5.42	122	6.42
8	141	5.58	117	6.67
9	133	5.63	116	6.67
10	136	5.83	105	6.60
11	122	6.08	91	6.00
12	122	5.92	87	6.17
13	104	5.92	87	6.17
14	102	5.83	88	6.50
15	95	5.83	79	6.33
16	89	5.80	71	6.75
17	77 N	5.75	70 N	6.25
18	81 N	5.50	71 N	6.92
19	84	5.58	66	6.50
20	79	5.75	69	6.67
21	78	5.83	75	6.42
22	95	6.17	78	6.17
23	87	6.17	71	6.17
24	79	6.08	76	6.17

S = Springs N = Neaps

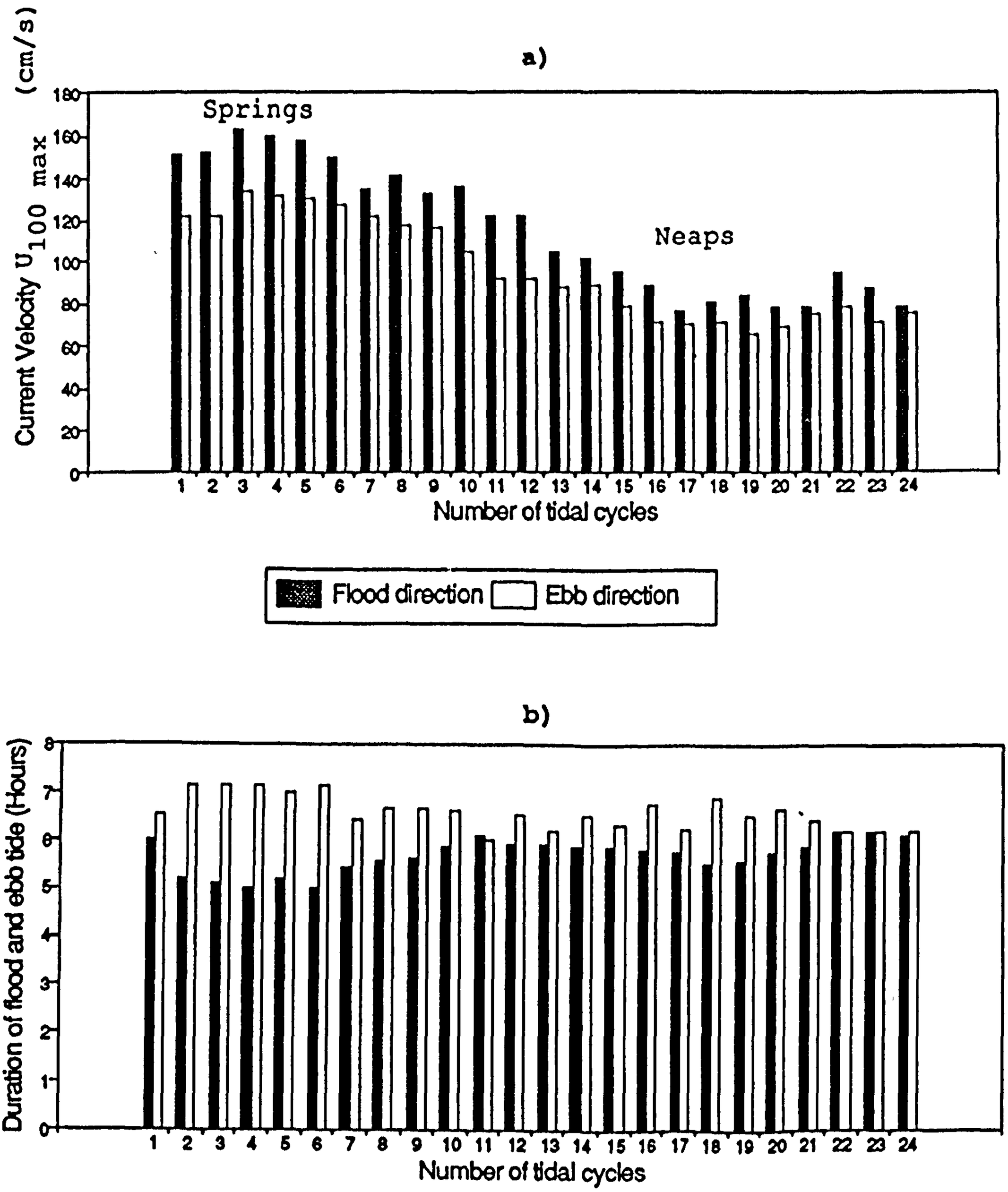

Fig: 4.5 **a)** Variations of maximum flood and ebb current velocities at station C1

b) Variations in the durations of flood and ebb tides during each tidal cycle at station C1

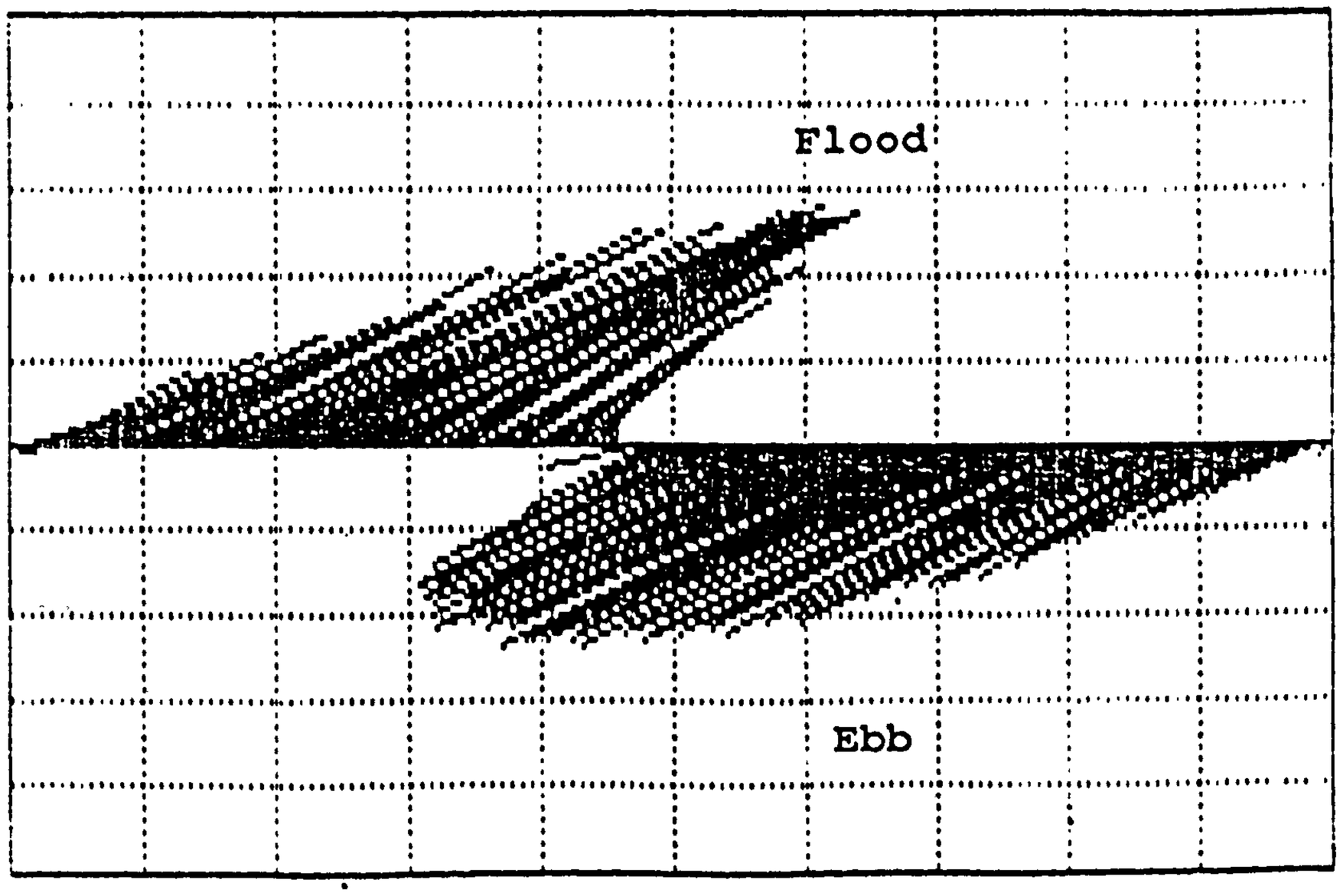

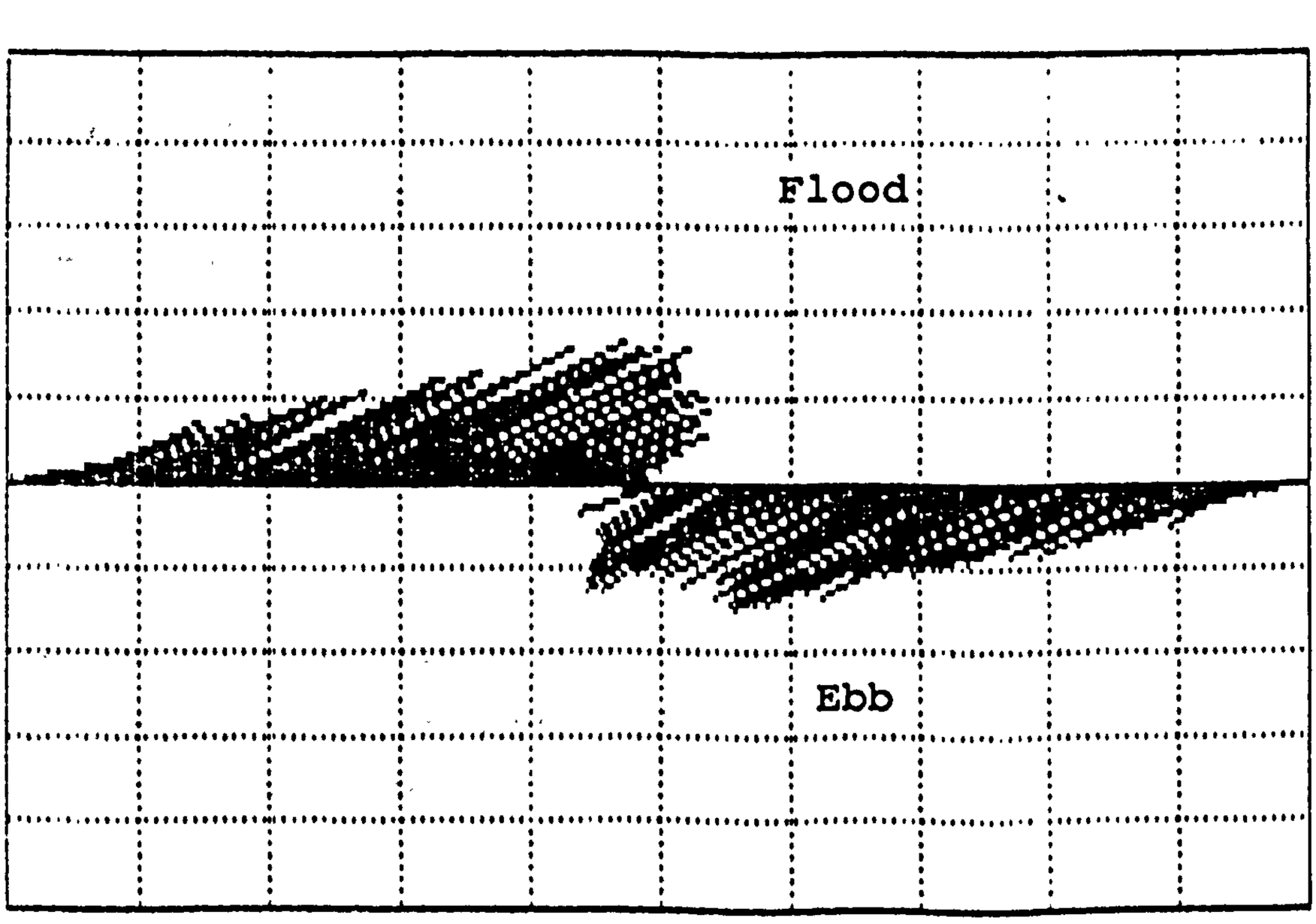

Fig: 4.6 Straw diagram of the velocity and direction of the tidal currents during spring (top) and neap (bottom) tidal cycles at station C1.

similarity in the current direction is the direct result of the location of the station C1 being just inside the Belan inlet where flood and ebb currents follow a natural direction of NE and SW respectively i.e. opposite to each other.

In addition, the residual currents at each of the three stations were calculated. The magnitude and the direction of the residual currents at station C1 over a period of 24 tides, a spring tide, and a neap tide are shown in Fig: 4.7. These results suggest a residual flow of water in the ebb (SW) direction. The results for the period of 24 tidal cycles (Fig:4.7a) may be unreliable because of the tilting of the current meter during the previously discussed flood tides - flood velocities greater than 130cm/s were not recorded and that would have definitely enhanced the SW component for subsequent ebb tides resulting in the relatively higher residual values. This high value, however, does not put into question the overall results as far as the direction of the residual currents is concerned. The residual currents (Fig: 4.7b) calculated for the tidal cycle No. 1 (this tidal cycle was recorded completely and appear similar to the actual spring tides) also suggest a southwesterly residual flow of 6.9cm/s. The same is true for the neap tide (Fig: 4.7c); however, the amount of residual currents in this case is considerably lower (0.6cm/s).

Overall the results from station C1 generally agree well with the general morphology of the location of the station and with previously conducted current measurements in the area. Similar conclusions - of southwesterly flow of residual water through the Menai Strait - have been reported by Harvey (1967), Jones and Haq (1963), and Jones (1984).

Nyandwi (1988), however, on the basis of VGU measurements at station A (for location refer to Fig: 4.4) reports higher ebb velocities than the flood velocities except on one occasion which he relates to the effect of strong southwesterly winds on that particular day. Another reason for this could be that it

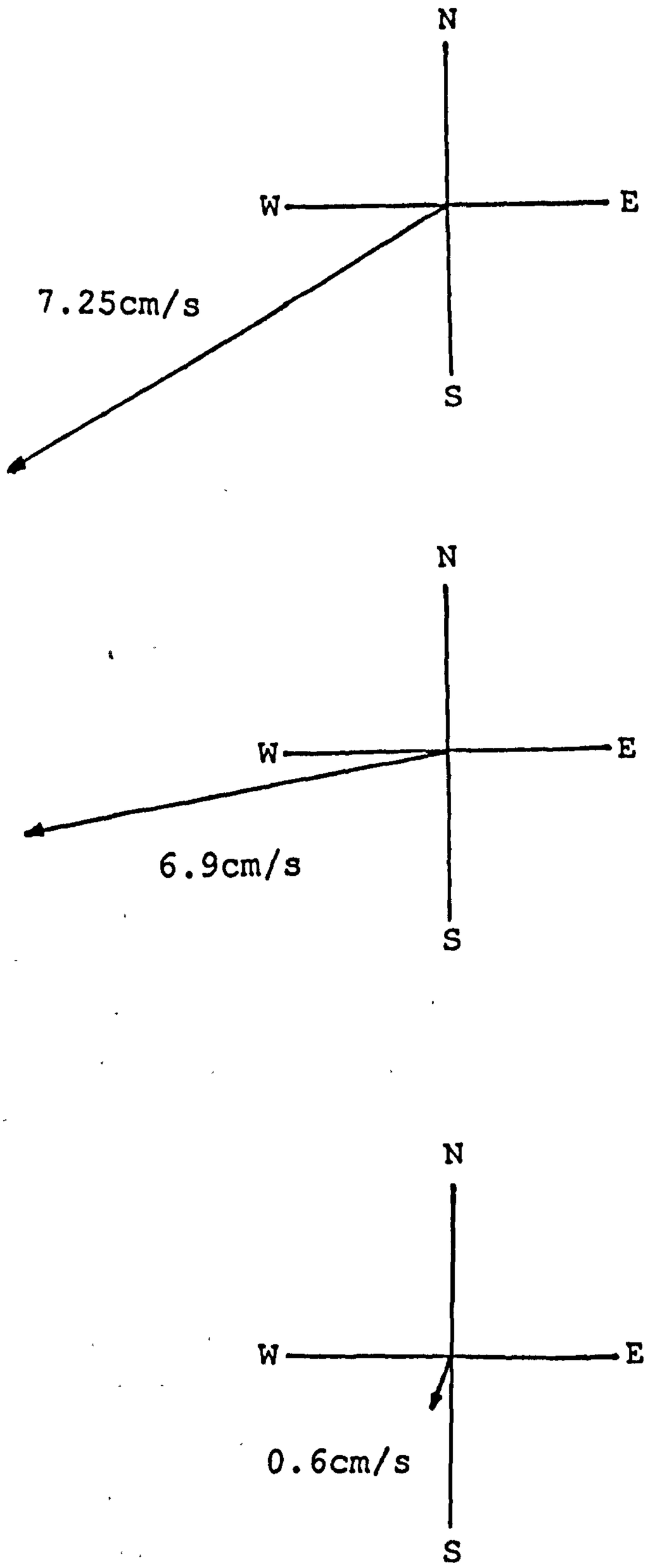

Fig: 4.7 Residual current velocity and direction at station C1.

a) Over a period of 24 tidal cycles.

b) During a spring tidal cycle.

c) During a neap tidal cycle.

is purely a result of the location of station A which is on the north side (Anglesey side) of the Strait whereas the main channel within the Strait at that particular location runs along the south coast (Caernarfon side) suggesting that away from the main channel, particularly along the Anglesey coast, ebb currents are dominating the area.

Station C2.

This station was occupied by the S4 current meter for a period of two weeks i.e. from 6/11/88 to 21/11/88. In total 27 complete tidal cycles were recorded successfully. As pointed out earlier, the iron frame containing the current meter could move under the influence of strong tidal currents. Therefore it was placed on the seabed, just off the main tidal sand body, in a relatively sheltered area. Because of the location of the station C2 the data do not exhibit any regular pattern as far as the direction of the currents is concerned. As such it was not practicable to separate the flood and ebb currents associated with individual tidal cycles. Consequently, at this station a different approach from station C1 had to be adopted. The whole data which consisted of 27 tidal cycles was split into individual tidal cycles for presentation.

The variations of the maximum tidal current velocities at station C2 over a period of 27 tidal cycles are presented in Table No. 4.2 and are shown in Fig: 4.8a. In general the current velocities in this area are of very low magnitude in comparison to station C1 suggesting that the local high velocity currents diminish in intensity before they reach station C2. It also appears that the regional currents are also considerably weaker at this position and they are making no significant impact either as far as the current velocity is concerned. The maximum and minimum current velocities recorded at this station are 43cm/s and 13cm/s respectively. The highest current velocities occurred only during spring tidal cycles (6 and 7) and then decreased quickly to an average value of 25cm/s.

Table No. 4.2

Maximum current velocity and dominant direction during each tidal cycle at station C3 and C2.
current velocity in cm/s. Direction in degrees.

Tide No.	Station C2		Station C3	
	Velocity	Direction	Velocity	Direction
1	36	215	11	340
2	33	217	18	017
3	30	330	28	232
4	32	350	28	338
5	33 S	355	18	026
6	43 S	338	17	018
7	42	342	28	024
8	26	353	27	020
9	29	212	30	016
10	29	350	31	026
11	28	346	33 S	029
12	25	360	42 S	018
13	27	357	30	022
14	25	006	24	019
15	26	341	32	017
16	24	358	24	030
17	29	344	23	025
18	22	338	20	026
19	23	328	20	022
20	30	350	17	022
21	32	191	14	018
22	18 N	023	15	024
23	23 N	355	12	022
24	13	360	13 N	017
25	34	213	11 N	020
26	23	001	--	---
27	33		--	---

S = Springs N = Neaps

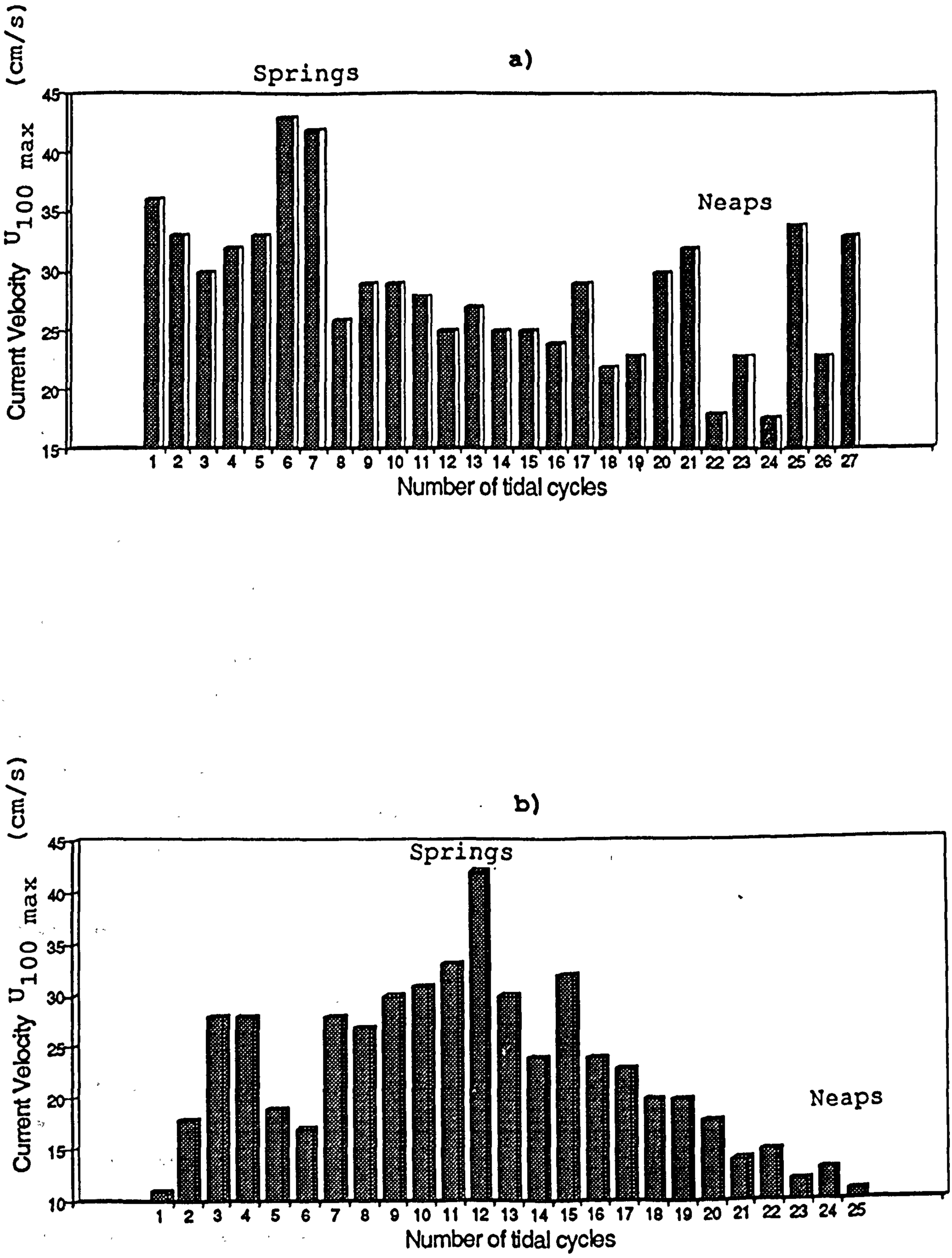

Fig: 4.8 a) Variations of maximum tidal current velocity at station C2 over a period of 27 tidal cycles.

b) Variations of maximum tidal current velocity at station C3 over a period of 25 tidal cycles.

The current direction varies considerably at this station during an individual tidal cycle (Fig: 4.9). The spring tidal currents (Fig: 4.9a) achieve maximum current velocity in a northerly direction and appears to be flowing in that direction for the best part of the tidal cycle while the rest of the currents flow with a southerly component. During a neap tide (Fig: 4.9b) the current pattern is markedly different than on the spring tide. The strongest currents tend to flow with a southerly component; however, the duration of the northerly flowing currents, as on springs, is relatively longer.

The residual currents shown in Fig: 4.10a also suggest that a strong northwesterly residual flow occurs at this station. The residual currents calculated over a period of 27 tidal cycles have a magnitude of 7.4cm/s with a strong northwesterly component. Similarly the residual currents obtained for a typical spring tide has a very high magnitude of 12.25cm/s (Fig: 4.10b) and they also flow to the NW direction. The neap tide results show relatively weaker residual flow towards the north (Fig: 4.10c).

Station C3.

At this station the S4 current meter was deployed from 19/10/88 to 3/11/88. In total 25 complete tidal cycles were recorded successfully. As at station C2, the data acquired at this station lacks any systematic current pattern which could differentiate flood and ebb periods of an individual tide. Therefore a similar approach of splitting the data into individual tidal cycles has been applied.

Maximum tidal current velocities at this station over a period of 25 tidal cycles are presented in Table. No. 4.2 and are shown in Fig: 4.8b. The velocities here appear to be generally lower than the velocities at station C2 and that is perhaps because of the relatively shoreward position of station C3. Maximum weak

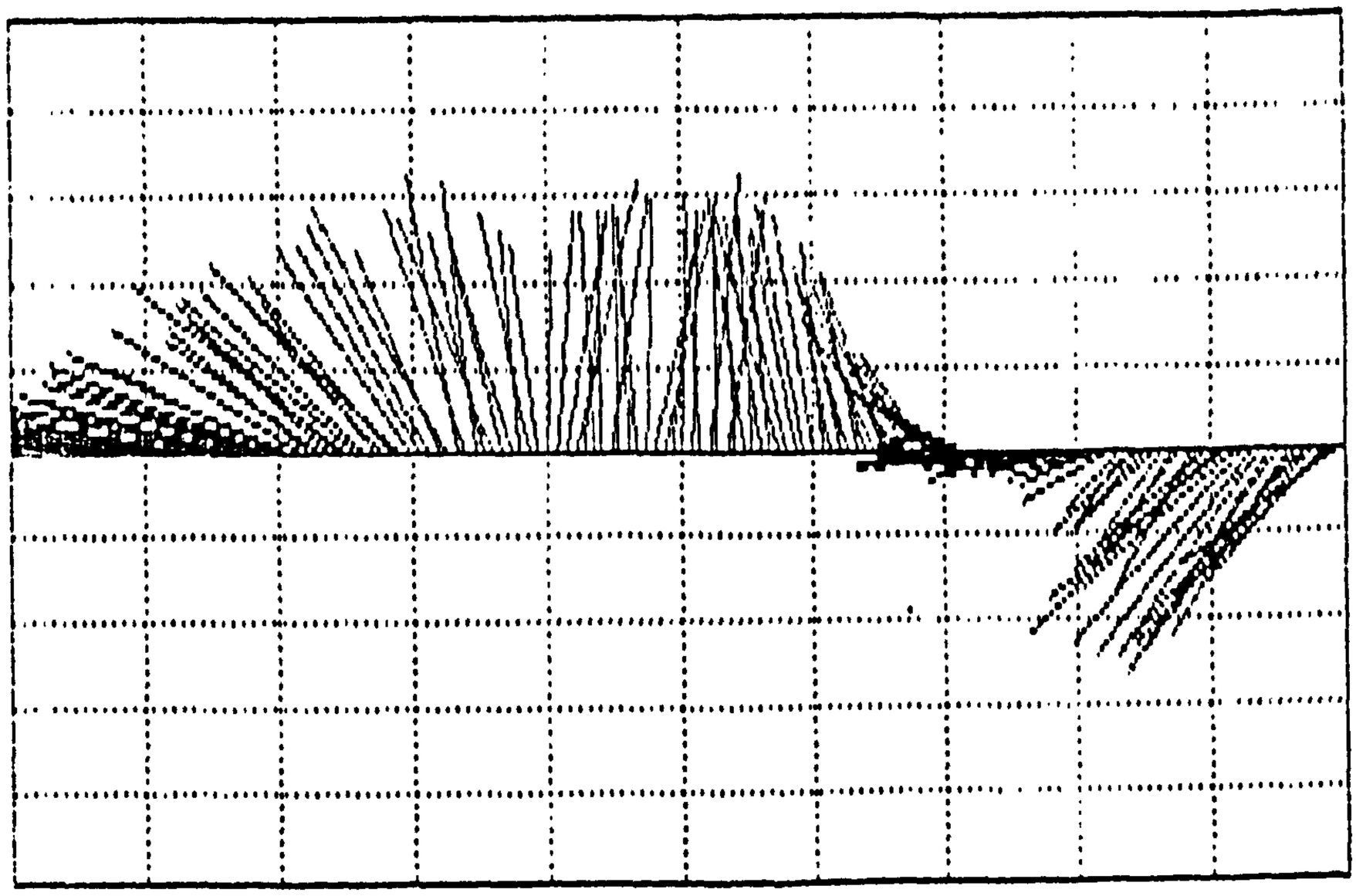

10cm/s/div

09/11/88, 00:18 09/11/88, 12:48

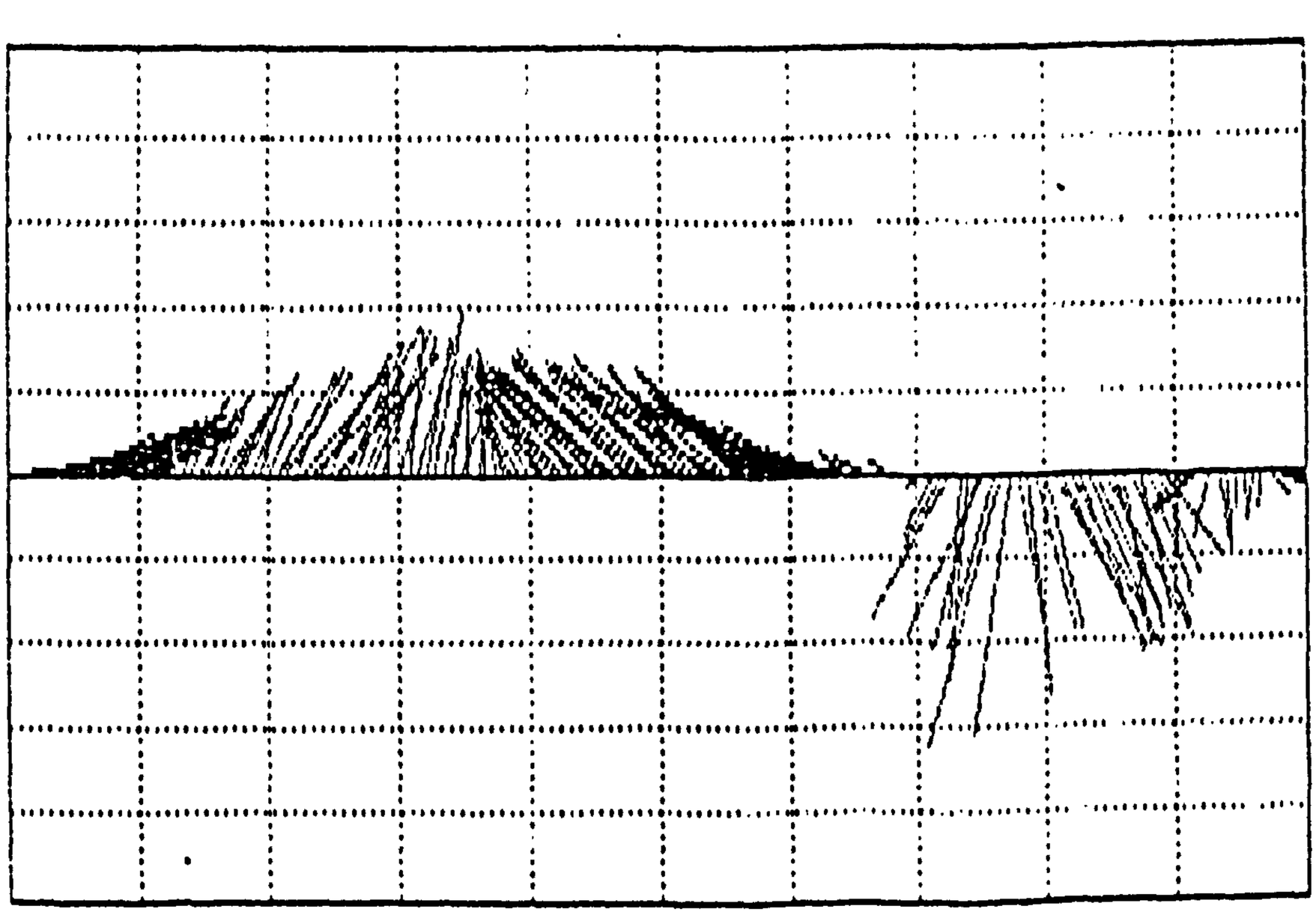

10cm/s/div

17/11/88, 20:53 18/11/88, 09:23

Fig: 4.9 Straw diagram of the velocity and direction of the tidal currents during spring (top) and neap (bottom) tidal cycles at station C2.

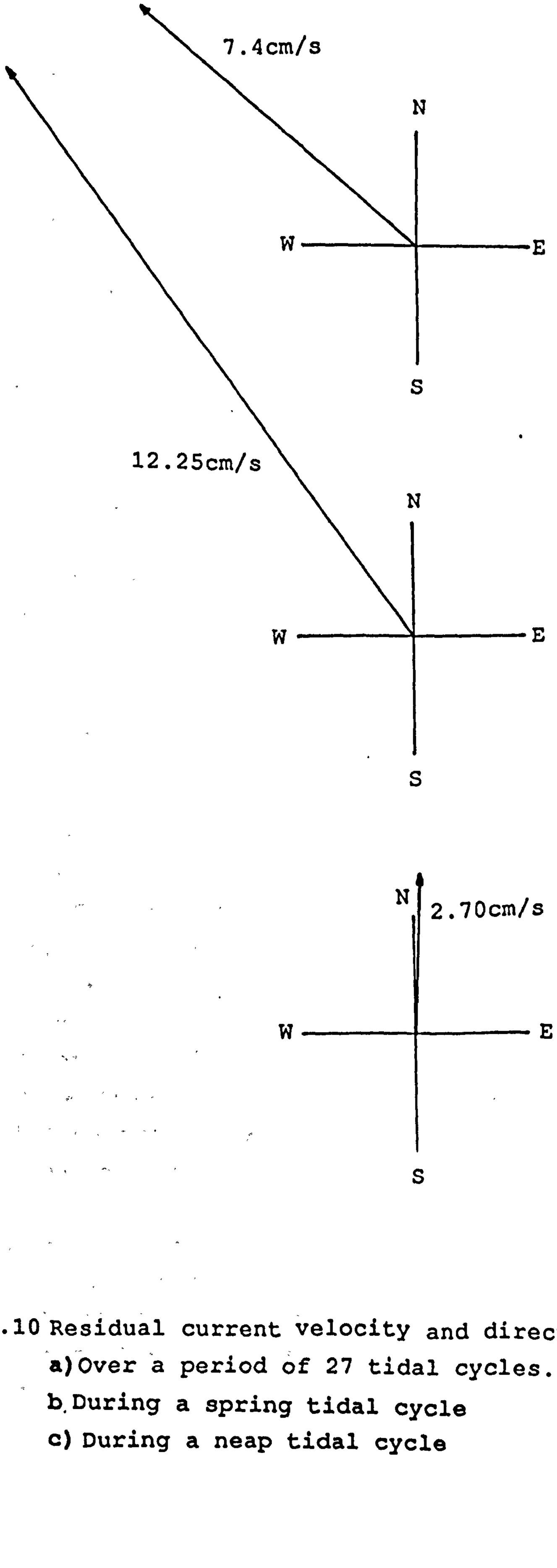

Fig: 4.10 Residual current velocity and direction at station C2.

a) Over a period of 27 tidal cycles.

b. During a spring tidal cycle

c) During a neap tidal cycle

current velocities of up to 42cm/s were recorded during the spring tidal cycles (tide Nos. 11 and 12) while the minimum weak current velocities reach as low as 11cm/s during the subsequent neap tide (tide No. 25). It appears that the maximum current velocities occur in the northeast direction which suggests that the flood currents are generally faster than the ebb currents. This phenomenon is clearly demonstrated in the Fig: 4.11a, where spring currents with a northerly component are dominant during a spring tidal cycle, this is not apparent (Fig: 4.11b) during a neap tidal cycle.

At this station, when the currents are not flowing to the north they show a strong westerly flow during a spring tide, but during a neap tide, the currents flow to the southwest with a strong southerly component. Thus during a spring tide, currents turn very quickly towards the west and flow out of Caernarfon Bay, whereas during a neap tide, as the currents are less intense and there is little flow towards the west, the currents appear to be rotating anti-clockwise during the course of the tidal cycle.

Although the above discussed data indicate thàt the stronger tidal currents flow towards the northeast, the residual currents calculated for this station (Fig: 4.12) flow in a northwesterly direction. As pointed out earlier, that during a neap tide the current pattern is markedly different from springs. Neap residual currents (Fig: 4.12c) flow towards the northeast with a magnitude of 1.68cm/s whereas the spring residual currents (Fig: 4.12b) flow towards the NW with a velocity of 11.5cm/s. The residual flow over a period of 25 tidal cycles (Fig: 4.12a) is also to the northwest though, its magnitude is less (4.35cm/s).

These results, specially those at stations C2 and C3, reveal interesting features of local and regional tidal currents. After deployment of the current meter at stations C2 and C3 it appeared that these were not the ideal locations for acquiring flow measurements in the area. However, while analysing this

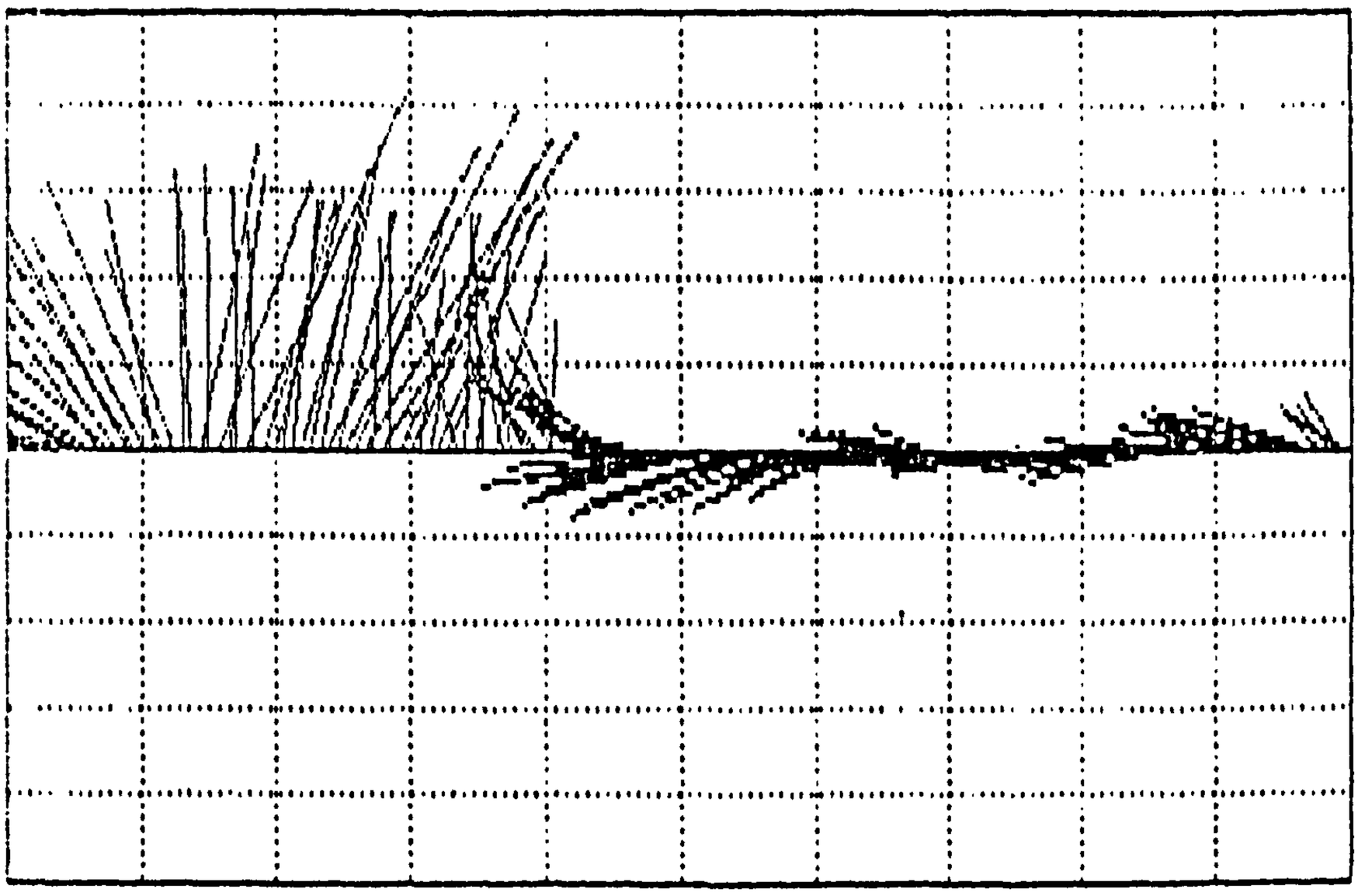

10cm/s/div

26/10/88, 04:17 26/10/88, 16:32

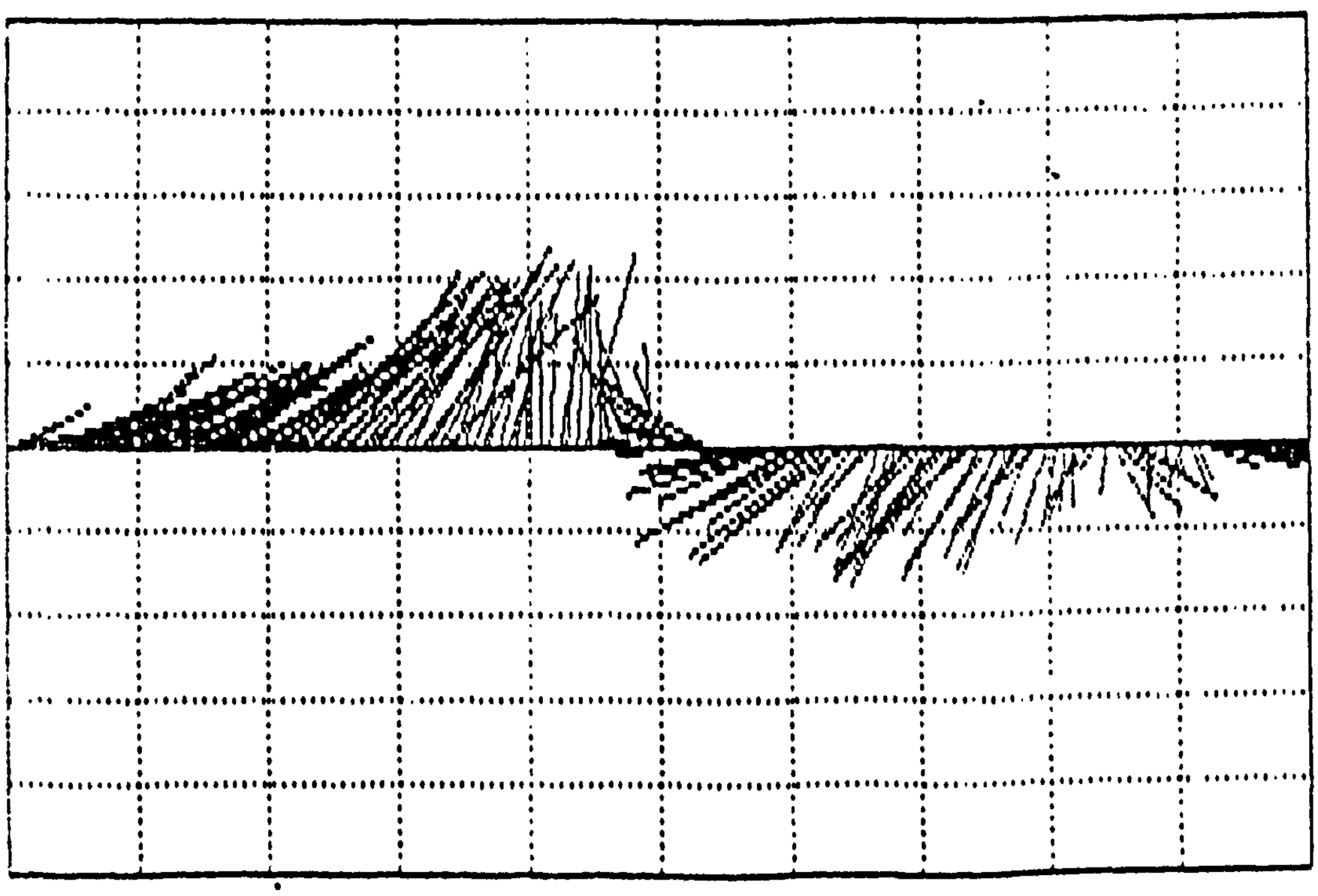

4cm/s/div

01/11/88, 20:42 02/11/88, 09:05

Fig: 4.11 Straw diagram of the velocity and direction of the tidal currents during spring (top) and neap (bottom) tidal cycles at station C3.

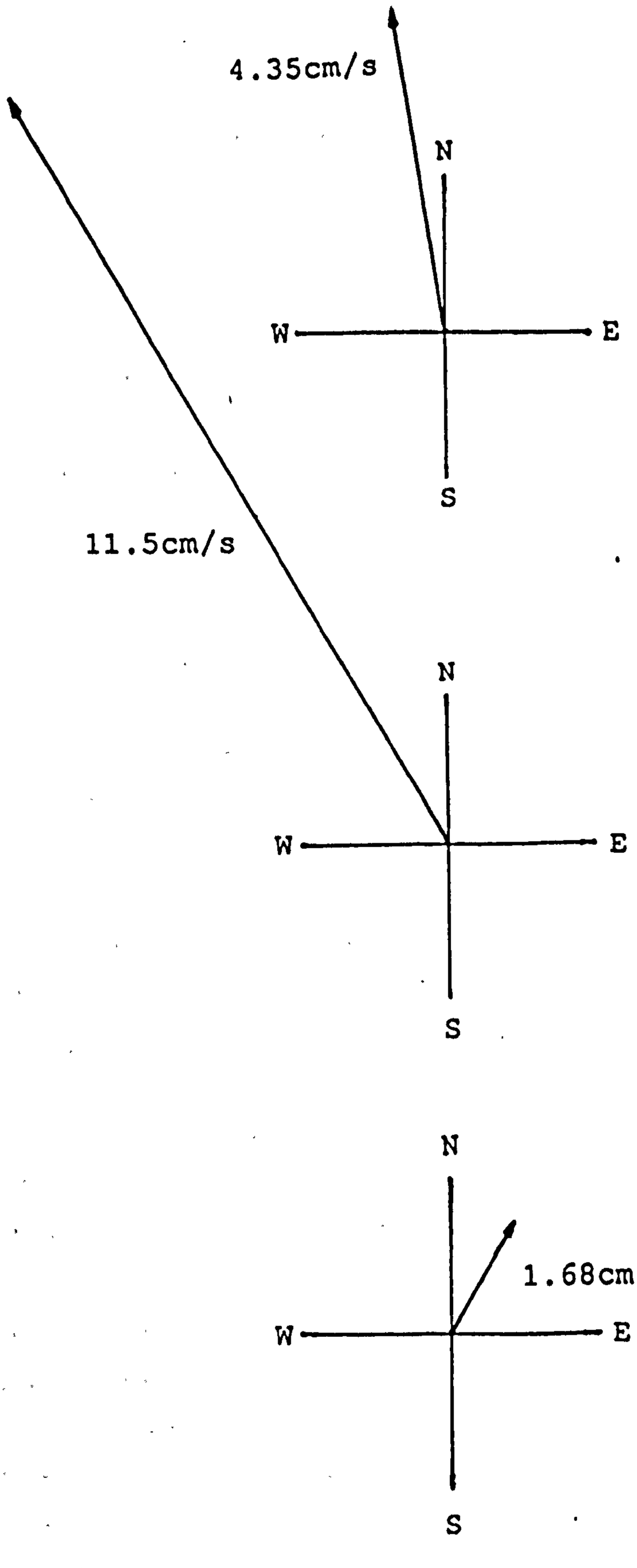

Fig: 4.12 Residual current velocity and direction at station C3.

a) Over a period of 25 tidal cycles.

b) During a spring tidal cycle.

c) During a neap tidal cycle.

data, the very low current velocities encountered at stations C2 and C3 seemed strange at first glance, but when detailed investigation was carried out, the data suggested that the area of stations C2 and C3 actually represents the zone where local and regional tidal currents interact. It appears that the tidal current velocity tends to increase on the either side of this area: towards Belan inlet it increases under the influence of local morphology while on the offshore side it increases under the influence of relatively faster regional tidal currents. On the basis of the results obtained at stations C1, C2, and C3 and station A, E, and F (current meter data for station E and F is given in appendix VI) shown on the location map (Fig: 4.4), an attempt has been made to draw a diagram of the general pattern of mid-flood and mid-ebb spring tidal currents in the area (Fig:4.13). On the basis of these diagrams some tentative points regarding the tidal current circulation in the study area can be made.

1) The tidal currents during a flood tide are generally stronger than the ebb tide currents. On the Anglesey side of the Strait, however, the ebb currents appear to be faster than the flood currents.
2) Within the Menai Strait the currents are relatively stronger on the Caernarfon side of the Strait.
3) The mid-ebb current velocity tends to decrease very quickly on the seaward side of the Belan inlet and reaches a minimum just off the main tidal sand body in the vicinity of stations C2 and C3.
4) Further offshore from stations C2 and C3 the mid tide current velocity appears to be increasing again because of the stronger regional tidal currents.
5) The mid-ebb tide currents, just after the stations C2 and C3 slowly start to turn towards the southwest and flow roughly parallel to the Lleyn peninsula coast.

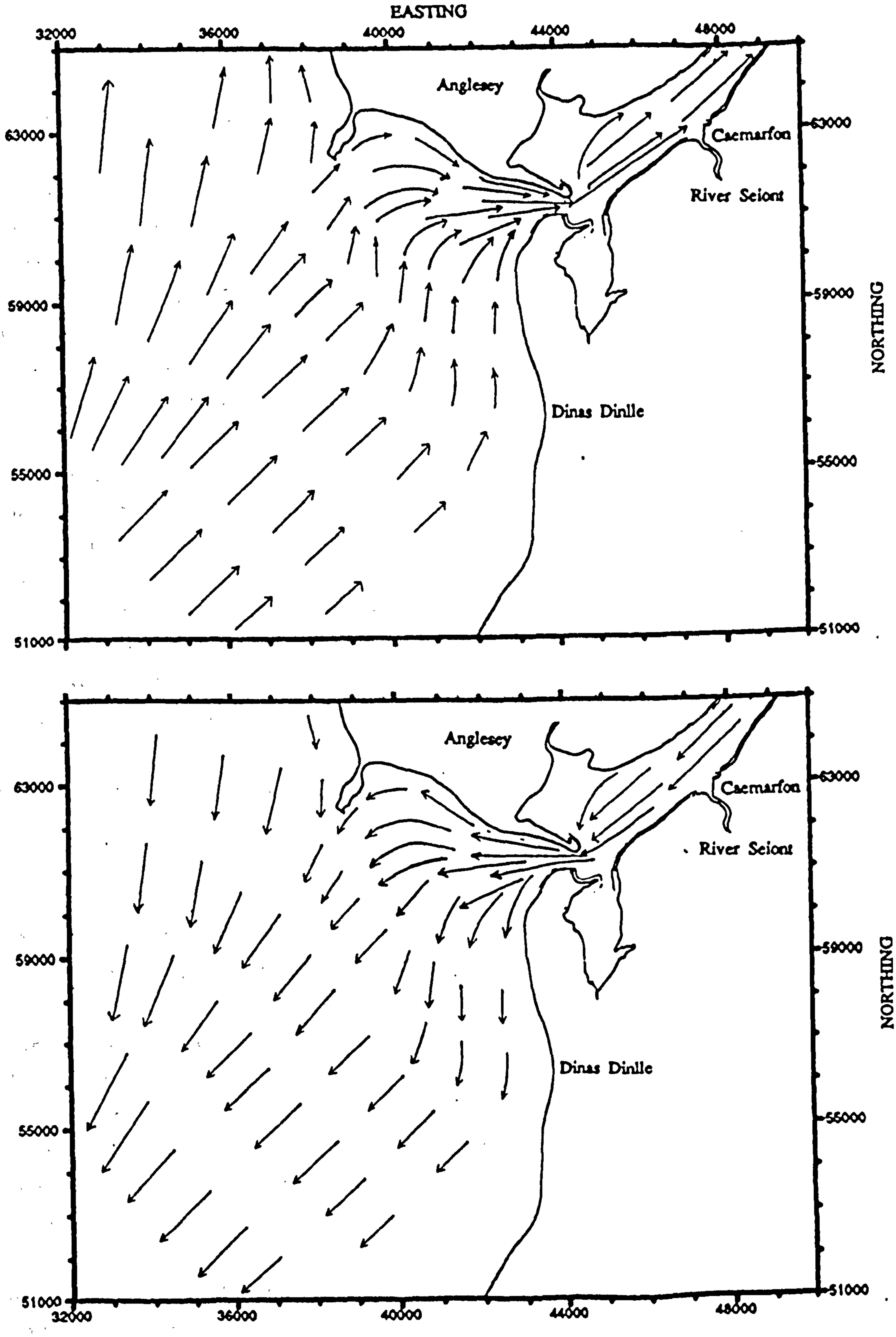

Fig: 4.13 Schematic pattern of mid-flood (top) and mid-ebb (bottom) spring tidal currents in the study area.
Length of arrow refers to the velocity of currents.
1.5cm = 100cm/s approx.

4.3 General morphology of the area.

As part of this study the general morphology of the study area has been inferred from satellite images taken by LandSat on 22 July, 1984 and various hydrographic maps. From these a diagram showing the morphology of the area has been produced and is shown in Fig: 4.14. The diagram clearly shows the Belan tidal inlet and associated sand bodies on either side of it, and a recurved spit (Aber Menai point).

The morphologies of the Belan inlet and associated sand bodies bear a general resemblance to a typical tidal inlet, as discussed by many workers (eg. Boothroyd and Hubbard (1975), Fitzgerald (1977), Hubbard (1977), Finley (1978), Hayes (1980), Imperto et al (1988), Knebel (1989), and Sha (1989)). It shows considerable diversity in its general setting and related processes. According to most of the studies referred to above, tidal inlets are formed between barrier islands along a coast, and in some instances they are related to estuaries. However, in this particular study, the Belan inlet is part of a complex morphologic and hydrodynamic system related to the main feature of study area, the Menai Strait-an open ended channel.

Through a typical tidal inlet system, almost equal amounts of water have to flow during ebb and flood tides (this statement would not hold for the inlets associated with seasonal rivers or the Menai Strait). In the case of the Menai Strait, more water flows from Beaumaris Bay into Caernarfon Bay during an ebb tide (as suggested by various studies in section 4.2). The general shape of the Menai Strait channel also does not show much resemblance to those areas usually related to a flood-tidal delta.

Within the study area the interior shoal does exhibit a flood ramp feature, from where the channel divides into two (just inside the Belan inlet where main channel and back channel are separated by sand banks). But then, instead of representing one

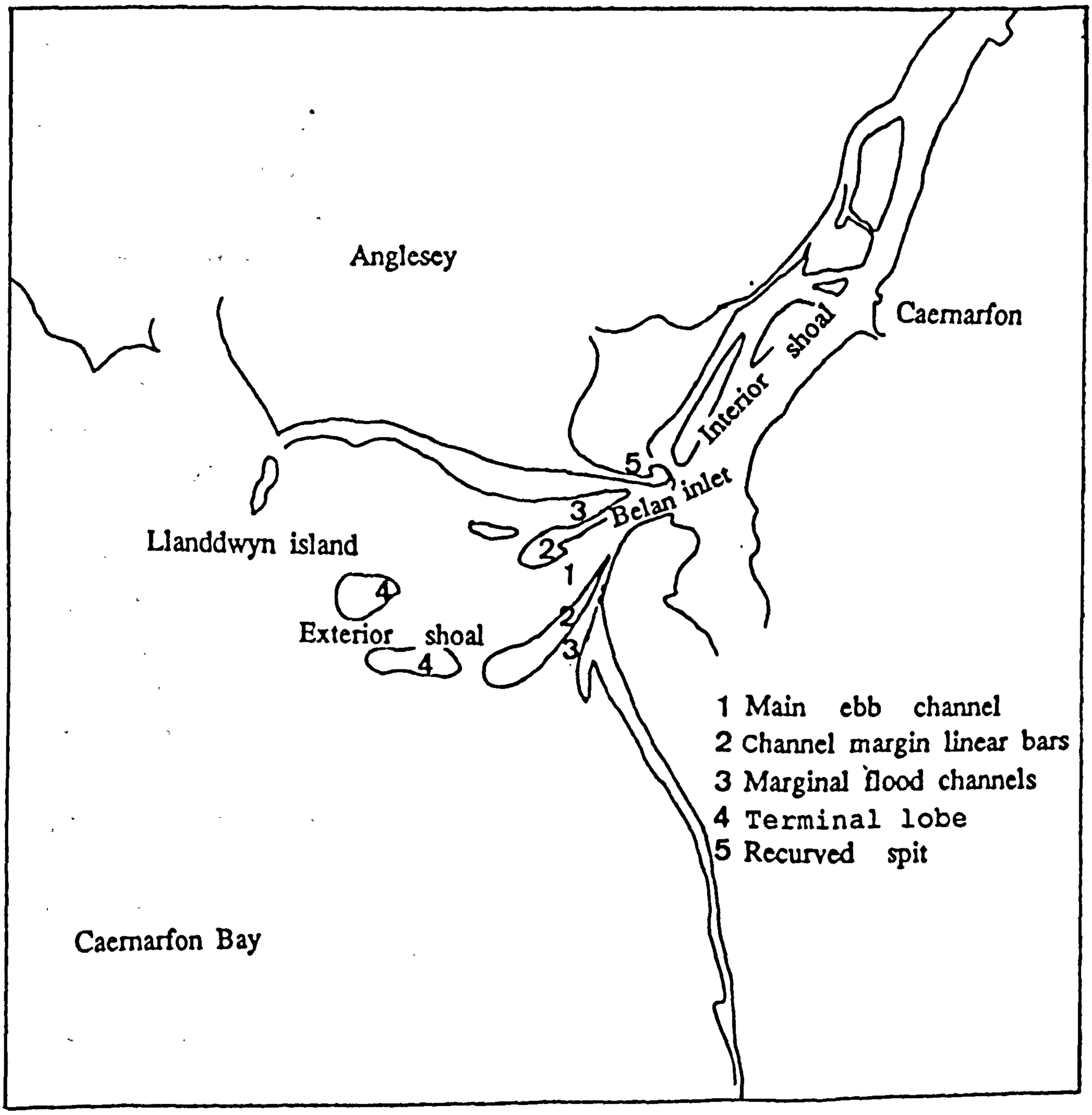

Fig: 4.14 Morphology of the Belan tidal inlet and exterior and interior shoal.

huge localised sand body with standard features, it elongates in its extent upstream, with the development of sand banks and sand ridges. The actual length of the interior shoal, starting from the Belan inlet, is nearly 6km. It also does not exhibit a well developed ebb shield and ebb spits.

However, it appears that the above mentioned diversities have very little effect as far as the general shape and extent of the exterior shoal is concerned. A detailed study of satellite images suggests that the exterior shoal does exhibit similar features to the standard model of an ebb-tidal delta described by Hayes (1980). The prominent features of the shoal include main ebb channel, channel margin linear bars, marginal flood channels, and a well developed terminal lobe (Fig: 4.14). Though the morphology of the exterior shoal in the study area appears to be similar to an ebb-tidal delta, it would be inappropriate at this stage to draw such a conclusion, without carrying out further investigations. Thus a detailed field study of the topography of these sand bodies and related channels was carried out and their findings are included in the next section.

4.4 Bathymetric studies.

In order to obtain up to-date information about the bathymetry of the area under current study, a series of echo-sounding surveys were carried out as listed in Table No. 4.3. A track chart of the surveys is shown in Fig: 4.15.

4.4.1 Equipment and procedures.

A Raytheon Model DE - 719 echo-sounder was used to obtain a continuous profile of the sea bed bathymetry. The Raytheon transducer was suspended about 0.5m into the water over the side of the vessel. At the start of the survey an echo-sounder calibration exercise was carried out by using the bar check method. This involves suspending a reflection plate at a known

Table No. 4.3

Date	Type of survey	Area covered	Position fixing
27 APR - 1 MAY 87	Echo-sounding + Side-Scan sonar	Menai Strait	Deca Trisponder system
22 JUN - 2 JUL 87	Echo-sounding + Side-Scan Sonar	Outside Belan Inlet	"
9-10 JUL 87	Echo-sounding + Side-Scan Sonar	Caernarfon Bay	Deca Navigation system
22 JUL 88	Echo-sounding + Side-Scan Sonar	Caernarfon Bay	"

Table 4.3 Details of the echo-sounding and side-scan sonar surveys carried out in the Menai Strait and Caernarfon Bay.

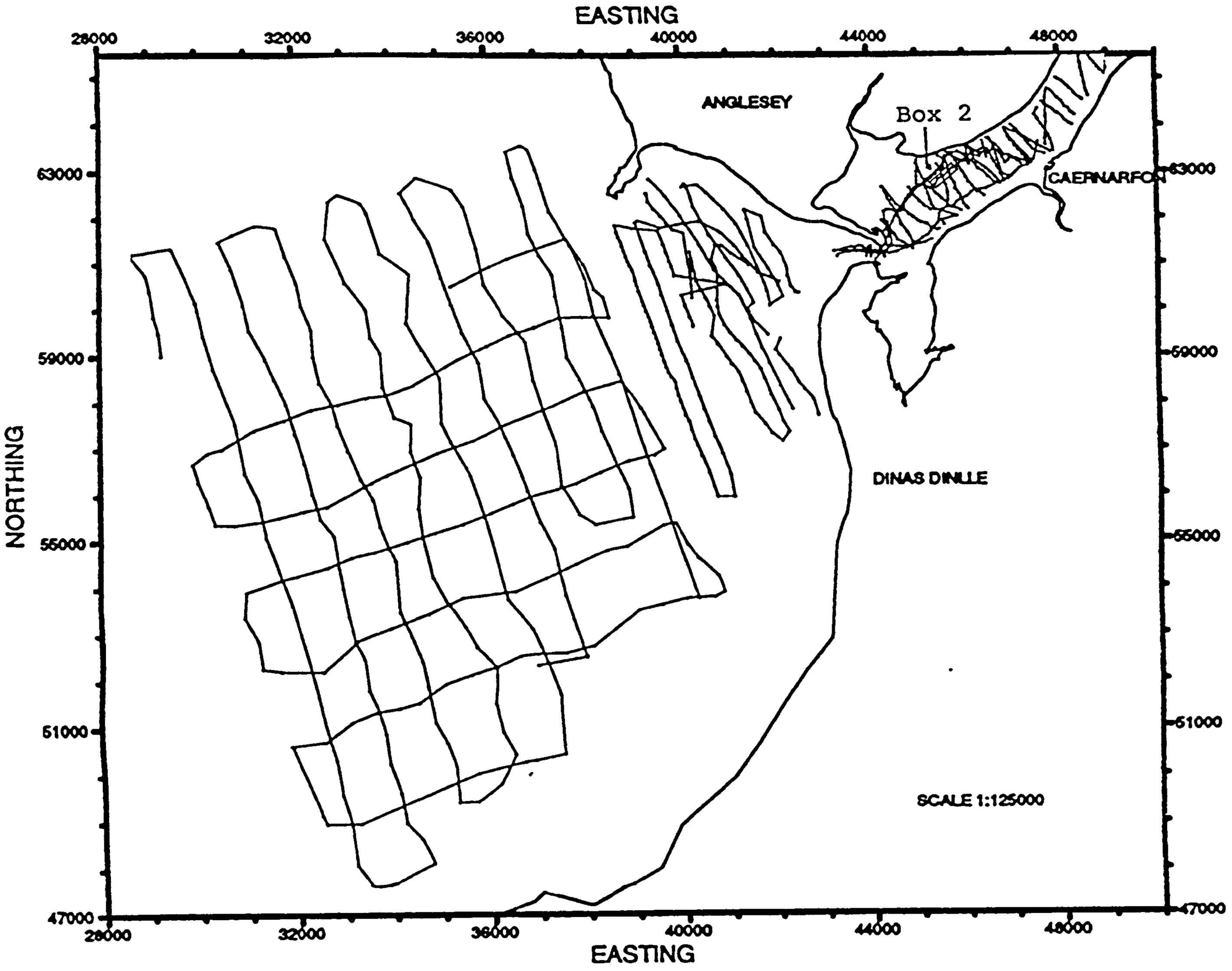

Fig: 4.15 Track chart of the echo-sounding survey.

depth below the transducer and correcting the vertical scale on the recorder accordingly. Once calibrated and in full operation the recorder produces a hard copy trace of the variation in water depth relative to the survey vessel's position.

Once all the echo-sounding surveys were completed and data was collected, interpretation of the echo-sounder records was carried out by correcting the recorded water depth for the tidal height variations. The bathymetric data was finally corrected to Ordnance Datum (Newlyn).

Equipment specifications can be found in appendix VII.

4.4.2 Bathymetric Chart.

From all the profiles obtained along the tracks shown in Fig: 4.15, a bathymetric chart of the southwest end of the Strait and Caernarfon Bay was compiled, and is presented as Fig: 4.16. The depth contours were drawn at an interval of 1m. However, at some places, particularly within the Menai Strait (eg. Fort Belan inlet), the depth variation in relatively small areas is so high that it was not possible to draw the complete sequence of 1m contours within the limits of selected scale. Therefore, in order to avoid any confusion in such areas, the contours were drawn at relatively higher intervals to show the major bathymetric features.

The most conspicuous features within the Strait are the main channel, back channel, and inter-tidal and sub-tidal sand banks and sand ridges (Fig: 4.16). The main channel runs from south of Llanddwyn Island towards the Caernarfon area. The greatest water depth along the main channel has been recorded at Fort Belan inlet, where it reaches to a depth of 25m, and the shallowest part of the channel lies northwest of Belan inlet, extending up to Llanddwyn Island and has a depth of 4m. Starting from Llanddwyn Island, the main channel initially runs parallel to the island and then to the Anglesey coast. After passing through

the Belan inlet it comes closer to the mainland coast and runs along the Caernarfon side of the Menai Strait.

Another major feature identified within the Strait, designated as back channel, runs roughly parallel to the main channel and extends from Aber Menai point to northwest of Caernarfon harbour. The maximum water depth of 11m has been recorded in the back channel just east of Aber Menai point, where a minimum depth of 3m occurs just northwest of Caernarfon harbour where the back channel meets the main channel. These two channels are separated by a flow parallel (or slightly oblique) sand ridge and sand bank.

In addition to these two channels, numerous minor channel features are also present between the sand banks. Large sand banks are situated in the northeast section of the Strait (indicated by arrows in Fig: 4.16).

Just seaward of the Belan inlet, the depth of the main channel gradually decreases and at a distance of about 3.5Km from the inlet it reaches a low of 6m. At this position , due to the presence of a large sand body in its course, the direction of the channel changes from southwest to northwest. This large sand body extends roughly from the south of Llanddwyn Island to the mainland coast near Fort Belan. It is cut by two narrow local channels, dividing it into north and south sand banks (also called Caernarfon bars), and a third sand body (preferably referred to as a flow parallel sand ridge) which extends up to the coast at Fort Belan, a distance of about 2Km.

The offshore limit of this large sand body in Caernarfon Bay is marked by the abrupt change in the contour pattern. From the 5m contour, which extends roughly from Llanddwyn Island to Dinas Dinlle beach, the water depth starts to increase relatively quickly and evenly.

Here one feature can be clearly noted: beyond the 11m contour

ANGLESEY

LLANDDWYN ISLAN

Sand banks

Back channel

Aber Menai point

CAERNARFON

RIVER SEIONT

Main channel

BELAN INLET

Caernarfon Bay

DINAS DINLLE

63000

59000

55000

51000

349000

228000

32000

36000

40000

44000

48000

O.S National grid scale 1:65000 approx

Fig: 4.16 Bathymetric chart of the SW end of the Menai Strait and Caernarfon Bay.
Contours at 1.0m interval below O.D

there is a considerable difference in the pattern of increasing depth between the northwest and southwest parts of Caernarfon Bay. In the northwest the water depth tends to increase sharply and reaches a maximum recorded depth of 31m below O.D, over a distance of about 8Km. On the other hand, in the southwest the contours are relatively widely spaced and the maximum recorded depth in this area reaches only 19m below O.D., over a lateral distance of about 4Km.

4.5 Bedform Studies.

In the current research project, the initial aims of the bedform studies were twofold. Firstly, on the basis of bedform occurrences, the aim was to obtain a preliminary understanding of the current flow paths in the southwest end of the Menai Strait and related coastal areas of Caernarfon Bay; secondly, it was intended to prepare a catalogue of occurrence, orientation, and changing pattern (under changing flow regimes of neap and spring tides and also the ebb and flood tidal currents associated with each of the above) of the bedforms.

The bedform studies described here are based upon the echo-sounding and side-scan sonar surveys listed in Table No. 4.3.

4.5.1 Equipment and procedures.

Side-Scan Sonar

An EG&G Mark 1B side-scan sonar system was used throughout the survey. The Mark 1B system consists of a dual channel graphic recorder, a transducer tow fish, and associated cables. The system can be powered by 24 volt DC batteries. The transducer fish is towed behind the survey vessel and lowered or raised in accordance with the water depth. The system is designed to produce a narrow side-ways-looking acoustic beam for examining reflection and scattering contrasts resulting from sea floor

morphology and sediment variability. During most of the current surveys the side scan beam was set up to scan an area of 125m either side of the transducer fish. The track chart of the side scan sonar survey is shown in Fig: 4.17.

Equipment specifications are given in appendix VIII.

4.5.2 Side-Scan Sonar technique and interpretation.

Side-scan sonar technique was first introduced in the U.K. in the 1950s (Leenhardt, 1974). The side-scan fish contains two sets of transducers, and these, using the acoustic beam, scan the seabed on either side (Fig: 4.18a). The acoustic beam is slightly depressed from the horizontal (10^{o} or 20^{o} depending upon the water depth and required range) in order to cover the whole distance from a point vertically below the fish to the limit of the maximum range.

An analogue side-scan record consists of a sheet of paper marked by shades of varying tonal intensity resulting from incoming acoustic signals. There are two primary mechanisms for the outgoing acoustic pulse to be returned to the sonar. These are reflection and backscatter. Reflection refers to direct echoes of sound bouncing off features and back to the sonar. Backscatter results from the interactions of the sound energy with the texture of the bottom material. If the sea floor were smooth like a mirror then no sound would get back to the sonar and side-scan would not be a very useful tool. Fortunately, no matter how smooth sea floor appears to be, there is always some roughness due to the grain size of particles which make up the bottom, whether sand, silt, clay, or gravel. The sand is rougher than silt and consequently records darker on the record. The intensity of the sound, scattered back to the sonar, is also a function of the angle of incidence. The shallower the angle, the weaker the signal.

Similar tonal variations are also caused by topographic

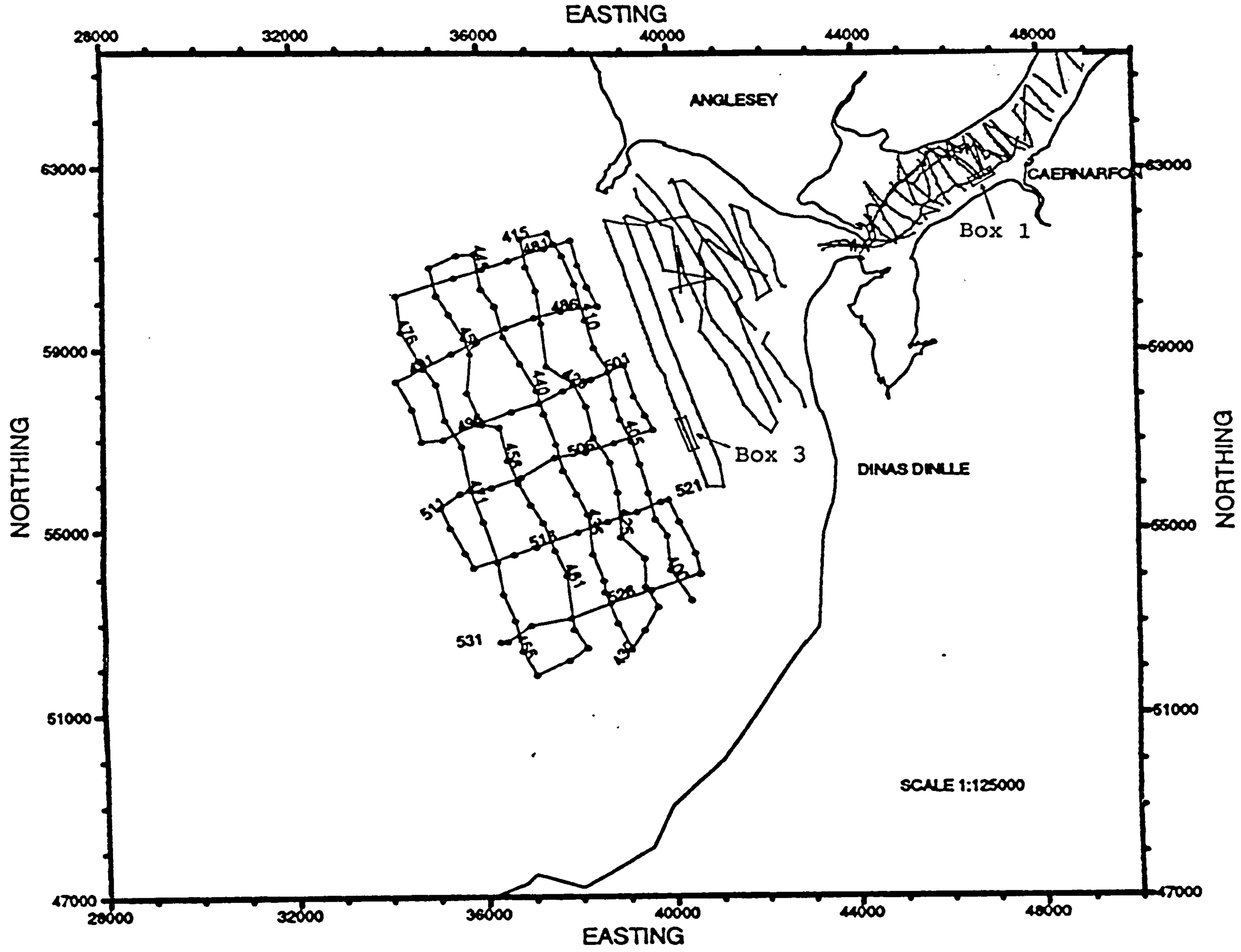

Fig: 4.17 Track chart of the side scan sonar survey

features. For example, in the case of bedforms, such as megaripples and sand waves, whilst the bedform side facing sonar beam will return strong signal and consequently record darker, the bedform side lying oblique to the sonar will return no signals and naturally be represented as a white area on the record. The projections on the seabed (such as rock or ship wreck) cause the formation of acoustic shadows on the record. A shadow is produced when something blocks the sound reaching a reflecting area on the seabed. If necessary, the shadow zone can be used to calculate the approximate height of a target above the surrounding sea floor.

In interpreting the side-scan records, in addition to observations of tonal changes, some other factors must also be taken into account which usually cause geometric distortion of sea floor features. An obvious distortion occurs parallel to the line of travel due to variable ship speeds, resulting in a compression of sonographs in this direction. Fig: 4.18b illustrates how the various geometric shapes are distorted with increasing ship speed. It shows that at about 2 knots virtually no distortion occurs. Another feature connected with the compression effect is the distortion of all linear displays. For example, a bedform, such as a megaripple or sand wave whose axis is at an angle of 45^{o} to the line of travel, records correctly at 2 knots, but records 63^{o} at 5 knots, and 74^{o} at 9 knots (Flemming, 1976).

The height of the transducer fish above the seabed causes a lateral distortion perpendicular to the line of travel. Due to the effect of this distortion the side-scan record represents an oblique distance (slant range) from the the fish to an object on the seabed. In order to determine the exact position of an object or feature relative to the line of travel, the horizontal range is calculated using Pathagoras' theorem. The horizontal range (Rh) (or better the true distance over the ground) is equal to the square root of the difference between the squares of the oblique distance (Od) and the height of the fish (Hf).

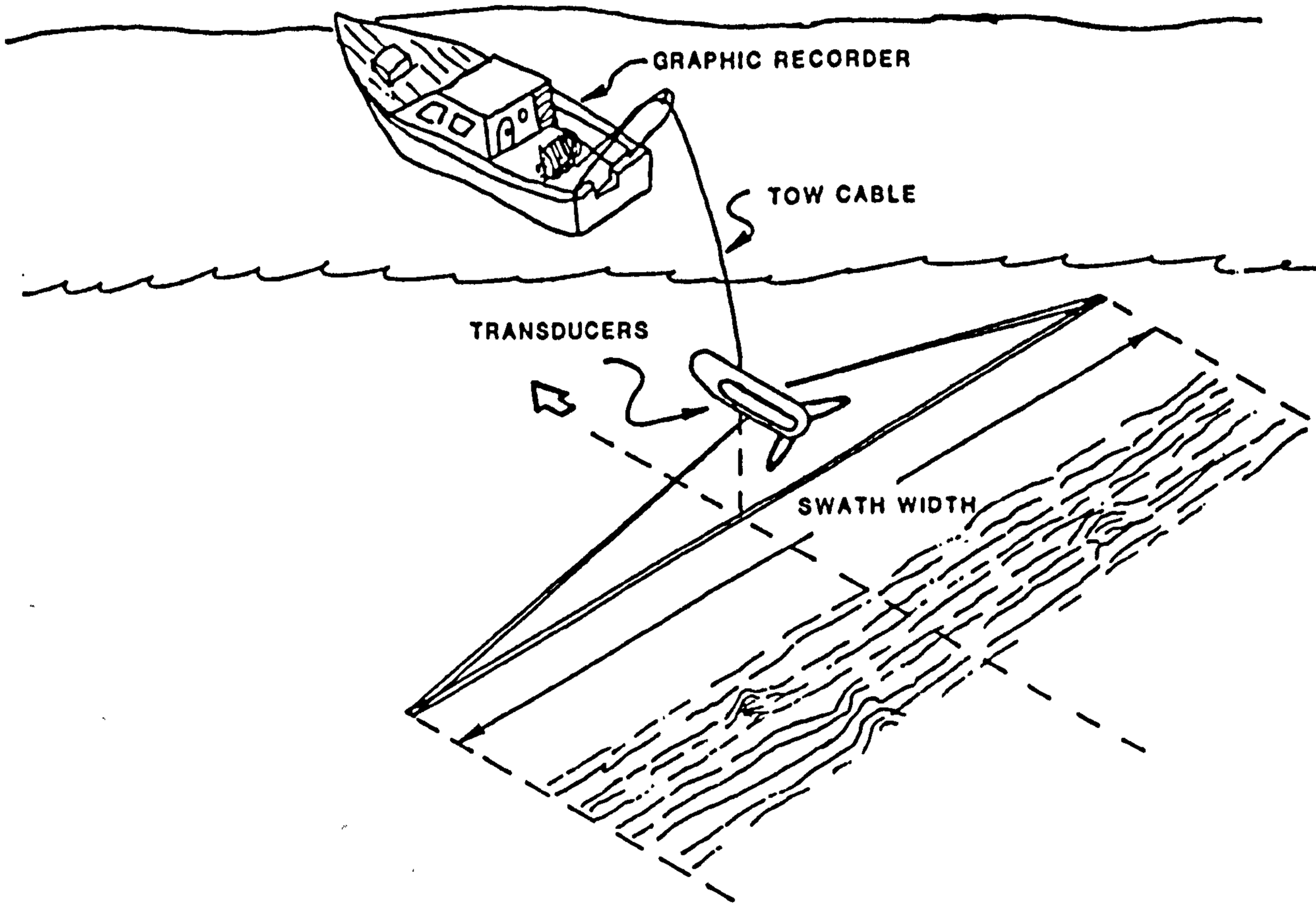

Fig: 4.18a The formation of seabed image using Side-scan sonar.

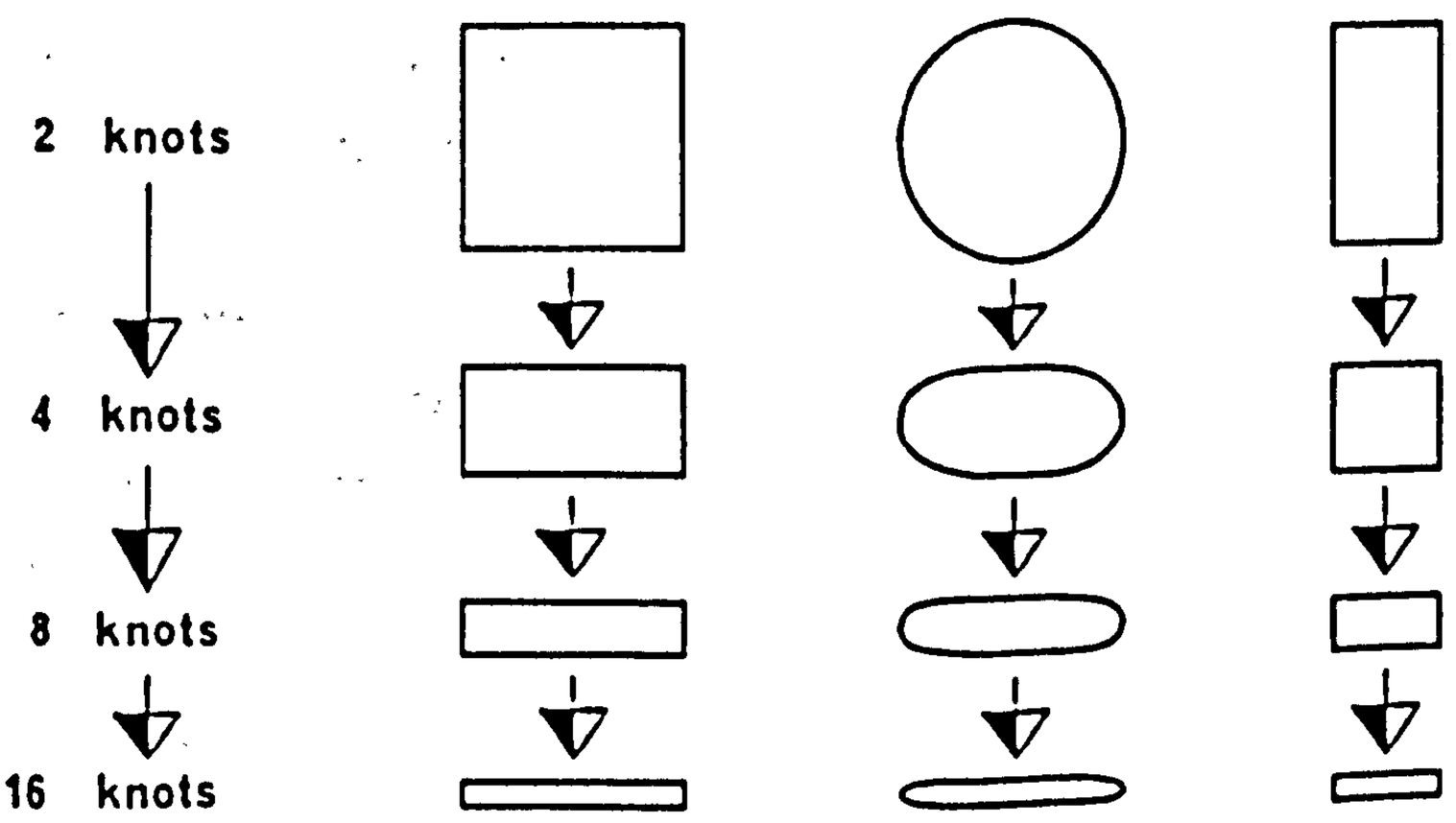

Fig: 4.18b Distortion effects on some common shapes parallel to the line of travel caused by various ship speeds (after Flemming, 1976).

Mathematically it can be written as;

$$Rh = \sqrt{Od^2 - Hf^2}$$

Sometimes however, various other distortions also occur as a result of working in rough weather conditions. Rolling of the ship, for example, alters the angle of the acoustic beam, and pitching affects the position of the fish with respect to the sea bed.

Within the study area, where water depth is very shallow in most parts, the angle of the acoustic beam was set to 20^{o}, in order to cover the maximum distance between the points on the seabed just below the fish to the limit of the maximum range. Since the aim of this survey was to map various bedform features present on the seabed within the Menai Strait and Caernarfon Bay, the interpretation of the side-scan records was carried out by correcting for variable ship speed and linear display distortions.

4.5.3 Bedform Terminology.

For the current study, Dalrymple et al's (1978) classification, which is based on the morphological characteristics of bedforms, will be used. In this classification, it has been noticed that sand waves display many similarities to type 1 megaripples. Because of the complex nature of overlapping morphological characteristics between sand waves and type 1 megaripples, it was felt that some sort of clear distinction between the two should be made to reduce any future confusion.

To distinguish sand waves from type 1 megaripples, two basic differences will be sought i.e. a higher wavelength and the presence of superimposed megaripples. Dalrymple et al suggests a maximum wavelength of 25m for megaripples, and so bedforms having higher wavelengths than 25m and/or having superimposed megaripples will be termed sand waves.

4.5.4 Bedform distribution in the area.

From all the side-scan record interpretations and aerial photographs (shown in Plates 1 & 2; for location refer to Fig: 4.24) a distribution map of the bedforms within the southwest end of the Menai Strait and in Caernarfon Bay has been produced and is shown in Fig: 4.19. The aerial photographs shown in Plate 1 and 2 were taken from an altitude of 3000 to 4000 feet during a low tide (between 18:10 to 18:35) on 19 July, 1989. Here one thing must be pointed out: most of the side-scan surveys were carried out during high spring tides (in order to maximise water depth and hence extend the areal range of the survey). Therefore, all the results must be seen accordingly. The spacing between the lines, which represents the areal distribution of the megaripple and sand waves on the map (Fig: 4.19), does not represent the wavelength of the bedform, However, their alignment approximately represents the dominant orientation of the bedform crestline.

Megaripples of various sizes, sand waves and sand ribbons have been widely identified in the area. The majority of the megaripples range in wavelength between 5-25m. However, some small scale megaripples of wavelength 1-5m also occur in the relatively deep water further offshore. Sand waves of up to 45m in wavelength have been mapped within the Strait. Sand ribbons are also one of the widely occurring features of the relatively deep water area extending further offshore from the outer limits of the Caernarfon Bay sand body.

Megaripples

Megaripples are the most common bedform recognised in the area; they occur mostly on the floors of the channels and on the sides of the sub-tidal and inter-tidal sand banks and sand ridges, the majority of them being type 1 (Dalrymple). However , in certain places, particularly over the top of the sand banks, sinuous crested and irregular shaped, (type 2) megaripples have also

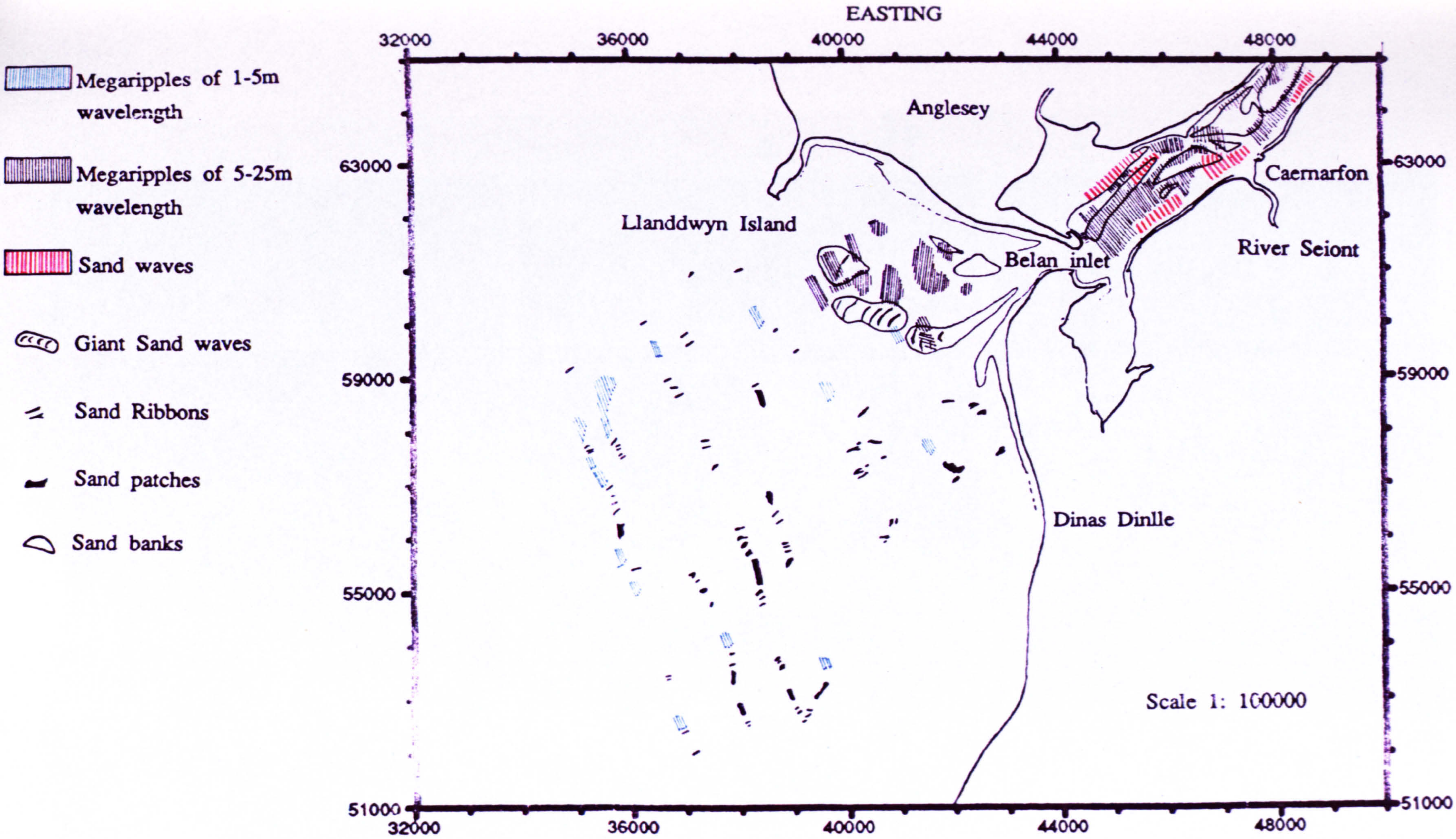

Fig: 4.19 Bedform distribution map of the SW end of Menai Strait and Caernarfon Bay.

Aerial photographs A, B, C (Plate 1) and D, E, F (Plate2) showing bedforms on inter-tidal and sub-tidal sand banks present in the Menai Strait.

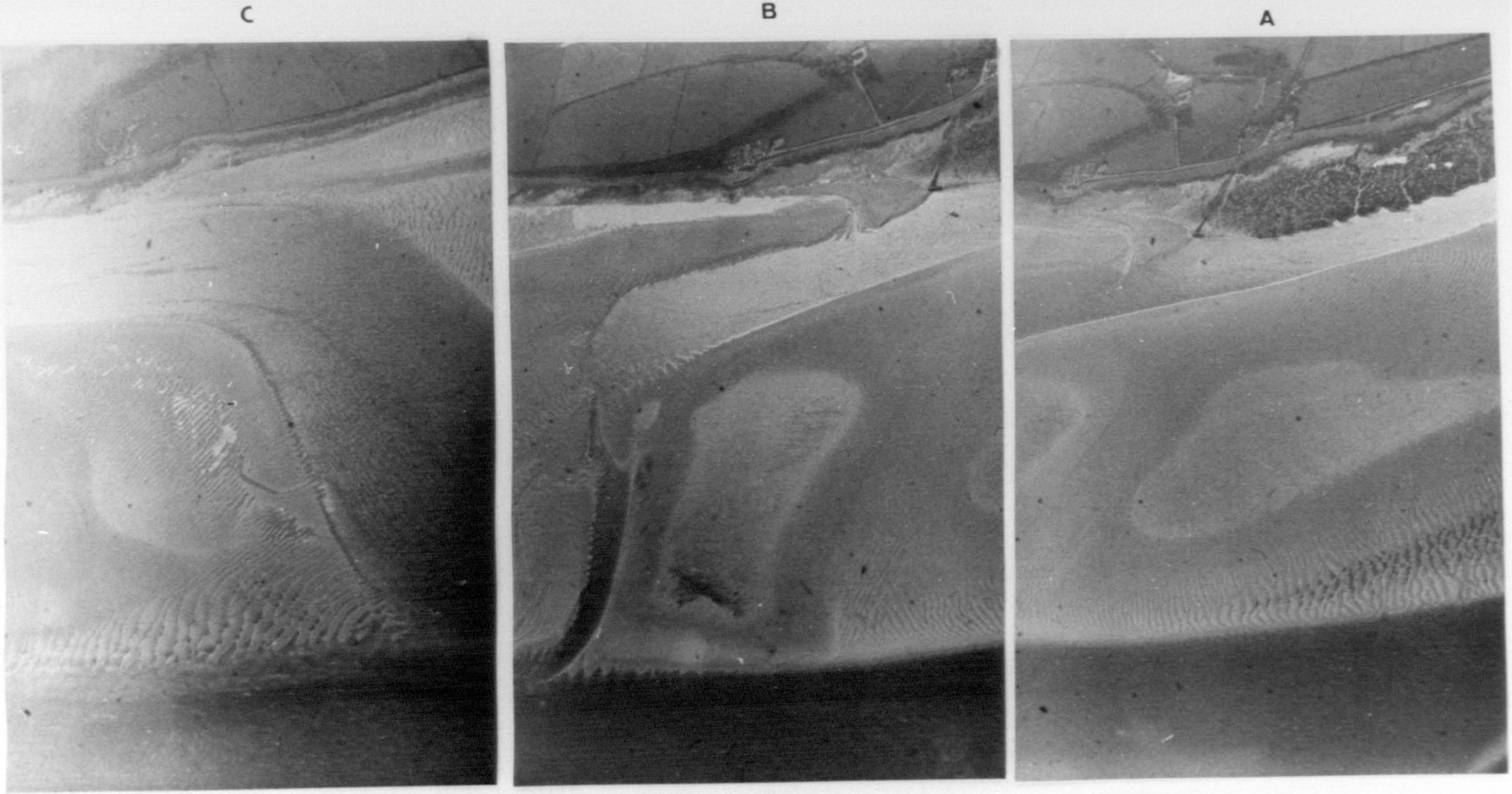

PLATE 1

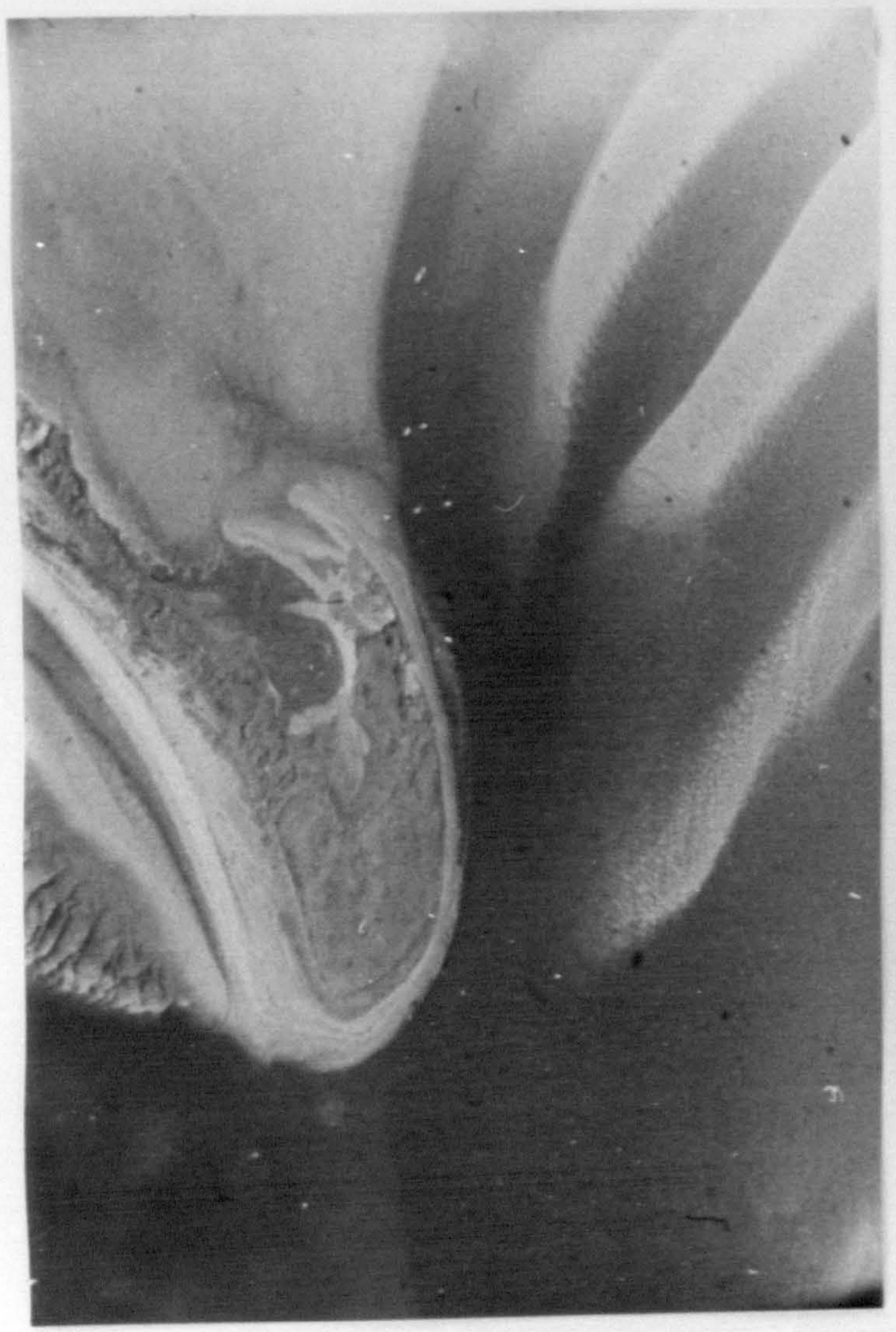

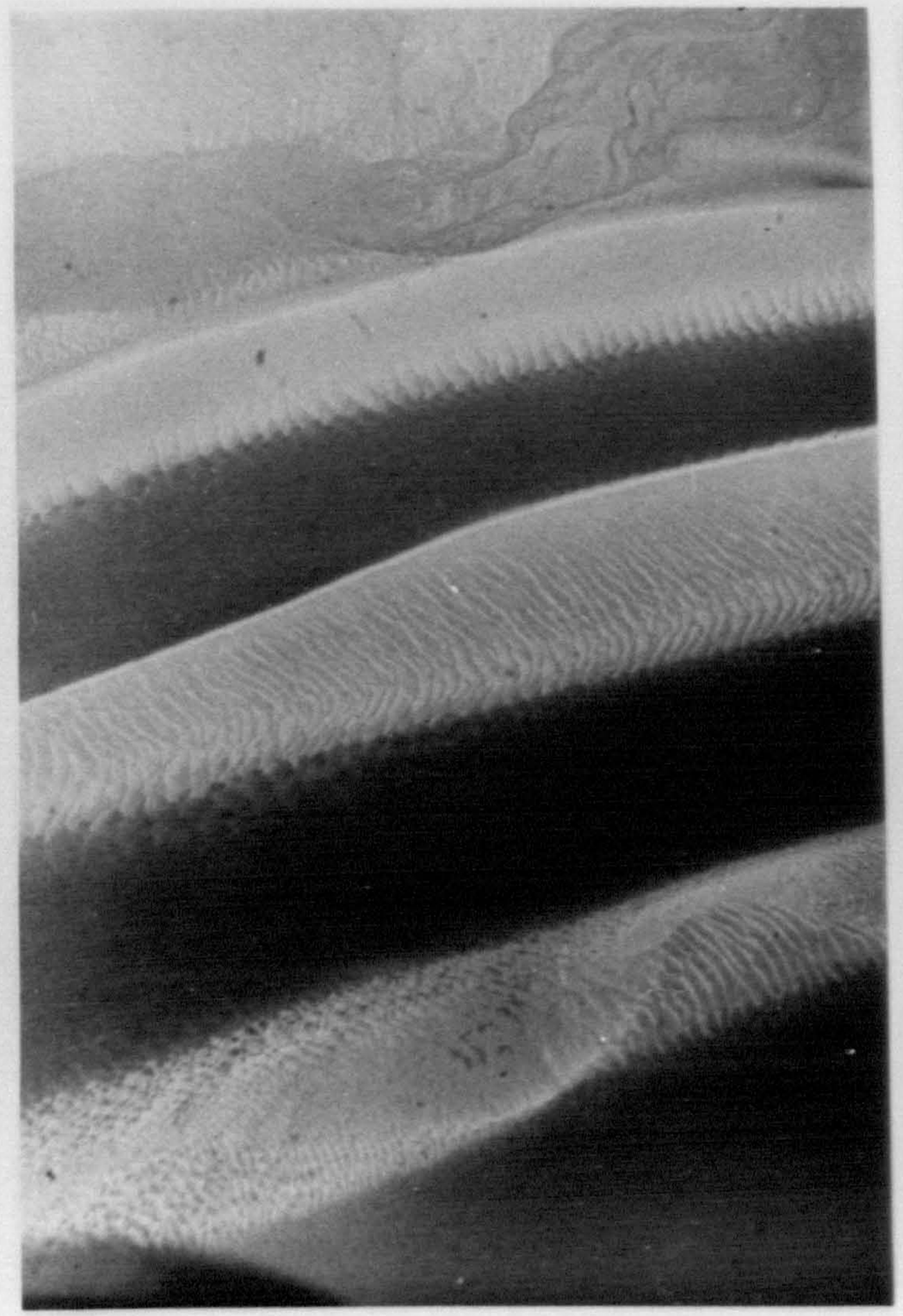

PLATE 2

been noticed (visual observation by the author). Type 2 megaripples were also reported by Jones (1984) in the vicinity of large sand banks occurring opposite and northeast of Caernarfon harbour.

Megaripples in the area range in size from 1 to 25m wavelength. These were further divided into small scale (1-5m wavelength) and large scale (5-25m wavelength) megaripples. This distinction was made purely on the basis of the occurrence of each megaripple set in a particular environment. For example, large scale megaripples predominantly occur in the relatively shallow, sandy, and hydrodynamically more active part of the study area. In contrast, the small scale megaripples are found in the relatively deep water extending from just seaward of the large sand body in Caernarfon Bay to further offshore. They usually occur in isolation as a small megaripple field. The majority of these fields appears to lie within the inferred course of the main channel. However, some scattered fields have also been identified in the southwest portion of the study area outside the main channel.

Large scale megaripples are the common bedform feature inside the Menai Strait and are almost equally well developed in the extension of the main channel outside Belan inlet. Throughout the study area, with a few exceptions, megaripples seem to be asymmetrical, with long, straight to sinuous crests in form. (The side-scan record shown in Fig: 4.20 is an example of the above type of bedform)

Sand waves

Sand waves predominantly occur in the areas surrounding the main and back channel within the Strait. In total, five sand wave fields have been identified, of which three are associated with the main channel course and the other two lie in the vicinity of the the back channel. The echo-sounder record showing the sand waves from the main channel area is included as Fig: 4.21. The occurrence of sand waves is not only restricted

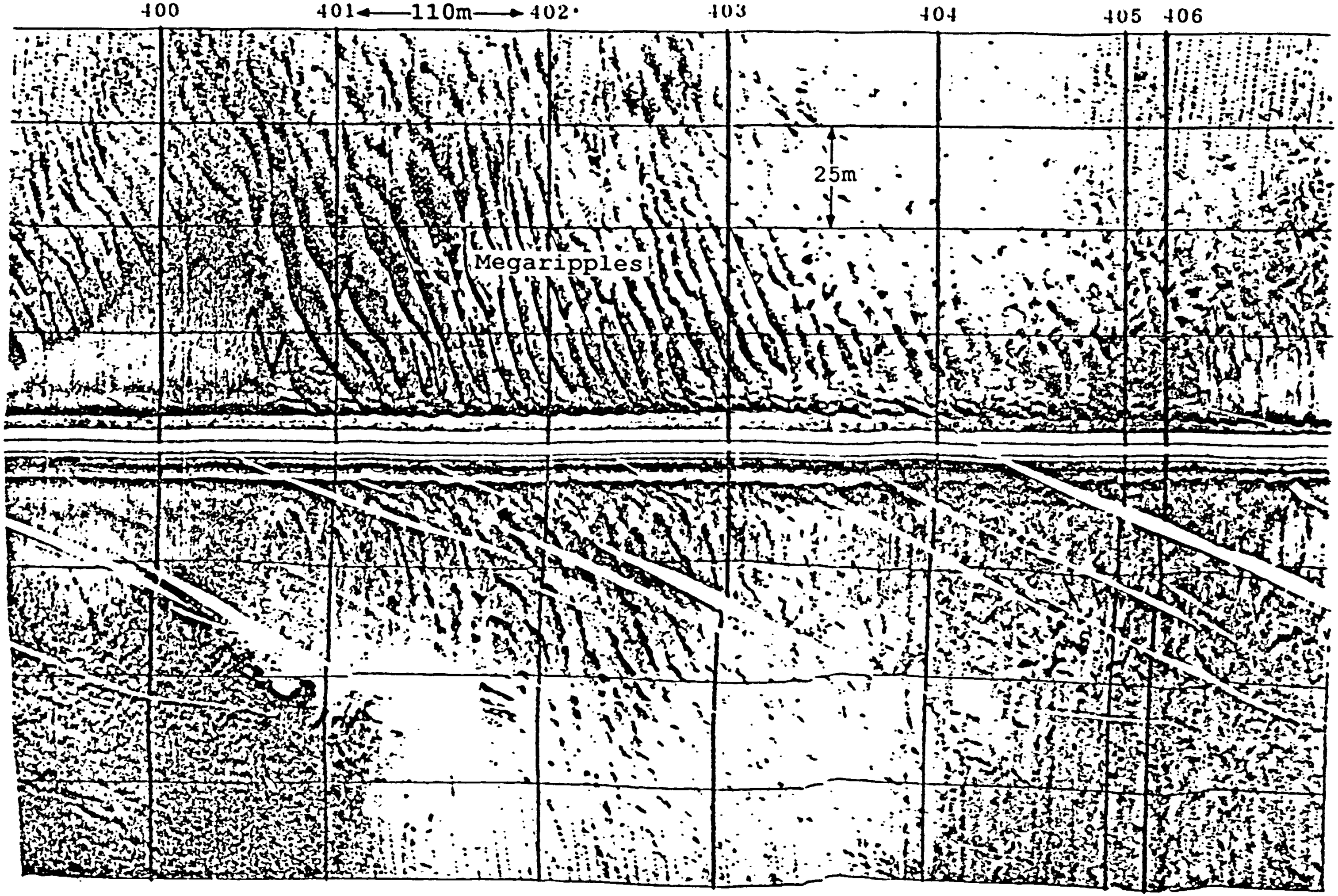

Fig: 4.20 Sonograph showing type 1 megaripples (location is marked as Box 1 in fig: 4.17).

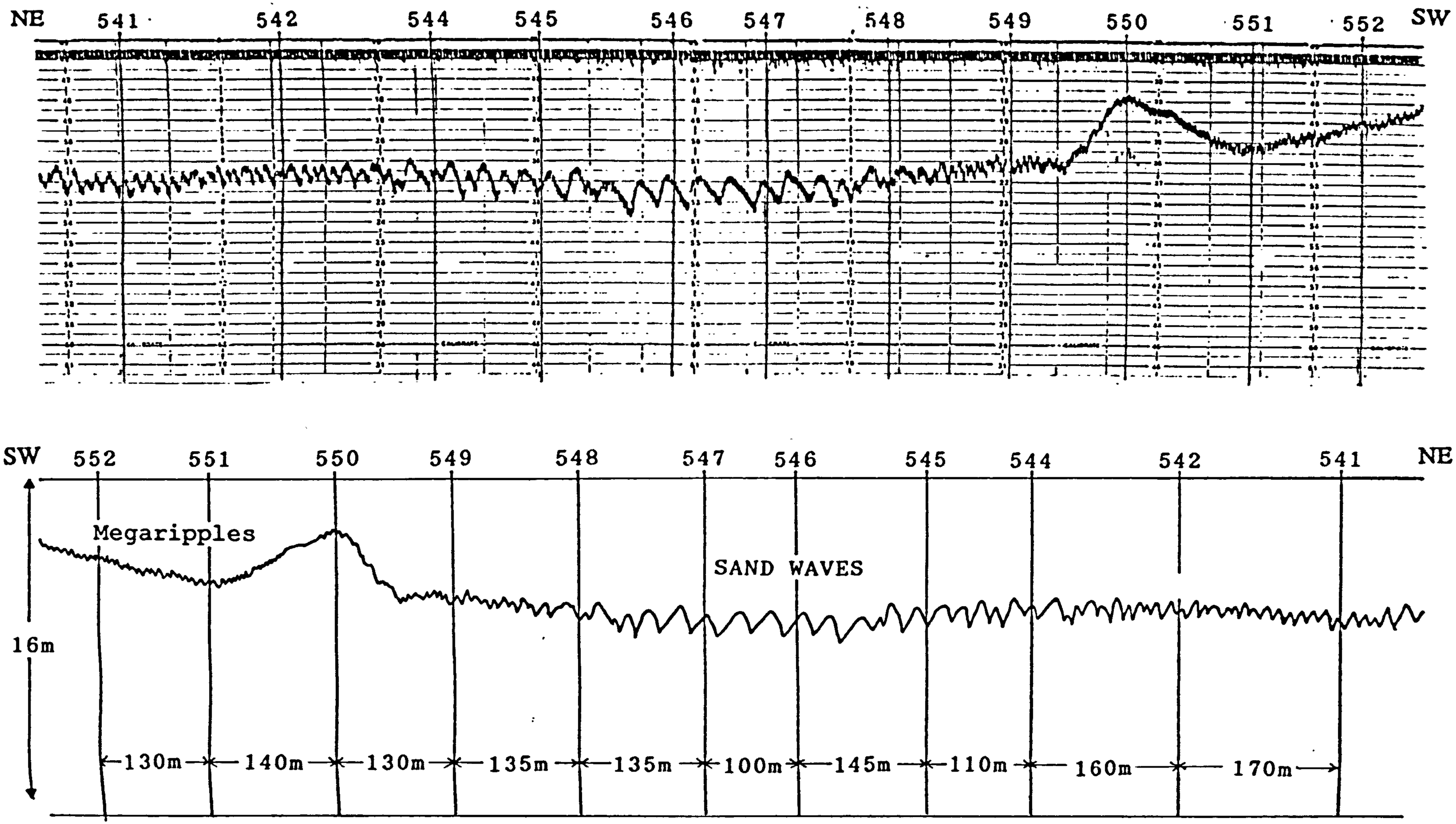

Fig: 4.21 **a.** Echo-sounder profile over sand waves and megaripple.
b. Interpreted diagram of the same record.
(location is marked as Box 2 in Fig: 4.15)

to the floor of the tidal channels. Some sand waves also extend over the sides of sand banks and sand ridges. An example of this kind can be seen in Plates 1 and 2. (For location of these photographs see Fig: 4.24)

Though the majority of the sand waves do not have superimposed megaripples, sand waves with superimposed megaripples have been encountered at two places (the NE and SW sand wave fields in the main channel). Virtually all the sand waves are asymmetrical, relatively long, with straight to sinuous crests and have a general height of 1m or less.

Sand ribbons

Sand ribbons up to 250m long and 30m wide have been mapped in the relatively deep water area of Caernarfon Bay and appear to be scattered in a wide zone extending just seaward of the main sand body. Fig: 4.22 shows an example of how such a bedform feature appears on a sonograph. The sand ribbons found in the area are covered with evenly spaced symmetrical to asymmetrical, long and straight crested megaripples of 1-2m wavelength.

4.5.5 Temporal variations over a neap-spring cycle.

The aim of this exercise was twofold. Firstly, to find out changes in the behaviour of bedforms under varying flow regimes resulting from the spring and neap tidal variations. Secondly, to see how these bedforms are responding to the changing flow conditions during flood and ebb tidal currents during one particular tidal cycle, i.e. whether any change is occurring in their size, shape, orientation and direction of movement, which could help in the final assessment of the direction of the net sediment transport in the area.

To achieve the above aims a series of surveys was carried out on a chosen line (Fig: 4.24) in the main channel extending from Llanddwyn Island to the northeastern limit of the study area (in the Menai Strait). The surveys were conducted on 23/8/88 (neap

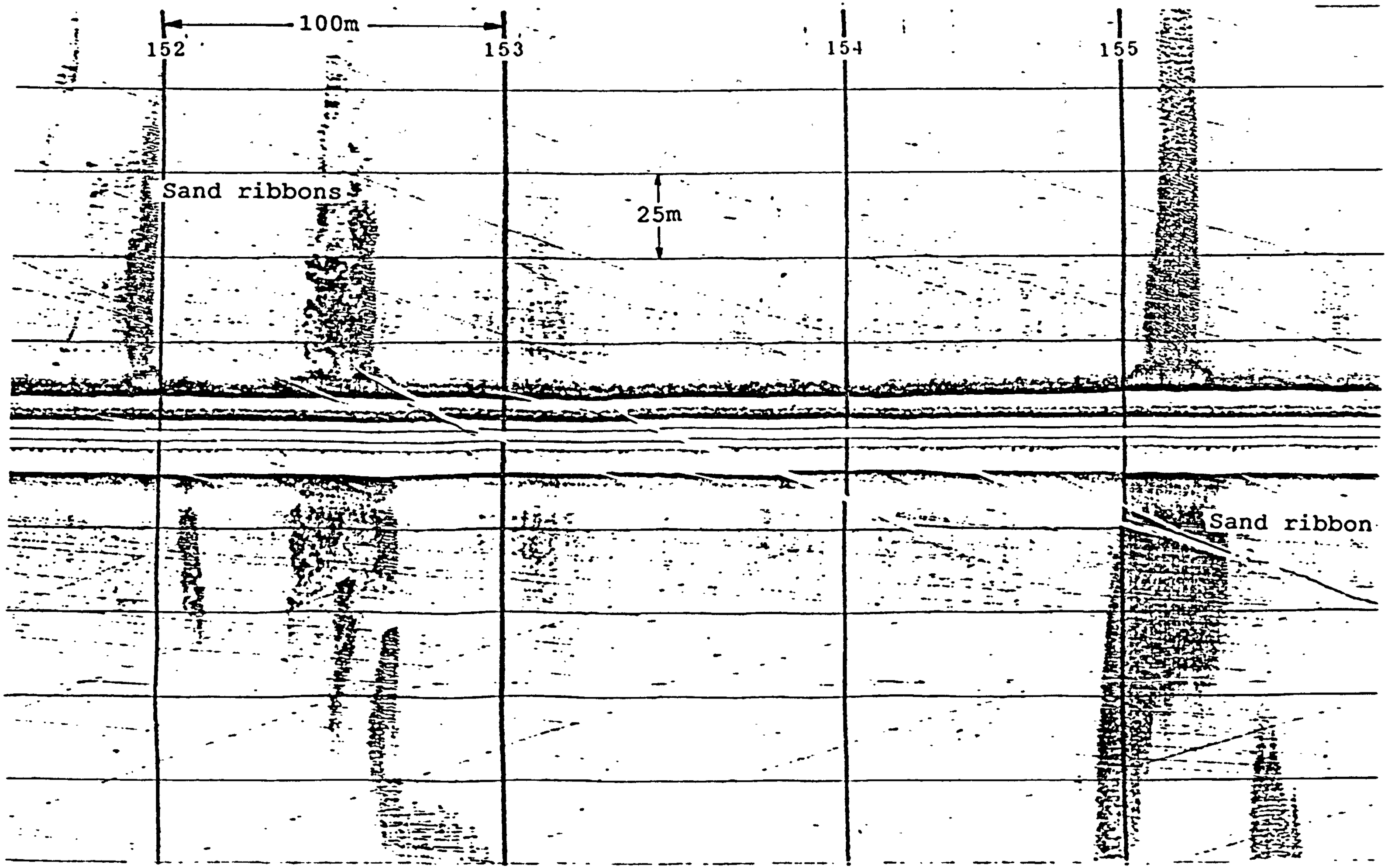

Fig: 4.22 Sonograph showing example of sand ribbons in the area.
(location is marked as Box 3 in fig: 4.17)

tide) and 30/8/88 (spring tide). The graph of the predicted tidal heights (from the Unit for Coastal and Estuarine Studies, UCNW Bangor), relative to chart datum at Caernarfon, for the above dates are shown in Fig: 4.23. Echo-sounding and pinger sub-bottom profiling systems were used simultaneously to collect the data.

The purpose of using the pinger sub-bottom profiler, in this particular exercise, was to acquire some knowledge about the thickness of the surficial sediment layer, and also to observe any changes occurring in its thickness during different tidal states.

During each (spring and neap) tidal cycle, the chosen line was surveyed twice; at high water and low water. UCNW's research boat "Lewis Morris" was used for the above surveys.

Results.

It would take considerable space to present the results of 4 different surveys of the complete survey line. Hence four echo-sounder sections A, B, C (within the Strait), and D (outside the Belan inlet), and two pinger sections E and F (also within the Strait) were selected from the repeated line for presentation and description. The location map of the echo-sounder and pinger sections is shown in Figs: 4.24 and 4.25, respectively.

Because of rough weather conditions and the very low water depth during low water at maximum springs, it was not possible to extend the survey up to Llanddwyn island and complete the line as planned. Consequently, the data remains incomplete and no sections have been selected for the survey line beyond the Belan inlet (except the echo-sounding section D).

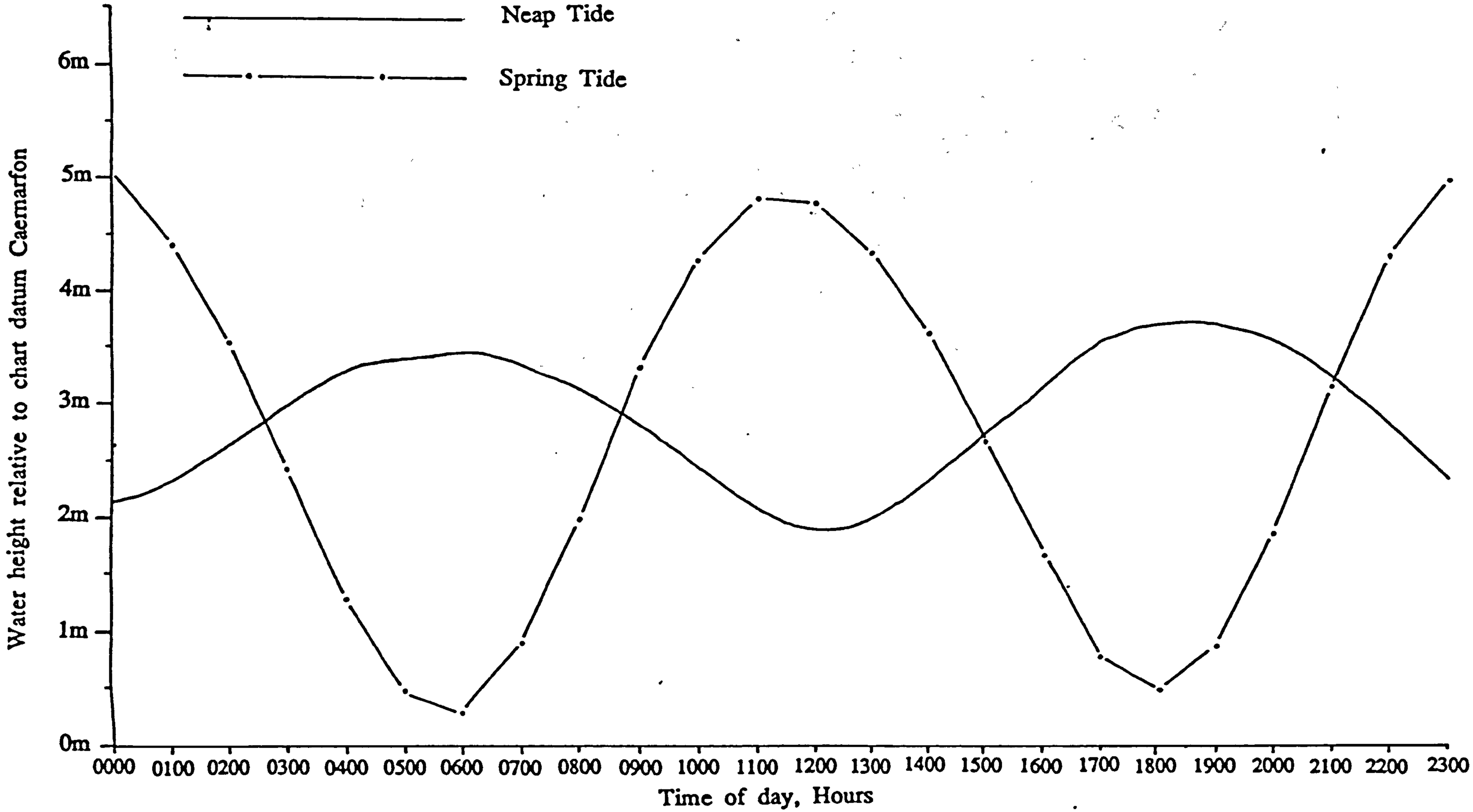

Fig: 4.23 Predicted tidal heights for 23/8/88 (neap tide) and 30/8/88 (spring tide) relative to chart datum Caernarfon (O.D. +2.722m).

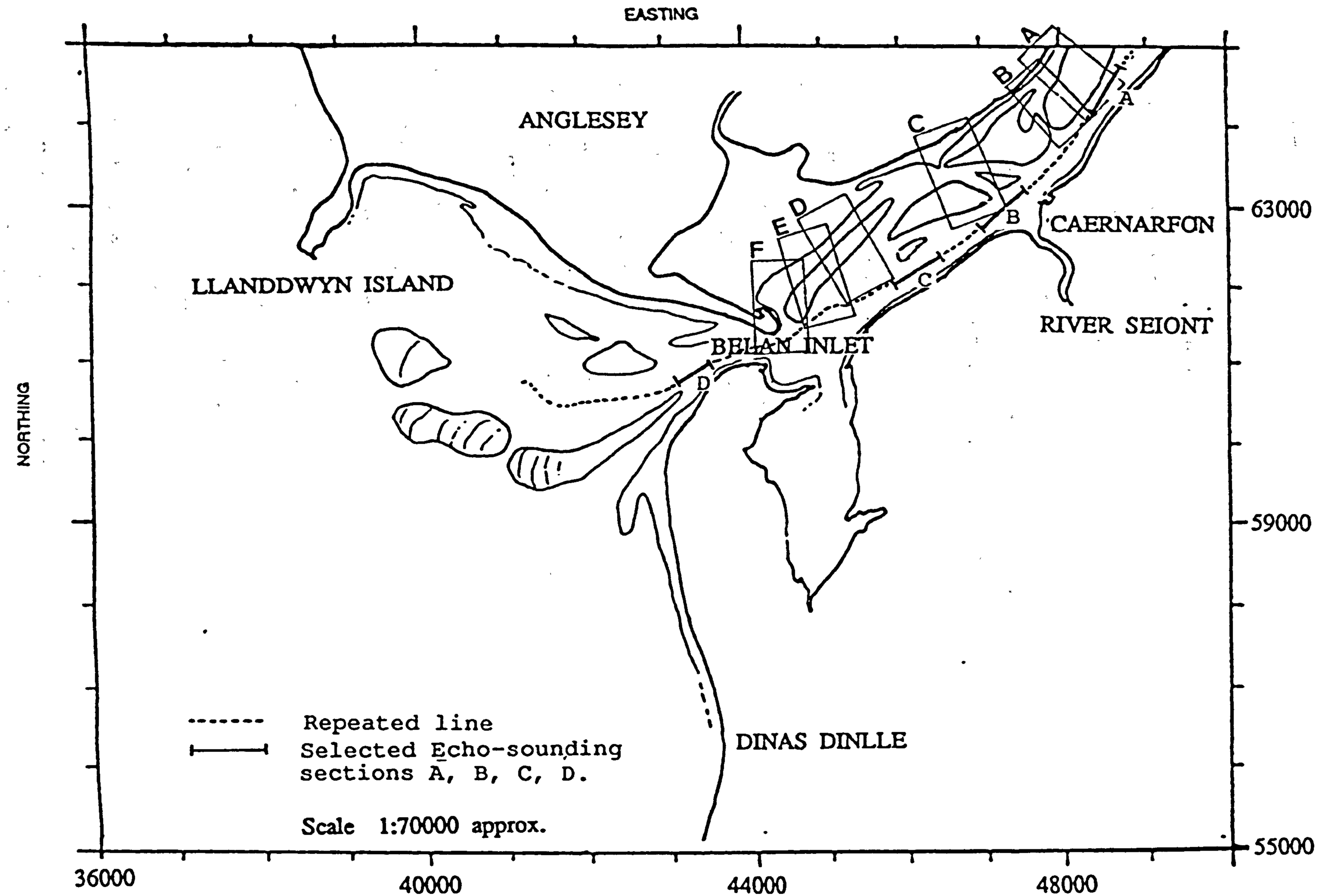

Fig: 4.24 Location map of a) the repeated line in the main channel and b) aerial photographs A, B, C, D, E, F (shown on plate 1 and 2).

Pinger results (sections E and F).

Two pinger sections E and F (for location see Fig: 4.25) were selected from the repeated line data to include here. These two areas were selected because they represented the best seismic record quality and gave an overall clearer picture of the surficial layer. The interpreted diagrams of sections E and F are shown in Figs: 4.26 and 4.27 respectively. An example of the raw pinger records (related to low and high neap/spring tidal cycles) is also presented in Fig: 4.26.

The water depth was corrected to Ordnance Datum (Newlyn). The thickness of the surficial sediment layer was calculated, using a seismic velocity of 1750 m/s. This velocity appears to be slightly higher for the surficial sediments; however, keeping in view the actual thickness of the layers (maximum 8m) involved here, the difference can be treated as insignificant.

From a first glance at the interpreted pinger results of sections E and F, it appears that substantial changes occurred in the thickness of the surficial sand, presumably as a result of changes in flow regime. For instance, interpreted section No. E4 (high spring (Fig: 4.26)) shows a variation of about 5m in thickness of surficial sand, relative to other sections (Nos. E1, E2, and E3). The same is true for the interpreted section No. F4 (high spring (Fig: 4.27)). After plotting the location of each survey line (Fig: 4.25) on a large scale map, it was noticed that the track lines of the individual surveys did not cover the exactly same area. A maximum displacement of 100m between the tracks, is apparent. However, the average displacement remains about 50m or less. The abrupt and substantial change in surficial layer thickness could probably be linked to the above effect. The larger displacements have been observed in the tracks of high and low springs and it could, perhaps, be an effect of relatively strong tidal currents on the course of the survey vessel. However, high and low neap tracks are reasonably close to each other.

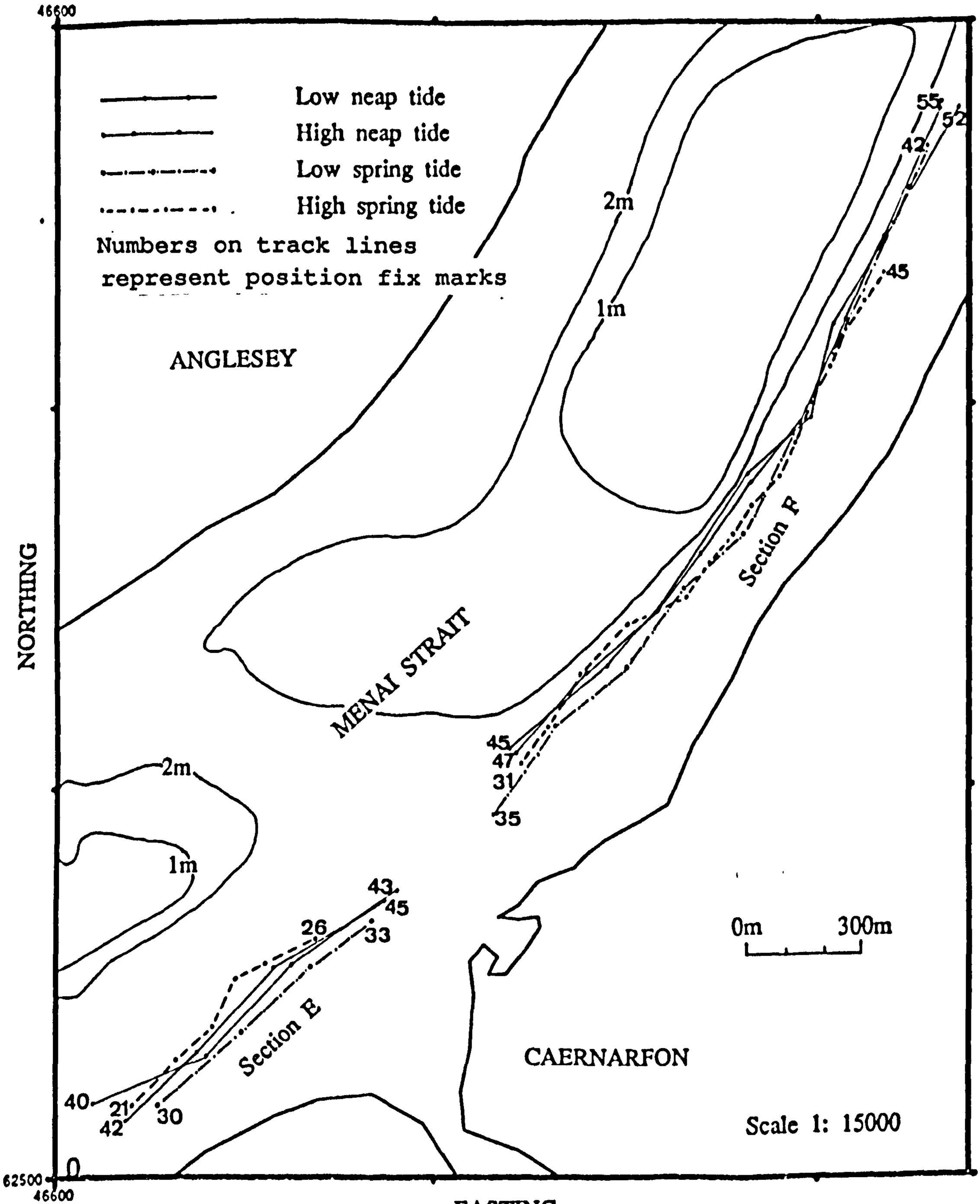

Fig: 4.25 Location map of the pinger sections E and F of the repeated survey line. (Depth contours below Ordinance Datum)

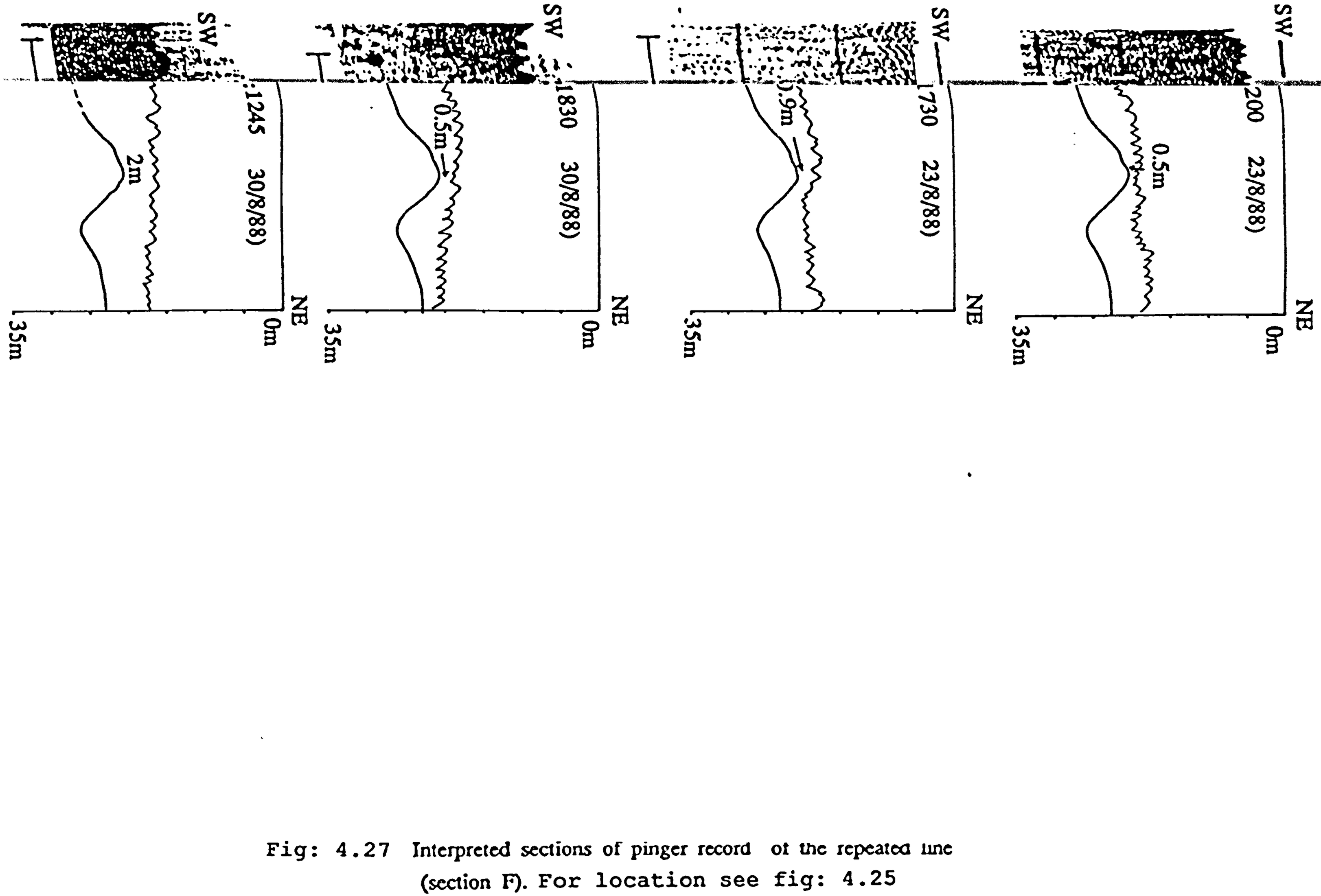

Fig: 4.27 Interpreted sections of pinger record of the repeated line (section F). For location see fig: 4.25

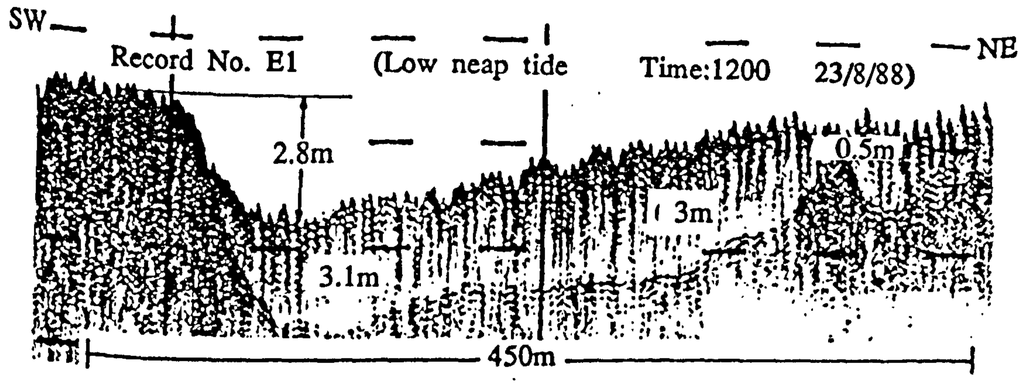

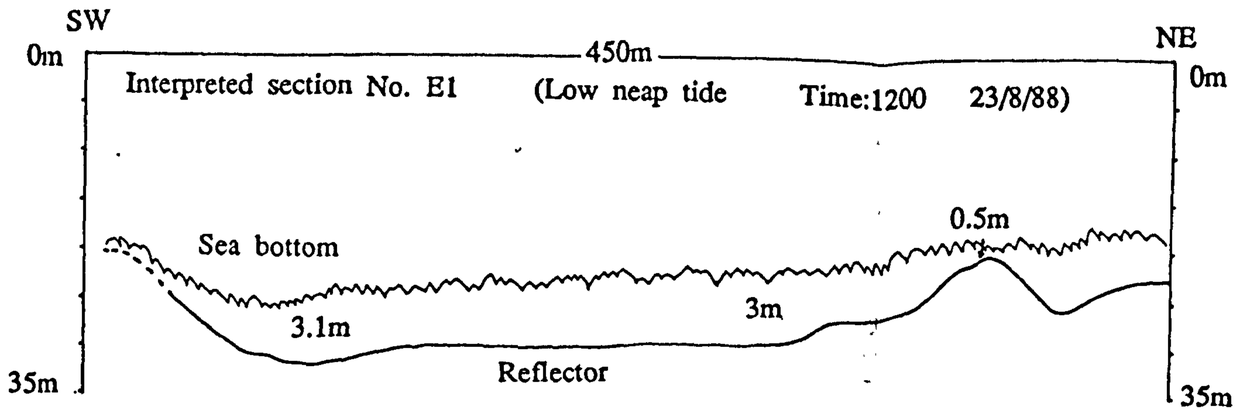

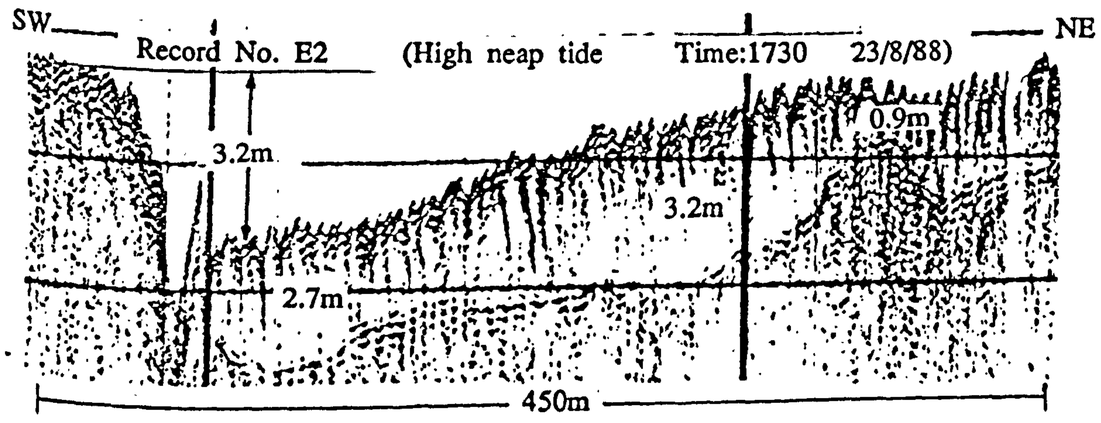

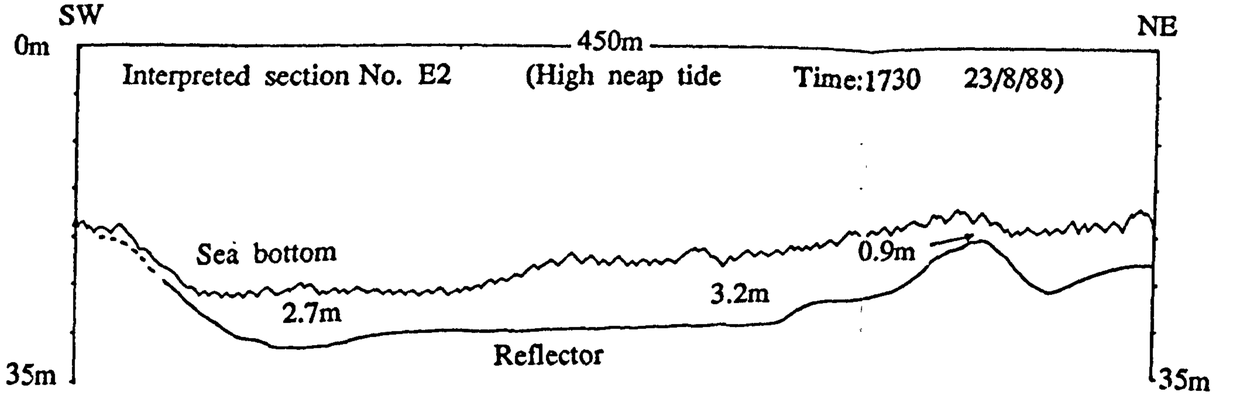

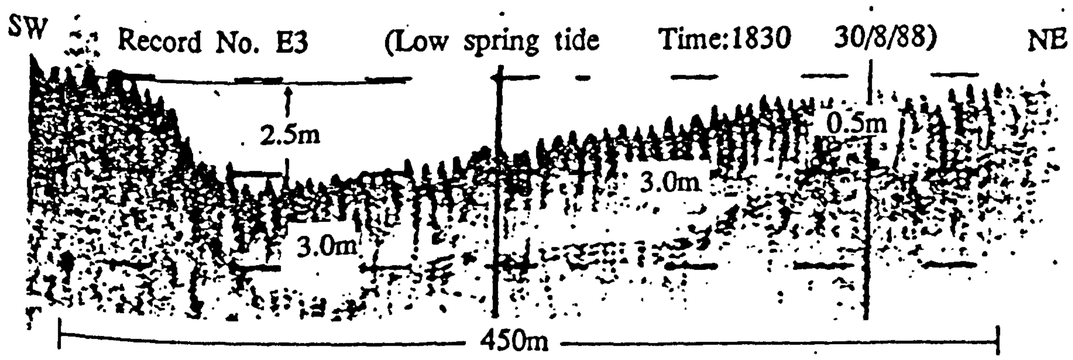

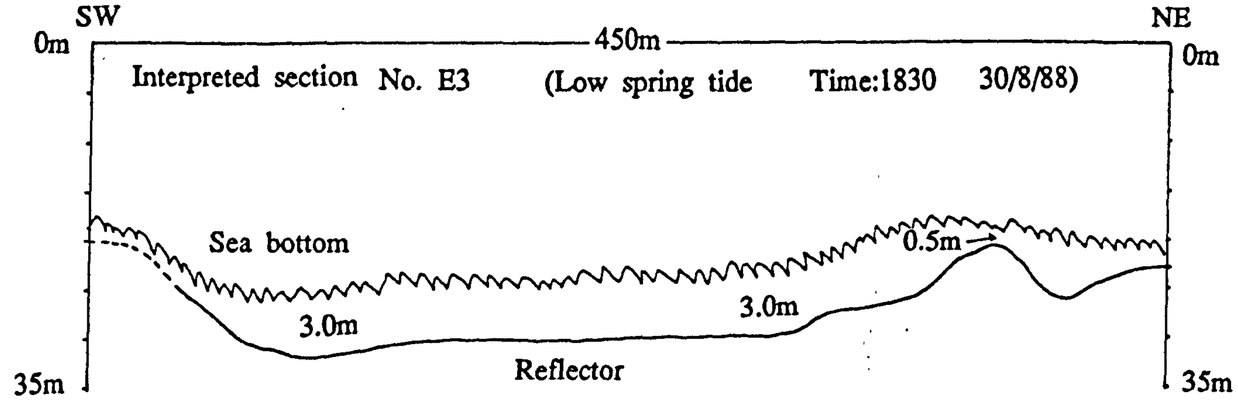

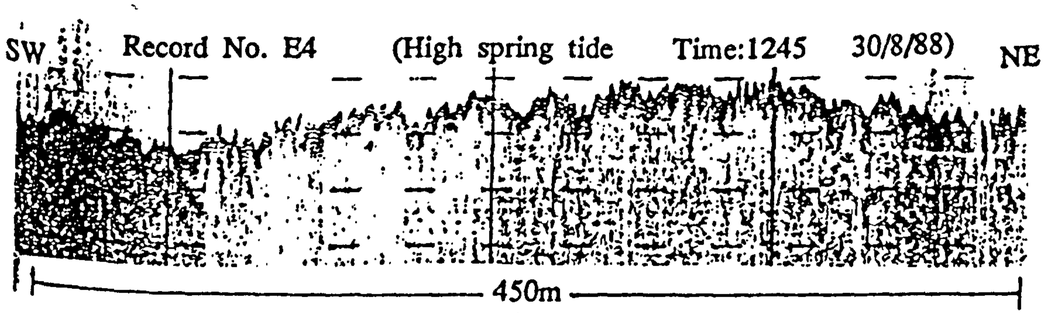

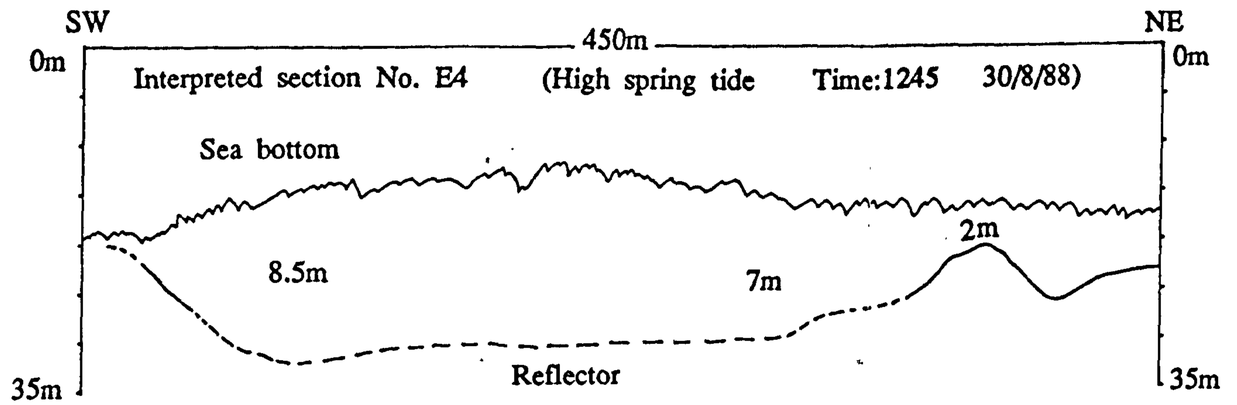

Fig: 4.26 Pinger records and their interpreted sections of the repeated line (section E). For location see fig: 4.25

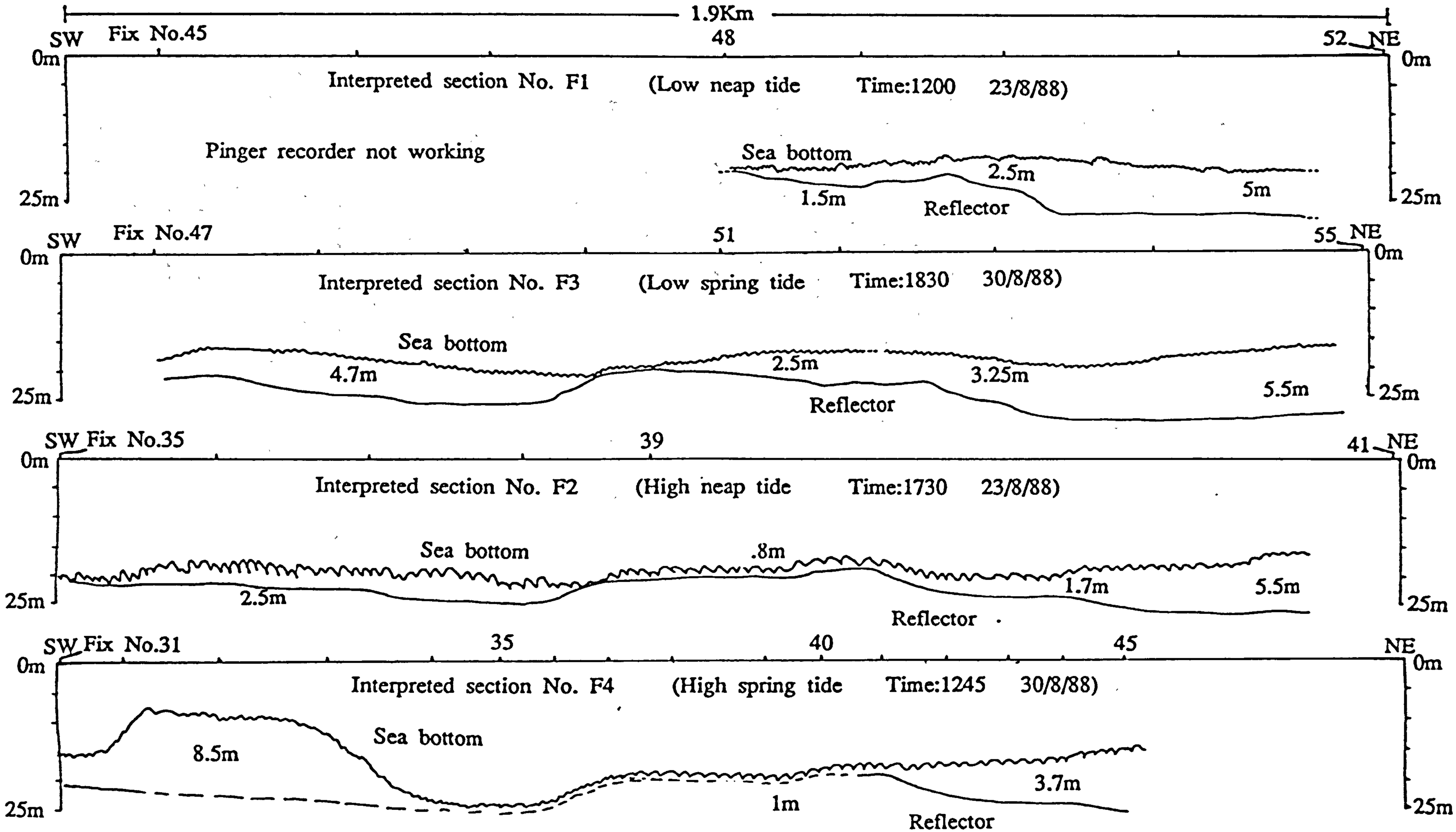

Fig: 4.27 Interpreted sections of pinger record of the repeated line (section F). For location see fig: 4.25

On the basis of the above mentioned facts it may be concluded that an attempt to carry out multiple surveys, to observe the effects of varying flow regimes over the thickness of the surficial sediments, failed to reach any significant quantitative conclusions as a result of navigational errors. However qualitatively, there appears to be some time-dependent variation in surficial sand thickness which probably relates to tidal flow. More conclusive and better results could be obtained if it was possible to overcome the navigational difficulties by, for example, using an automatic trisponder position fixing system, which displays the course of the track line and relative position of the boat on a computer monitor. The system allows a repeat of the same track line using real line display to correct for boat wandering provided that an appropriate boat and personnel are available. Such results would significantly enhance the value of this type of study.

Echo-sounding results (sections A, B, C, and D).

The above sections are shown in Figs: 4.28a, 4.28b, 4.28c, and 4.28d. Each consists of four echo-sounder records of the same area surveyed at high and low waters during spring and neap tidal cycles. On the basis of examining each record individually for significant bedform features, some important conclusions can be drawn.

Firstly, it appears that enormous changes are taking places in the size, shape and orientation of the bedforms during one tidal cycle. The same is true for the neap and spring tidal variations as well. Repeated echo-sounder records of the same area on each section appear reasonably different to one another, as far as the size of the bedforms is concerned. However, low water neap and low water spring records show consistency in a sense that the bedforms remain ebb oriented. On the other hand, records of the high water neap and high water spring are somewhat complex. They show that during high water springs the majority of the

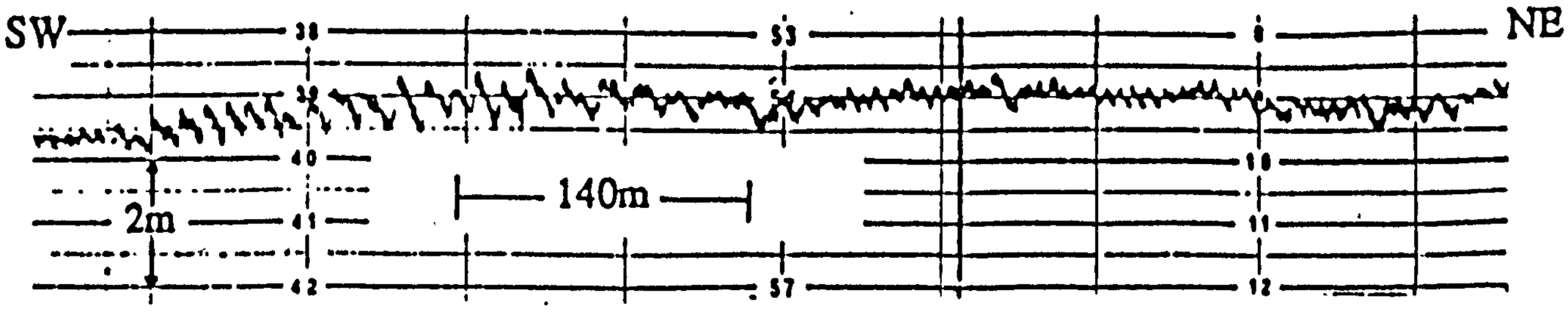

Record No. A1 (Low neap tide Time:1200 23/8/88)

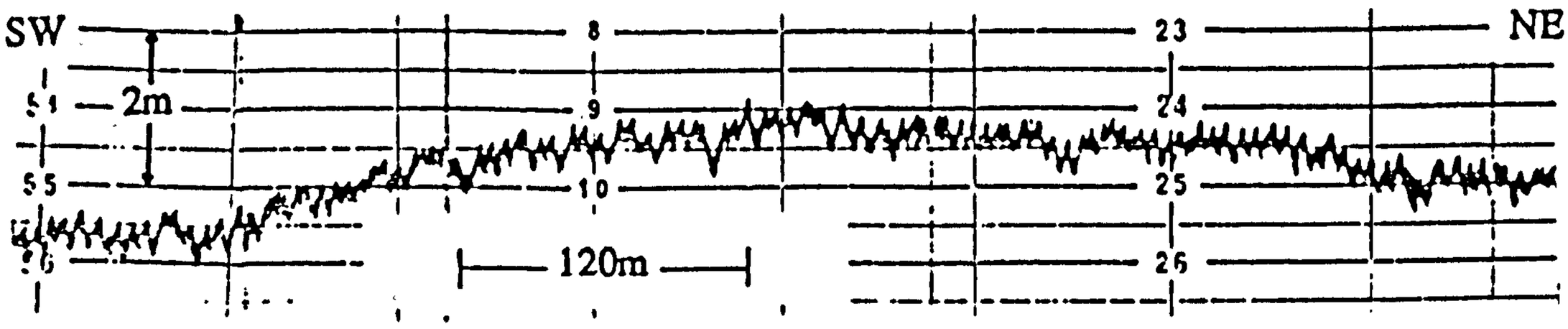

Record No. A2 (High neap tide Time:1730 23/8/88)

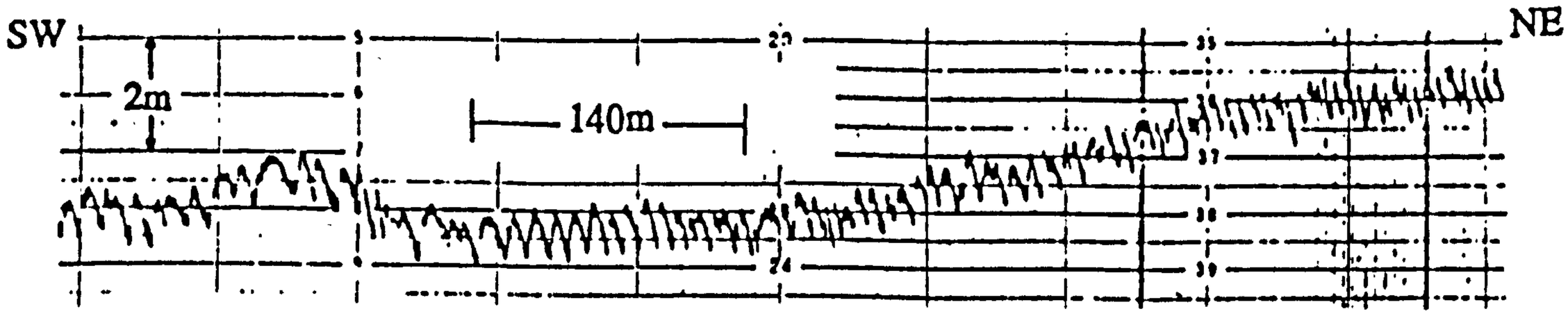

Record No. A3 (Low spring tide Time:1830 30/8/88)

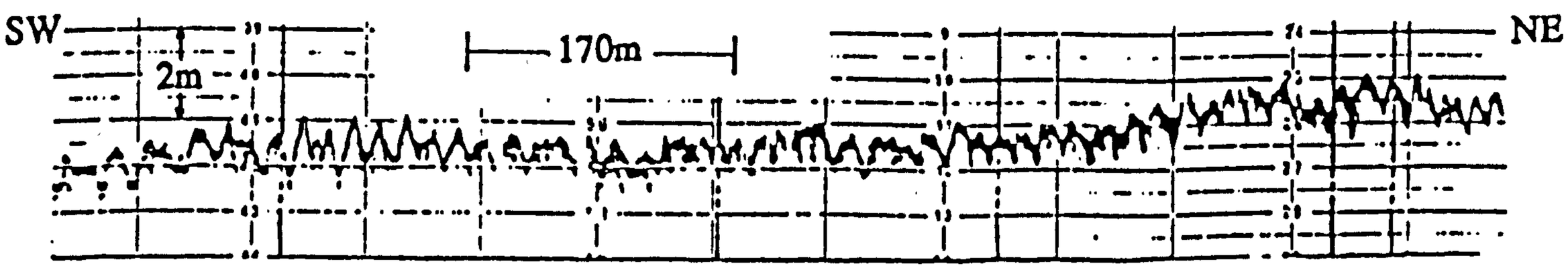

Record No. A4 (High spring tide Time:1245 30/8/88)

Fig: 4.28a Echo-sounding records of the repeated line (Section A).

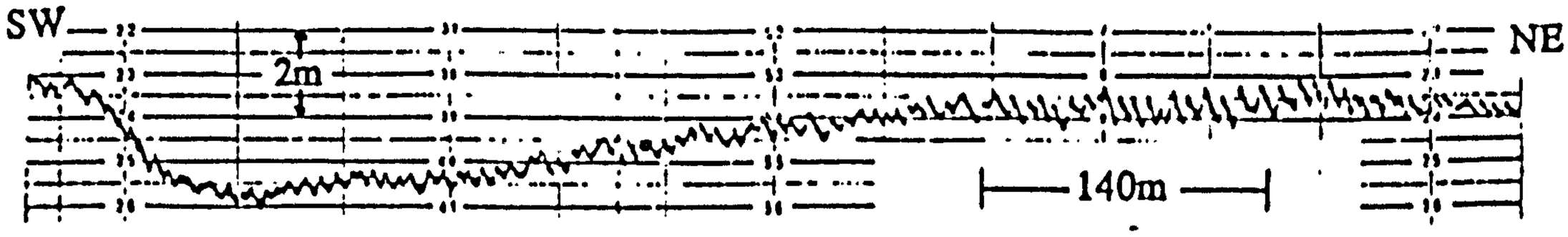

Record No. B1 (Low neap tide Time:1200 23/8/88)

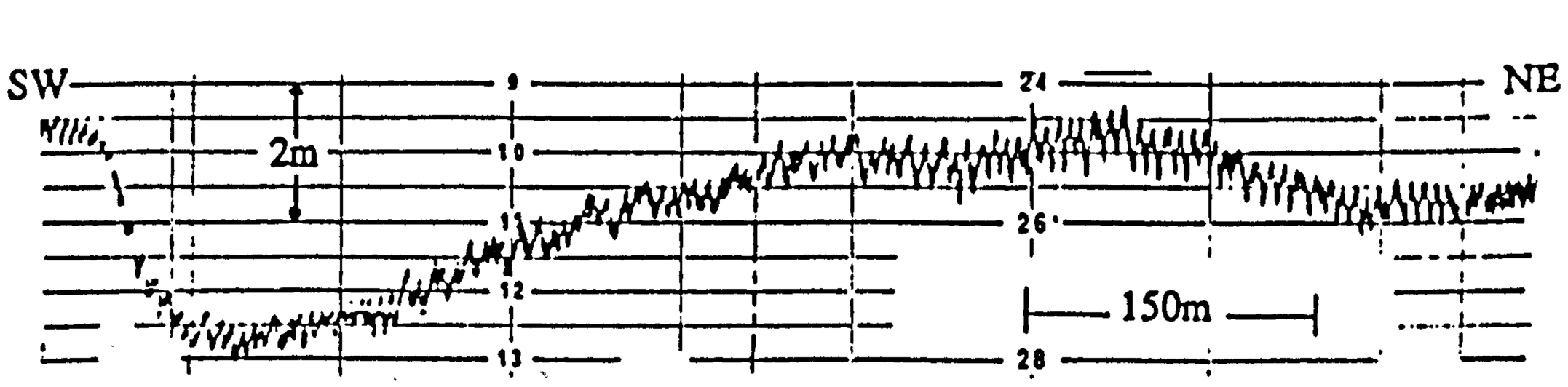

Record No. B2 (High neap tide Time:1730 23/8/88)

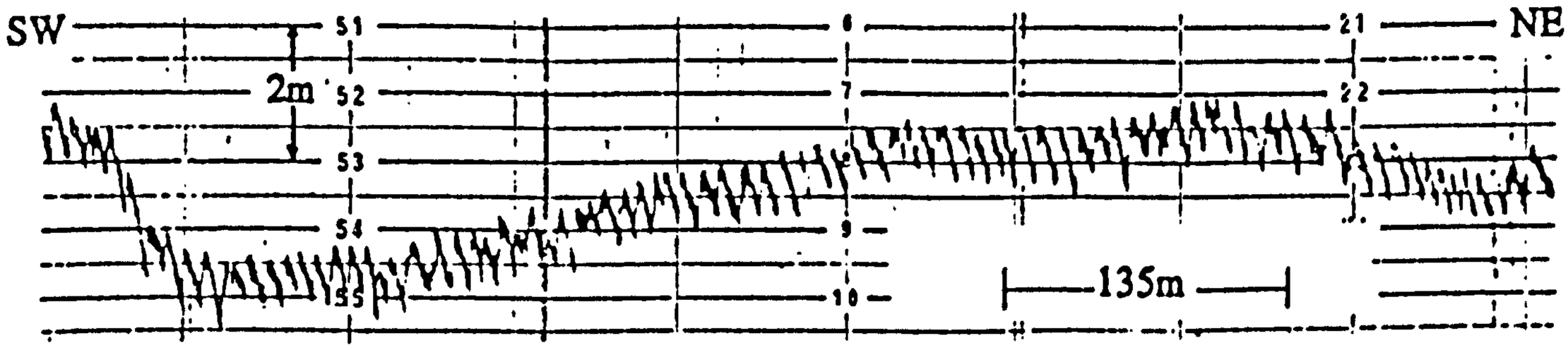

Record No. B3 (Low spring tide Time:1830 30/8/88)

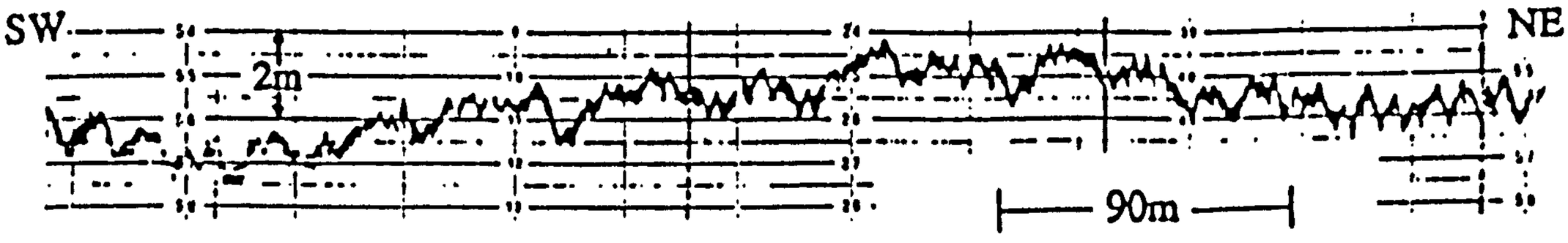

Record No. B4 (High spring tide Time:1245 30/8/88)

Fig: 4.28b Echo-sounding records of the repeated line (Section B).

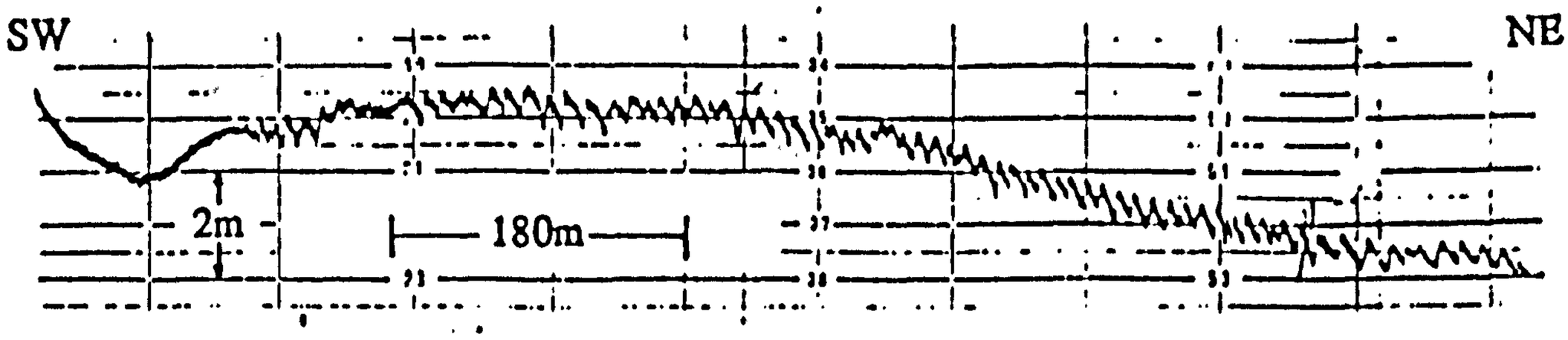

Record No. C1 (Low neap tide Time:1200 23/8/88)

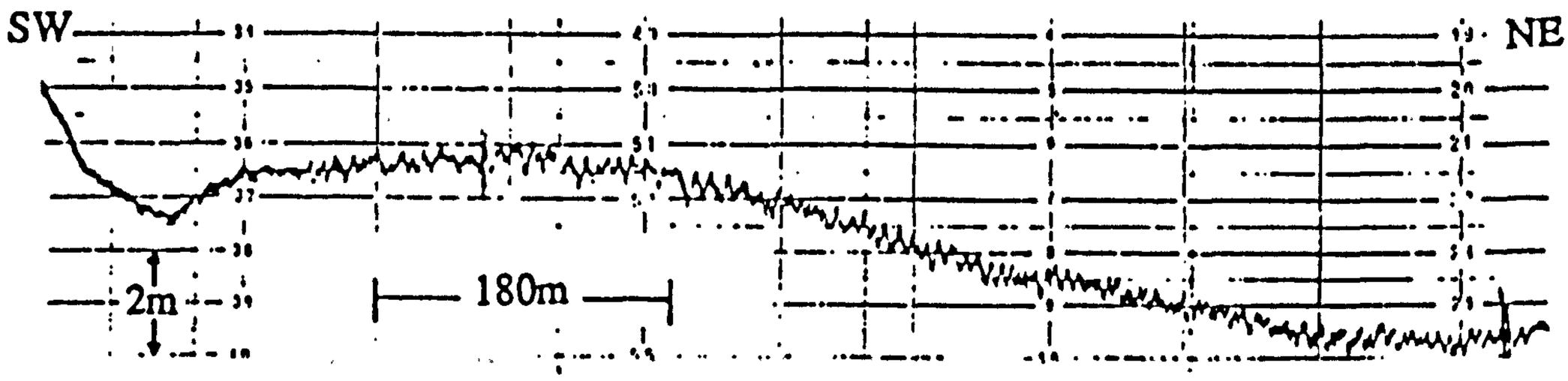

Record No. C2 (High neap tide Time:1730 23/8/88)

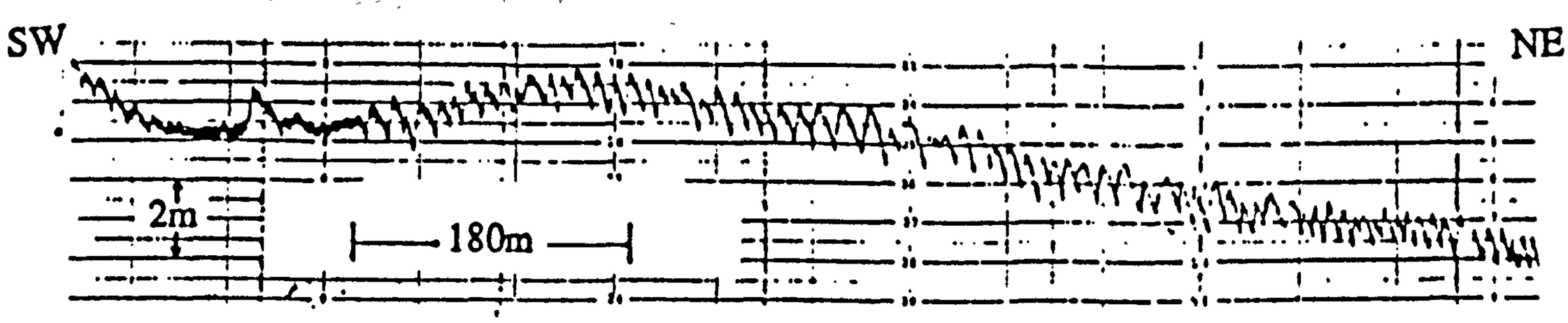

Record No. C3 (Low spring tide Time:1830 30/8/88)

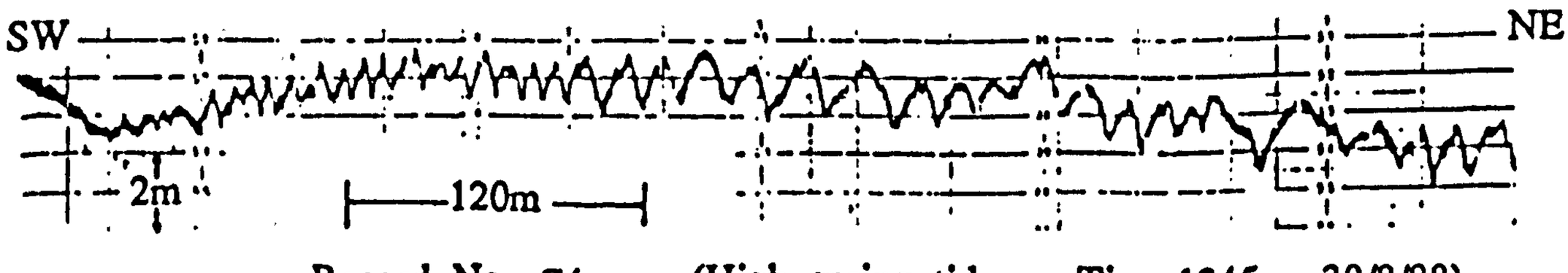

Record No. C4 (High spring tide Time:1245 30/8/88)

Fig: 4.28c Echo-sounding records of the repeated line (section C).

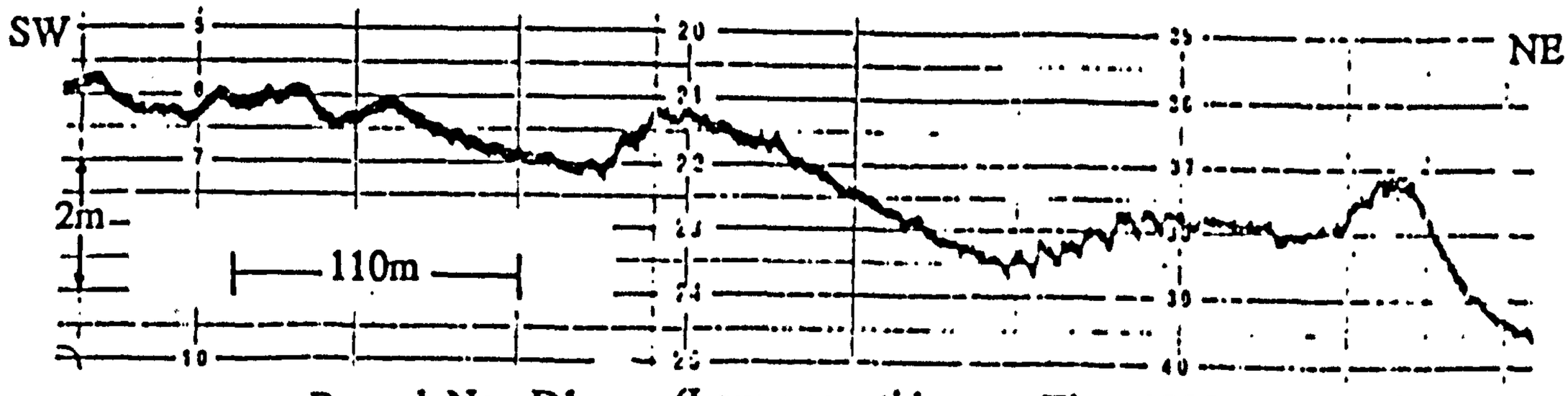

Record No. D1 (Low neap tide Time:1200 23/8/88)

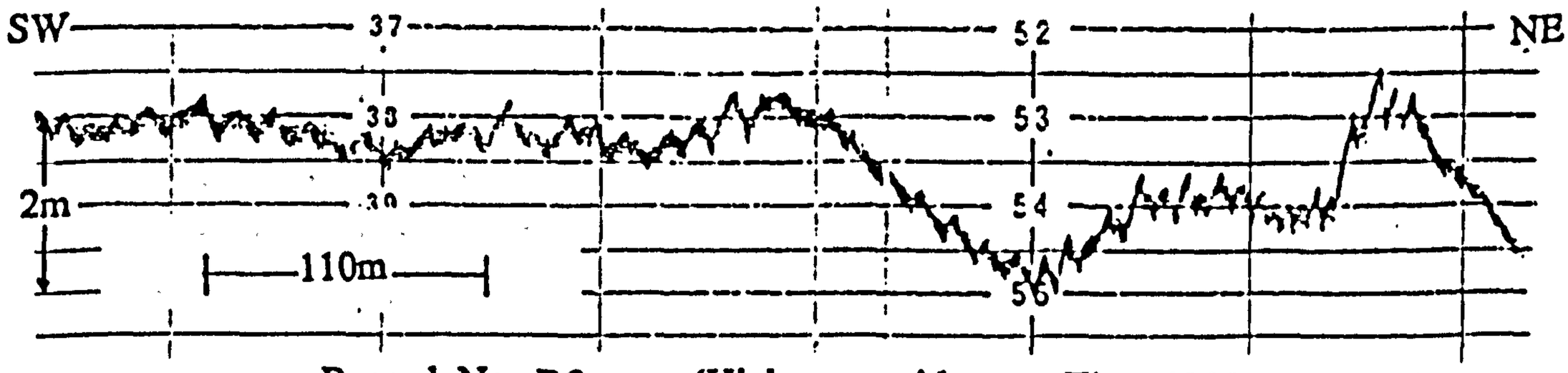

Record No. D2 (High neap tide Time:1730 23/8/88)

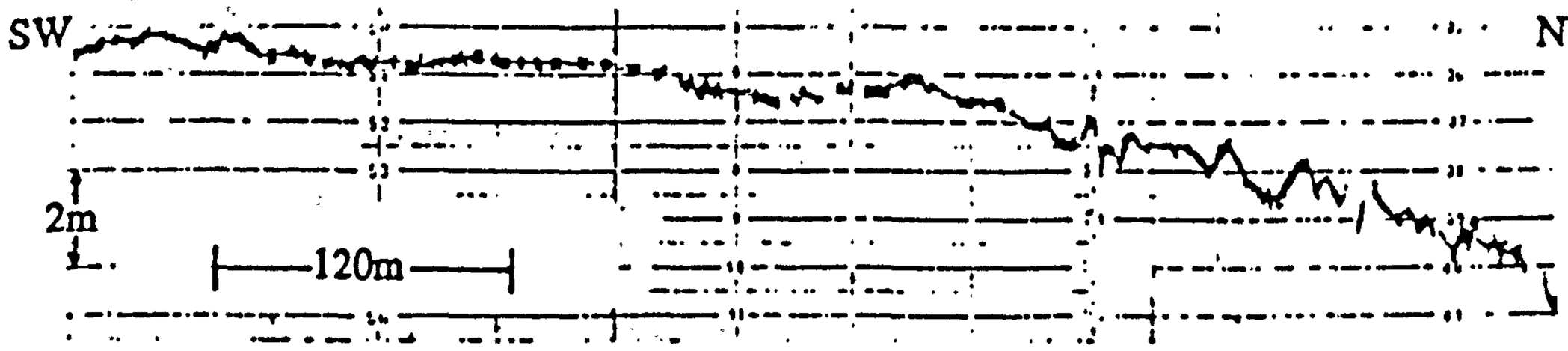

Record No. D3 (Low spring tide Time:1830 30/8/88)

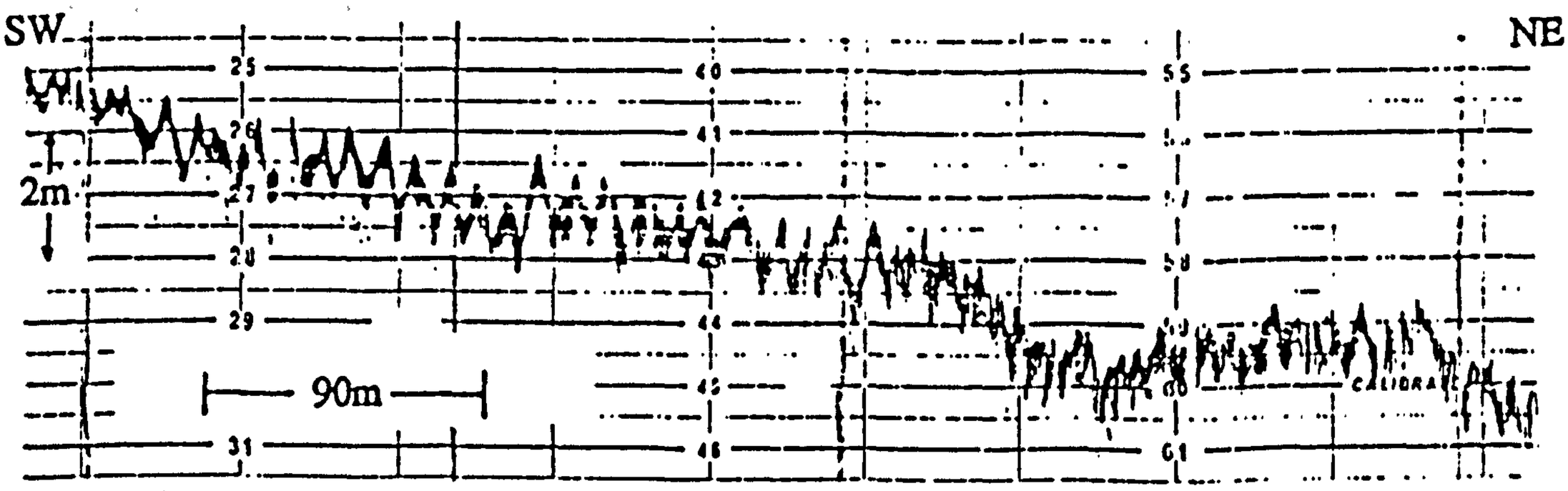

Record No. D4 (High spring tide Time:1245 30/8/88)

Fig: 4.28d Echo-sounding records of the repeated line (section D).

bedforms are flood oriented, whereas records taken at high water neap (except section D) suggest that most of the bedforms are near symmetrical.

Secondly, it has also been observed that bedform characteristics show considerable change from one section to another during one particular survey. That may be indicative of the variability of the flow conditions along the Strait. The largest bedforms (sand waves) occurred on record No. B4 (Fig: 4.28b) taken during a spring tide, where flood oriented sand waves of up to 45m wavelength with superimposed megaripples can be seen. On the same record megaripples of 7.5m wavelength can also be seen on the extreme right portion of the record.

Thirdly, a comparison of the four sections reveal that the echo-sounding records of section A, B, and C, except for a few diversities in size of the bedforms, show a general resemblance in orientation i.e. the bedforms are ebb oriented at low water and are partially flood oriented at high water. However, the records of section D (Fig: 4.28d) do not follow the same pattern. For example, record No. D2 (high neap) shows ebb oriented bedforms and record No. D4 (high spring) shows a majority of symmetrical bedforms unlike other sections where most of the bedforms are flood oriented. This diversity among the records taken within the Menai Strait and outside the Strait, perhaps, is the effect of the sudden changes in hydrodynamic conditions which occur as a result of the morphology of the Belan tidal inlet.

Quantitative analysis of the echo-sounding sections A, B, C and D.

An analysis of morphological characteristics such as height and wavelength of the bedforms appearing on echo-sounding records of all four sections was carried out to draw some general conclusions regarding the effect of changing tidal current intensity and direction during the ebb and flood tides of the

neap/spring cycle. Then, on the basis of the above analysis, a model of bedform size and shape related to the low and high neap/spring tidal currents could be produced. Quantitative analysis of the morphological characteristics of bedforms was carried out using the following method:

In order to calculate the average apparent wavelength (L) and height (H) of the bedforms on one particular echo-sounder record, 3-5 sub-sections (number of observations) were selected and measured to ensure that average values represent much of the record. This process was repeated for each of the echo-sounder records on all four sections. The number of observations per record was dictated by the frequency of the change in bedform size; records representing frequent change in bedform size have a higher number of observations and vice versa.

Since all the bedform height and wavelength measurements from the echo-sounder records were carried out manually, it must be borne in mind that the precise accuracy of these results is subjected to some observational error. However, the final results do agree with the general patterns of the size, shape and orientation of the bedforms visually observed on echo-sounder records. It suggests that the effect of observational error is insignificant and the results still reveal a great deal regarding the behaviour of bedforms in relation to various states of the tidal cycle.

The results of the above exercise have been summarised in Table No. 4.4 where the wavelength/height ratio and the dominant orientation of the bedforms have also been mentioned.

Results

On the basis of quantitative values shown in Table No. 4.4 some important points regarding height, wavelength, steepness index and orientation of bedforms can be made.

Table No. 4.4

Section & Record.No	Height		Wavelength		W/H	orient-ation	No.of obs ervations
	Range	Average	Range	Average			
Section A							
R.No. A1	0.16-0.64	0.32	6.7-13.3	9.3	29	ebb	4
" . A2	0.19-0.38	0.28	6.7-20.0	12.1	43	sym	4
" . A3	0.33-0.67	0.54	5.2-13.5	10.11	19	ebb	5
" . A4	0.4 -0.9	0.63	11.3-22.7	15.6	25	sym	5
Section B							
R.N0. B1	0.22-0.55	0.36	5.8- 7.8	6.8	19	ebb	5
" . B2	0.14-0.43	0.30	5.0-25.0	10.85	36	F/sym	4
" . B3	0.29-0.57	0.50	6.4- 9.0	8.36	17	ebb	4
" . B4	0.5 -1.25	0.90	7.5-45.0	24.4	27	flood	4
Section C							
R.No. C1	0.19-0.38	0.28	10.0-15.0	11.8	42	ebb	4
" . C2	0.15-0.38	0.25	5.0-10.0	6.85	27	sym/ebb	4
" . C3	0.29-0.76	0.53	7.5-15.0	12.4	24	ebb	4
" . C4	0.51-1.28	0.91	8.9-32.0	22.0	24	flood	4
Section D							
R.No. D1	0.12-0.34	0.23	6.1- 9.1	7.6	33	ebb	4
" . D2	0.17-0.26	0.26	9.2-14.7	12.0	47	ebb	4
" . D3	0.21-0.63	0.39	4.0-16.0	10.0	26	ebb	3
" . D4	0.23-0.76	0.54	5.0-12.0	8.5	17	sym	3

Values in meters

Details of the morphological characteristics of the bedforms determined from the echo-sounder records of section A, B, C, and D. For location see Fig: 4.14a. (W/H = Steepnex index; F = Flood; sym = Symmetrical).

Range values are also average values calculated from more than one point (in Table written as No. of observations) on a particular echo-sounder record.

Record Nos. A1, B1, C1, D1 correspond to Low Neap
" . A2, B2, C2, D2 " High Neap
" . A3, B3, C3, D3 " Low Spring
" . A4, B4, C4, D4 " High Spring

Height

Several authors (eg. Allen and Friend (1976), Boersma & Terwindt (1981) Dalrymple (1984), Terwindt & Brouwer (1986)) have reported that tidal bedforms increase in height during a spring tide and decrease towards a neap tide. Similar tendencies have been observed during this work, where average bedform height during high spring tide reaches up to 0.91m, whereas during a neap tide it remains around 0.3m. It has also been observed that there is considerable difference between the average bedform height during low water springs (0.54m) and high water springs (0.91m). In contrast to the spring tide, neap tide bedforms attain higher average heights at low water.

Wavelength

The spring tide also causes dramatic changes in the wavelength of the bedforms, where average apparent wavelength reaches up to 24m. Like height, the wavelength of the bedforms also reaches to maximum during the high spring tide. This may be the result of the merging of two or more megaripples into one large sand wave reaching up to 45m in wavelength. Some of these sand waves carry superimposed megaripples. This tendency has only been observed for section B (Fig: 4.28b). The same trend also appears on record No. B2 (high tide neap) of the same section, where only 4-5 sand waves, up to 25m long, with superimposed megaripples can be seen.

It has also been observed that wavelength tends to increase in size towards high water neap and decrease towards low water neap. Wavelength also shows a change in size during one particular survey, along the chosen survey line. For instance, during low neap, megaripple wavelength increases from an average of 6.8m at section B to an average of 11.8m at section C. The same is true for other sections and surveys.

Steepness index

The highest and lowest steepness indices of 46 and 16.7 have been calculated for high water neaps and low water springs

respectively. A similar tendency for steepness index to decrease towards spring tide has also been reported by Terwindt & Brouwer (1986). There appears to be a little variation in steepness index between high water and low water springs, which perhaps, indicates systematic changes in the height and wavelength of the bedforms during high water and low water springs. In contrast, the difference in steepness index is considerably greater between high water and low water neap.

Orientation

A detailed study of echo-sounder records for the sections A, B, C, and D indicates that megaripple and sand wave orientations do change between the ebb and flood tide. However, a complete reversal of the bedforms has been recorded on only two sections (B and C) between the high water and low water springs. In sections A and D the high spring records show symmetrical bedforms. This change shows a tendency of irregularity, predominantly related to the flood tide. As a result, the orientation of the flood tide bedforms generally varies from near symmetrical to flood oriented, while in one instance (Record No. C2; Fig: 4.28c), the flood tide record shows symmetrical to ebb oriented bedforms.

4.5.6 Bedform structures related to neap-spring cycle.

The results of the average apparent wavelength and height of bedforms, produced in Table No. 4.4, were further analysed in order to, determine the general shape and size of the bedforms relative to each of the above mentioned tidal conditions. This exercise was carried out in a way that the results of each particular survey, for example, in the case of 3 echo-sounder records of low water neap i.e. A1, B1, C1 (each from sections A, B, C) were further analysed to calculate the mean average values for the wavelength and height of the bedforms. The standard deviation of both was also calculated. The results for section D were not used in above calculations for two reasons. One relates to its location, which, being outside the Belan

inlet is substantially different to the remaining three sections (within the Menai Strait). Secondly, its results show considerable diversity to the general pattern of change observed in other sections.

The final results of the above exercise are summarised in Table No. 4.5 and discussed below.

From the mean average values of height and wavelength, a model of bedform size and shape related to the neap/spring tidal cycle was constructed, which is shown in Fig: 4.29. On the basis of this model the following points can be made.

1) The overall size of the megaripples/sand waves is relatively larger during high water spring than any other state of the tidal cycle.
2) The mean average wavelength of megaripples does not change much between low water and high water neap. However, the mean average height is greater during low water neap.
3) The model suggests an increasing trend in the mean average wavelength of the megaripple from low water neap to high water spring. The biggest increase, however, occurs between the low water and high water springs.
4) The megaripples are always ebb oriented during low water neap and spring tides.
5) During high water neap, while the majority of megaripples exhibit symmetrical orientation, some flood and ebb oriented megaripples may occur.
6) A complete reversal of megaripples/sand waves occurs only partially at high water spring and neap tides.
7) The frequency of complete reversal of megaripples at high water spring is considerably greater than at high water neap.

From the above study, it can be concluded that the bedforms (megaripples/sand waves) in the study area i.e. within the Menai Strait are dominantly ebb-oriented to symmetrical during most of

Table: No. 4.5

Tide	R. No. (height, wavelength)	Height		wavelength		Orientation
		Mean average	Standard deviation	Mean average	Standard deviation	
Low neap	A1. (0.32, 9.3) B1. (0.36, 6.8) C1 (0.28, 11.8)	0.32	0.033	9.3	2.0	ebb
High neap	A2 (0.28, 12.1) B2 (0.30, 10.9) C2 (0.25, 6.7)	0.28	0.021	9.9	2.24	flood/ sym/ebb
Low spring	A3 (0.54, 10.1) B3 (0.50, 8.4) C3 (0.52, 12.4)	0.52	0.016	10.3	1.7	ebb
High spring	A4 (0.63, 15.6) B4 (0.90, 24.4) C4 (0.91, 22.0)	0.81	0.13	20.7	3.7	flood/ sym

Values in Meters

Mean average values of the height (H) and wavelength (W) and dominant symmetry of the bedforms related to low and high neap/spring tides in SW Menai Strait.

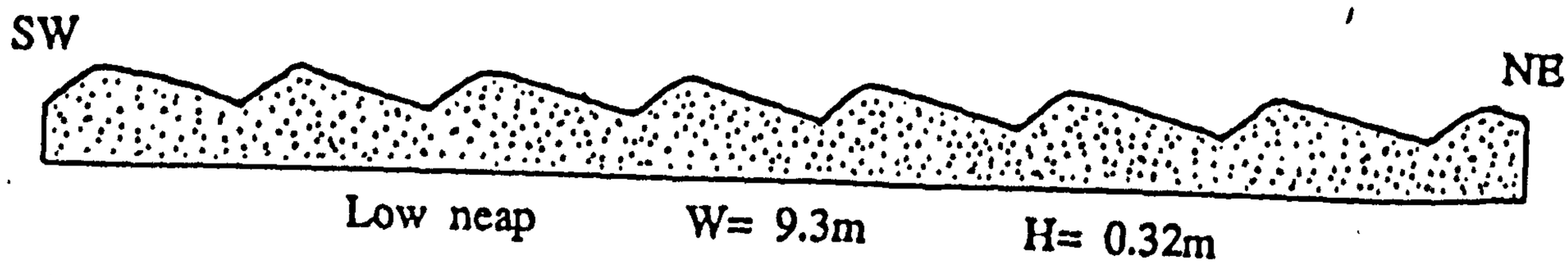

Fig: 4.29 Model of bedform size and shape related to various tidal states (wavelength (W) and height (H) values are the mean average values).

the neap/spring tidal cycle. It suggests that ebb currents are the dominant features of the hydrodynamic system prevailing in the area. Similar conclusions have also been drawn by Jones (1984) working in the area of large sand banks opposite Caernarfon. He suggests that the megaripples in this area remain ebb-dominated for most of the time, with flood domination occurring only at high water springs.

4.6 Conclusions.

1) There is a southwesterly residual flow of water through the Strait.
2) Large sub-tidal and inter-tidal sand banks occur within the Menai Strait and Caernarfon Bay which are very much influenced by the Fort Belan tidal inlet morphology.
3) The morphology of the tidal sand body outside the Belan inlet (exterior shoal) shows resemblance to the standard model of the ebb-tidal delta as suggested by Hayes (1980).
4) Because of the general setting of the Menai Strait the flood tidal delta morphology is very different to the standard model of Hayes (1980).
5) The bedforms found in the study area range from small scale megaripples (1 to 5m wavelength) to sand waves of up to 45m in wavelength.
6) The sand waves predominantly occur in the Menai Strait area, while the small scale megaripples are found in the deeper parts of the study area in Caernarfon Bay.
7) Sand ribbons occur extensively in the deeper parts of the study area i.e. extending from the outer limits of the ebb-tidal delta to further offshore. All the sand ribbons have superimposed ripples of 1 to 2m in wavelength.
8) Most of the bedforms found within the Menai Strait are asymmetrical in form and appear to be active during much of the neap/spring tidal cycle.
9) The largest bedforms (sand waves) predominantly occur in the areas of the channels i.e. main channel and back channel.
10) The majority of the bedforms within the Menai Strait remain

ebb oriented during most of the tidal cycles, while the partial reversal of the bedforms to flood orientation occurs only during the spring flood tide.

11) Outside the Belan inlet the great majority of the bedforms occur in the areas of the main channel. While the largest bedforms occur nearer to the Belan inlet, they decrease in size moving away from the inlet.

CHAPTER 5

GRAIN SIZE ANALYSIS: INTERPRETATION AND SIGNIFICANCE OF SEABED SEDIMENT DISTRIBUTIONS

5.1 Introduction.

Since the early twentieth century, grain size measurements of transported and deposited sediments has been one of the most widely used analytical tools in sedimentological studies. Udden (1898) realised that some kind of relationship must exist between the size distribution of clastic sediments and the environment of deposition.

The concept behind this study is that when any medium (water, ice, wind) is subjected to motion it produces a shear stress which affects materials, such as sediments, with which it is in close contact. In the case of the water column, the fluid shear stress results in the movement of sediments present at the sediment/water boundary. Generally, finer sediments are more easily moveable than coarser sediments. Thus different intensities of fluid motion are required to move sediments of different size and this provides a clue towards the understanding of hydrodynamic conditions existing within any particular area. On this basis, numerous studies have been carried out world wide to quantify various grain size parameters and their significance in terms of a depositional environmental interpretation.

Grain size studies of sediment samples should provide information about the prevailing hydrodynamic conditions in areas, such as the Menai Strait and Caernarfon Bay, areas which are primarily under the influence of tidal currents. Such knowledge of grain size provides a basis also for interpretation of past sedimentary environments in the geological record and also aids the prediction of future movement of sediments in related areas. Such studies will also

enhance the overall understanding of the nearshore tidal system and its relationship with adjacent offshore environments.

In addition to Udden's work (1898, 1914), some other early contributions include the work of Wentworth (1922, 1929), Trask (1932), Krumbein and Pettijohn (1938), Otto (1939), and others who applied various statistical methods to characterise the size distribution of clastic sediments.

Because of the immense significance of grain size studies, a large amount of literature has been produced over the years, relating to the topic of interpretation of environments of deposition from studies of clastic sediments. Several useful papers dealing with the subject include Doeglas (1946), Folk and Ward (1957), Passaga (1957), Mason and Folk (1958), Harris (1958), Fuller (1961), Moss (1962), Spencer (1963), Klovan (1966), Visher (1969), Glaister and Nelson (1974), Mclaren (1981), and Mclaren and Bowles (1985).

Here it is worth mentioning some literature which is of relevance to the current study. Krumbein and Aberdeen (1937) studied the sediments of Barataria Bay, USA. On the basis of computed statistical parameters they noticed that a regular variation in sediment character occurs from deeper to shallower parts of the Bay. Similar remarks were made by Hough (1942) while studying the sediments of Cape Cod Bay Massachusetts, USA.

Friedman (1961) suggested that on the basis of mean grain size and skewness parameters, dune and beach sediments could be separated as dune sands were more positively skewed at each mean size. In addition plotting sorting against skewness clearly distinguished river and beach sands, with the river sands more positively skewed and less well sorted. Friedman (1967) however, argued that the same sign of skewness may arise under different environmental conditions, for example positive skewness of dune sands results from a truncated coarse tail, but in river sands the same effect is produced by the presence of a fine tail.

Duane (1964), on the basis of a study of recent sediments in Western Pamlico Sound, North carolina, USA, suggested that negative skewness was caused by removal of fine particles from the sediments by a winnowing action, whereas positive skewness resulted from the accumulation of fine grains in sheltered environments.

Krumbein (1938) indicated the significance of progressive or continuous changes in grain size distribution from source to final depositional location. Progressive changes have also been recognised by several other workers (Slaper and Tamer (1975), McCave (1978), Haner (1984)).

Mclaren (1981) concentrated on the trends in grain size measures. He suggested that these trends could be used to identify both the probable source and the probable deposit, and this might help to identify net sediment transport paths among sedimentary deposits. He argues that, if a source sediment undergoes erosion, and the resultant sediment in transport is deposited completely, the deposit must be finer, better sorted, and more negatively skewed than the source (càse I). The lag remaining must therefore be coarser, better sorted and more positively skewed (case II). If the sediment in transport undergoes selective deposition, the resultant deposit may either be finer (case IIIA) or coarser (case IIIB) than the source, but the sorting will be better and the skew more positive.

Mclaren and Bowles (1985) attempted to scrutinize more vigorously the validity of the trends mentioned by Mclaren (1981), and suggested two modifications to the original model. These are that;

a) successive deposits occasionally become more poorly sorted than their source, and
b) when sediments become finer, their skew must become more negative.

In the current study, an investigation of grain size distributions in the tide-dominated nearshore environment (i.e. part of the Menai Strait and Caernarfon Bay), and to some extent in an interrelated offshore environment (of Caernarfon Bay) was carried out. The objectives were, firstly to study the characteristics of grain size distributions and their relationship to the prevailing hydrodynamic system in the study area, and secondly, to identify any grain size trends occurring in the area which could be used -together with other results (in Chapters 4 and 6)- to identify possible sediment transport pathways among the sand deposits.

5.2 Sediment sampling.

In order to collect sediment samples representative of all the environments under examination, special attention was given to the planning of the sample collection exercise. Realising the extent of the area and number of samples required, the idea of composite sampling seemed impractical, and hence spot samples were collected. The area does display considerable diversity from one part to another, as far as its topography and hydrodynamic conditions are concerned. As a result two different sediment samplers (Van Veen and Shipek grab samplers) and various boats were needed to collect the samples from the three different areas. For convenience and ease of understanding, these three areas will be referred to as Area 1, Area 2, and Area 3. Site locations of sediment sample stations are shown in Fig: 5.1 and a brief discussion of the three areas is given below.

Area 1

In this area sampling on a rigorous grid was impossible because of the difficulty of small boat handling in the shallow water. Consequently random sampling was carried out using a small boat and a Van Veen grab sampler. Some selective sampling was also attempted in the main and back channels and at other important

Fig: 5.1 Location map of the sediment sample stations
(Area 1, Area 2, and Area 3).

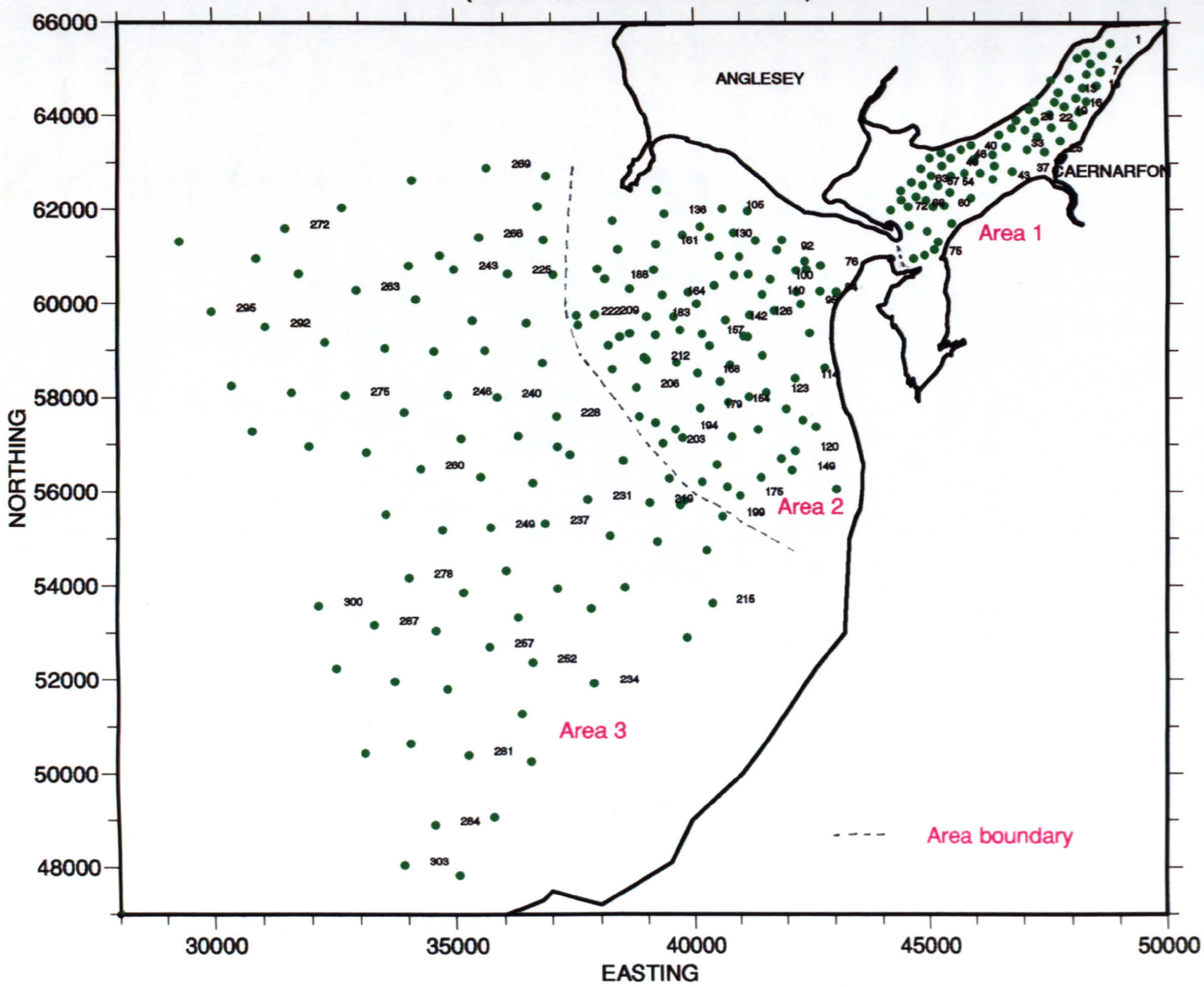

topographic features. Folk (1974) pointed out that one should search for and sample the coarsest and finest sediment obtainable as well as sediments most typical of the area studied.

Because of the relatively light weight of the Van Veen grab sampler, some problems were encountered in collecting samples, particularly in the areas of relatively deeper water and/or strong tidal currents. In these areas, the sampler tended to swing away from its vertical drop course and did not hit the sea bottom cleanly. Consequently, in some instances it failed to collect a sample. This problem was overcome, partly by tying equal lead weights on both sides of the grab, and partly by sampling such areas during or near the slack water period. The location of each sample was fixed using a trisponder positioning system. In total 68 samples were collected from this area giving an average sample interval of about 300m.

Area 2

This area extends from Fort Belan inlet up to the offshore limits of the Caernarfon Bay sand body, and is referred to as the ebb-tidal delta. Area 2 is similar to Area 1 in that it also contains large sand deposits and is largely influenced by flood and ebb tidal currents. However, the intensity of the currents is much less in this area and the water depth is greater. The sampling exercise in this area was carried out using the research boat "Lewis Morris" and a Shipek grab sampler. Again, because of the large sub-tidal sand bodies and difficult bathymetry no fixed grid pattern could be followed and random sampling was carried out. In total 85 sediment samples were collected from this area (with an average interval of about 500m) and the same trisponder system was used for position fixing of the sample stations.

Area 3

One limit of this area is defined by the distal boundary of the ebb-tidal delta and the relatively deeper offshore sediments.

Because of the greater water depth in Area 3, the larger research vessel "Prince Madog" was employed and sampling was carried out using a Shipek grab sampler. This area was sampled on two different occasions (1987 and 1988). During these two exercises, sampling was carried out according to a pre-planned grid pattern. In the shoreward part of Area 3, sampling was carried out at an average interval of 700m and was gradually increased to 1km in the seaward part. In total 87 samples were collected from area 3 and the location of the sample stations was fixed with the aid of the Decca navigation system.

5.3 Sample preparation.

Preparation in the case of those samples composed predominantly of sand was fairly straightforward. However, the presence of gravel, and/or silt and clay in a fair number of samples greatly complicated the preparation procedure. The sample preparation procedures adopted for various fractions are described below.

5.3.1 Preparation of sand sized samples.

The samples were thoroughly washed through a 63μm sieve and then transferred to an evaporating dish and stored overnight in an oven to dry. Once dried, the sample was split into smaller portions using a Citenco rotary type splitter. Since all the sand sized fractions were analysed by a Fall Tower method, the weight of the sample used for analysis was kept to an average of 5 grams (the significance of this will be discussed in a separate section on the Fall Tower). This was achieved by continuous splitting of the sample until the required amount was obtained.

5.3.2 Preparation of composite sediment samples.

Preparation of those sediment samples composed of a mixed sand and gravel fraction was carried out in an identical way to the above, except that the dried sample was passed through a 2mm

sieve to separate gravel from sand. The gravel fractions were analysed using the sieve technique and, in most cases a maximum of 100g was used for the analysis. In the case of sediment samples with little gravel, however, the weight of the sample used for analysis was inevitably less.

For the sediment samples containing sand, gravel and/or silt and clay fractions, a lengthy treatment had to be adopted. Initially, using the 63μm sieve, wet sieving of the sample was carried out. The sediments were thoroughly washed to disaggregate the sand and fine particles. The silt and clay sediments were washed through the sieve together with water, and were collected in a bottle kept underneath the sieve. Then, in order to separate the fine sediment from the water, the sample bottles were put into a centrifuge for about 20 minutes. At the end of this period the fine sediment completely settled on the bottom of the bottle and all the water was decanted. The remaining fine sediments were treated with dispersing liquid (Calgon) and finally a mixture of sediment and dispersing liquid was produced. The total volume of the sample was measured at this stage, from which, depending upon the quantity, about 30 to 40% was transferred into crucibles to dry in order to calculate the total percentage of fine sediment in the sample. The rest of the sample was kept in a beaker and later prepared for analysis by Sedigraph.

Preparation of silt and clay samples for Sedigraph analysis.

Complete dispersion of the sample in a liquid of known density and viscosity is the prime requirement of sample preparation for Sedigraph analysis. However, there are no established techniques by which complete particle dispersion is routinely achieved. Stein (1985) suggests that about 15 minutes ultrasonic treatment is necessary to achieve fairly good dispersion of the sample. In this particular analysis the sample was kept in an ultrasonic device for about 15-20 minutes. In most cases a magnetic stirrer was also used to aid the dispersing process.

Before putting the sample into the Sedigraph for analysis, a final check was carried out by examining the sample under a microscope to make sure that a reasonable dispersion had been achieved. The magnetic stirring was continued, even inside the Sedigraph, with an inbuilt stirrer, until the grain size analysis process was initiated.

5.4 Grain size analysis methods.

The methods commonly used for grain size analysis by sedimentologists include the use of sieves, settling tubes, and microscopes. Each method has its advantages and limitations. For example, practical difficulties prohibit the use of settling tubes for sediments with particles greater than 2mm in diameter. Therefore sediments with particle sizes larger than 2mm are analysed by sieving techniques. Both techniques (sieving and settling tubes) are inadequate, however, if the sample is composed of indurated materials and under such conditions size distribution of the sediments may be obtained by microscopic study of thin sections.

In the current project the greatest proportion of the sediment samples were effectively all sand. However, a fair number of sediment samples, collected mostly from Area 3, also contained a considerable amount of gravel and/or silt and clay as well as sand. The gravel sized fractions were analysed using the sieving technique, and sand and finer sediments were analysed using Settling tube and Sedigraph techniques respectively. A brief discussion of the techniques used, is given below.

5.4.1 Sieving.

Gravel (pebble) fractions were analysed using the standard sieving technique described by Krumbein and Pettijohn (1938) and Folk (1968). A set of British standard Endecott sieves with an aperture interval of 0.25ϕ (Krumbein, 1934) was used. The coarsest sieve was extended up to -4.75ϕ. Shaking of the sieves

was performed by a mechanical shaker.

It should be noted that sieving involves the measurement of the intermediate diameter of the grains i.e. between two sieve sizes, and can be considered as only an approximation to the actual grain size. Rittenhouse (1943) reports that the diameters of grains retained on any sieve show a considerable range in intermediate diameter. The weight of the sample suitable for size analysis by sieving is determined by two factors i.e. it must not be too much that individual sieves become choked, and its lower limit must not be too low that the sample no longer represents the bulk sample. Rogers (1959) recommends 30-50g for most sands and 100 to 200g for coarser sediments. Griffiths (1967) suggests 100-150g for the average sediment sample. For the current study, a maximum of 100g was used for sieve analysis. After 10 minutes of shaking, each fraction was weighed using an electronic balance with a quoted accuracy of one hundredth of a gram. A record of the cumulative weight was kept.

5.4.2 Fall Tower.

A fall tower (settling tube or sedimentation colùmn) is a device which measures the fall time versus distance (i.e. distribution of settling velocity) of the grains released at the top of a water filled column. The general aim is to convert the fall velocities to a grain size distribution. There have been many studies which attempt to relate settling properties of grains to a measure of its physical size. Some examples are those of Stokes (1851), Emery (1938), Gibbs et al (1971), Migniot (1977), Baba and Komar (1981), and Slot (1984). Yalin (1972) points out that, in addition to grain size, the settling velocity is also a function of grain volume, density, sphericity, roundness, and fluid viscosity. Stokes (1851) theoretically deduced a relationship between fall velocity and sphere size which is known as Stokes' Law and is written as,

$$w = gD\ (\rho_s - \rho) / 18\ \nu$$

where w is the fall velocity, D is the particle diameter, ρ_s and ρ are the particle and fluid densities respectively, g is the gravitational acceleration, ν is the fluid kinematic viscosity. Various other studies carried out on the settling velocities of grains include; Hallermier (1981), Yalin (1977), etc.

The weight of sample used has also a great influence over the accuracy of the final calculated settling velocity. Hulsey (1961) concluded that, with increasing sample weight, the faster falling larger grains fall faster, and the smaller grains at the trailing boundary fall slower. Hulsey did not explain this effect, but it appears that it is probably related to sample concentration effects. These are the effects of grain to grain interactions, in terms of grains being slowed in the turbulence produced by other grains falling through the water column. This effect is at its maximum immediately after a sample is released in the water, where the high concentration of grains may result in a density current effect before each grain attains its individual velocity. The experimental work of Slot and Geldof (1986) on different grain size and sample weights showed that a sample weight of 2-4g produced errors of less than 1-5% due to this concentration effect. Rigler et al (1981) used samples usually 4-5g in weight in his analysis in a settling tube of 19cm diameter.

Emery (1938) proposed the use of a settling velocity type of analysis for sand sized particles. However, due to the fact that his settling tube device and measurement methods were crude, his technique was not accepted. The post-1945 advances in electronic instruments added new impetus to the design and construction of more sophisticated settling tubes. The Woods-Hole (USA) rapid sediment analyser (Zeigler, Whitney and Hayes, 1960) was one of the first of these new generation settling tubes. Since then many settling tubes of different type and size have been put into use.

The fall tower (settling tube) system used for the analysis of sand-sized sediment samples in the current study comprises four main components:

- a 2m long plastic tube with an inner diameter of 28.5cm.
- a sample releasing system.
- an electronic balance.
- a Commodore Micro-computer.

In general, the procedure of sediment analysis using this system involves passing about 5g of a pre-prepared sand sample through the sample releasing system and continuously monitoring the weight of the sediments settling on the bottom of the tube. Once it was checked that all the parts of the fall tower were fully functional, the required sand sample was evenly distributed in the water around a large plug at the top of the tower (an integrated part of the sample releasing system which facilitates holding the sample until sampling is started; further details of the Fall Tower can be found in appendix IX). Sampling is initiated by a lever which raises the plug thus releasing the sample into the water column. The lever simultaneously activates a micro switch to set the timing system to zero and begin the recording sequence. After a few seconds, depending upon the size of the individual grains, the grains start to settle onto a balance pan which is suspended at the base of the tube by nylon threads connected to a balance fitted above the settling tube. The readings of the balance are automatically logged on to a floppy disk by the computer in the form of time versus weight. The data from floppy disks were ultimately transferred to the Vax main frame for further analysis.

5.4.3 Sedigraph.

The Micromeritics Sedigraph 5000ET particle size analyser was used for analysis of silt and clay sized fractions. This technique is similar, in principle, to the settling tube described above, but differs in the operation mechanism. The

Sedigraph measures the sedimentation rates of particles dispersed in a liquid and automatically interprets these data to yield a cumulative mass percent distribution in terms of equivalent spherical diameter. The Sedigraph makes use of a fine beam of X-rays to determine the concentration of particles remaining at decreasing sedimentation depths in a sedimentation cell as a function of time. The difference between initial (time=0) and instantaneous (time=t) transmitted X-ray intensity is electronically translated and presented as cumulative mass percent finer against particle diameter. The sedimentation cell itself is about 25mm (1 inch) in length, which is just enough to obtain accurate data for the fall rate of particles of 100 micrometer in diameter. In the case of particles of smaller sizes (0.1 to 0.2 micron in diameter), however, the time required to settle a similar distance (25mm) can be as much as 200 hours. To overcome this problem, the position of the sedimentation cell is automatically moved downward relative to the detecting X-ray beam. This cell movement is independently coordinated with the x-axis of the x-y recorder to indicate the equivalent spherical diameter.

The diameter range over which the analysis is required and the time of analysis depend upon particle and liquid densities, liquid viscosity, and the starting particle diameter. On the basis of the values of the above terms, a preliminary "rate" calculation is made. Selecting this rate on the Sedigraph programmes the instrument for the specific requirement. For further details on the Sedigraph technique and instrumentation reference should be made to Vitturi and Rabitt (1980), Stein (1985), or the Micromeritics instrumentation manual for the Sedigraph 5000ET.

The calculated rate used for the current study was set to analyse particles ranging in diameter between 70μm and 0.25μm. The system was attached to a Viglen micro-computer which enabled continuous recording of the data onto a disk and simultaneous plotting of the data on screen as the sample was

being analysed. In total, 40 silt and clay sized fractions of the samples collected in the 3 Areas were analysed using this system.

5.5 Final processing of the grain size data.

After laboratory analysis of gravel, sand, silt and clay sized fractions of all the samples, the results were analysed using various computer programmes. Complete processing of the data was achieved by using 5 different computer programmes at various stages. A schematic diagram of the processing sequence of grain size data using computer programmes is shown in Fig: 5.2. A brief introduction to each of the programmes used is given below.

1) **FT1.For** :- This programme is used at an initial stage to translate the time weight data of the fall tower analysis into cumulative weight percentage against grain diameter.

2) **GSCALC.FOR**:- This programme performs all the calculations involved in determining the moment and Folk grain size parameters. It also plots the cumulative and frequency distribution curves. A hardcopy record of both parameters and curves, can be obtained via an appropriate printing device. The samples composed of 100% sand are directly processed by this programme, while the samples containing composite fractions (gravel, sand, and fines) are passed through another programme in order to combine the data.

3) **GSIN.FOR**:- This allows the fall tower data (FT1.FOR output) to be combined with Sedigraph data. The samples composed of sand and fines are combined directly using this programme. However, in the case of those samples composed of gravel, sand, and fines, another problem is encountered, since GSIN.FOR does not allow sieve data to be

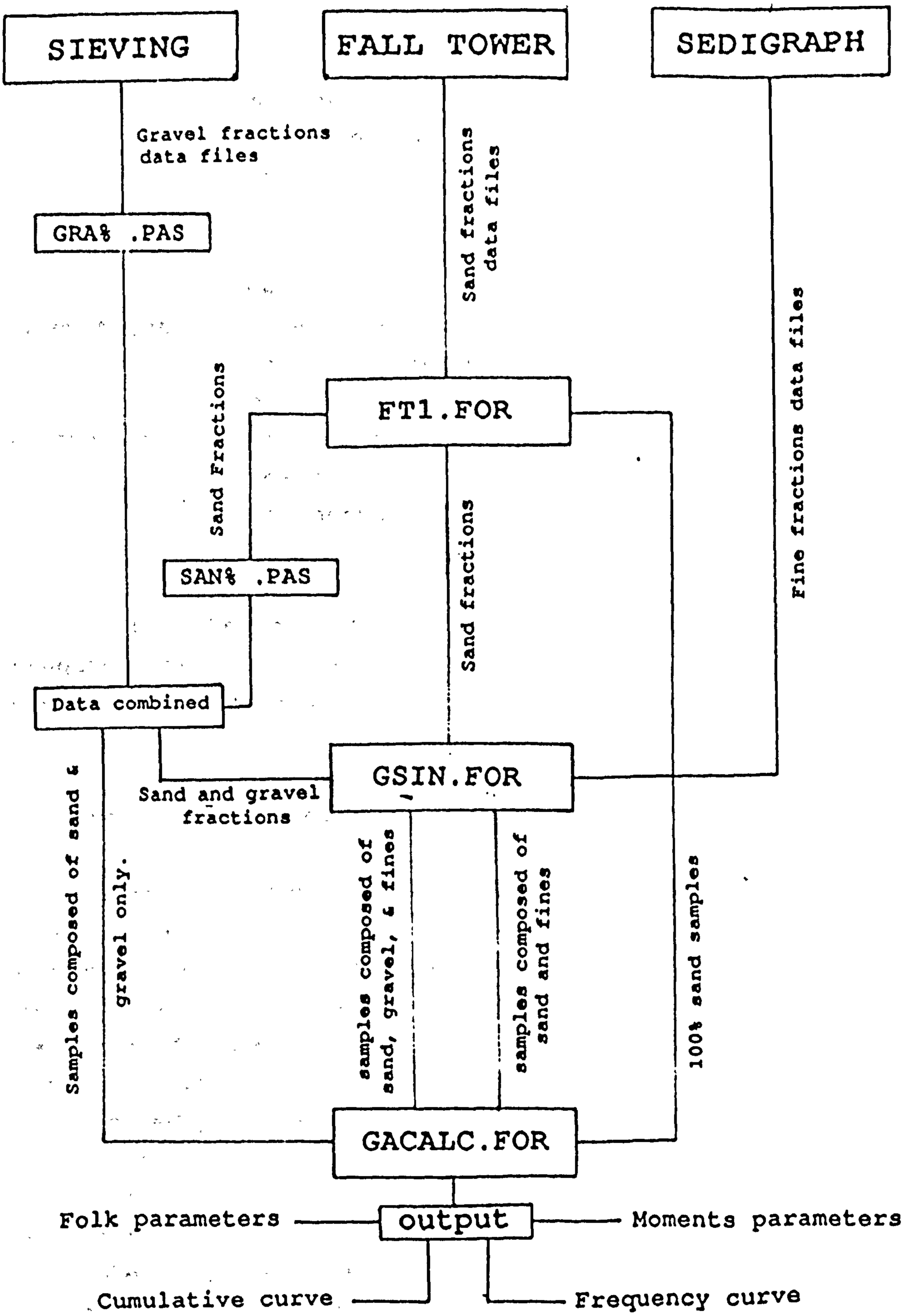

Fig: 5.2 Schematic diagram of the sequence followed for the processing of grain size results.

combined with fall tower and Sedigraph data. To overcome this problem the sieve data is combined with the fall tower data files obtained by FT1.FOR. In order to do this two additional new programmes, GRA% .PAS and SAN% .PAS were used.

4) **GRA% .PAS:-** This programme transforms the cumulative weight data of gravel, obtained by sieving, into cumulative weight percentage.

5) **SAN% .PAS:-** This facilitates the adjustment of the fall tower data files (FT1.FOR output), according to the actual percentage of sand in a sample, thus enabling the gravel data to be added.

At the end, the results were ultimately obtained in the form of frequency curves, cumulative frequency distribution curves, and moment and Folk grain size parameters for each of the sediment samples.

5.6 Grain size distribution curves.

Once the sediment samples had been analysed using the appropriate laboratory techniques, the next important step was presentation of the data. The most useful way of presenting the grain size data is either by grain size distribution curves (allowing further quantitative readings to be made) and/or by statistically calculated parameters. Folk (1966) strongly recommended plotting distribution curves for each analysis, even if the grain size parameters are obtained statistically. He argued that, by not drawing the distribution curve, it is not possible to get the "feel" of the data and it is also not possible to detect bimodality and see genetic relationships. He further emphasised that there is really no substitute for constructing a distribution curve if there is a need to visualize mixed populations.

Buller and McManus (1979) distinguished four main types of

distribution curves; a) histogram of frequency distribution, b) frequency distribution versus log diameter, c) cumulative frequency distribution, and d) cumulative frequency distribution as a probability plot (Fig: 5.3).

Histograms of typical grain size spectra result in an asymmetrical distribution with the mode remaining on the fine side of the mean diameter. It is well known that the grain size distribution is generally log-normal, and it is now general practice to use the logarithm of the grain size (Spencer, 1963). Plotting the frequency distribution curve (type b) using the logarithm of diameter removes the asymmetry from the frequency curve. Pettijohn (1957), however, states that many sediments are not log-normal and even those that are approximately so show some departure from a strict log-normal distribution. Spencer (1963) suggests that these skewed log-normal curves may be best explained by considering them as mixtures of three or less log-normal populations of grain size (this concept will be discussed further in section 5.7). As such, the frequency distribution curves are very important in indicating mixed populations.

Another common method of plotting grain size data is by means of a cumulative frequency curve. These curves are obtained by plotting the cumulative percentages against log diameter. Cumulative curves are very useful as the data can readily be visualised and correlated with other samples, and errors in weighing or caused by faulty sieves can easily be detected (Folk, 1966).

The grain size data can also be plotted as a cumulative frequency distribution on probability paper. The plotting of a log-normal sediment population on probability paper appears as a straight line, and is far superior to other curves where interpolation is required.

For presentation of data for this project two types of curves,

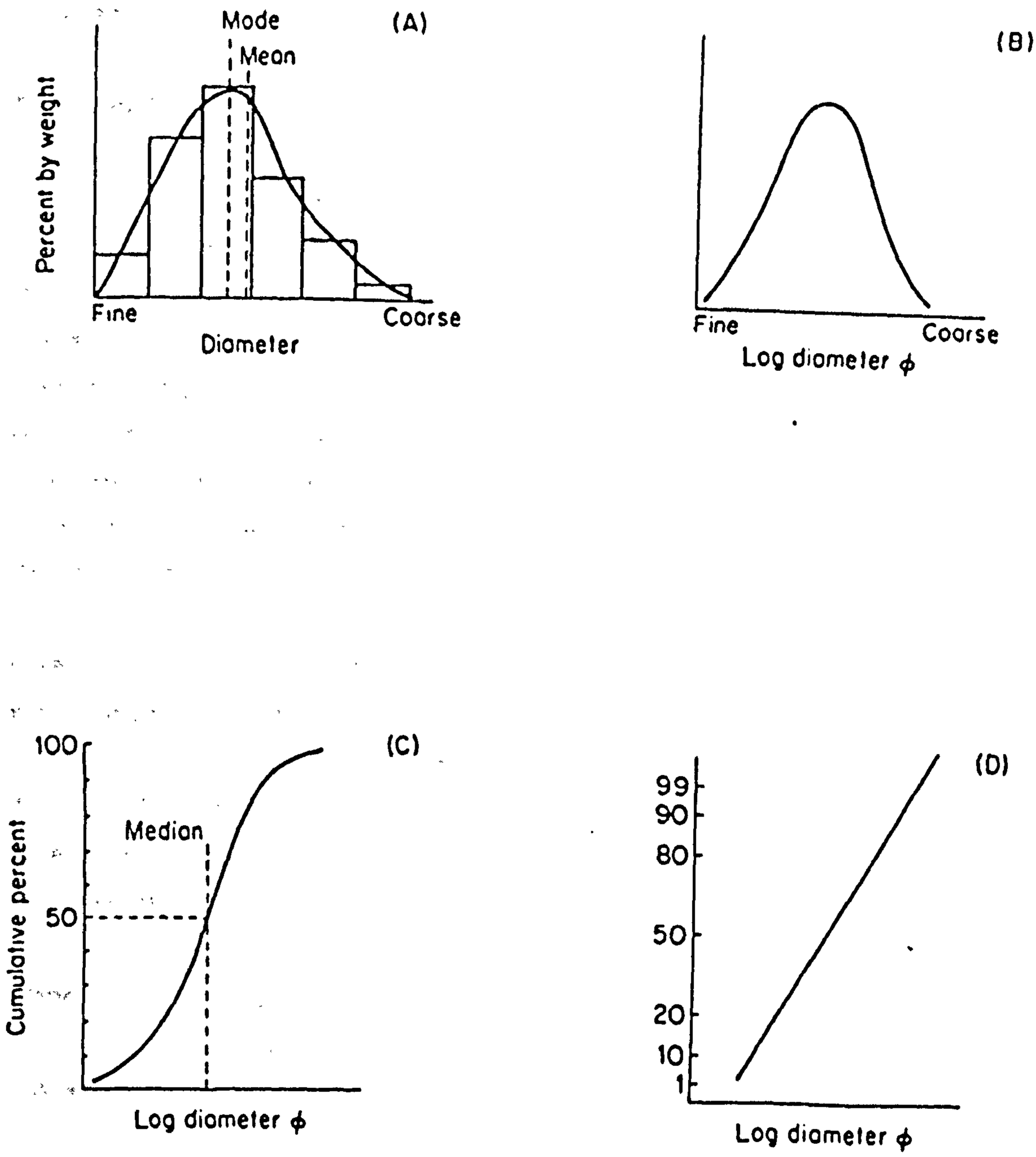

Fig: 5.3 Various types of grain size distribution curves.
a) Histogram of frequency distribution.
b) Frequency distribution versus log diameter.
c) Cumulative frequency distribution curve.
d) Cumulative frequency distribution as probability plot. (after Dyer, 1985)

cumulative frequency and size frequency, were drawn for each of the samples, and these will be discussed later.

5.7 Grain size parameters.

Numerous quantitative parameters obtained from grain size analyses have long been used to interpret environments of deposition. These parameters range in complexity from those obtained by computing the various moments (Krumbein and Pettijohn, 1938) of the sample distribution about some central measure of sediment diameter, to those obtained by selecting a few points (graphical measures) from the cumulative frequency curves of the sediments (Otto (1939), Inman (1952), Folk and Ward (1957)).

One of the basic purposes in determining the grain size parameters is to facilitate comparison of samples and to aid in the correlation between sediment type and environment (Inman, 1952). The most widely used grain size parameters include: mode, mean, sorting, skewness, and kurtosis. Sahu (1964) suggested the following definitions for the above parameters.

Mode:- It indicates the most frequently occurring size of the sediment in a grain size distribution.

Mean:- It indicates the overall average size of the sediment.

Sorting:- It is the measure of the uniformity of the sediment.

Skewness:- Measures the asymmetry of the frequency distribution.

Kurtosis:- Indicates deviations from the normal distribution at the extremities of the sediment distribution.

To determine these grain size parameters two different methods were used in this study and are described below.

5.7.1 Method of moments.

Method of moments was first proposed by Van Orstrand (1925) and Krumbein (1936) later adapted the technique for use with his phi scale ($\phi = -\log_2 D$, where D is the grain size in mm). This technique involves the computation of grain size parameters by taking into account the entire frequency distribution. For example, the calculation of mean by moment method takes into account the weight percentages and mid point in each of the size grades. Further details on the moment method are well documented in Krumbein and Pettijohn (1938).

Folk (1966) described the moment method as the most elegant technique. However, he argued that despite its aesthetic satisfaction for natural sediments, the method of moments does have some serious drawbacks. For example, in the case of his studies, Folk (1966) reported that the moment method assumes that the particles with a size grade (1ϕ to 2ϕ) have a centre of gravity at the half way mark (i.e. 1.5ϕ) while his calculations showed that it is in fact 1.71ϕ and that could give an erroneous sorting value of 0.76ϕ instead of an actual value of 0.70ϕ. As far as the calculation of grain size parameters in this study is concerned, the above mentioned error is of little significance, because the size grade interval of 0.10ϕ has been used in most of cases.

5.7.2 Graphical measures.

Various graphical measures of average grain size have been proposed (Trask (1930), Otto (1939), Inman (1952), Folk and Ward (1957)). The graphic measures are obtained by reading percentiles from a cumulative curve. In general, it is accepted that the more percentiles read, the more accurate the method should be (McCammon, 1962). As such, in deciding which graphic method to use, it is necessary to compromise between simplicity and accuracy. From that point of view, the graphical measures proposed by Folk and Ward (1957) appear to be the best suited

for calculation of the grain size parameters.

Folk and Ward (1957) suggest that, the commonly used graphical measures are inadequate, particularly when frequency curves are non normal, because they are based on only two or three points read off the cumulative curve. Consequently, they proposed a new series of statistical measures which include more points on a curve. In addition to quantitative measures, Folk and Ward (1957) also suggested verbal limits for the skewness and sorting, and these are listed in Table No. 5.1.

5.8 Multimodal distributions.

Non-normal skewness and kurtosis values are held to be the identifying characters of bimodal sediments even where such modes are not evident in the frequency curves (Folk and Ward, 1957). Several workers attribute the bimodal populations within a grain size distribution to different sediment transport mechanisms (Visher (1969), Sagoe and Visher (1977)). Inman (1949) defines three distinct methods of sediment transport:

1. **Surface creep:-** It is also called a bedload phenomenon in which the material slides or rolls along the bottom with the velocity less than that of fluid current.
2. **Saltation:-** It is a jumping motion in which the particles momentarily bounce above the bottom and travel with the velocity of the fluid.
3. **Suspension:-** The suspension of the sediment is caused by fluid turbulence. The size of the sediment that may be held in suspension is dependent upon the intensity of turbulence. Consequently the break or truncation point between suspension and bedload transport may be highly variable on a cumulative curve and reflect physical conditions at the time of

Table No. 5.1

Verbal limits of sorting and skewness according to Folk and Ward (1957)

Sorting	
Very well sorted	0.00 - 0.35
Well sorted	0.35 - 0.50
Moderately sorted	0.50 - 1.00
Poorly sorted	1.00 - 2.00
Very poorly sorted	2.00 - 4.00
Extremely poorly sorted	>4.00
Skewness	
Very negative	-1.00 - -3.00
Negative	-0.30 - -0.10
Nearly symmetrical	-0.10 - +0.10
Positive	+0.10 - +0.30
Very positive	+0.30 - +1.00

deposition (Visher, 1969).

5.9 Significance of the grain size parameters.

Each of the grain size parameters may be useful in an interpretation of the physical processes acting on the sediment. The mean grain diameter of a sediment population, for instance, indicates the average energy of the depositing agent. Sahu (1964), however, states that the average size of a sediment is dependent also upon the size distribution of the available source material.

The sorting indicates the range of the energy (velocity) of the depositing agent. When a sediment is produced by two different modes of deposition, such as a combination of bedload and suspended load, the sorting may indicate the difference in the velocity associated with these modes of deposition. The skewness measures the asymmetry of the grain size frequency distributions. If the skewness is negative, the sample is coarsely skewed and where the skewness value is positive the sample is described as finely skewed. Assuming sufficient quantities of material of different sizes are available, a coarsely skewed sample implies that the velocity of the depositing agent operated at a higher value than the average velocity for a greater length of time than normal and/or the velocity fluctuations towards the higher values occurred more often than normal (Sahu, 1964).

5.10 Areal distribution of the bottom sediments in the study area.

The bottom sediments of the study area show a wide variation from one part of the area to another. In some cases the bottom sediments of one particular location contain a mixture of gravel, sand, and fine (silt & clay) sediments. However, in general, two main types of bottom sediments can be distinguished in the area. These are

1) very fine to very coarse sands.
2) fine gravel.

The areal distribution of these two types of sediments in the Menai Strait and Caernarfon Bay is shown in Fig: 5.4 (the grain size results obtained for each sample using Moments and Folk methods are listed in appendix X). The type 1 sediments (very fine to very coarse sand) are the predominant type from the inner limits of the area within the Menai Strait to the outer limits of the ebb-tidal delta in Caernarfon Bay. In the outer zone i.e. further offshore the dominancy of the sand sediments is partially interrupted by type 2 sediments (gravel) which occur as discrete patches. However, the type 1 sediments continue to extend down to the deeper water parts of the study area. The type 2 sediment does not show any obvious trend in areal distribution and occurs only as isolated patches.

In order to get a better understanding of the areal distribution of the type 1 and 2 sediments, an effort was also made to produce separate contour diagrams of the % of sand and gravel within the sediments in the area (Figs: 5.5 and 5.6 respectively). The contour diagram of sand % clearly reveals that most of the study area is covered with 100% sand sediments. The lowest value of the sand % in the area reaches a value of less than 40%, and that only occurs at one place i.e. near Llanddwyn island. Fig: 5.4 shows that the sediments with mean grain size $>-1\phi$ occur in small isolated patches. Figure 5.6 provides a detailed picture of the areal distribution of the % of the gravel fraction in a sample, and from that it can be noted that gravelly sediments occur in a fairly large part of Caernarfon Bay. Another important factor that can be noted here is that, although the gravel sediments are spread over large parts of Caernarfon Bay, the % of gravel appears to increase towards three distinct parts of the area where gravel % reaches to over 60%.

Fig: 5.4 Aerial distribution of the bottom sediments
in the Menai Strait and Caernarfon Bay.

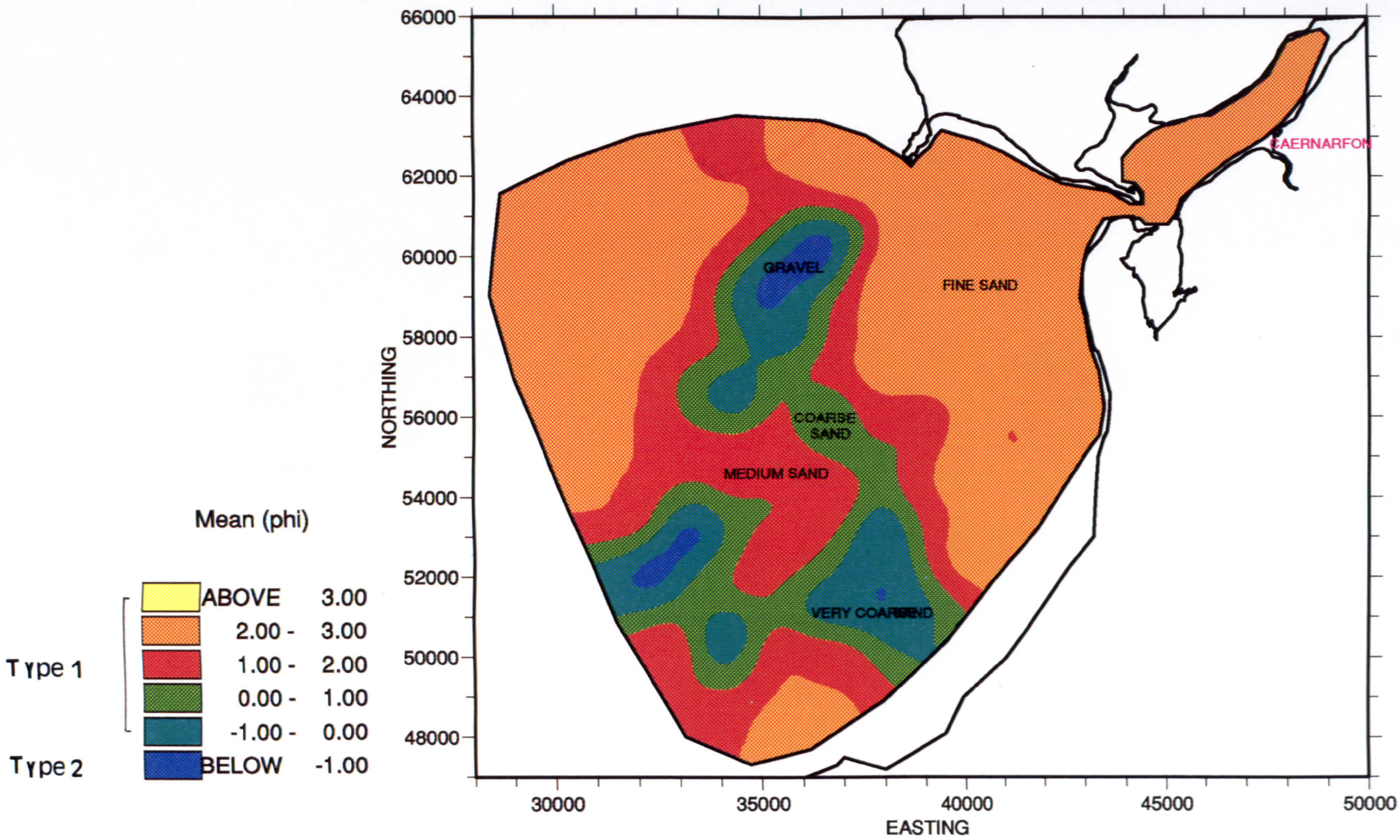

Fig: 5.5 Contour diagram of the percentage of sand in the study area.

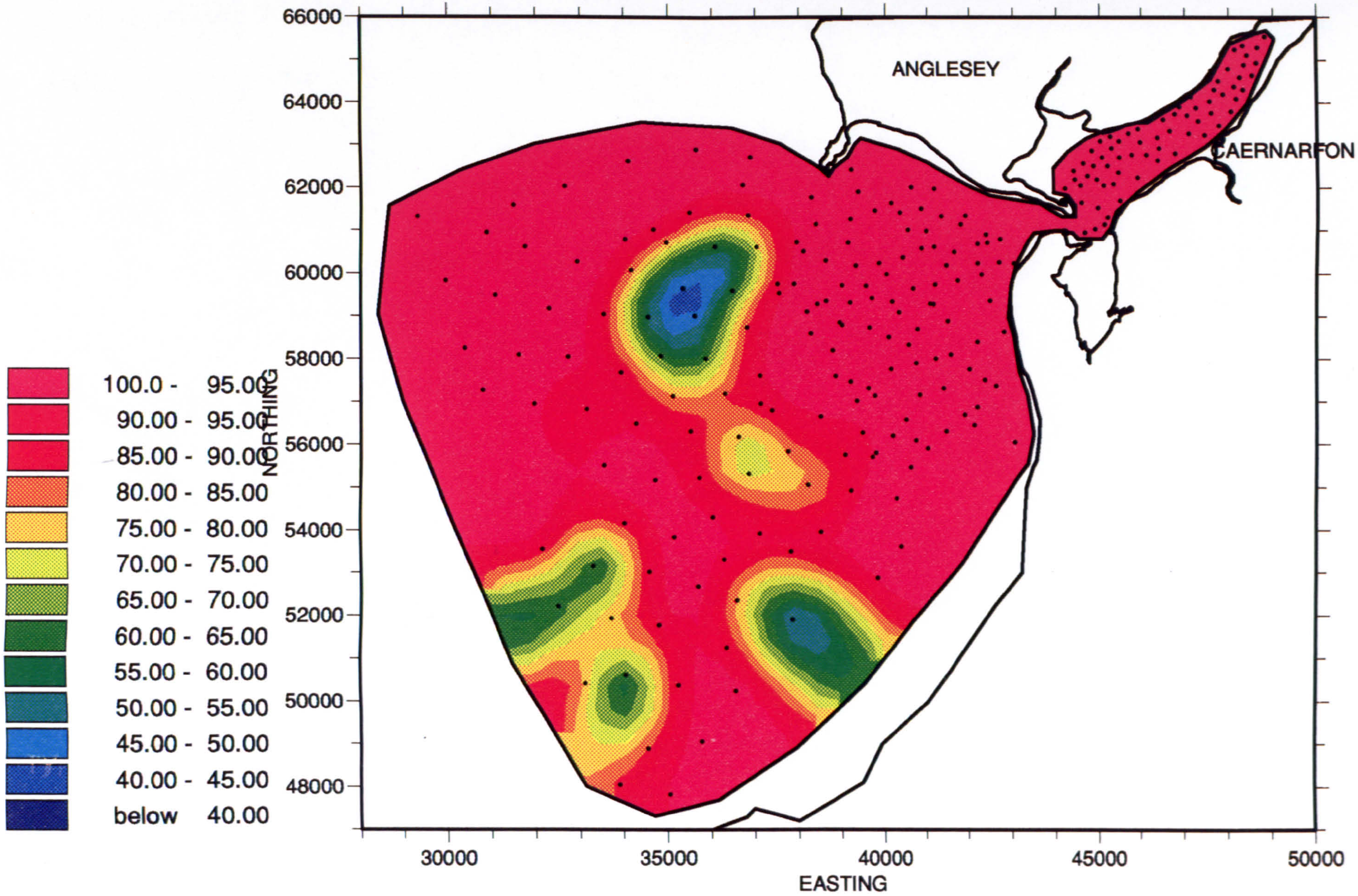

Fig: 5.6 Contour diagram of the percentage of gravel in the study area.

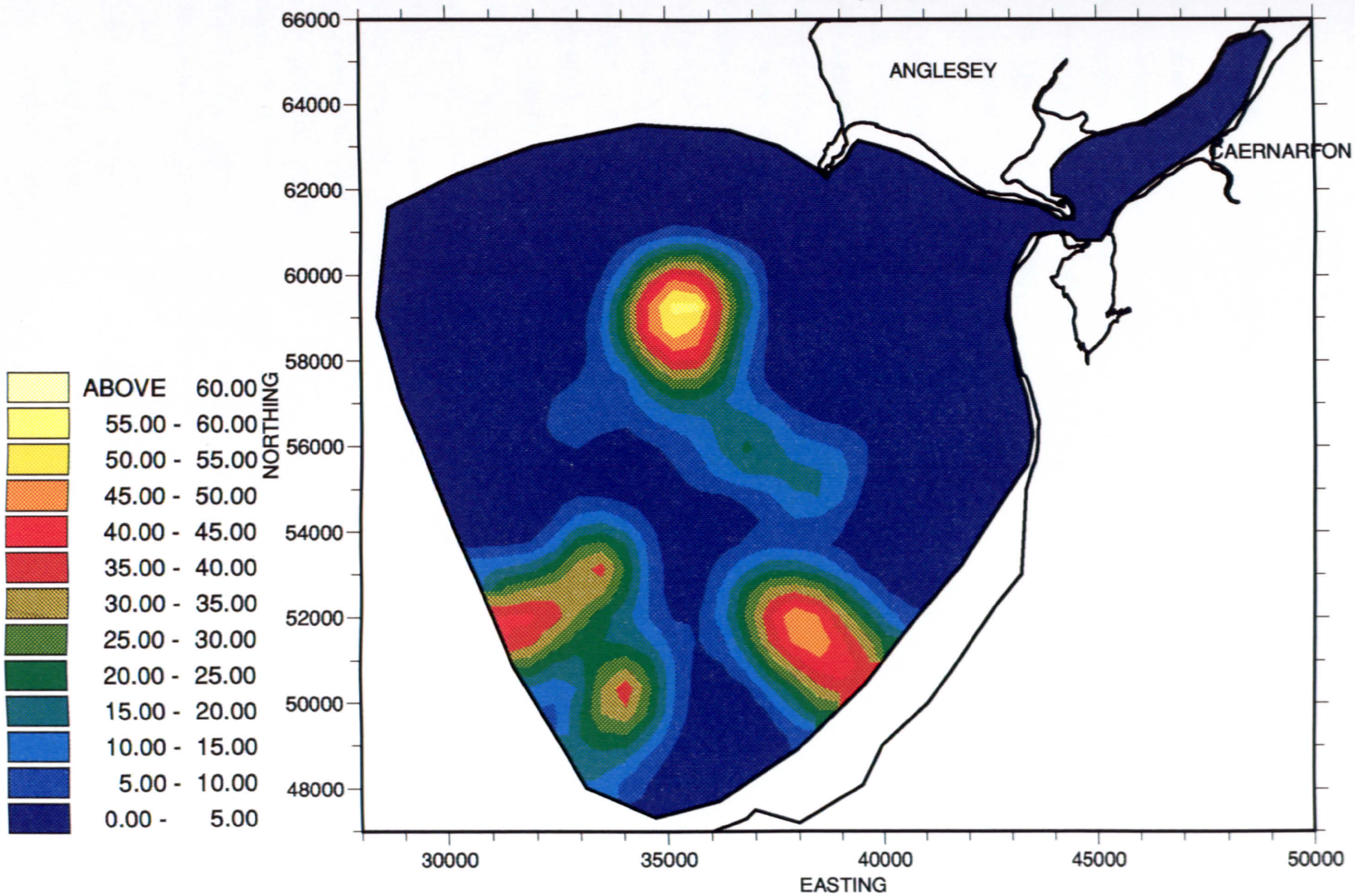

5.11 General features of the cumulative curves.

The cumulative grain size curves representing the samples from different parts of the study area exhibit marked difference in the type and size of the sediments. In order to characterise these bottom sediments, typical cumulative curves were chosen from each of the Areas i.e. 1, 2, and 3 (as mentioned in section 5.2), and are shown as Figs: 5.7a, 5.7b, and 5.7c respectively.

One of the most interesting features of the cumulative curves is that they show a change in the percentage of dominant sediment population type from Area 1 to Area 3. For instance, Fig: 5.7a (Menai Strait area) indicates that the sediments are almost entirely composed of one main log-normal grain population (sand) whereas the typical curves of Area 3 (Fig: 5.7c), indicate the presence of more than one dominant sediment mode (though some curves are similar to those of Area 1 (sample Nos. S265 & S300)). This diversity results from the fact that a number of sediment samples of Area 3 are composed of two main fractions i.e. sand and gravel and to some extent also silt and clay. Since various techniques were used to analyse the gravel, sand, and silt and clay fractions of each sediment sample, it was felt that, in order to justify the combination of results obtained by three various techniques, the cumulative distribution curves for a) each of the fractions and b) the whole sediment sample should be plotted separately. Examples of this kind are demonstrated in Figs: 5.8 and 5.9. These indicate that the curves of the various fractions give a sufficiently close fit to allow a continuous line to be drawn for each sample.

The mean grain size of the sediments of Area 1 range between 2.7ϕ (fine sand) and 1.9ϕ (medium sand). Most of the curves are log-normal, with only a few exceptions where the sediments are either slightly +ve or -ve skewed. The majority of the Area 2

sediment curves are similar in general shape and character to the Area 1 curves, although the samples collected from the area near to the outer (offshore) limits of the ebb-tidal delta (Sample Nos. S175 & S182) are composed of more than one mode and are relatively coarser. One thing that must be noted here is that the latter sediment type (such as sediment samples S175 & S182) in area 2 represents approximately less than 10% of the sediment sampled, whereas the majority of the samples are represented by samples S82 and S96 (Fig: 5.7b).

Typical curves from Area 3 (Fig: 5.7c) indicate enormous diversity in their general shape and sediment type. In addition to sand, gravel is one of the major sediment fractions present in this area. Fine particles (silt & clay) also constitute a relatively small fraction of the Area 3 samples, although the fine particles seldom cross the 3-4% limit. The mean grain size of the sediments of this area range between 2.7ϕ (fine sand) to -2.7ϕ (medium gravel).

5.11.1 Multimodal cumulative curves.

From a study of the cumulative curves shown in Figs: 5.7a, 5.7b, and 5.7c, it can be seen that some of the sediment samples obtained from Area 3 and to a certain extent from Area 2, appear to be a mixture of more than one mode. For example Area 2 cumulative curves shown in Fig: 5.7b (Sample Nos. S175 & S182) show breaks at two places in the slopes of the cumulative curves. These breaks occur at about 2ϕ and at 0.5ϕ. Very similar breaks (at 2ϕ and 0.8ϕ in value) in the slopes of the cumulative curves have also been reported by Fuller (1961) while studying the shallow marine sediments off the Cape of Good Hope, South Africa. Fuller gave various explanations for this phenomenon, such as possible systematic error in analysis technique or more probably the layering of the surficial sediments of various grain size. The explanation he favoured most was that these breaks in the slopes of the cumulative curves possibly result from the differing transport mechanisms such as saltation,

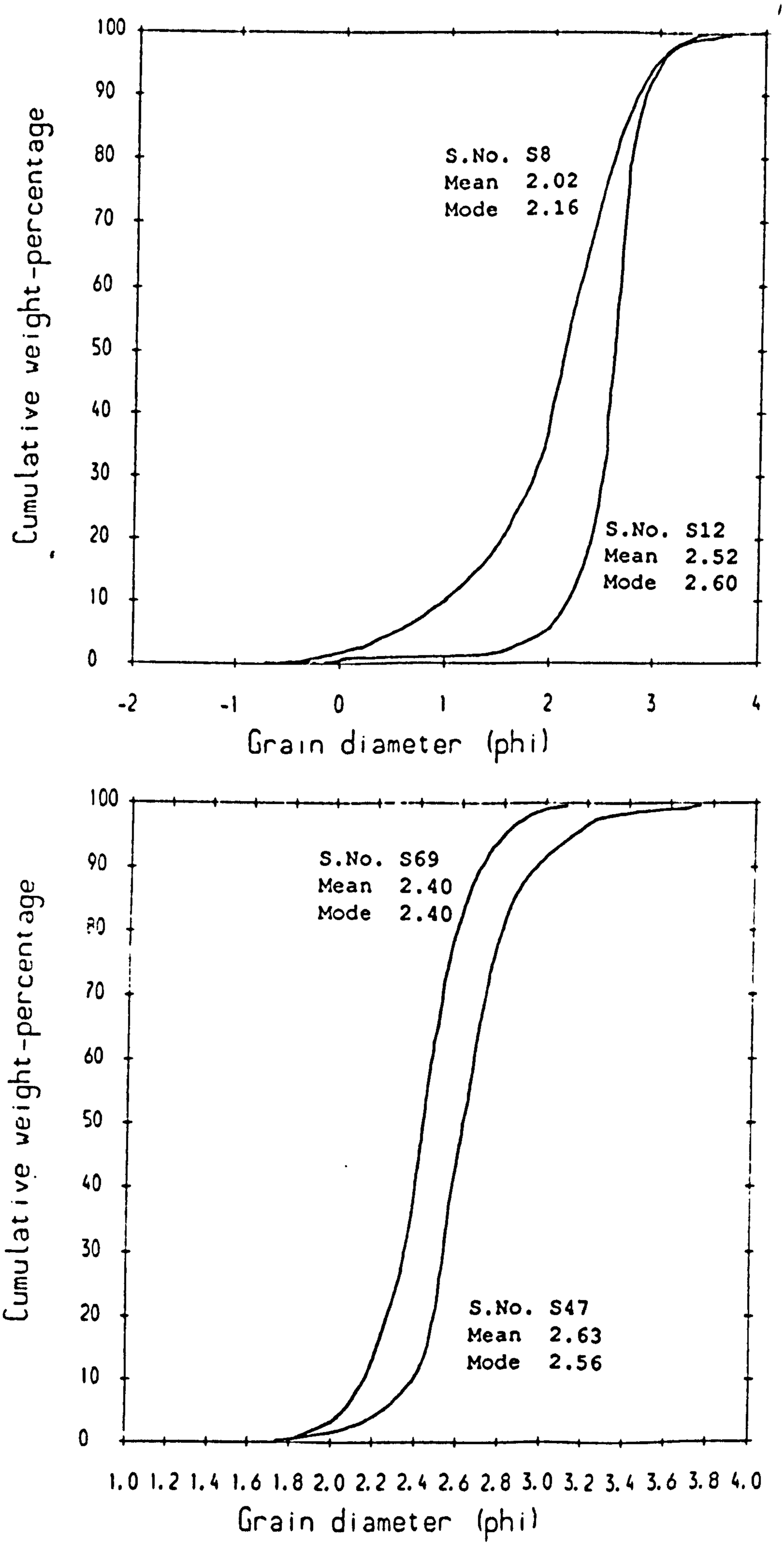

Fig: 5.7a Typical cumulative curves of Area 1.

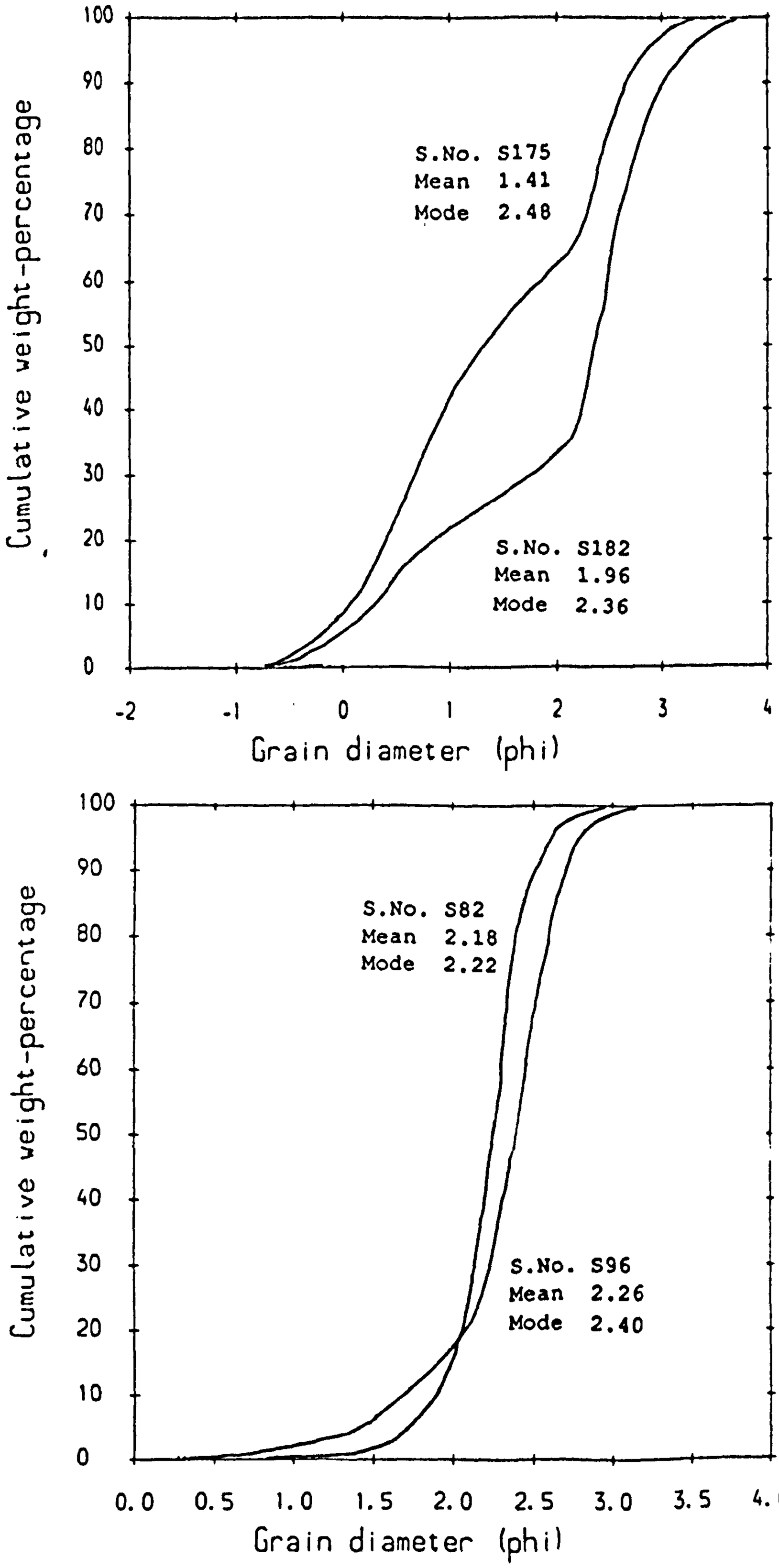

Fig: 5.7b Typical cumulative curves of Area 2.

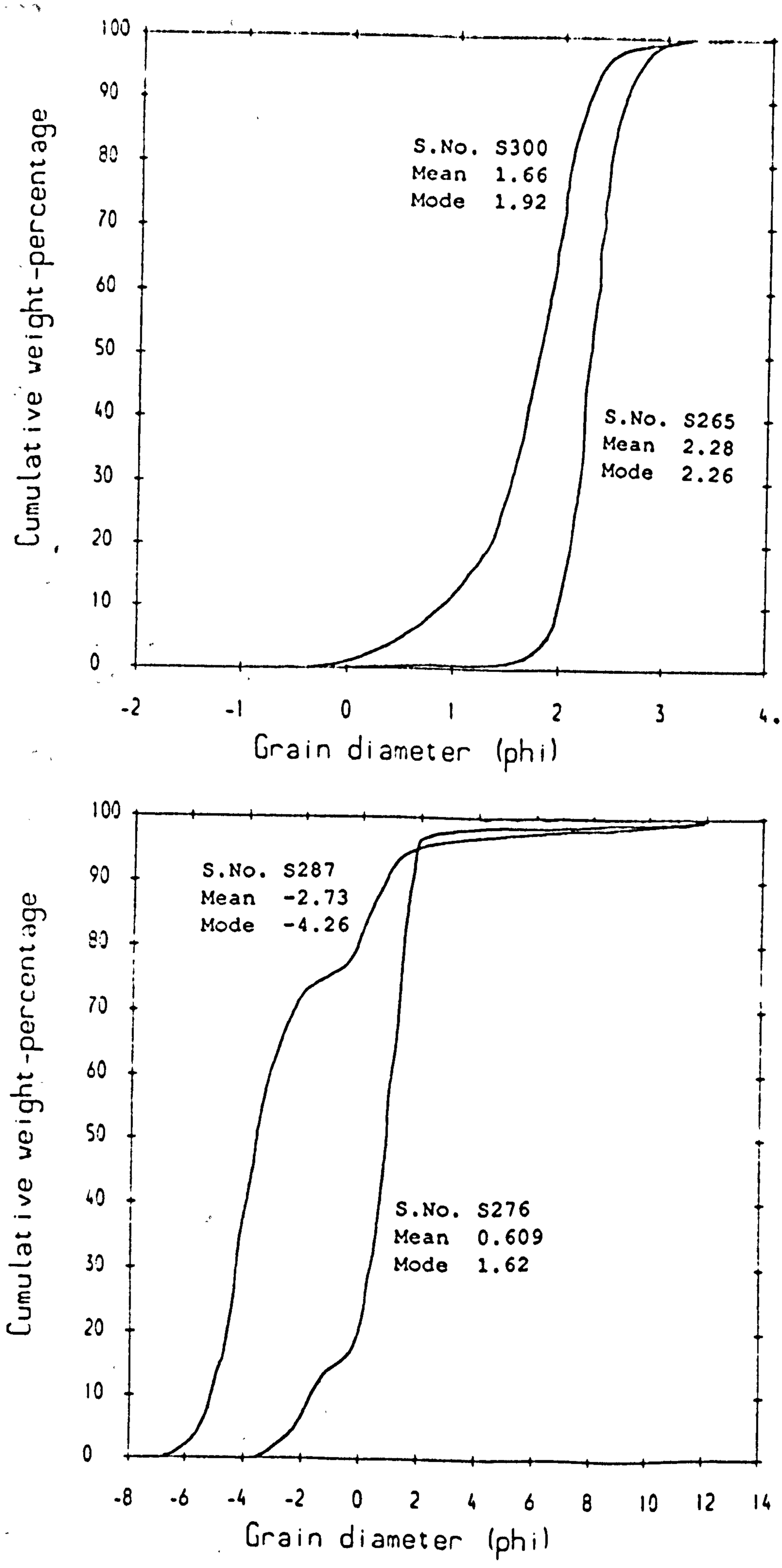

Fig: 5.7c Typical cumulative curves of Area 3.

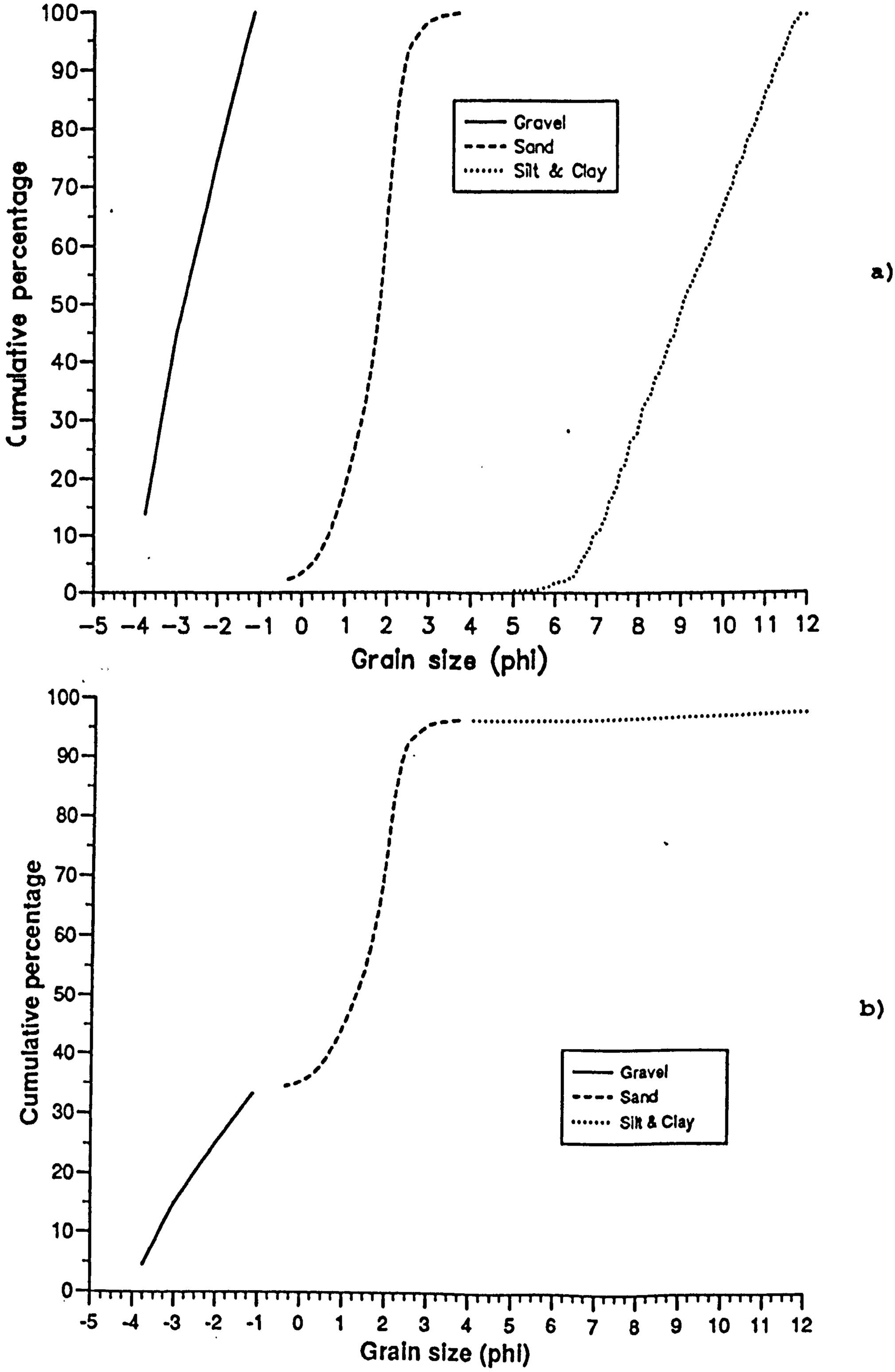

Fig: 5.8 a) Separate cumulative distribution curves of gravel, sand, and silt and clay fractions present in sediment sample No. S258.
b) Cumulative distribution curve of sediment sample No. S258.

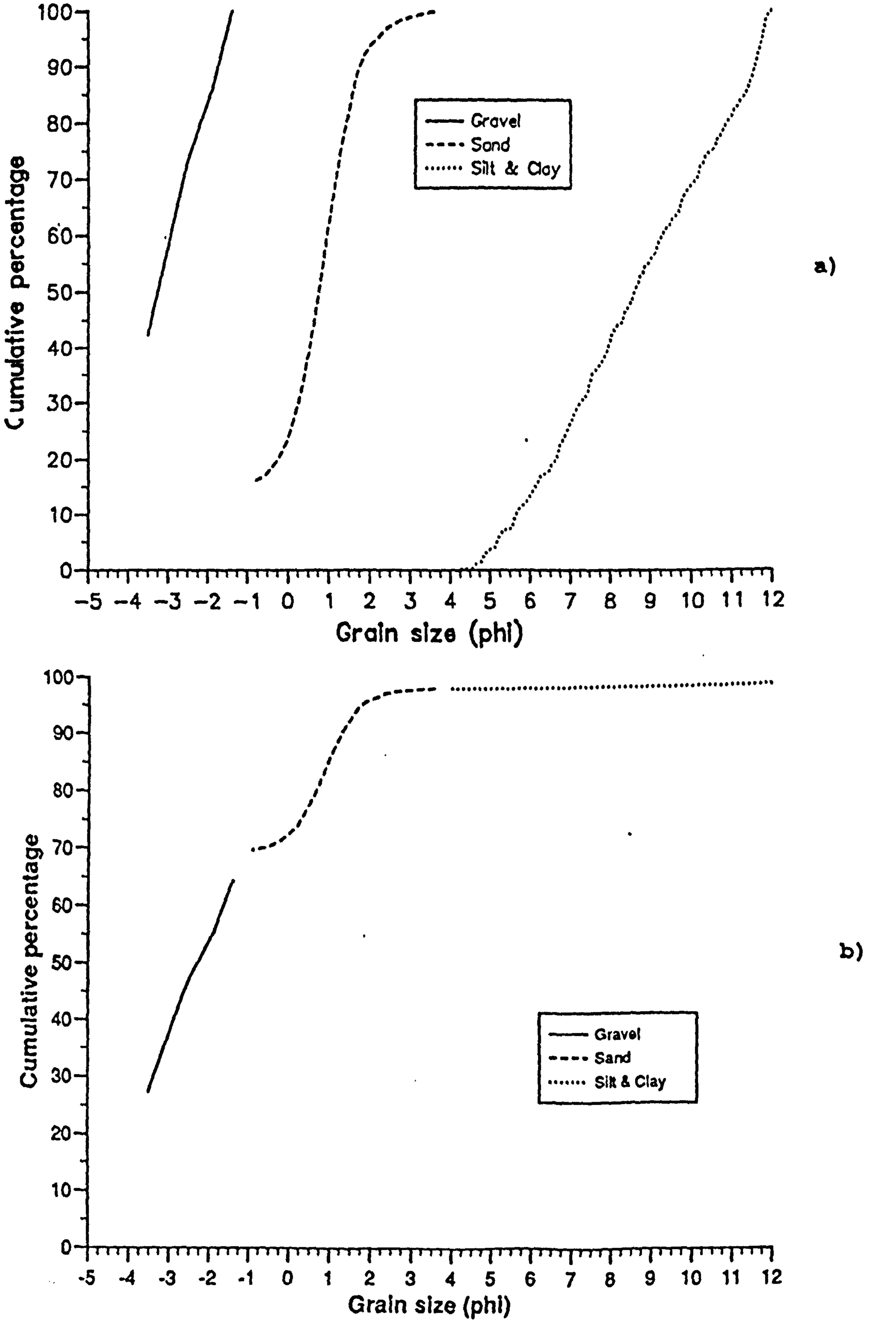

Fig: 5.9 **a)** Separate cumulative distribution curves of gravel, sand, and silt and clay fractions present in sediment sample No. S260.
b) Cumulative distribution curve of sediment sample No. S260.

traction, and suspension. A similar explanation is also given by Visher (1969).

The multimodal curves from Area 3, however, show two different points on the cumulative curves where breaks in the slopes of the cumulative curves occur. Two obvious breaks can be observed at 0ϕ and -2.5 to -3.5ϕ. In the case of samples containing fine particles, an additional break in the slope of the cumulative curve usually occurs between 3 and 3.5ϕ.

5.12 Grain size results - general summary.

In order to gain a clearer understanding of the areal distribution of the grain size parameters in the study area as a whole, an effort was made to produce contour diagrams of the sorting and skewness of the sediments according to the verbal limits of Folk and Ward (1957). The main aim was to use these contour diagrams for a general consideration of the trends in sorting and skewness of the diverse bottom sediment types, before presenting the fine details of the various grain size parameters.

Folk and Ward (1957) suggested verbal limits only for sorting and skewness. However, once these two diagrams were produced there was strong evidence that a similar type of diagram for mean grain size would be needed to describe the results of skewness and sorting in relation to mean. Thus a contour diagram of the mean grain size (Fig: 5.12) was also produced at a contour interval of 0.2ϕ value.

The most interesting and important feature revealed by these diagrams is the general trend of variation between the sediments of the Menai Strait and in the deeper offshore parts of the area. For instance, Fig: 5.10 shows that the sorting of the sediments becomes poorer in a seawards direction from the Menai

Strait and other coastal areas. The diagram also suggests that within the Menai Strait and just outside the Belan inlet in Caernarfon Bay the sediments are very well sorted. This trend continues until it is disrupted by a consistent band of well sorted sediment, that extends from Llanddwyn Island to Dinas Dinlle beach. This band of well sorted sediment probably represents the zone between the ebb-tidal delta and offshore sediment, because from here seawards (further offshore) the sorting of the sediment tends to decrease.

The mean grain size contour diagram (Fig: 5.12) indicates that this parallel band of well sorted sediment represents the finest sediment found in the study area. It also indicates that the mean grain size of the sediment tends to increase on either side of this band of well sorted fine sediment. It also supports the interpretation that this band represents the zone where environmental change is taking place.

Detailed examination of the sorting and mean size contour diagrams (Figs: 5.10 and 5.12 respectively) also suggests that there is a strong link between the mean grain size and sorting of the sediments. The sorting tends to decrease with increasing grain size and vice versa. As such the sediments in the gravelly areas are very poorly sorted whereas the fine to medium sand sized sediments in the areas of the tidal deltas are very well sorted.

The sediment skewness shown in Fig: 5.11 also matches well with the sorting and mean size diagrams, particularly in the areas predominantly covered by pure sand sized sediments (Menai Strait and just outside the Belan area). In these areas the skewness values of the sediments remains +/- 0.1 and the frequency curves are generally symmetrical or near symmetrical. However, the skewness of the sediments further offshore is less clear and shows poorer correlation with mean and sorting results.

Fig: 5.10 Sediment sorting according to the verbal limits of Folk & Ward (1957).

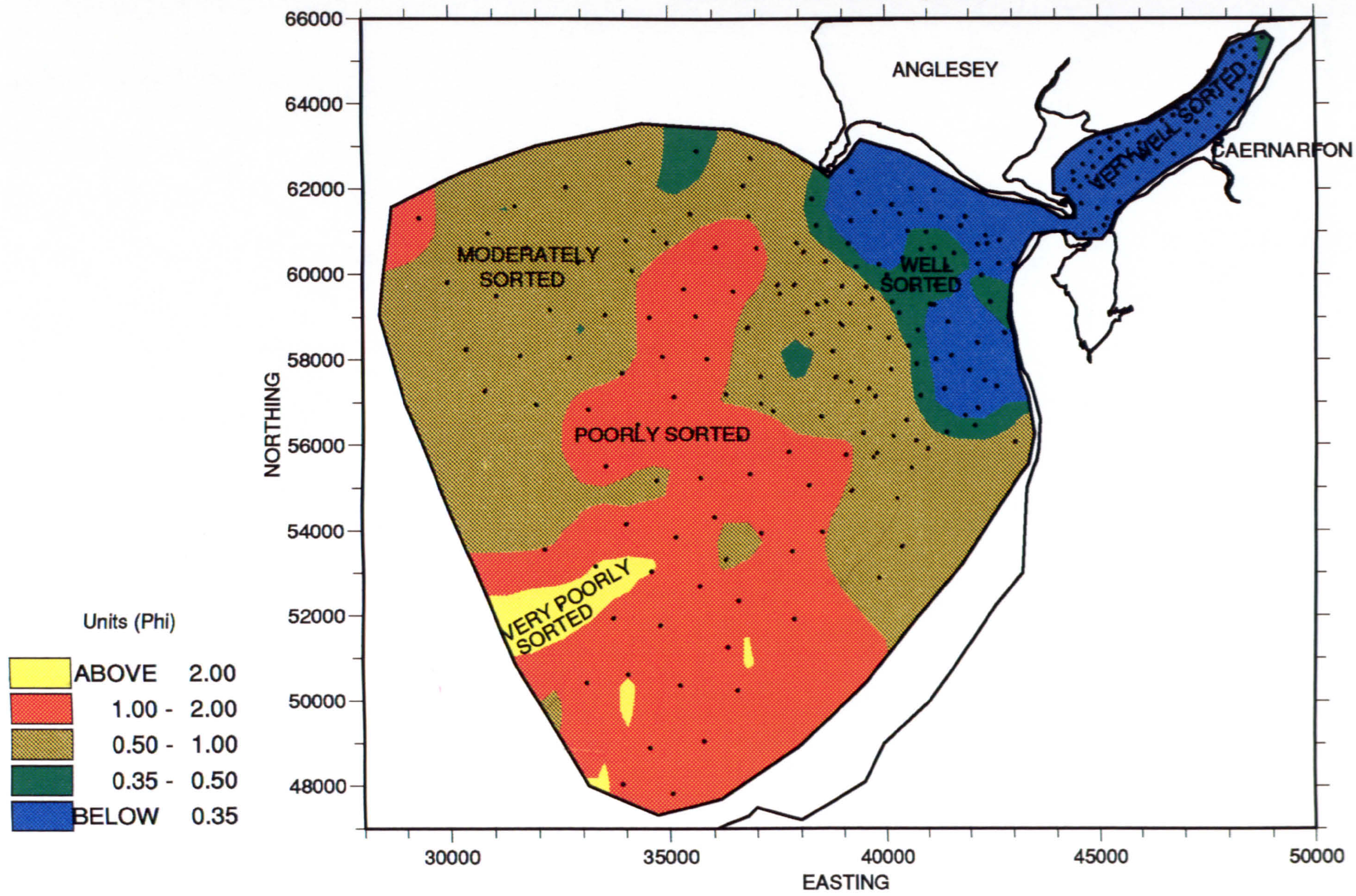

Fig: 5.11 Sediment skewness according to the verbal limits of Folk & Ward (1957).

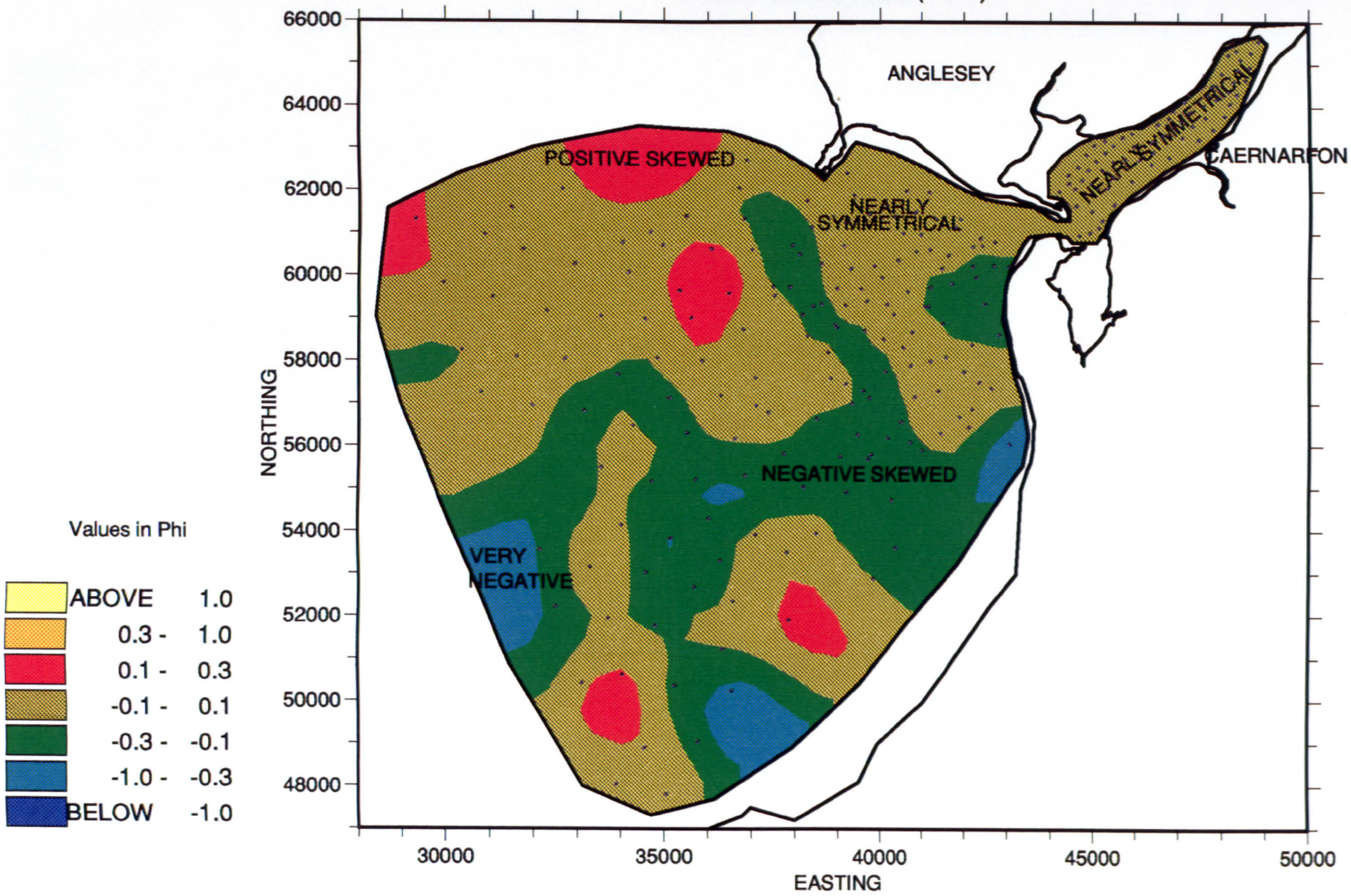

Fig: 5.12 Contour diagram of mean grain size
in phi (moments)

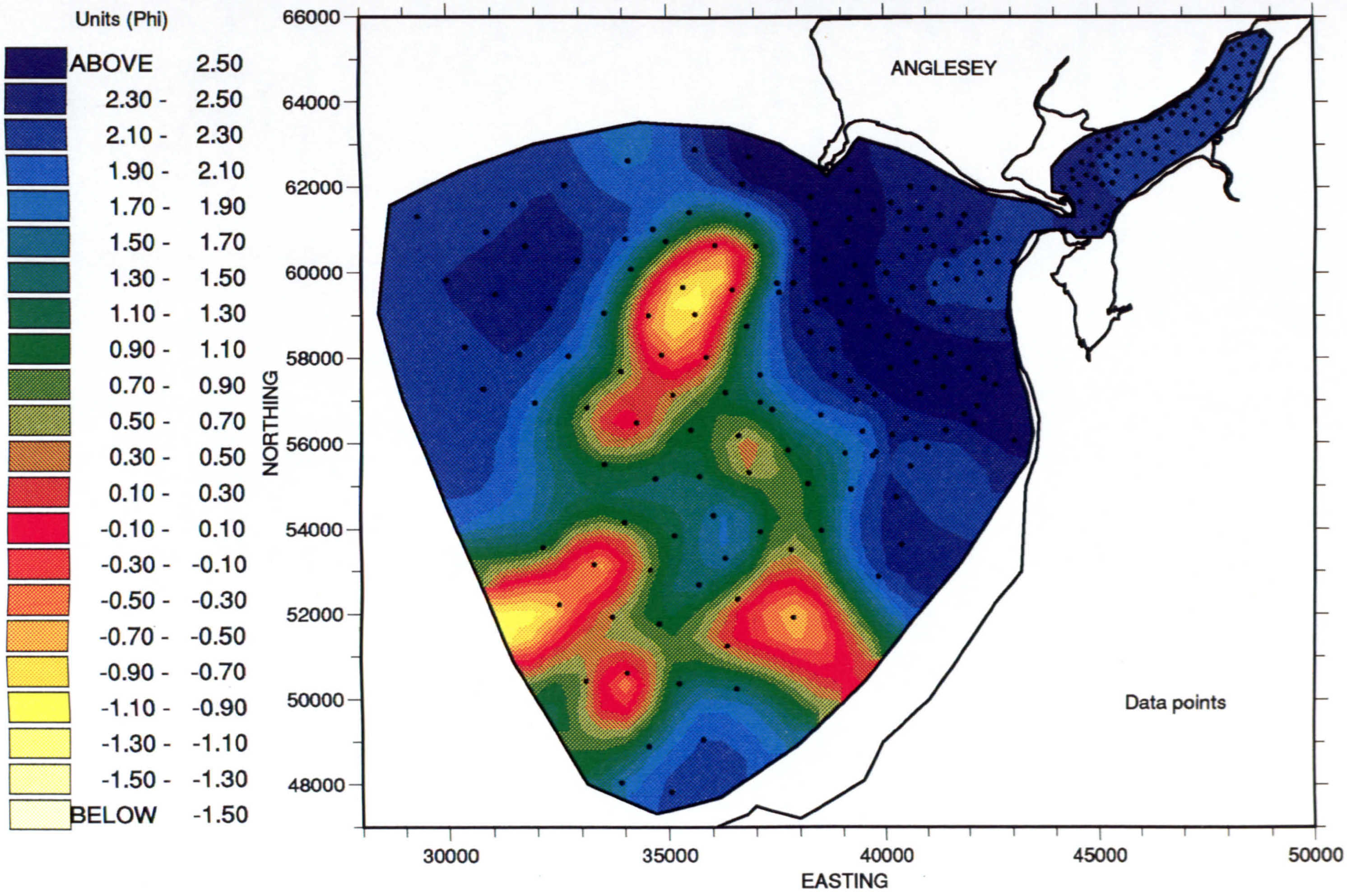

5.13 Grain size results - specific detail.

Up until now efforts have been devoted towards the understanding of the major features related to grain size distribution in the study area. In order to obtain a deeper insight into the fine details of the various grain size parameters, line contour diagrams have been produced for each of the parameters obtained by moments and graphical methods. While preparing these diagrams it was felt that it would not be practical to contour the whole study area using a constant contour interval. The main reason for this was that within the Menai Strait and in the area of the ebb-tidal delta just outside Belan inlet, the values of grain size parameters change only slightly while there are more major changes in the remaining area. For example, within the Menai Strait and in the area of the ebb-tidal delta the mean grain size ranges between 1.9ϕ and 2.8ϕ (moments), whereas in the remaining offshore area the mean ranges between -2.5ϕ and +2.5ϕ. Consequently, two different contour intervals were used to prepare the diagrams.

To facilitate this presentation the whole study area was split into two new zones i.e. A and B (which are different to previous areas 1, 2, and 3). This division was essentially roughly along the offshore limits of the ebb-tidal delta in Caernarfon Bay. For the exact location of these two areas reference should be made to Fig: 5.13.

In addition, bearing in mind that the areas of tidal sand deposits were regarded as more important from the present study's point of view, it was decided to define the grain size distribution for area A in more detail and consequently, contour diagrams for this area were produced at 0.1ϕ interval, whereas in area B a contour interval of 0.5ϕ was chosen (except in the case of skewness where the same interval of 0.1ϕ was used for both areas). The contour diagrams are presented in such a way that the moment and Folk results for each of the parameters (mean and sorting) related to either area A or B appear on the

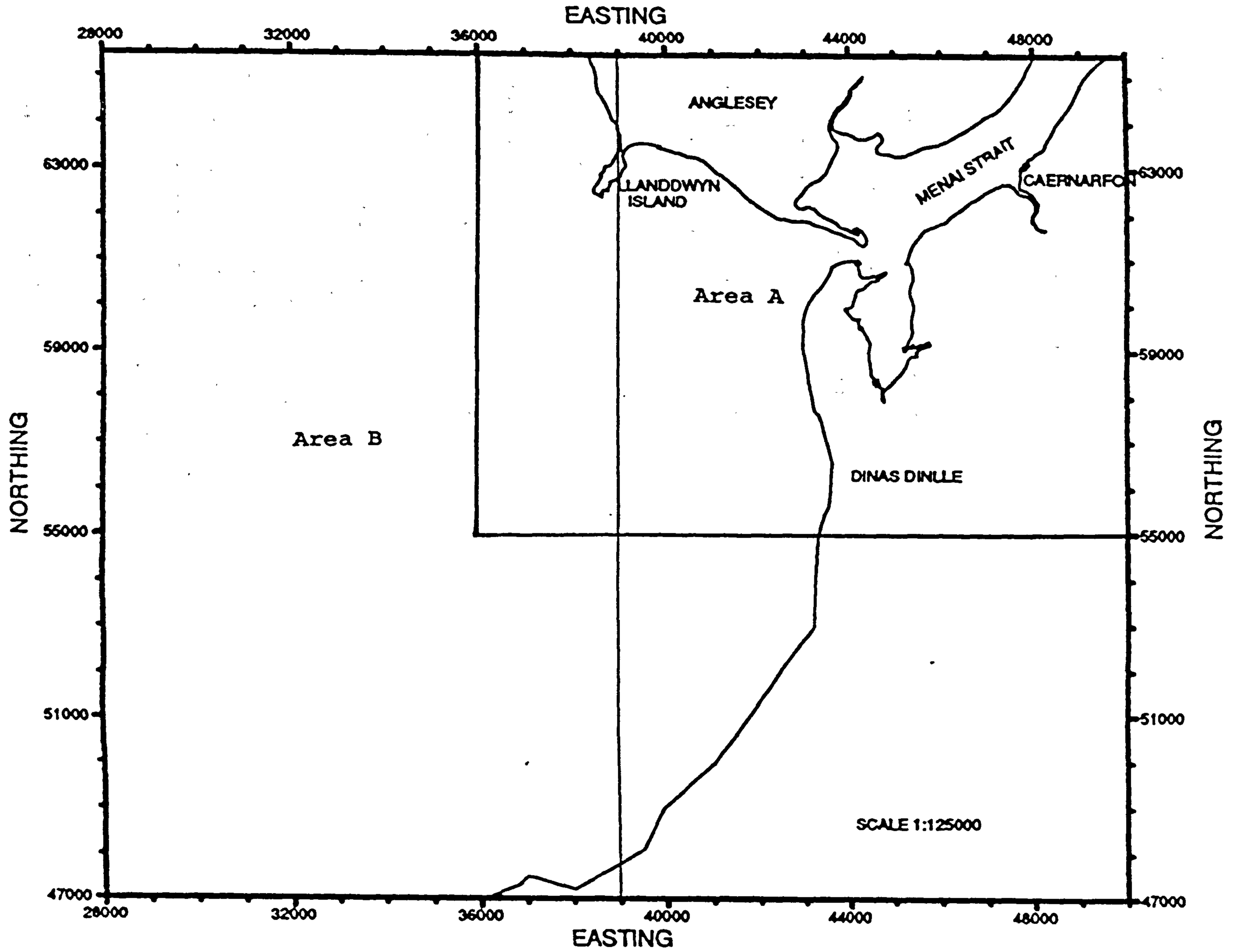

Fig: 5.13 Location map of the areas A and B.

same page for comparison purposes. For example, in Fig: 5.14, diagram A1 represents moment mean of the sediments occurring in area A, whereas the Folk mean of the same area is presented in diagram A2. The related diagrams of area B are presented in a similar fashion in Fig: 5.15.

5.13.1 Mean grain size

Looking at the general contour diagram of the mean grain size (Fig: 5.12), it appears that this is uniform over large sections of the study area. However, the detailed line contour diagrams of the same parameter presented in Figs: 5.14 and 5.15 reveal that this is not the case, and under the influence of the local morphological changes and prevailing hydrodynamic conditions the mean size tends to show considerable variation in relatively small areas. Both the mean diagrams i.e. moments and Folk, are discussed below.

Moments mean

The overall mean grain size in the study area ranges between -2.5ϕ and +2.9ϕ. About 74% of the total samples, however, remain within the mean grain size range of 2ϕ - 2.8ϕ, whereas samples with mean grain size less than 1ϕ make up only 11% of the total samples.

As described previously, the finest sediments (represented by the contours of 2.7ϕ and 2.8ϕ in Fig: 5.14, A1) occur as a conspicuous band along outer limits of the ebb-tidal delta, roughly stretching from Llanddwyn Island to Dinas Dinlle beach. From this band of fine sediments there is a trend of increasing mean grain size in directions towards the Belan inlet and moving further offshore. Since the mean grain size contours on either sides are roughly parallel to each other, this increasing trend appears to be reasonably consistent along the entire stretch of the fine band of sediments. These parallel contours are relatively well developed on the offshore side, while towards Belan inlet, it appears that this trend of parallelism is

interrupted because of the morphological variations occurring due to the ebb-tidal delta.

Within the Menai Strait the coarsest sediments are generally found in the tidal channels. For example, the main tidal channel area is characterised by the contours ranging between 1.8ϕ and 1.9ϕ. In contrast, fine sediments usually occur in the areas of inter-tidal and sub-tidal sand deposits adjacent to the channel. The mean size also appears to decrease towards the shoreline as can be seen in close proximity to Belan inlet on both sides (shores) of the Strait. Looking at the general appearance of the contours within the Strait nothing definitive can be said about any obvious trend in mean grain size. This is because most of the changes in the mean value are tied to the local topographic features. However, the contours of the ebb-tidal delta appear to show a decreasing trend in the mean size away from the inlet. The contour nearest to the Belan inlet shows a mean value of 1.8ϕ and that decreases to 2.8ϕ around the presumed limits of the ebb-tidal delta. In contrast to the Menai Strait, the sediments outside the Belan inlet show the opposite trend in that the coarser sediments tend to occur over and around the sand banks, whereas the finer sediments are found in the area of the main channel. This opposite trend in the occurrence of fine and coarse sediments could possibly be the result of a decrease in the intensity of the ebb tidal currents as soon as they pass the Belan inlet. The diminishing ebb tidal current velocity probably results in the quick deposition of coarse grained sediments in the shallow areas of the sand deposits, whereas the remaining fine sediments tend to be deposited further away in the main channel. If this is true, it may provide a vital clue towards the understanding of sediment transport pathways in the area.

Further offshore from the 2.8ϕ contour, the mean grain size tends to increase and very quickly reaches -1.5ϕ in the southwest of Llanddwyn Island and in the southeast corner of the map (Fig: 5.15 A1), and then decreases again before attaining

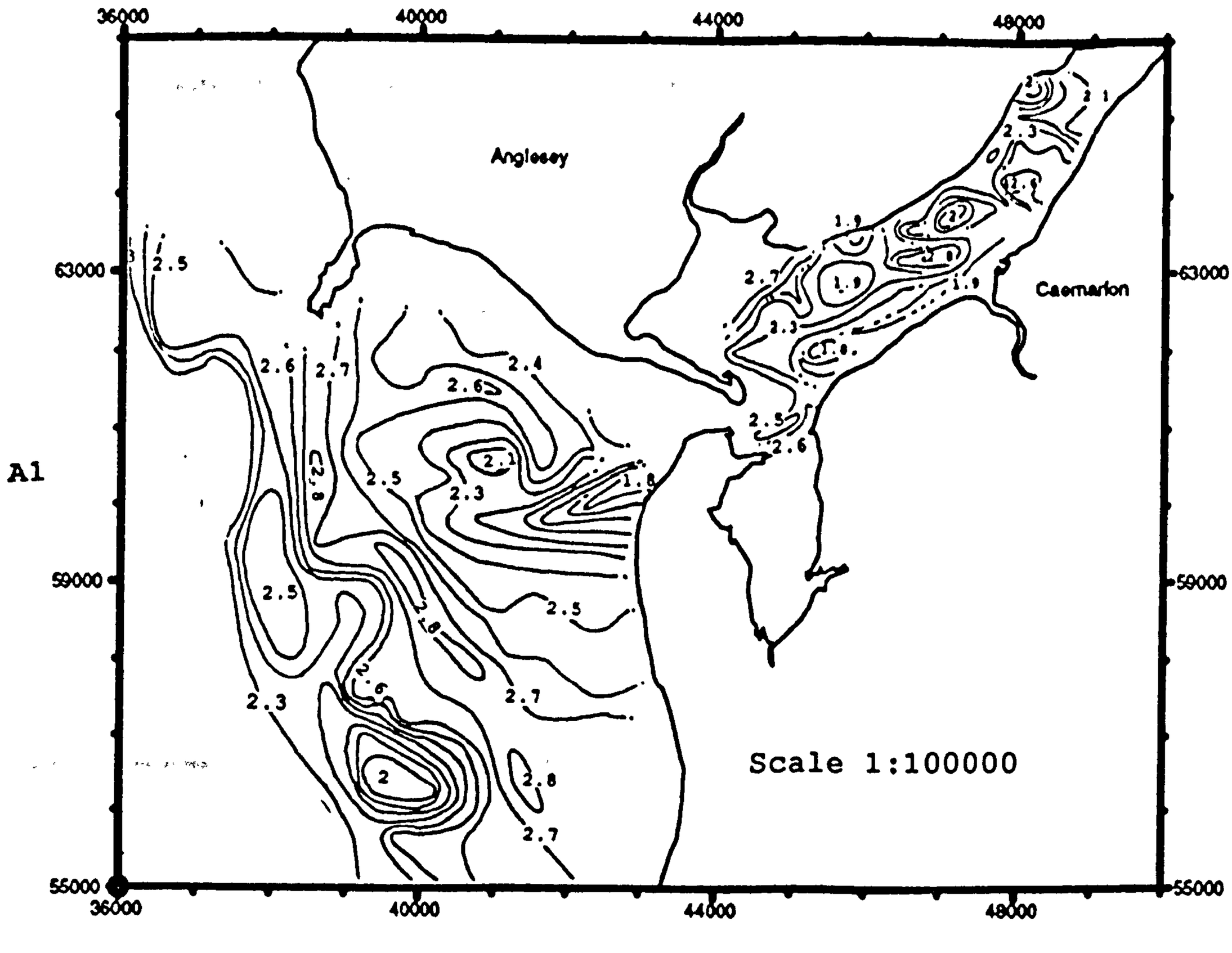

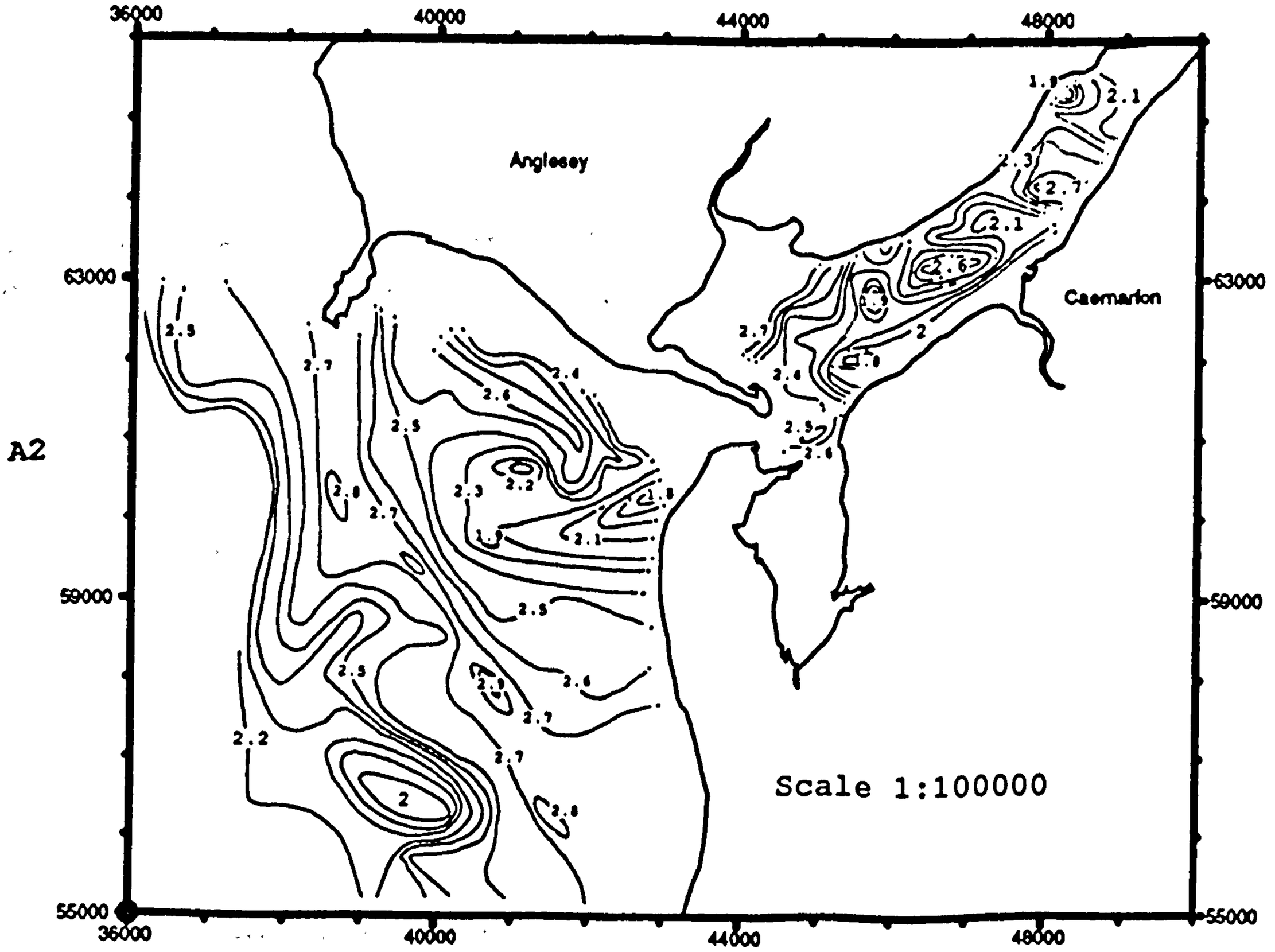

Fig: 5.14 Contour diagram of the mean grain size of area A.
A1) Moments A2) Folk. (contour interval .1 phi)

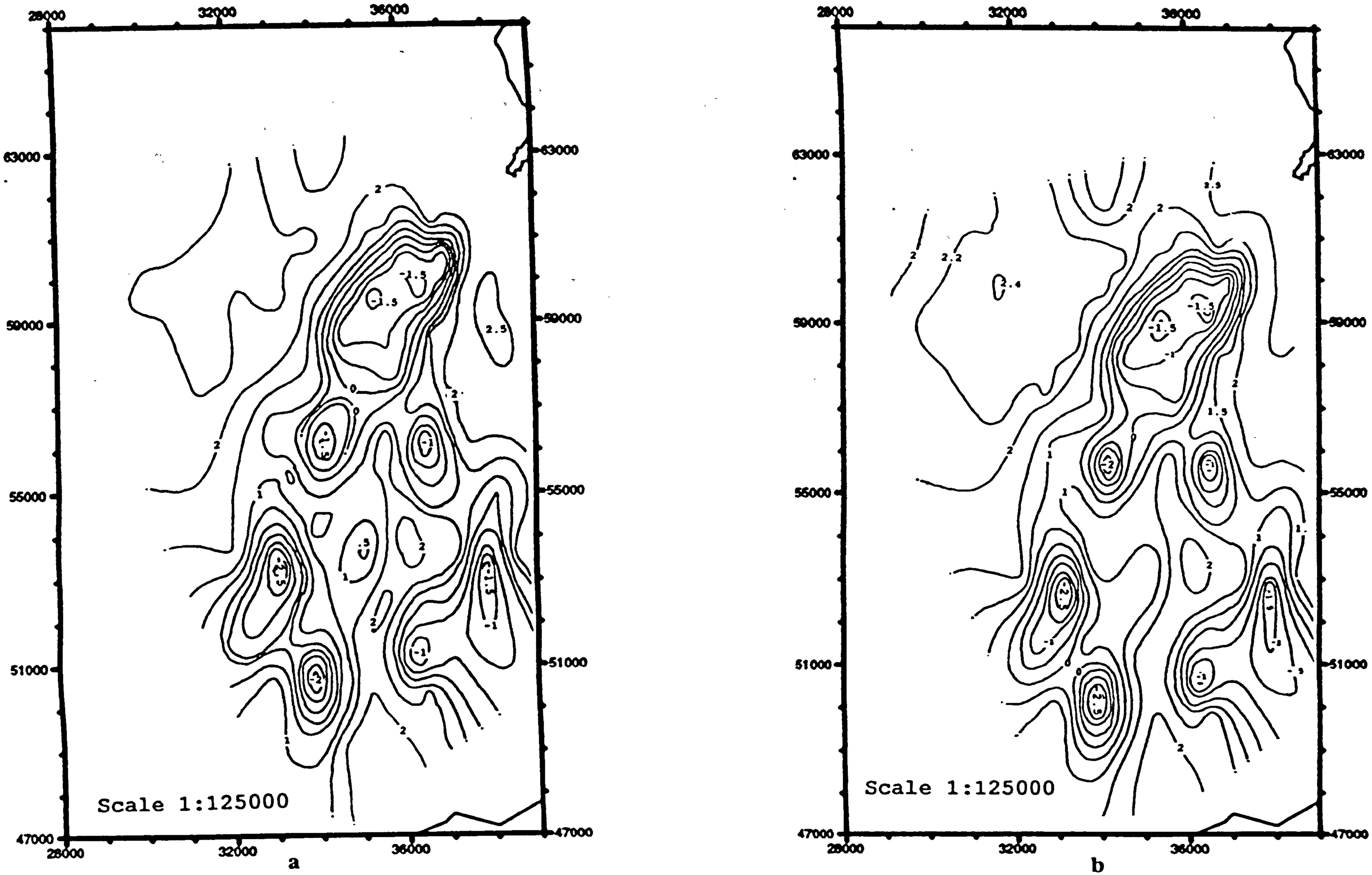

Fig: 5.15 Contour diagram of the mean grain size of area B.
B1) Moments B2) Folk. (contour interval .5 phi)

the maximum value of -2.5ϕ near the offshore extremities of the study area. However, the samples with mean grain sizes less than 1ϕ make up only 11% of the total sediment samples, although, one thing that must be noted here is that they are scattered over a fairly large area which is obvious from the diagram shown in Fig: 5.15 A1 (which indicates that the sediments coarser than 1ϕ form the shape of several small and large patches separated by relatively finer sediments).

Folk mean

The Folk mean diagram is very similar in general appearance to the moment mean diagram. Contour shapes and positions are almost identical except in a few places, such as south of Llanddwyn Island. Here contours show marked differences in shape and position, although there is very little difference in the contour value. The Folk mean size ranges between -2.5ϕ and 2.9ϕ.

5.13.2 Mode grain size.

The mode grain size ranges between -4.5ϕ and +2.8ϕ in the entire study area. The majority of the sediment samples, however, fall in the range between +2ϕ and 2.8ϕ. The sediment samples with mode grain size value less than +2ϕ makeup about 19% of the total samples, whereas the sediment samples having mode grain size coarser than -2ϕ represent only 4% of the total samples and are predominantly from the areas of gravel patches. The sediments having mode size less than 2ϕ predominantly occur in the areas well away (further offshore) from the tidal sand deposits of the Menai Strait and Caernarfon Bay, with only two exceptions where mode values of 1.8ϕ and 1.9ϕ have been encountered in the vicinity of the ebb-tidal delta in Caernarfon Bay.

Mode grain size is held to be a more reliable parameter than mean grain size for environmental studies (Folk, 1966). The distribution of the mode grain size is shown in Fig: 5.16. Schlee (1973) states that pronounced modal gradients, that is,

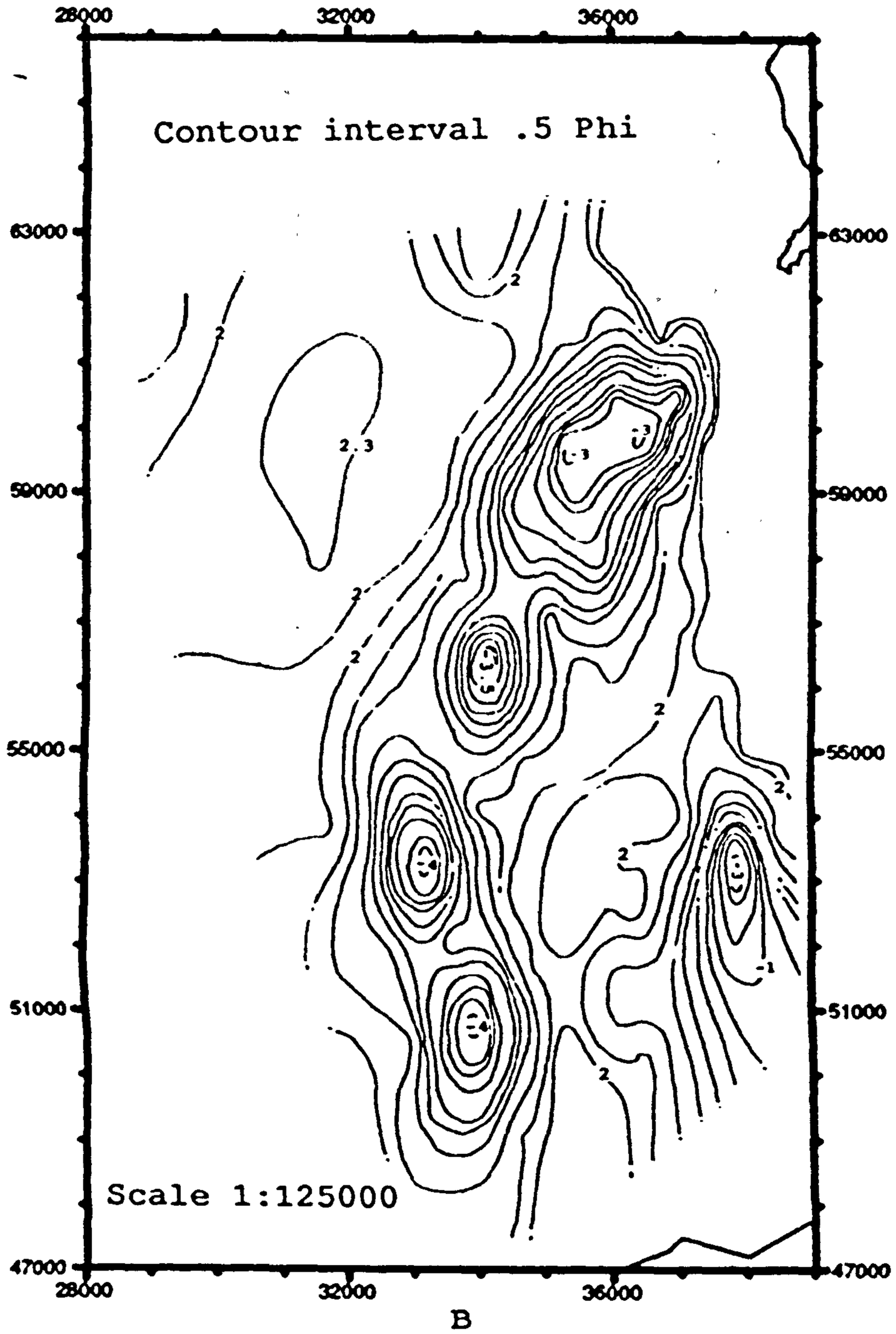

B

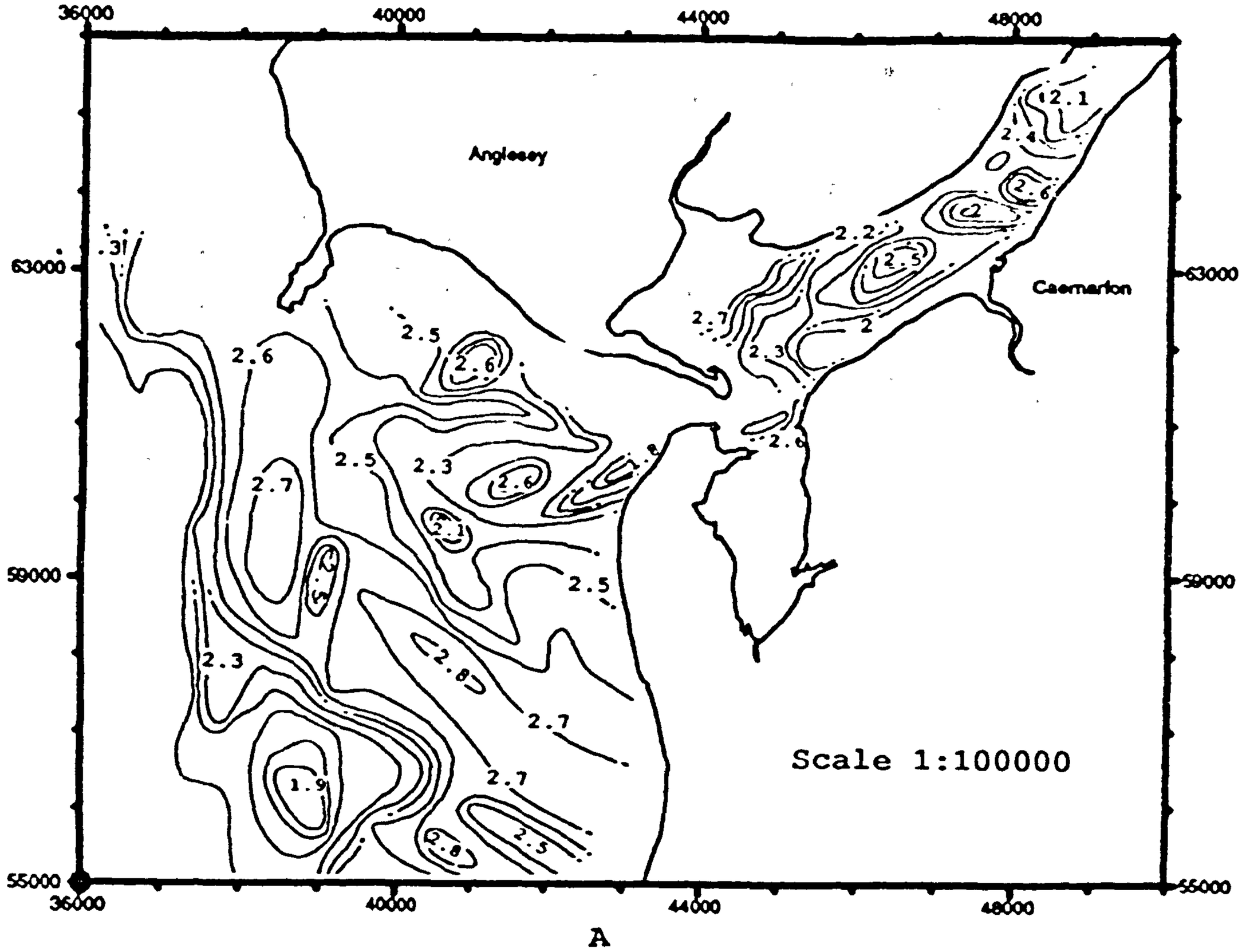

A

Fig: 5.16 Contour diagram of the mode grain size of the areas A & B. A) contour interval .1 phi B) contour interval .5 phi

several modal intervals forming a consecutive sequence over a limited distance, have been taken to imply potential sediment transport directions. In the study area the modal gradients occur in several locations. The most pronounced modal gradient can be seen in the vicinity of the ebb-tidal delta, where mode grain size tends to decrease away from the inlet. Within the Menai Strait a relatively smaller modal gradient appears in the NE of Belan inlet and indicates that the mode grain size decreases towards the inlet.

One thing that must be noted here is that the pattern of the mode grain size contours along the presumed limits of the ebb-tidal delta is almost similar to the contours of mean grain size as suggested by the contours of 2.7ϕ and 2.8ϕ which are roughly parallel to each other.

About 50 sediment samples collected from the offshore part of the study area show more than one grain size mode i.e. more than one peak on the frequency curve. More than one mode in a grain size distribution occurs predominantly in sediments composed of more than one sediment fraction (i.e. mixture of sand, silt and clay, and gravel). However, some sediment samples, particularly those collected along the offshore limits of the ebb-tidal delta (which are entirely composed of sand-sized particles), also show bimodality. Further offshore, the sediments are usually polymodal and mostly represent the areas of gravel patches. In between these gravel patches, however, it can be noted that most of the sediments have a mode grain size of 2ϕ.

From the general pattern of mode grain size contours for the offshore area (Fig: 5.16b) it appears that the mode grain size, moving offshore, tends to decrease rapidly and attains the lowest mode value of -4ϕ in the SW of area B. Within the Menai Strait it can be noted that the sediments having mode size of 2ϕ, generally occur in the main channel.

5.13.3 Sediment sorting.

Moments sorting

The sorting of the sediments within the study area ranges between 0.16ϕ and 3ϕ units. About 76% of all the samples, however, have a sorting value between 0.16ϕ and 0.50ϕ, whereas 12% of samples fall in the sorting range between 0.5ϕ and 1.0ϕ, and the samples with sorting between 2ϕ and 3ϕ makeup only 5% of the total. That shows that the majority of the grain size distributions obtained from the area are very well sorted to well sorted. These sediments generally represent the large tidal sand deposits on either sides of the Belan inlet. The remaining 24% of the samples represent the sediments mainly composed of more than one mode grain size and generally occur in the offshore part of the study area (Fig: 5.18). These sediments are usually composed of sand, gravel and/or silt and clay fractions.

The contour diagram of the moment sediment sorting shown in Fig: 5.17 indicates that, within the Menai Strait, the sorting values vary between 0.2ϕ and 0.5ϕ. The diagram does not suggest any obvious trend in the varying sorting value which could directly be linked to the general pattern of the tidal currents in the area. Instead, it reveals that most of the change is a result of the minor and major topographical features. For instance the high sorting value of 0.5ϕ opposite Caernarfon town occurs in the area where the back channel joins the main channel. It also appears that over the flanks of the sand banks and in the area of the main channel the sediments are relatively better sorted. The sorting of the sediments is best around the Belan inlet and could be attributed to the higher current velocity in this region. Just outside the Belan inlet three areas of relatively better sorting separated by a thin belt of relatively less well sorted sediments can be distinguished. These areas represent the terminal lobe of the ebb-tidal delta which is composed of north and south sand banks and a sand ridge, while the less sorted belt of sediments perhaps indicates that this area is sheltered. The better sorting over the sand deposit area probably indicates

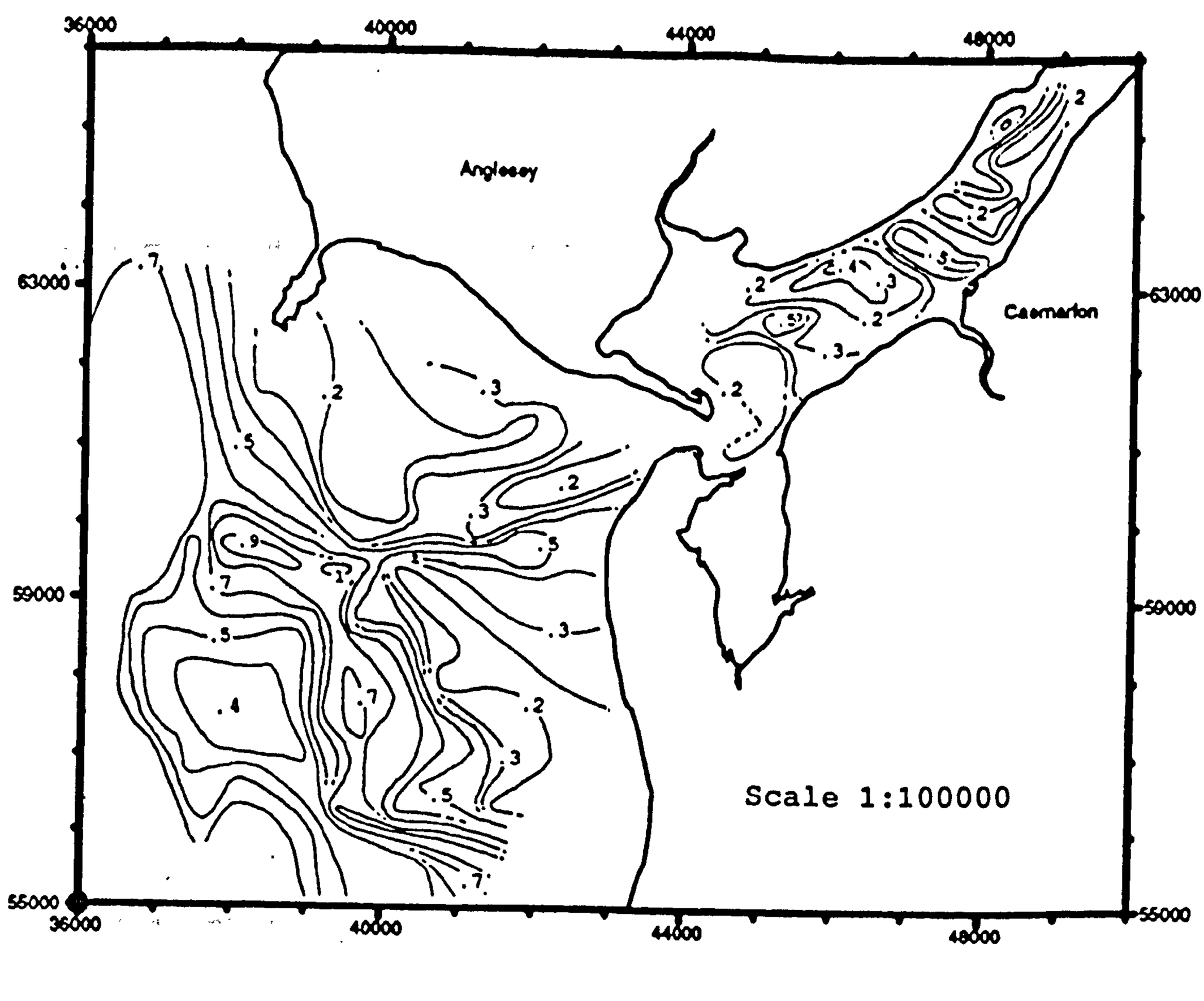

A1

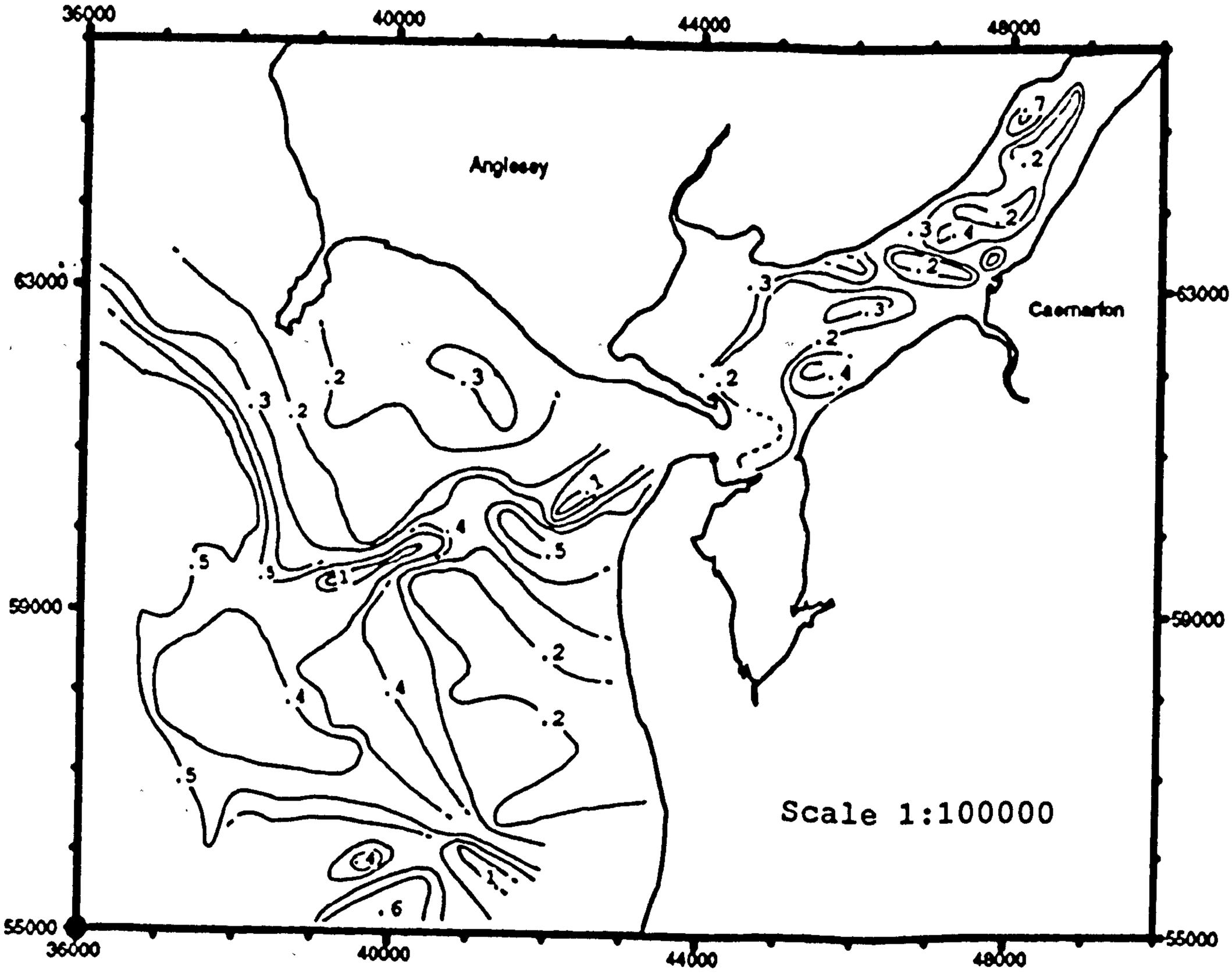

A2

Fig: 5.17 Contour diagram of the sediment sorting of area A.
A1) Moments A2) Folk. (contour interval .1 phi)

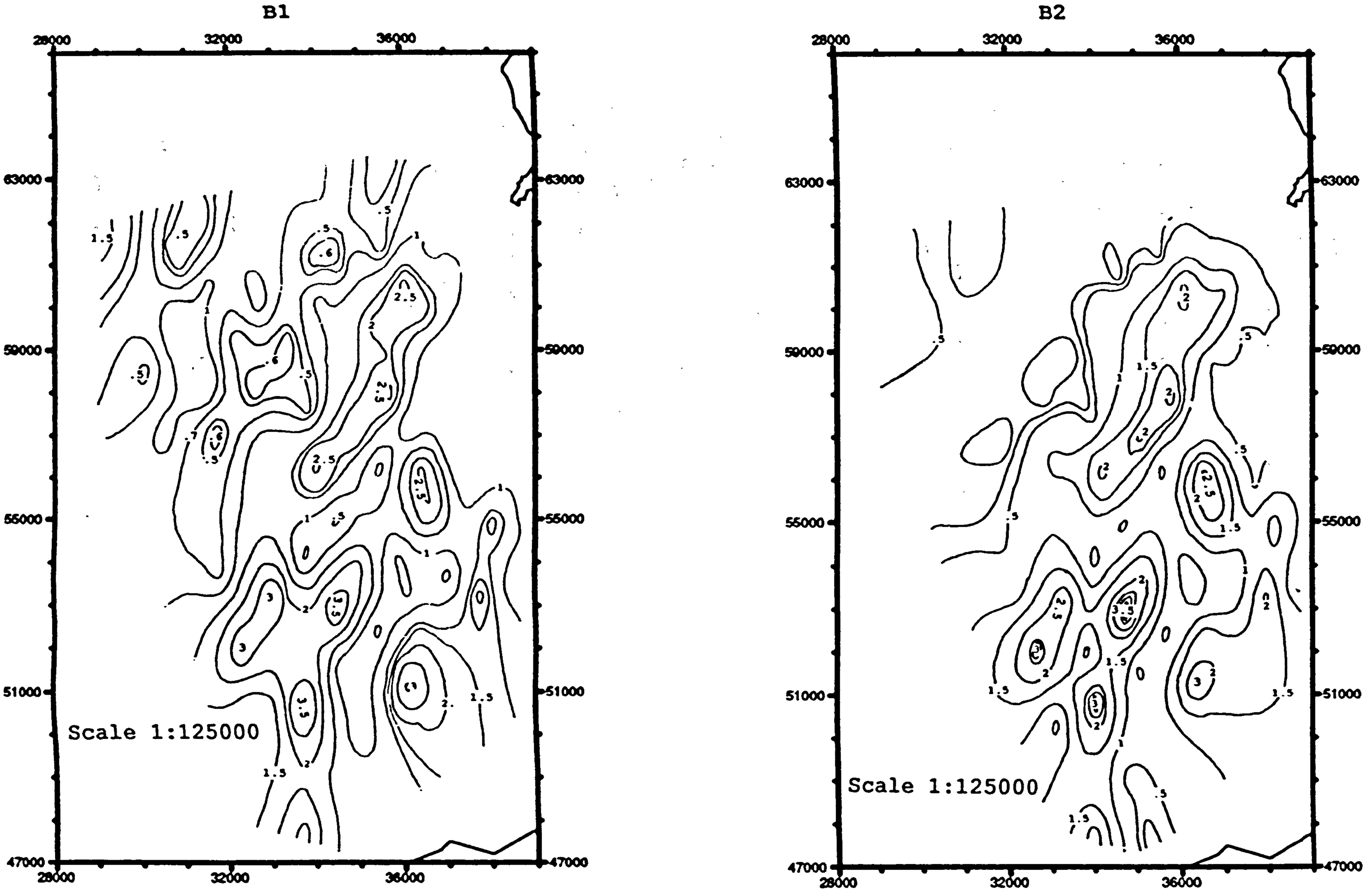

Fig: 5.18 Contour diagram of the sediment sorting of Area B.
B1) Moments B2) Folk. (contour interval .5 phi)

that sorting in this particular area is a function of shallow water depth and wave activity. In the location of the parallel band of fine sediments discussed in the section on mean grain size, very interesting changes in the sorting value have been noticed. The diagram indicates that in the vicinity of this band the sediments are relatively poorly sorted in comparison to the sediments on either side. This also supports the point made previously that this area represents the zone where interaction between the local and regional tidal currents is taking place.

The highest values of sorting (extremely poorly sorted sediments) have been encountered in the area shown in Fig: 5.18 and in the mainly polymodal sediments occurring in gravel patches and surrounding areas.

Folk sorting

Generally, the Folk sorting results are similar to moment sorting. However, they do tend to show some variation, particularly in areas where sorting of the sediments is influenced by local morphological changes, such as the sand bodies on either side of the Belan inlet (Fig: 5.17). The Folk sorting contour diagram of a deeper part of the study area (Fig: 5.18) shows almost identical features to the moment diagram.

5.13.4 Sediment skewness.

The comparison of the two sets of skewness values, obtained by moment and graphical methods, indicates that there is a marked difference between the two. The skewness values obtained by the moment method are of generally high magnitude and particularly in the case of the sediments containing a minor amount of fine particles (silt and clay), the skewness values are extremely high. The skewness ranges between -4ϕ and +9ϕ units, whereas the Folk skewness values range between -0.6ϕ and +0.6ϕ units. since the skewness diagram presented previously in Fig: 5.11 is also based on the Folk results, the detailed line contour diagram for current discussion was also drawn only for Folk values and is

shown in Fig: 5.19.

Though the overall skewness ranges between -0.6ϕ and +0.6ϕ in the study area, 90% of all the samples have skewness values ranging between -0.3ϕ and +0.3ϕ. However, the sediments having skewness values less than -0.3ϕ and more than +0.3ϕ make up only 8% and 2% respectively of the remaining 10% of the samples. About 53% of all the sediment samples are negatively skewed. Thus the majority of the samples have a tail to the left i.e. an excess of coarse material for a normal curve. This figure can be misleading though if we want to consider the various areas separately. For instance, within the Menai Strait there are fewer negatively skewed sediments (38%) than outside the Belan inlet (59%) and further offshore in the deeper water region (60%). Within the Strait it can also be noted that almost all the negatively skewed samples occur in the tidal channel areas and around the flanks of the sand banks.

It had been suggested that positive skewness i.e. an excess of fine material, may indicate an area of deposition, while negative skewness, i.e. an excess of coarse material, may indicate an area from which fine grades have been winnowed. This interpretation of skewness has been widely used by various workers. Some examples include Hough (1942), Spencer (1963), Friedman (1967), and Swift (1969). On the basis of the above hypothesis it can be said that the negative skewness occurring in the channel areas within the Menai Strait indicate the effect of strong tidal currents which erode the fine sediments from these areas. The negative skewness values around the main channel area outside the Belan inlet also indicate a similar situation; however, the skewness value here are smaller (-0.1ϕ) which is presumably because of the weaker tidal currents in that area.

Very negative values near the mainland coast (SW of Belan inlet) are probably caused by the strong tidal currents during the early stages of the flood tide. Most of the sediment samples

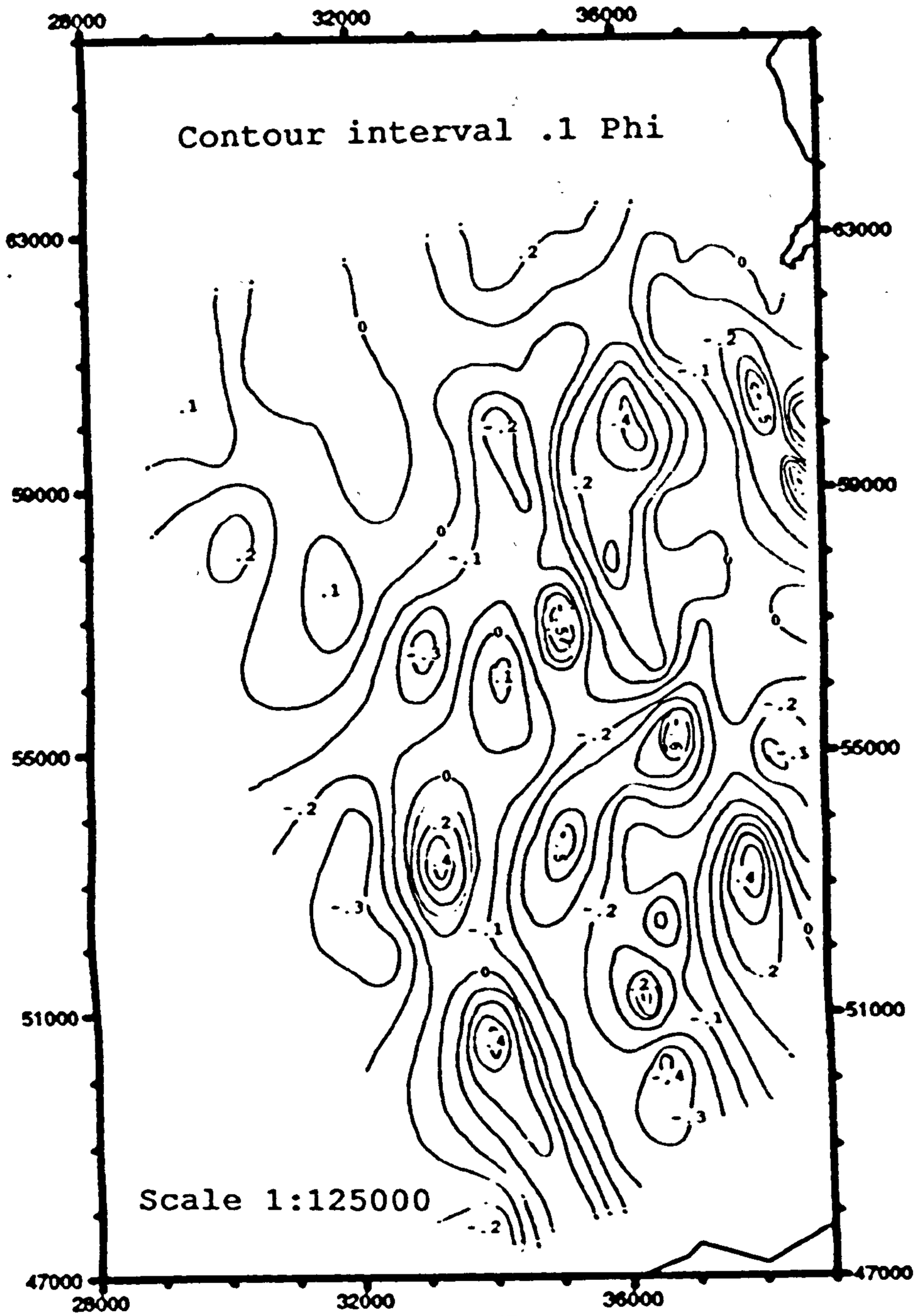

B

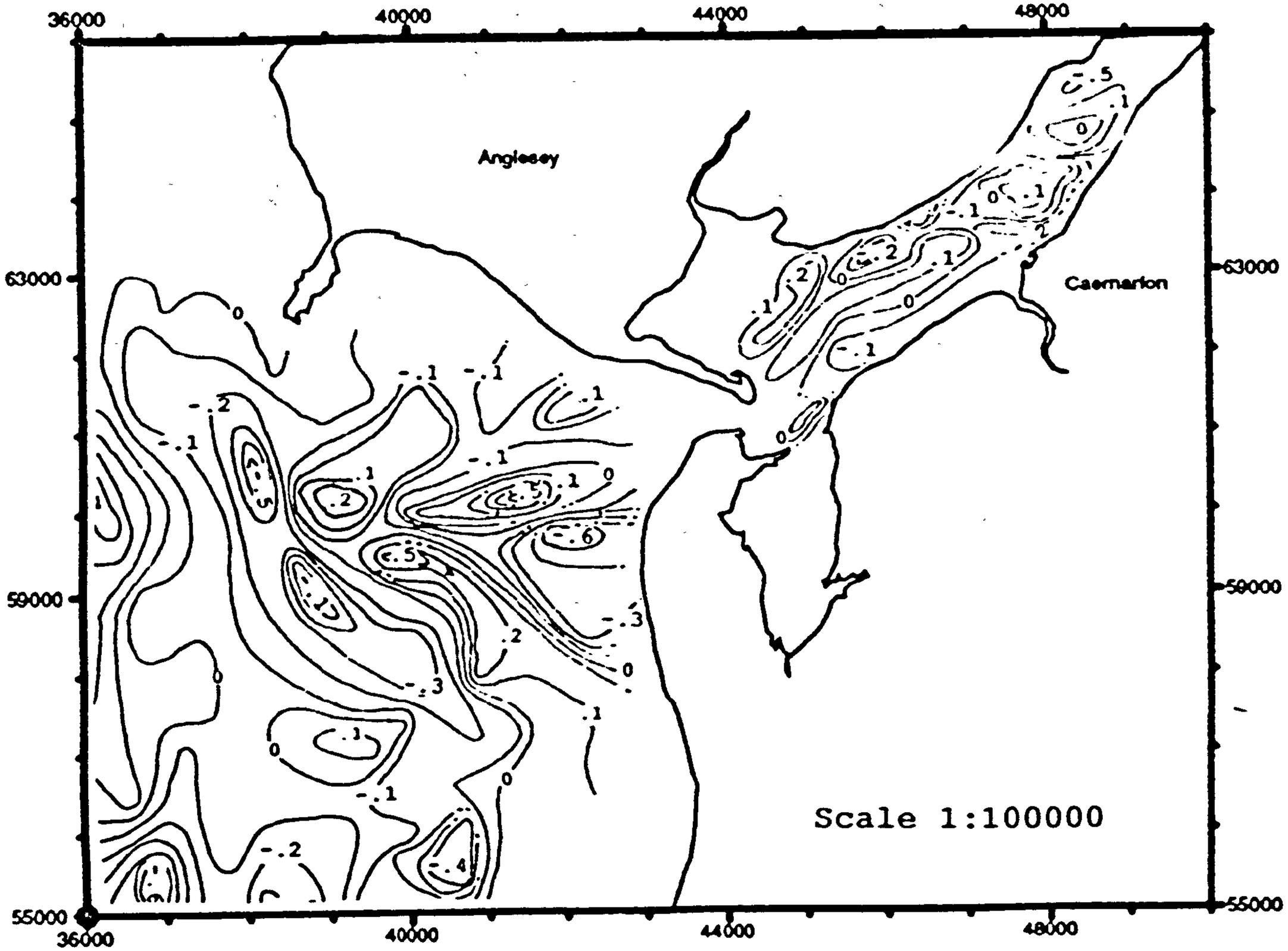

A

Fig: 5.19 Contour diagram of the sediment skewness (Folk) of the areas A & B (contour interval .1 phi).

collected from the vicinity of the presumed offshore limits of the ebb-tidal delta (parallel band) also show negative values. This also supports the previously made point that this area represents a complex zone, where perhaps, strong interaction is taking place between the locally influenced and regional tidal currents.

Skewness is very positive in areas of gravel (pebble) patches, while the sediments occurring in the area separating the higher mean/mode value regions are negative to very negatively skewed. Very positive values in the former area are the result of a tail of sand and/or fine sediments, whereas in the latter case the negative to very negative values are due to the coarse sand sediments. From this it can be seen that these negative to very negative values in the middle of the study area indicate a possible winnowing action of the tidal currents.

5.14 Conclusions.

1) Primarily two types of bottom sediments; i) fine to coarse sand and ii) fine gravel may be identified in the study area.
2) The overall mean grain size in the area varies between 1.9ϕ and -2.5ϕ.
3) Fine to coarse sand predominantly occurs within the Menai Strait and in the areas around the Belan inlet.
4) The gravel sized sediments are found in relatively deeper parts of the study area and probably represent relict glacial sediments.
5) Since gravel sediments occur as random patches, they appear to be playing little part in the present day processes.
6) Within the Menai Strait, the coarser sediments generally occur in the channel areas, whereas the finer sediments are found in the sub-tidal sand deposit areas.
7) Outside the Belan inlet, however, the coarser grained sediments occur in the areas of sub-tidal sand deposits, while the finer sediments occur on the flanks of sand banks and in the area of the main channel.

8) The finest sediments in the study area occur along the outer limits of the ebb-tidal delta in Caernarfon Bay, from where the mean grain size tends to increase on the both sides.

9) A fair amount of the bottom sediments of the deeper parts of the study area is composed of gravel, sand, and silt and clay fractions; however, the results suggest that sediments other than sand sized play very little or no role in the present day sedimentological environment prevailing in the study area.

10) The grain size parameters within the Menai Strait do not exhibit any obvious trends, However, just outside the Belan inlet grain size trends may be identified.

CHAPTER 6

SEDIMENT TRANSPORT

6.1 Introduction.

Estimations of the sediment transport rate and direction in the marine environment are of great importance to sedimentologists, marine engineers, and oceanographers. Sedimentologists and oceanographers are frequently required to predict sediment transport patterns in the coastal zones and over the adjoining shelves. A prior knowledge of sediment activity in any particular area is vital, whether the area is to be exploited for engineering purposes or its coast is to be protected from the damaging effects of erosion. In addition, an understanding of modern sediment transport systems will also aid interpretation of sedimentary deposits in the geologic record.

Sediment transport is a particularly difficult process to measure. However, it is a well established fact that sediments in the marine environment can be transported as a suspended load and/or bed load. The suspended load travels usually at a velocity equal to the transporting currents. Bed load transport is limited to a thin zone immediately above the bed where the current velocity is slower than the mean water mass current, and as a result, the bed load moves at a relatively lower velocity (Bagnold, 1956).

Measurements of sediment transport rates are usually made with relation to one or more empirical formulae eg. those suggested by Bagnold (1956, 1963, 1966), Yalin (1963), Engelund and Hansen (1967) and others. However, some methods for direct measurement of sediment transport, for example using sediment traps and studying the movement of bedforms and tracers (Finely (1978), Heathershaw (1981) Langhorne (1981), have also been used.

In areas of large bedforms, sediment transport rates can be measured by periodic surveys along a line of moving bedforms (Kachel and Sternberg (1971), Jones (1984)). Such surveys are generally carried out in the inter-tidal zone during low tide and require detailed mapping in order to reveal the constant pattern of sediment transport.

Estimation of sediment transport can also be carried out using radioactive tracers. Attaching certain tracers to the sediment grains and monitoring their movement over a certain period of time with the help of a scintillation or geiger counter provides enough evidence to calculate the net sediment transport rates. This type of study has been carried out by Heathershaw (1981) in Swansea Bay to calculate the amount and direction of the net sediment transport in the area.

The most widely used method of estimating sediment transport rates, however, is based on the physical relationship between the sea bed sediments and flow strength. Over the years various sediment transport formulae have been proposed. Most of these formulae are a function of several parameters, such as mean grain size, current velocity, water and sediment density, viscosity, temperature and surface roughness. Accurate information on all these parameters is not easy to obtain and it is even more difficult to accommodate them in a formula. As such, only a few of these parameters such as current velocity and grain size are measured directly whereas the remaining are combined as a constant to be determined experimentally.

Using such formulae and current meter observations Gadd et al (1978) carried out sediment transport studies on the New York shelf. On the basis of results obtained by using various bed load sediment transport formulae they concluded that bed load transport exists at the New York harbour entrance and that ebb directed transport exists in the central channel of the harbour entrance.

Heathershaw (1981) compared the measured and predicted sediment transport rates in tidal environments on the British continental shelf. He concluded that the directions of sediment transport are governed primarily by the tidal currents. However, he pointed out that the transport rates may be enhanced appreciably by wave activity. He also reports that while existing theories may give widely differing estimates of sediment transport, the direction of net sediment movement in the study area is in general agreement with other sedimentological results (eg. sand wave asymmetry and orientation and sand ribbon alignment).

The response of shelf sediments off North Yorkshire to the contemporary hydraulic regime was examined by Jago (1981). On the basis of tidal current data he suggested a southerly residual sediment transport during neap and spring tidal currents with a shoreward component. Estimates of similar kind were also made by Yang (1985) in the Oosterschelde tidal basin (Netherlands) using current velocity measurements. He concluded that estimates of the long term sediment budget showed that large amounts of sand have been eroded from the Oosterschelde basin and transported to the ebb-tidal delta.

In a small part of the current study area, just opposite Caernarfon harbour, Jones (1984) conducted a study of megaripple movement over a period of 34 days. His observations reveal that megaripples migrated a distance of 12.07m in a southwesterly direction over a period of 34 days. Nyandwi (1988) carried out current meter measurements using a Velocity Gradient Unit (VGU). Using various sediment transport equations he also reached a similar conclusion as Jones (1984) that there is a residual sediment transport to the southwest in the area.

Other sediment transport studies related particularly to tidal inlet systems similar to the one (Fort Belan inlet) involved in the current study include: Oertal (1972, 1975), Finely (1975), Hayes (1975, 1980), Hine (1975), Hubbard (1975), Fitzgerald et

al (1984), and Sha (1989).

In the current study the sediment transport patterns within the Menai Strait and in Caernarfon Bay will be examined using the tidal current data presented in Chapter 4. The extent of the variability of the sediment transport during flood and ebb tides and during spring-neap tidal cycles will be determined. The dominant direction of net sediment transport at each of the stations will be calculated. Once this basic information for individual stations is gained, then on the basis of this new information together with the previous results obtained in Chapter 4 and 5, an effort will be made (in Chapter 7) to determine net sediment transport pathways prevailing in the study area.

6.2 Threshold velocity.

As fluid velocity increases over a bed of sediments, it exerts a stress and a situation is eventually reached such that any additional increase in stress will cause particles to be moved from the bed and be transported. The velocity slightly less than that required to put a sediment into motion is called a threshold velocity. The circumstances necessary to initiate sediment motion are a function of the characteristics of the sediment (density, size, packing, sorting, shape, etc.), the fluid (density and viscosity), and the fluid average velocity (Miller et al 1977).

Since threshold velocity is of critical importance in the calculation of sediment transport, a number of graphical relationships have been proposed in an effort to define the threshold condition. The most quoted references on the above topic include: Hjulstrom (1935, 1939), Shields (1936), Sundborg (1956), Guy et al (1966), Sternberg (1972), and Miller et al (1977). Before Miller et al's work the most used graphs were of Hjulstrom and Shields. The Hjulstrom's graph relates the mean velocity of fluid flow in a river to the grain size of the bed

sediments. Though his graph does not really apply to conditions other than a river, because of its simplicity it found wide acceptance amongst the geologists and oceanographers.

Sternberg (1972) carried out a study of the threshold of grain motion in a shallow marine environment by conducting experiments on rippled, random, and rocky bed configurations. His work includes measurements of the velocity distribution within 1.5m of the seabed and the visual observation of the sediment water interface using an under water television camera system. He concludes that his results differ slightly from the Sundborg's (1956) threshold mean velocity and Shield's (1936) entrainment function θt versus grain diameter curves which were initially constructed from the data obtained for uniform sediments.

Miller et al (1977) re-examined the various pre-existing curves which were commonly employed to predict the threshold of grain motion. Miller et al selected only those data sets which were obtained by conducting experiments in laboratory flumes with parallel side walls under conditions of uniform steady flow over an initially flattened bed and the particles used were rounded or spherical of nearly uniform size. On the basis of this study Miller et al (1977) modified various existing curves related to threshold (Shields (1936), Inman (1949), Lane (1955), Sundborg (1956), Yalin (1972)) of grain motion. The proposed modified Sundborg's curve of the grain diameter D versus the flow velocity 100cm above the seabed U_{100} is shown in Fig: 6.1. Miller et al, however, warn that the application of this modified curve to the conditions other than those similar to the original experiments may give considerably differing results.

Gadd et al (1978), on the basis of re-analysis of Guy et al's (1966) flume data, report that the sediment transport rate for the sediment grain sizes 0.18mm and 0.45mm approaches zero at a threshold velocity near 20cm/s. Therefore in their studies of the estimation of the sediment transport on New York shelf they used the threshold velocity of 17cm/s and 19cm/s for the

sediment grain sizes 0.18mm and 0.45mm respectively. Mahamod (1989) also carried out re-analysis of Guy et al's flume data and suggests similar values for the threshold velocity necessary to transport the grains with 0.18mm and 0.45mm size. The plot of the threshold velocity against sand grains proposed by Mahamod is shown in Fig: 6.2 which suggests considerably lower threshold velocities.

6.3 Bed load Transport Equations.

Various sediment transport equations have been suggested to calculate the bed load transport rates in marine environments. These equations have largely been a result of flume experiments in laboratories. Most of the formulae are completely based on empirical relationships between the rate of sediment transport and flow characteristics of the fluid such as mean velocity or shear velocity. The most widely used sediment transport equations are those of Bagnold (1956, 1963, 1966), Yalin (1963), Engelund and Hansen (1967), Gadd et al (1978), and Hardisty (1983).

Bagnold's Equation

According to Bagnold (1966) the amount of bed load transport may be taken as proportional to the frictional energy expended upon the sea bed by the fluid. This concept is expressed by the following relationship:

$$q = \frac{\rho_s}{(\rho_s - \rho)\ g}\ k\ \omega \qquad (6.1)$$

Where q is mass sediment transport per unit width (gm cm^{-1} s^{-1}), ρ_s and ρ are sediment and fluid densities respectively, g is acceleration due to gravity, k is an experimentally determined coefficient, and ω is stream power (energy expended per unit time by the flow which can be written as τu, where τ is shear

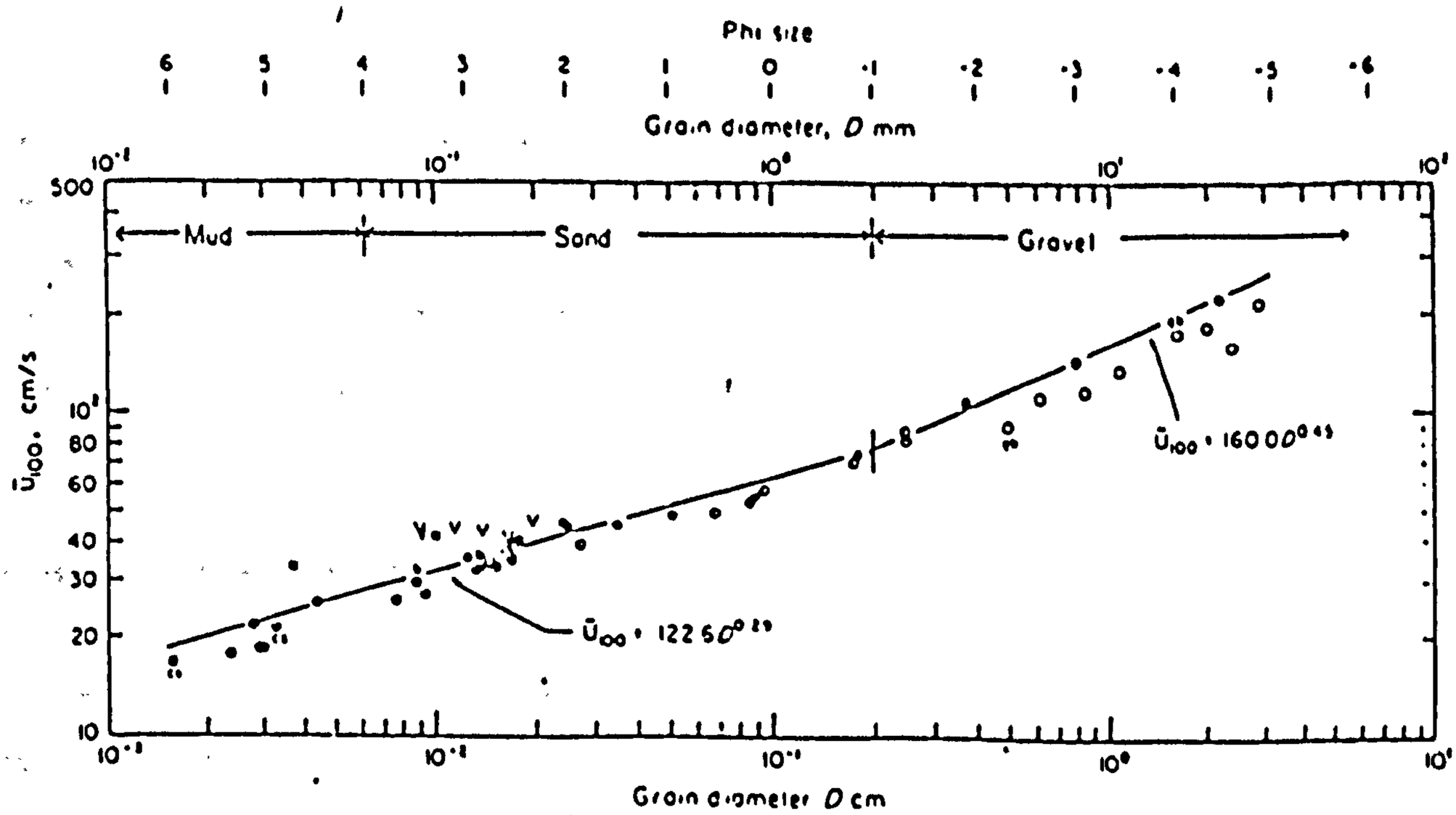

Fig: 6.1 Threshold velocity U_{100} against grain diameter (Miller, 1977).

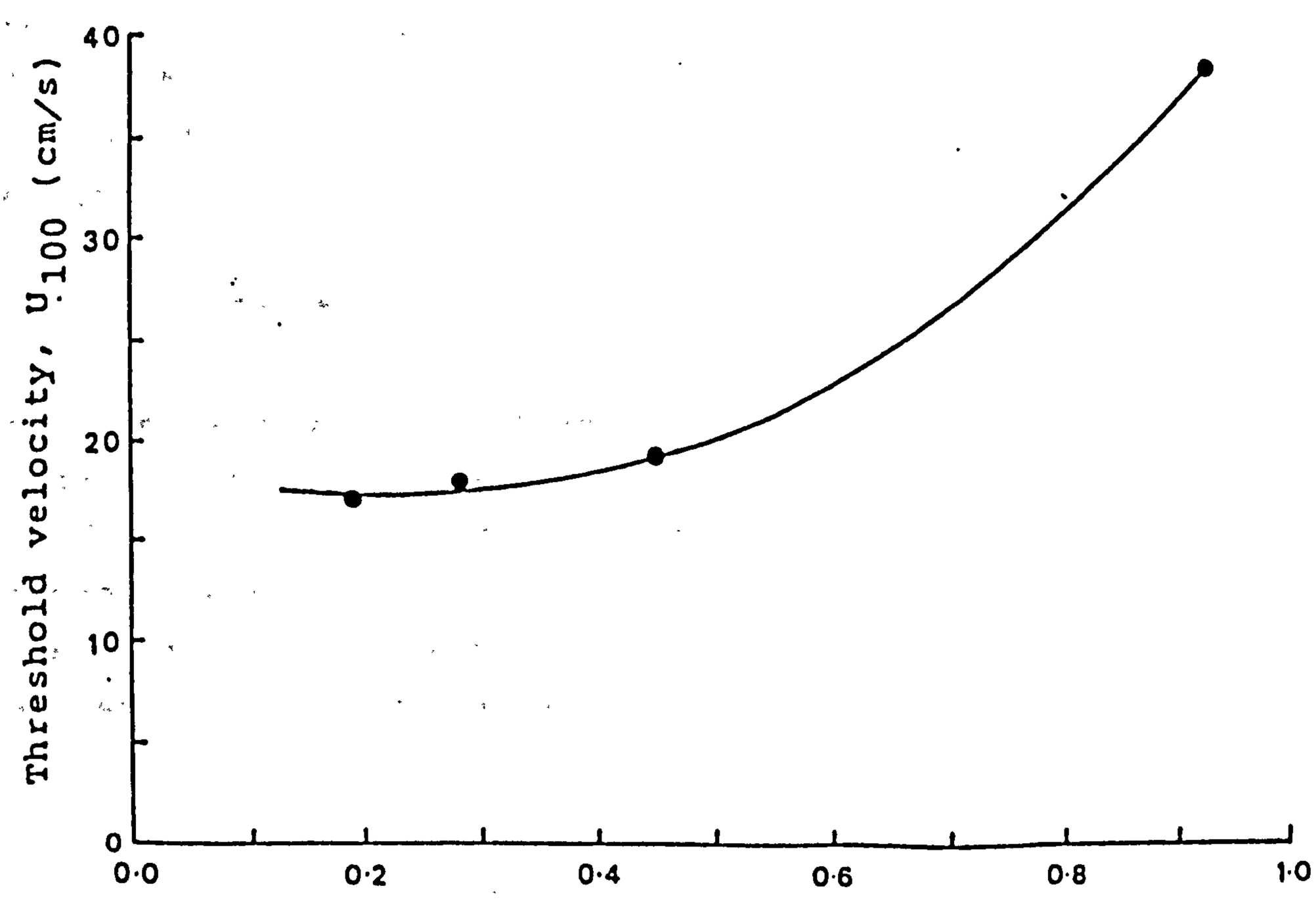

Fig: 6.2 Threshold velocity U_{100} against grain diameter (Mahamod, 1989).

stress and u is flow velocity). It was originally thought (Bagnold, 1963) that k depends on sediment characteristics only. However, it has subsequently been shown (Kachel and Sternberg, 1971) that k also depends on the excess shear stress $(\tau - \tau_{cr})/\tau_{cr}$, where τ is shear stress and τ_{cr} is the threshold stress.

Gadd et al's Equation

Using Guy et al's (1966) data Gadd et al (1978) removed the dependence of k on excess shear stress and expressed Bagnold's original equation in terms of the near bed current velocity (U_{100}) and a threshold velocity (U_{cr}) so obtaining;

$$q = \beta \, (U_{100} - U_{cr})^3 \qquad (6.2)$$

Where β is a coefficient of proportionality obtained from the flume data of Guy et al, U_{100} is a current velocity measured at the height of 100cm above the sea bed, and U_{cr} is the threshold velocity.

Hardisty's Equation

Following a suggestion from Vincent et al (1981) that the shear stress $[u^2(t) - u_{th}^2]u(t)$ lifts the sediment from the bed while the flow then transports the sand at a rate proportional to the instantaneous flow velocity u(t), Hardisty (1983) calibrated this relationship using Guy et al's (1966) and Williams (1967) sediment data and suggested the following equation.

$$q = k \, (U_{100}^2 - U_{100cr}^2) \, U_{100} \qquad (6.3)$$

$$k = (1/(6.6\ D_{mm}^{1.23}))10^{-5}$$

Where k is the calibration coefficient which is strongly related to the grain size (D_{mm}) of the sediment. Hardisty suggests that this equation is closer to the original concepts of Bagnold's work than is the excess velocity formulation suggested by Gadd et al (1978).

Engelund and Hansen's Equation

Engelund and Hansen's (1967) equation expresses the total load q in terms of a friction factor Cf, a dimensionless sediment discharge ϕ, and a dimensionless bed shear stress θ.

$$Cf\ \phi = 0.1\ \theta^{5/2} \qquad (6.4)$$

where $\phi = q/\rho \quad (g \left[\frac{\rho_s}{\rho} - 1 \right] d_{50}^3)^{1/2}$

$$\theta = \left(\frac{\tau}{(\rho_s - \rho)\ g\ D} \right)$$ 5/2 A. ALI

$$Cf = \frac{2u_*^2}{U^2}$$

where d_{50} is grain diameter and u_* is shear velocity. Substituting for above values in equation (6.4) gives;

$$q = 0.05\ \rho_s\ U^2 \left\{ \frac{d_{50}}{\left[\frac{\rho_s}{\rho} - 1 \right] g} \right\}^{1/2} \left\{ \frac{\tau}{\left[\rho_s - \rho \right] g d_{50}} \right\}^{3/2}$$ A. ALI

This formula is calibrated for materials coarser than 0.15mm (Raudkivi, 1976).

Discussion.

For the purpose of the estimation of sediment transport in the current study Hardisty's excess shear stress formulation was used. This equation was selected for various reasons. One is that it takes into account the threshold velocity and secondly that it uses the flow velocity measured 100cm above the bed and as such the acquired current meter data in the present study can directly be used. Hardisty (1983) reports that the constant k in his equation is strongly related to the grain size of the sediment and as such it should increase the accuracy of mass sediment transport rate determination. Mahamod (1989) argues that since Hardisty's equation is calibrated only for the velocities up to 55cm/s it would over estimate the sediment transport rate at higher velocities. Similar arguments can also be made for other sediment transport formulae since all the formulae are based on empirical relationships, they will always carry an element of inaccuracy. Gadd et al (1978) reports that various sediment transport formulae (Bagnold (1963), Yalin (1972), etc.) used in the sediment transport studies on New York shelf vary amongst themselves by as much as an order of magnitude.

Most of the other sediment transport equations are based on the shear velocity, and that itself, if calculated from U_{100} using empirically determined drag coefficient C_{100}, will introduce a considerable error into the calculations. Engelund and Hansen's (1967) equation does not take into account the threshold velocity and therefore calculates the sediment transport for all the velocities. As such it appears that all the sediment transport equations suffer from one or other drawback and none of them is actually capable of estimating the amount of sediment transport accurately. It does not, however, invalidate the use of these equations but it does emphasizes that it must be borne in mind that estimation of the amount of sediment transport on the basis of the any equation will always carry a certain amount

of uncertainty which varies according to the varying conditions from area to area under which sediment transport is taking place.

The detailed investigation of the literature related to the threshold condition of grain motion reveals that the threshold curves presented by various workers differ amongst themselves by an order of magnitude. For example, Miller et al's (1977) curve of U_{100} against grain diameter presented in Fig: 6.1 gives a threshold velocity of about 38cm/s for the sediments of 0.18mm grain size. Whereas the results of Gadd et al (1978) and Mahamod (1989) suggest a threshold velocity of about 17cm/s for the sediments of the same grain diameter. One of the reasons responsible for this huge discrepancy appears to be that Miller et al's curve is based on the results of flume experiments which were conducted on the flat beds with uniform sized grains. On the other hand the Gadd et al's and Mahamod's results were drawn from the re-analysis of the original flume data of Guy et al (1966) who conducted experiments for all kinds of bed roughnesses i.e. ranging from flat beds to antidunes. Therefore it appears that the presence of bedforms on the seabed greatly enhances the chances of sediment to move under the influence of relatively lower current velocities. Though this factor seems to be responsible to some extent for these differing threshold values, the difference is such that this alone may not be enough to explain the discrepancy completely. Owing to this discrepancy, it was decided to use both (Miller et al's and Mahamod's) threshold values to calculate the sediment transport at stations C1, C2, and C3. The results of the sediment transport calculations obtained on the basis of the lower and higher threshold values will be examined in relation to other results and an attempt will be made to determine which of the two results fits most closely to the prevailing hydrodynamic system in the area.

6.4 Sediment Transport in the study area.

To estimate the sediment transport in the present study the current meter data (discussed in Chapter 4) was used in a way that each velocity reading was transformed into sediment transport rates (g/cm/s). In case of station C2 and C3 these sediment transport rates were summed up for the time interval between the velocity readings (in the case of the present study, 5 minutes) and then their north and east components were calculated for a period of a complete tidal cycle. Finally these north and east components were vectorally resolved to calculate the amount and direction of the residual sediment transport over a period of a tidal cycle. In the case of station C1, where the tidal currents predominantly flow in two directions i.e. flood and ebb, the total sediment transport for the flood and ebb periods of an individual tidal cycle were calculated separately. On the basis of these, finally the net sediment transport for each tidal cycle was also calculated. The obtained results are discussed below.

6.4.1 Station C1.

The calculation of the sediment transport at this station was carried out for the 24 tidal cycles. As mentioned previously, during the tidal cycle Nos. 2-6 (due to the tilting of the current meter), some of the flood tide data were lost and these were later extrapolated. All the results which will be given here are obtained based on this extrapolated data. However, in order to give an idea of the recorded error in the velocity data of the above mentioned flood tides, the graphs shown in Fig: 6.3 were produced by using the original data. At this station the dominant mean grain size of the seabed sediments is 0.18mm, therefore a threshold velocity of 38cm/s was used. The graph shown in Fig: 6.3a clearly indicates that the determined sediment transport during the flood tides Nos. 2-6 is almost half in comparison to subsequent ebb tides. As a result the net sediment transport (Fig: 6.3b) during these flood tides, in

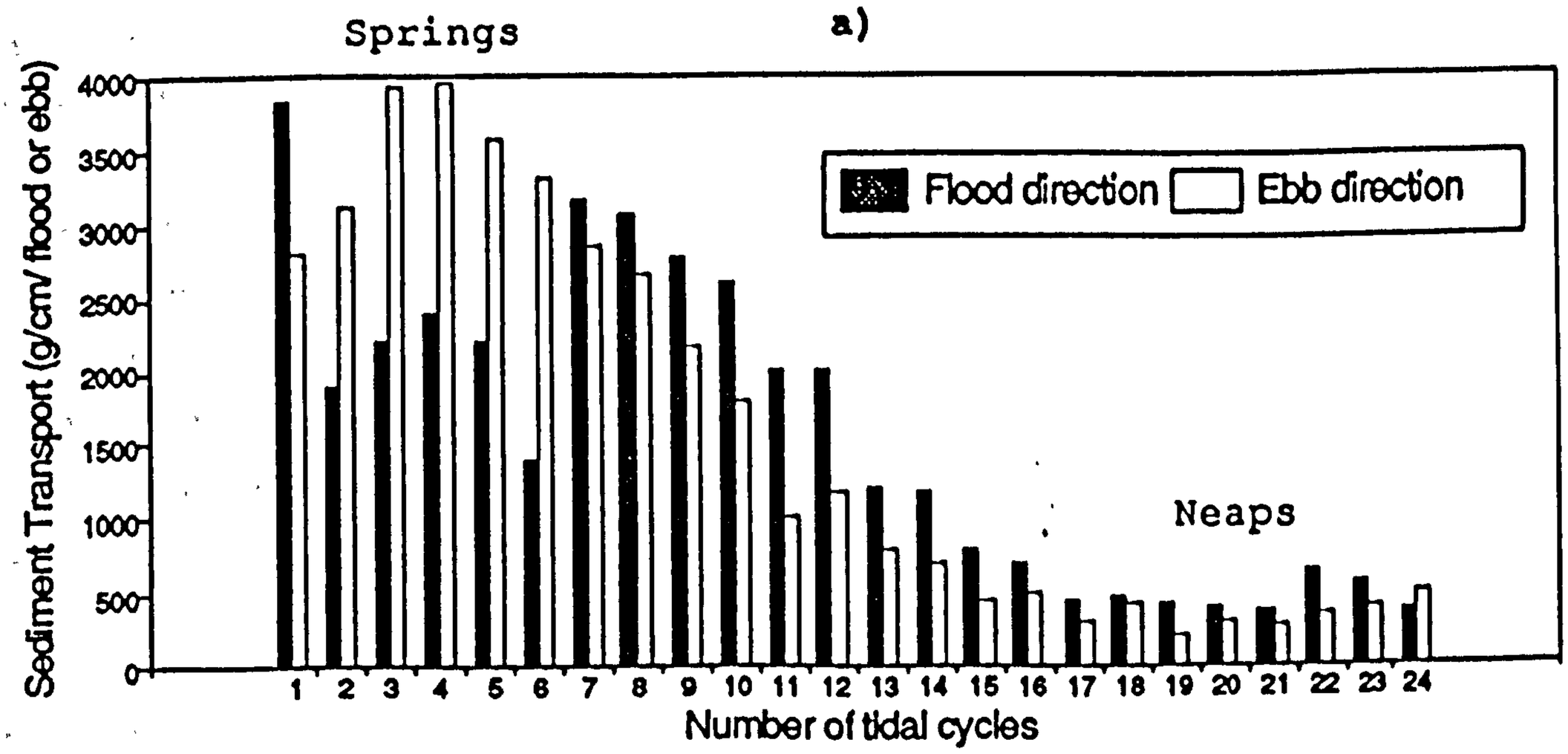

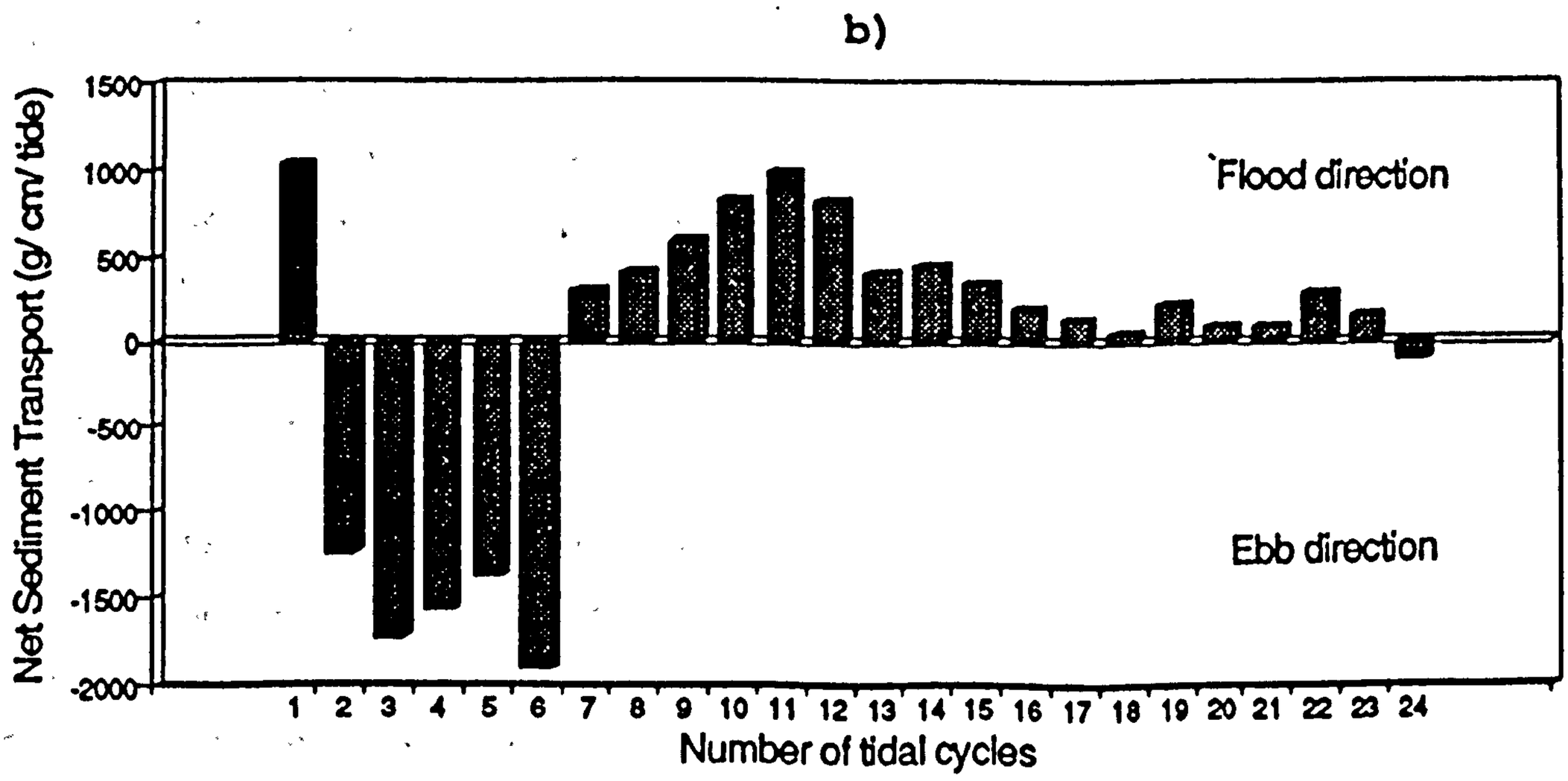

Fig: 6.3 **a)** Variations of sediment transport in the flood and ebb directions for each tidal cycle at station C1.

b) Net sediment transport during each tidal cycle at station C1.

Mean grain size 0.18mm Threshold velocity 38cm/s

contrast to rest of the data, show ebb direction. In order to avoid these clearly erroneous results the extrapolation of the data seems reasonable. The results based on the partially extrapolated data are given below.

Threshold velocity 38cm/s

The results obtained using threshold velocity of 38cm/s are presented in Table No. 6.1 and graphs are shown in Fig: 6.4. The results suggest that the maximum sediment transport on flood and ebb tides occurs during a spring tide; however, the net sediment transport appears to reach its maximum in between neap and spring tide. These results (because of the extrapolated data) carry an element of doubt, but this extrapolated data is only a small portion of the data and the rest of the data also suggest a similar trend of decreasing net sediment transport towards spring and neap tides. The results also suggest that during all the tidal cycles but one (No. 24) the net sediment transport occurs predominantly in the direction of the flood tide.

Threshold velocity 17cm/s

As expected, the amount of the sediment transport obtained by using a lower threshold velocity is considerably higher. The results of these calculations are presented in Table No. 6.2 and the graphs of sediment transport against tidal cycles are shown in Fig: 6.5. The results suggest that maximum flood and ebb sediment transport of 4992 and 4365 g/cm/flood and ebb respectively occurred during the spring tide (tidal cycle No. 4), while the minimum sediment transport of 567 and 474 g/cm/flood and ebb respectively occurred during the neap tide (tidal cycle No. 21). These results also suggest a similar trend of maximum net sediment transport occurring in between the neap and spring tidal cycles. However, the amount of net sediment transport in the flood direction is relatively smaller.

Table No. 6.1

Sediment Transport at station C1 (g/ cm/ flood or ebb)
Net sediment transport (g/ cm/ tide)
Mean grain size .18mm Threshold Velocity 38cm/s

Tide No.	Flood	Ebb	Net	Direction
1	3846.29	2808.64	1037.65	NE
2	4167.94	3118.44	1049.50	NE
3	4534.39 S	3931.52 S	602.87 S	NE
4	4611.15 S	3950.92 S	660.23 S	NE
5	4104.79	3584.67	520.12	NE
6	3813.15	3302.59	510.56	NE
7	3160.55	2853.66	306.89	NE
8	3062.49	2660.80	401.69	NE
9	2778.37	2192.51	585.86	NE
10	2625.19	1791.91	833.28	NE
11	2007.86	1005.48	1002.38	NE
12	2007.17	1172.09	835.08	NE
13	1196.88	780.03	416.85	NE
14	1156.59	700.12	456.47	NE
15	800.30	444.94	355.36	NE
16	683.37	487.28	196.09	NE
17	444.76	302.77	141.99	NE
18	473.33	425.20	48.13	NE
19	429.45	214.51	214.94	NE
20	402.49 N	313.47 N	89.02 N	NE
21	382.50 N	286.77 N	95.73 N	NE
22	632.22	342.37	289.85	NE
23	561.33	410.23	151.14	NE
24	387.82	485.91	-98.09	SW

S = Springs N = Neaps

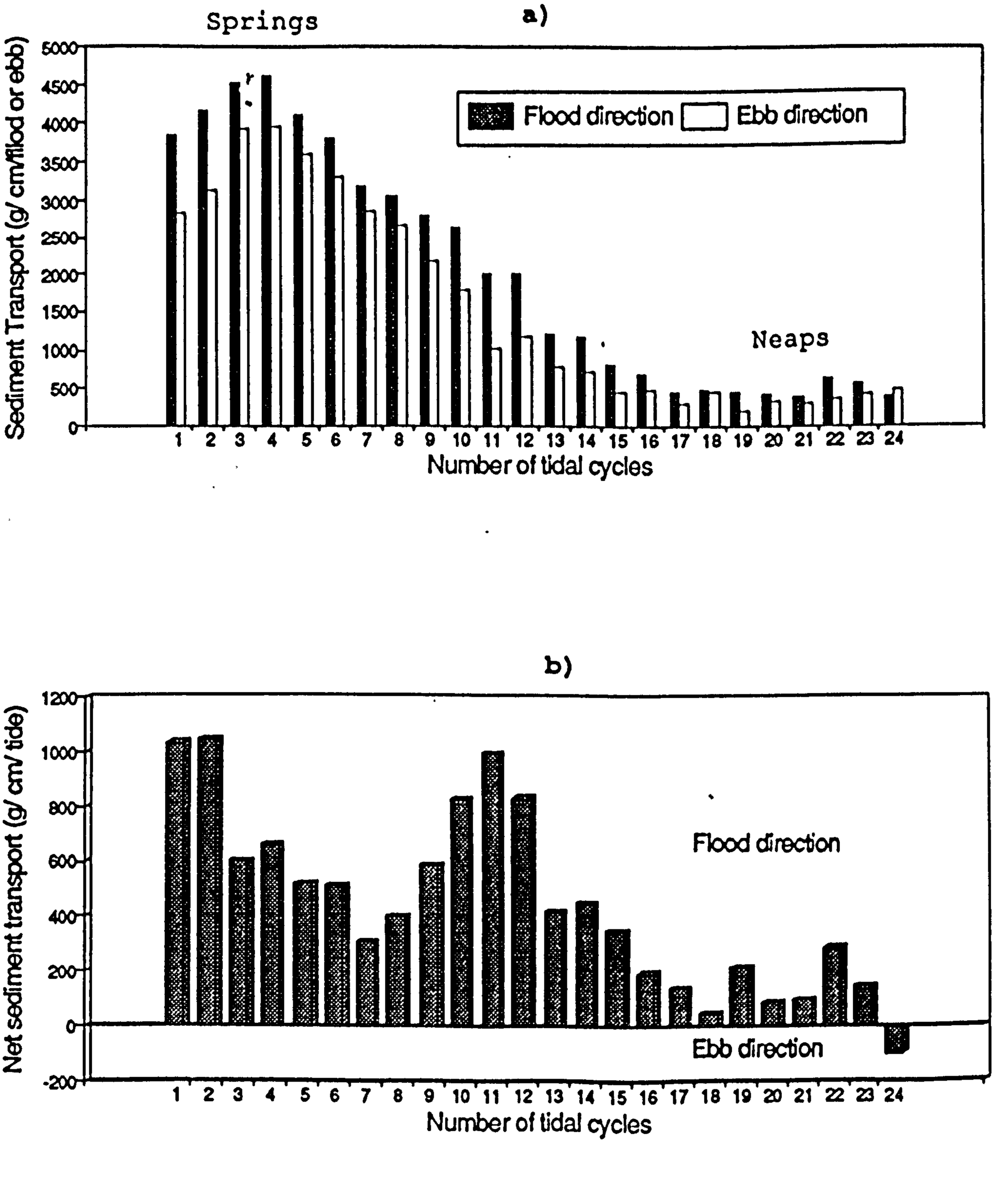

Fig: 6.4 **a)** Variations of sediment transport in the flood and ebb directions for each tidal cycle at station C1.

b) Net sediment transport during each tidal cycle at station C1.

(This graph is based on the extrapolated data for flood tide during the tide Nos. 2 - 6)

Mean grain size 0.18mm Threshold velocity 38cm/s

Table No. 6.2

Sediment Transport at station C1 (g/ cm/ flood or ebb)
Net sediment transport (g/ cm/ tide)
Mean grain size .18mm Threshold velocity 18cm/s

Tide No.	Flood	Ebb	Net	Direction
1	4200.72	3188.22	1012.5	NE
2	4523.91	3506.56	1017.35	NE
3	4919.89 S	4345.43 S	574.46 S	NE
4	4992.92 S	4365.83 S	627.09 S	NE
5	4513.24	3981.79	531.45	NE
6	4187.04	3705.10	481.94	NE
7	3501.16	3234.64	266.52	NE
8	3403.63	3037.09	366.54	NE
9	3107.86	2538.80	569.06	NE
10	2955.30	2124.69	830.61	NE
11	2313.18	1271.64	1041.54	NE
12	2319.35	1470.54	849.34	NE
13	1458.08	1033.53	424.55	NE
14	1419.98	949.56	470.39	NE
15	1033.89	665.82	368.07	NE
16	905.66	724.07	181.59	NE
17	636.86	497.42	139.44	NE
18	667.04	651.94	15.10	NE
19	614.08	397.73	216.35	NE
20	583.56 N	526.53 N	57.03 N	NE
21	567.69 N	474.80 N	92.89 N	NE
22	854.02	542.23	311.79	NE
23	773.97	615.53	158.44	NE
24	578.53	713.15	-134.62	SW

S = Springs N = Neaps

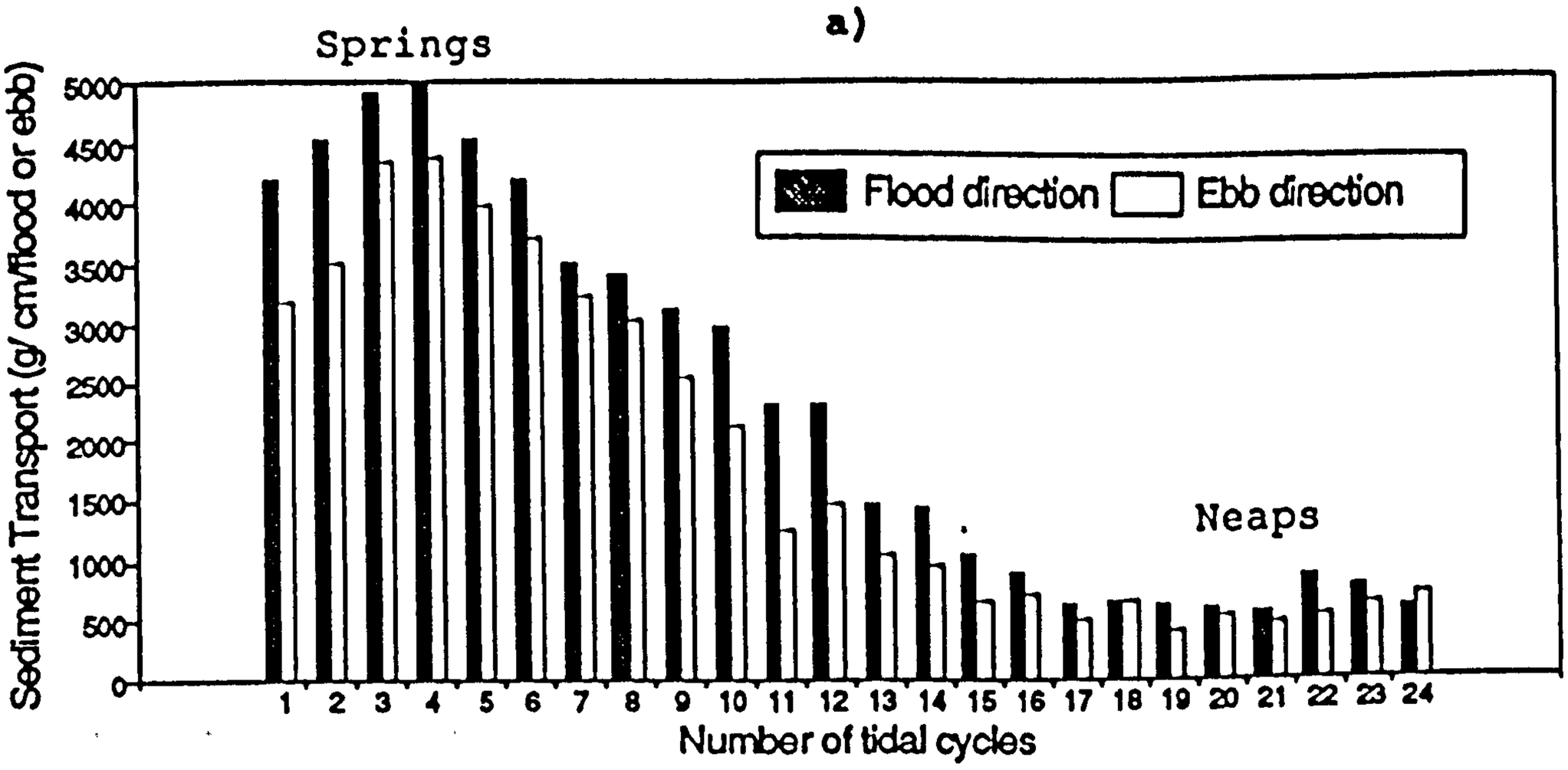

Fig: 6.5 a) Variations of sediment transport in the flood and ebb directions for each tidal cycle at station C1.

b) Net sediment transport during each tidal cycle at station C1.

(This graph is based on the extrapolated data for flood tide during the tide Nos. 2 - 6)

Mean grain size 0.18mm Threshold velocity 17cm/s

6.4.2 Station C2.

Threshold velocity 35cm/s

In this area the mean grain size of the sediments is in the range of 0.16mm, so a lower threshold velocity of 35cm/s was used. Since at this station the current velocity only occasionally exceeds the threshold velocity of 35cm/s, the obtained results show very little residual sediment transport. During most of the tidal cycles the sediment transport appears to remain zero. However, some activity seems to occur during the spring tidal cycle (tidal cycle No. 12). The results of the 27 tidal cycles are presented in Table No. 6.3 and the related graphs are shown in Fig: 6.6a. This graph suggest that even where sediment transport had occurred it is as little as 9 g/cm/tide.

Threshold velocity 16cm/s

When a lower threshold velocity was applied at station C2, the amount of residual sediment transport increased considerably and reached a maximum of 102 g/cm/tide during a spring tide. The results presented in Fig: 6.6b suggest that the minimum sediment transport occurred during a neap tide. It also suggests that the residual sediment transport suddenly dropped just after the spring tides and then remained in the range of about 10 g/cm/tide for the rest of the tidal cycles. The results indicate that the direction of the residual sediment transport at this station remained very consistent throughout the recorded tidal cycles and shows a strong northwest trend.

6.4.3 Station C3.

Threshold velocity 37cm/s

Because of the even weaker currents at station C3 the results obtained by using the higher threshold velocity suggest that there is no bedload transport at all except during a spring tide. The results of the 25 tidal cycles recorded at this station are presented in Table No. 6.4 and the graph of the same

Table No. 6.3

Amount and direction of residual sediment transport at station C2 (g/ cm/tide). Direction of sediment transport in degrees.

Tide No.	Thresold VEL 35cm/s		Threshold VEL 16cm/s	
	Sed. Transport	Direction	Sed. Transport	Direction
1	1.19	212	14.21	248
2	0.78	207	11.91	232
3	0	----	16.90	340
4	0	----	30.52	347
5	0.21	4	45.53	347
6	9.41	342	102.43 S	343
7	9.91	348	74.27 S	346
8	0	----	7.47	343
9	0	----	8.44	310
10	0	----	16.44	330
11	0	----	13.90	326
12	0	----	7.16	245
13	0	----	8.15	328
14	0	----	5.28	303
15	0	----	10.91	351
16	0	----	7.60	359
17	0	----	13.57	350
18	0	----	2.25	311
19	0	----	7.11	346
20	0	----	17.58	346
21	0	----	5.17	182
22	0	----	0.56 N	30
23	0	----	6.94 N	352
24	0	----	3.69	293
25	0	----	14.53	302
26	0.18	214	11.16	226
27	0	----	22.28	302

S = Springs N = Neaps

a)

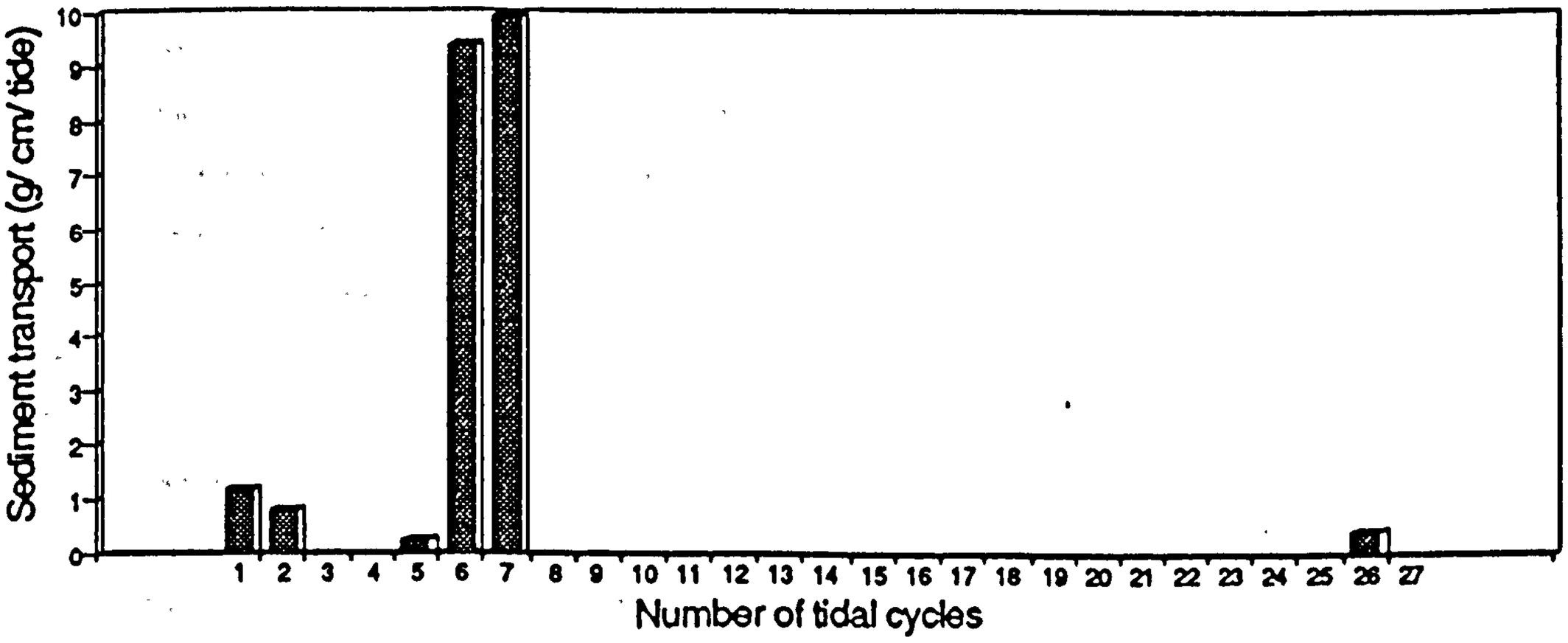

b)

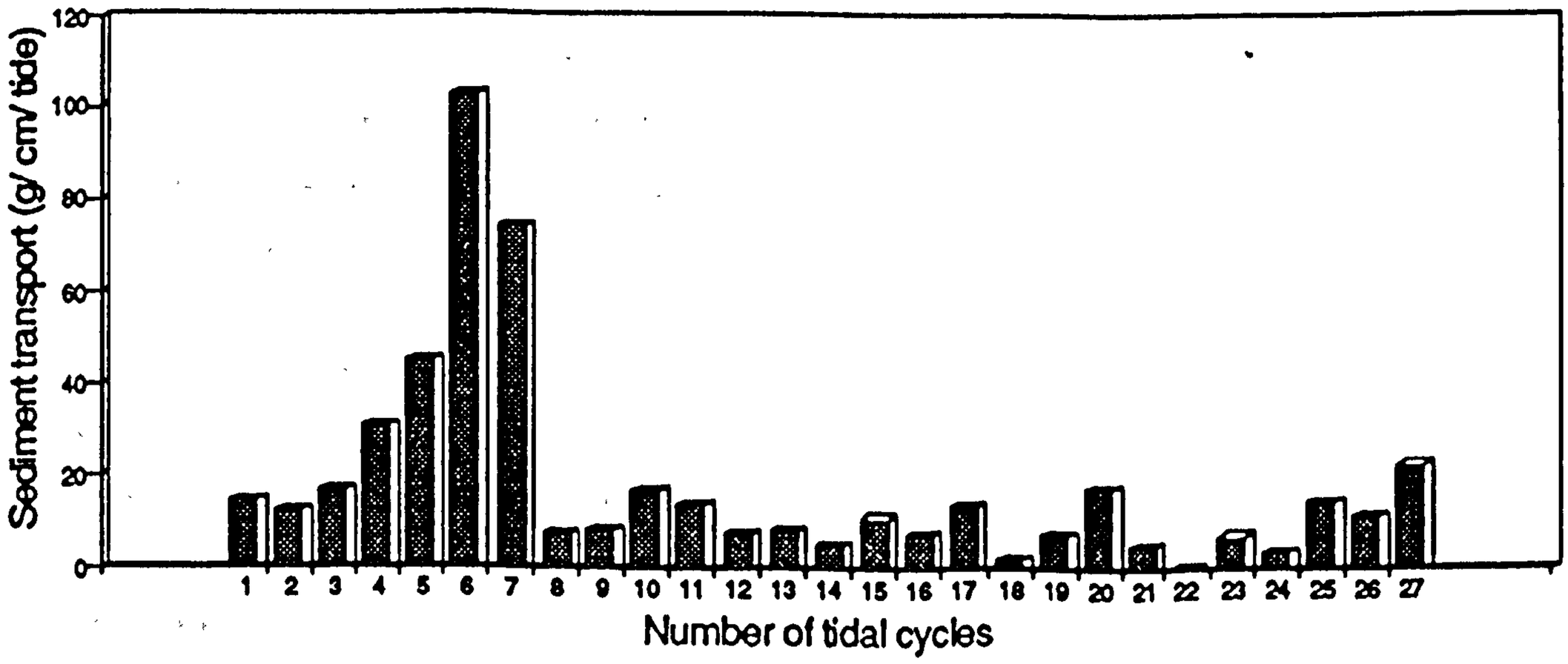

Fig: 6.6 **a)** Residual sediment transport at station C2. Direction of transport NW. (Threshold Velocity 35cm/s)

b) Residual sediment transport at station C2. Direction of transport NW. (Threshold Velocity 16cm/s)

is shown in Fig: 6.7a. This graph suggests that the residual sediment transport took place only during tidal cycle No. 12 in a northeast direction.

Threshold velocity 17cm/s

The lower threshold values, suggested a relatively higher amount of sediment transport. The plot of the obtained results is shown in Fig: 6.7b. These results also suggest that the residual sediment transport mainly takes place around the spring tide while it approaches zero during neap tide. The dominant direction of the transport at this station is towards the northeast.

On the basis of the sediment transport results obtained at station C1, C2, and C3 an attempt was made to clearly show the amount and direction of sediment transport during spring and neap tides in relation to the location of these stations. Arrows were drawn at each station in accordance with the amount and direction of the sediment transport at that station. Here it must be made clear that the arrows drawn at the station C1 represent the net sediment transport while the arrows drawn for station C2 and C3 represent the residual sediment transport. The diagrams related to spring and neap tides are shown in Fig: 6.8 and Fig:6.9 respectively. The magnitude of the arrows indicate the values obtained using lower threshold velocities.

The spring tide results indicate that at the station C1 the net sediment transport of 627 g/cm/tide takes place in the flood direction. Whereas the arrow drawn for station C2 suggest a residual sediment transport of 102 g/cm/tide in the northwesterly direction. At station C3 the amount of residual sediment transport is even less than station C2; however, there is very little difference between the direction of transport at station C1 and C2 which has strong northerly component.

The neap tide results (Fig: 6.9) indicate that a very little sediment activity occurs in comparison to a spring tide. The net

Table No. 6.4

Amount and direction of residual sediment transport
at station C3 (g/ cm/ tide)
Direction of sediment transport in degrees

Tide No.	Thresold VEL 37cm/s		Threshold VEL 17cm/s	
	Sed. Transport	Direction	Sed. Transport	Direction
1	0	----	0	----
2	0	----	0	----
3	0	----	2.61	235
4	0	----	3.06	330
5	0	----	0.02	26
6	0	----	0	----
7	0	----	4.95	21
8	0	----	7.54	17
9	0	----	9.67	14
10	0	----	14.85	25
11	0 S	----	16.01 S	28
12	2.12 S	18	39.03 S	351
13	0	----	9.73	17
14	0	----	3.14	11
15	0	----	14.75	13
16	0	----	3.03	24
17	0	----	1.54	23
18	0	----	0.62	26
19	0	----	0.15	22
20	0	----	0	----
21	0	----	0	----
22	0	----	0	----
23	0	----	0	----
24	0 N	----	0 N	----
25	0 N	----	0 N	----

S = Springs N = Neaps

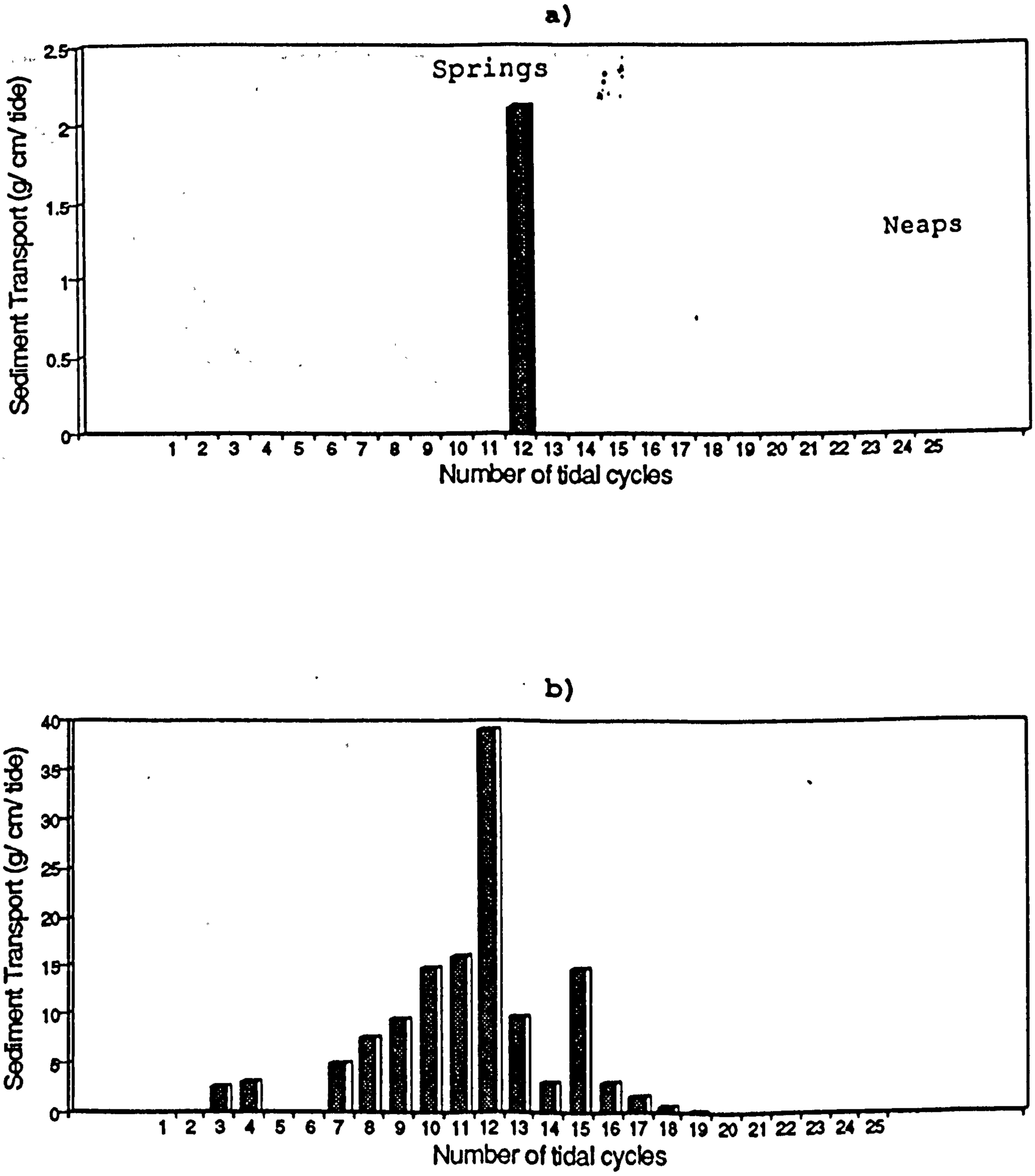

Fig: 6.7 a) Residual sediment transport at station C3. Direction of transport NE. (Threshold Velocity 37cm/s)

b) Residual sediment transport at station C3. Direction of transport NE. (Threshold Velocity 17cm/s)

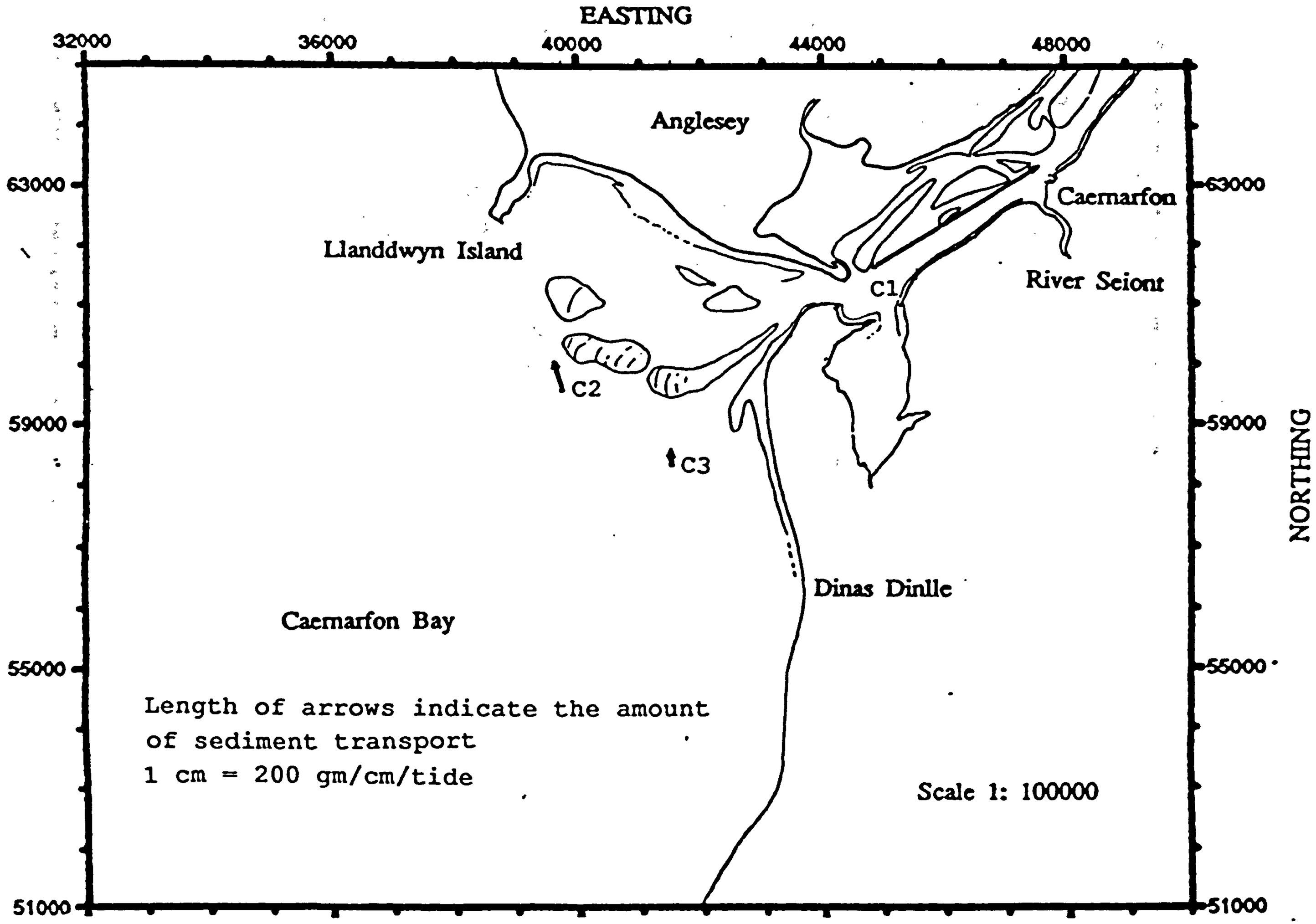

Fig: 6.8 Sediment trnasport at station C1, C2, and C3 during a spring tidal cycle.

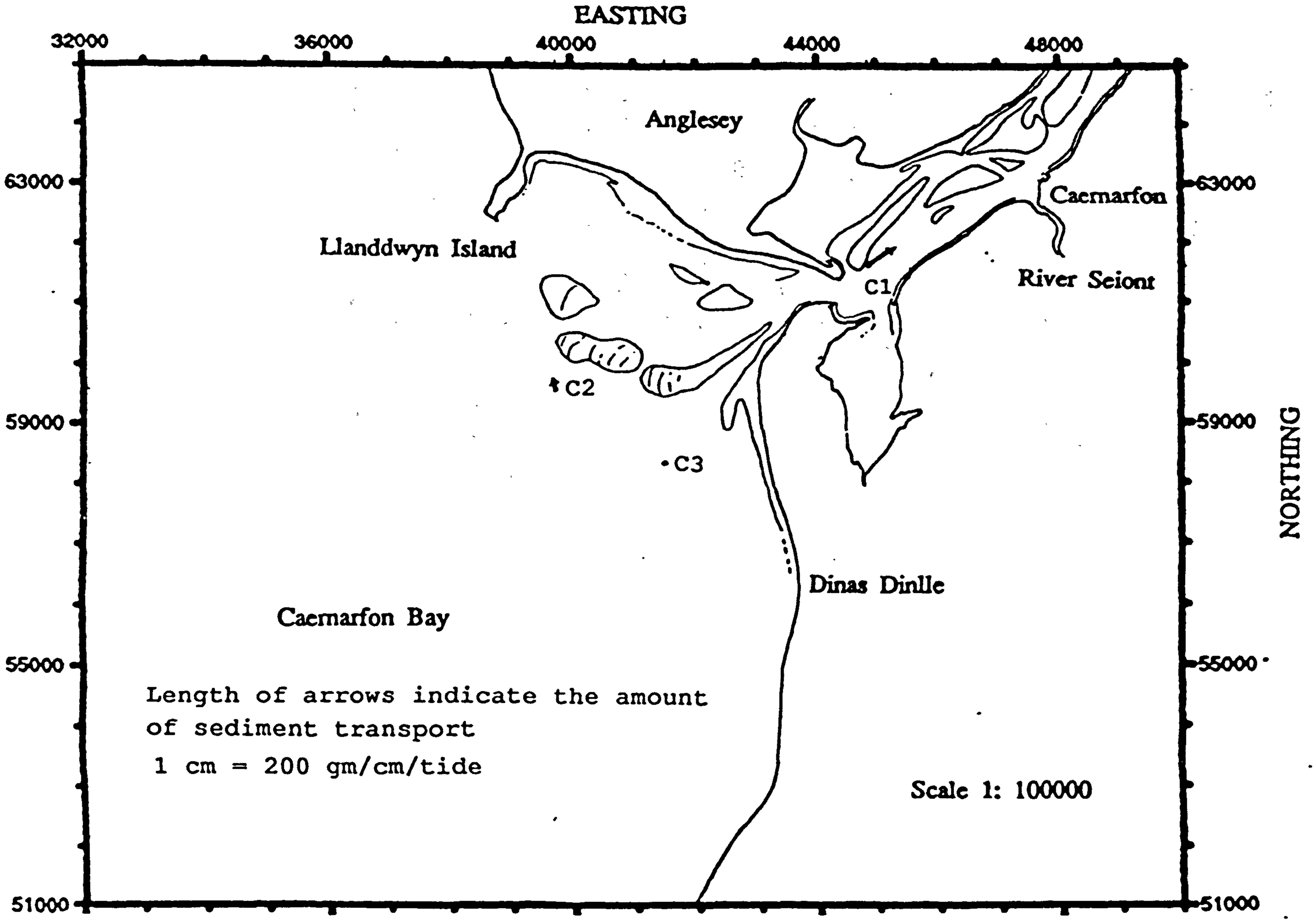

Fig: 6.9 Sediment transport at station C1, C2, and C3 during a neap tidal cycle.

sediment transport at station C1 decreases to as low as 57 g/cm/tide; however, the direction of transport remains the same. Outside in Caernarfon Bay there appears to be no sediment activity at station C3, while station C2 shows very little residual sediment transport (4 g/cm/tide) in a northwesterly direction.

The results from current meter observations at station C1 (inside the Strait) suggest that a considerable amount of sediment is transported in and out of the Belan inlet where the net sediment transport appears to be to the northeast (flood direction). This northeasterly net sediment transport direction at station C1 is however in total contrast to the present (bedfrom and grain size results) and previous (Jones (1984), and Nyandiwi (1988)) studies which suggest a southwesterly net sediment transport. It is probable therefore that the result is a function of instrument failure (tilting) during measurements made at this station. The results from the stations C2 suggest that a northwesterly residual sediment transport occurs in that area. Whereas, at station C3 the residual sediment transport mainly takes place in the northeast direction.

Whilst the results obtained using Miller et al's (1977) threshold values, particularly for station C2 and C3, indicate a little sediment activity in those areas, the results obtained using Gadd et al's (1978) and Mahamod's (1989) threshold values suggest relatively higher residual sediment transport.

CHAPTER 7

DISCUSSION

7.1 Quaternary history of the Caernarfon Bay and Menai Strait.

Results obtained from continuous seismic profiling in the study area provide strong support to those who speculated that a considerable quantity of Quaternary material must be present in Caernarfon Bay (Foster (1968), Dobson et al (1971), and Al-Shaikh (1971). Their speculations were based largely on evidence gathered from Quaternary studies of neighbouring areas (Cardigan and Tremadoc Bays), and especially concerning the course of the Irish Sea glaciations. Greenly (1919) and Embleton (1964) suggest that the Irish sea ice was deflected away from the mainland Welsh coast by the Welsh glaciers in the vicinity of the Menai Strait. It is therefore assumed that Irish Sea ice moved over Caernarfon Bay and must have resulted in the deposition of sediments of glacial and glacio-fluvial origin.

Seismic evidence (Fig: 3.16 and 3.17) reveals that the Quaternary sediments in the deeper parts of Caernarfon Bay are mainly composed of glacial and postglacial sediments and are overlain by a thin blanket of recent sand and gravel. In the vicinity of the tidal inlet the thickness of recent sediments appears to be considerably higher. The maximum thickness of Quaternary sediments in Caernarfon Bay is 77m.

7.1.1 Buried valleys in Caernarfon Bay.

The sparker seismic sections (Figs: 3.17) clearly indicate two buried valleys (previously described as a double branching valley) with a NE-SW dominant trend. On the basis of gravity, magnetic and seismic profiles Al-Shaikh (1971) reported similar types of features and linked the origin of these valleys to the Berw and Dinorwic faults (seismic results obtained from the area lying further offshore of the present surveys). However, because

of a lack of direct evidence he could not be certain about the offshore extension of the Dinorwic fault, but he speculated that it may extend into the central Irish Sea Basin. Bott and Young (1971), on the basis of gravity surveys, also reported the occurrence of depressions in the vicinity of the Berw and Dinorwic faults. Although no direct evidence of these faults can be seen in offshore seismic records in this study, the location and NE-SW trend of these buried valleys clearly links them to the Berw and Dinorwic faults. These features reach a maximum depth of -98m O.D. in some places. The northern valley (related to the Berw fault) appears to be slightly deeper than the southern valley (related to Dinorwic fault).

From the evidence it appears that although the origin of these buried valleys, which are incised into the bedrock, is related to the Caledonian and subsequent Hercynian earth movements, their typical U-shaped glacial form suggests that their present form was generated by glacial action during Quaternary glaciations. The relative deepening of the valley in the vicinity of the Berw fault could be result of the probable increase in the intensity of the Irish sea ice flow as it was less retarded by the Welsh ice. Similar U-shaped buried valleys have also been reported from the neighbouring Cardigan and Tremadoc Bays (Blundell, 1969).

7.1.2 Bedrock control on Quaternary sedimentation in the study area.

The distribution and deposition of Quaternary sediments in the study area is largely influenced by the bedrock topography. The greatest thicknesses of Quaternary sediments occur in the valleys, whilst in the area represented by the middle part of the N-S trending sparker sections (Fig: 3.17) i.e. where the bedrock rises upwards, it is overlain directly by postglacial sediments of glacio-fluvial origin and consequently the thickness of glacial sediments reaches to zero.

Seismic evidence indicates (Fig: 3.17) that the depth to bedrock increases gradually moving further offshore, suggesting that the bedrock dips gently towards the west. This produces a gradual thickening of the glacial sediments in the offshore direction. Blundell et al (1969) reported a similar trend of bedrock deepening westwards in Cardigan and Tremadoc Bay. They suggested that the glacial and postglacial sediments, which lie unconformably over the bedrock, also tend to increase in thickness westwards.

7.1.2 Quaternary sedimentation in Caernarfon Bay (glacial and postglacial).

Borehole data from the study area indicate that Quaternary deposits in Caernarfon Bay consist of 4 lithostratigraphic units. A boulder clay layer (unit 1) lies unconformably on the top of the bedrock. This is followed by a thin layer of sand and gravel (unit 2). Above the sand and gravel layer a second boulder clay layer (unit 3) was deposited and later, at the onset of the Holocene sea level rise, a layer of postglacial sediment (unit 4) was deposited.

The three lithostratigraphic units (boulder clay, sand and gravel, and boulder clay) within the glacial sequence (identified from the borehole data) are in agreement with the tripartite sequence suggested by Jehu (1909) and Greenly (1919). Jehu (1909) linked the two separate boulder clay layers and intermediate sand and gravel layer to two ice advances and an inter-glacial period respectively. Bowen (1973) states that, with the exception of Jehu's (1909) use of this scheme in the western Caernarfon region, tripartite schemes used in demonstrating two ice advances are of dubious validity in Wales. He does not however, give any justification for this.

In contrast to the borehole data, the seismic evidence collected as part of this project (Fig: 3.17), reveals only a single lithological unit (except section GG' where another reflector

within the presumed glacial layer can be seen). An additional reflector identified in section GG' perhaps indicates the presence of an intermediate sand and gravel layer which might be present over a considerable part of Caernarfon Bay. Since the seismic sections obtained during the current study suggest a single acoustically homogeneous layer, which is taken to represents the glacial sequence, is treated as a single unit. A similar acoustically homogeneous glacial sequence has also been reported for Barmouth Bay area (Larcombe, 1991). There are two explanations for this phenomenon; i) the glacial sequence may be basically composed of a single lithological unit ii) the seismic sensing technique used in both areas i.e. in the Caernarfon and Barmouth Bays, was unable to distinguish internal reflections within the glacial sequence. Since the borehole data from the study area indicates that the glacial sequence is in fact composed of more than one lithological unit the first explanation is obviously unacceptable and the problem appears to be one of seismic resolution or lack of acoustic impedance contrast between the lithologic layers.

The postglacial sediments in the area are composed mainly of sands and gravels and shelly material. The borehole data suggests that the thickness of the postglacial sediments in the immediate locality is about 11m. Such a figure does in fact broadly represent the average thickness of the postglacial sediments in Caernarfon Bay. The overall thickness of the postglacial sediments ranges between 3 and 15m. The isopach map of the thickness of the postglacial sediments (Fig: 3.23) reveals that there are large variations in the thickness of the sediments in relatively small areas. This suggests that there must have been a transitional period between the end of glacial deposition and the onset of marine sediment deposition during which time the top of the glacial sequence was severely altered and channelised. This may have been associated with glacio-fluvial erosion. These channel areas filled with postglacial sediments, can clearly be seen in the Fig: 3.23 (represented by the red to yellow colour). The alignment of

these channels appears to be roughly in line with the Menai Strait and Malltreath valleys and may have served as the extension of the river valleys, related to the above depressions, discussed by Greenly (1919). From this it appears that the deposition of postglacial sediments in Caernarfon Bay was strongly controlled by the surface topography of the top of the glacial sequence.

The results of the current study together with those of Blundell (1969) for Cardigan Bay, suggest that the deepest postglacial sediments in the area are at about -30m O.D.; this indicates that when postglacial deposition commenced in these areas sea level must have been about -30m O.D. Sea level curves (Heyworth and Kidson, 1982) obtained for various parts of Britain suggest that c. 9000 years B.P. sea level in this area was around -35 to -30m O.D. Larcombe (1991) reported for Barmouth Bay that the transition between glacial and marine sedimentation occurred between -40 and -30m O.D. Thus the Mawddach valley fill above the -35m O.D is probably estuarine in origin.

The evidence suggests that it was not until perhaps c. 9000 years B.P. that postglacial sediments started to be deposited in a marine environment of Caernarfon Bay. Initial deposition must have taken place in the relatively deeper channel areas cut into the glacial sequence. As sea level rose, and gradually the thickness of the postglacial sediments increased, various types of channel fill sequences were deposited. The internal pattern of these channel fill sequences indicates a rise in the sea level after c. 9000 years B.P.

7.1.4 Evolution of the present day morpho-hydrodynamic system in the study area.

The relevant literature and the present results indicate that rising sea level during the Holocene transgression, when reached to an approximate level of -2m O.D., must have resulted in the flooding of the Menai Strait depression. Embleton (1964)

speculated that the flooding of the Menai Strait took place between 6000 to 7000 years B.P. Bowen (1973) states that a comparatively limited amount of information is available on the Holocene sea level rise in the Wales. Bowen (1974) reported sea level results obtained by Tooley (1969, 1974) which suggest that marine conditions affected the coastal zone of Wales between 8500 and 4700 years B.P. The sea level at Abergele (North Wales) is thought to have been -2.8m O.D. between 7600 - 7200 and -0.24 to -0.77 between 6885 - 6025 respectively. Therefore Embleton's (1964) speculation that the Menai valley was flooded between 7000 to 6000 years B.P. appears to be reasonable.

In addition to the permanent flooding of the Menai Strait by sea water, the second major feature, which must have also played a major role in the evolution of the present day hydrodynamic system is the recurved spit at the mouth of the Belan inlet. It may be speculated that as the sea reached nearer to its present level, the sand, probably of offshore origin, started to be deposited along Newborough and Dinas Dinlle beaches. Subsequently, under the influence of southwesterly winds prevailing in the study area, the sand was blown from the beach and started to deposit on relatively higher ground along the coast. The rising sea level and increasing wave and tidal current activity in the vicinity of the recurved spit (Aber Menai point) must have contributed to the present form of the spit. Similar spits within the Dyfi (Wilks, 1977 and 1979) and Mawddach (Larcombe, 1989) estuaries are thought to have been formed around 5000 years B.P. Comparing this with the recurved spit in the present study area it can be speculated that the completion of the present day morpho-hydrodynamic system in the area took place about 5000 years B.P.

The evolution of such a major morpho-hydrodynamic system in the study area, dramatically changed the tidal current pattern around Anglesey and along the related coastal areas of the mainland in general, and within the Menai Strait and Caernarfon Bay in particular.

In the coming sections, emphasis will be given to the distribution and transportation of the recent sediments with special reference to the newly evolved morpho-hydrodynamic system in Caernarfon Bay and Menai Strait.

7.1.5 Deposition of the recent sediments.

Under the influence of the resulting morpho-hydrodynamic system, strong flood and ebb tidal currents flowing through the Strait twice a day emerged as major features of the tidal current pattern in the study area. Harvey (1968) indicated northward going currents in the west of Anglesey which curve around the island and move towards Beaumaris Bay. This coupled with the southwesterly residual flow (suggested by previous and present studies) through the Menai Strait suggests a circular movement of water around Anglesey. As a result of this current pattern large amounts of recent sediments accumulate in Beaumaris Bay, at the southwest end of the Menai Strait (opposite Caernarfon town), and in Caernarfon Bay (just outside Belan inlet).

Fouere (1966) states that the origin of the present surface sediments in Beaumaris Bay (NE end of the Strait) is most likely related to the tills and fluvio-glacial deposits being eroded along the Anglesey coast. Grain size and current meter results obtained by Ali (personal communication), from Beaumaris Bay, suggest that there is net transport of sediments into the Strait. All this evidence suggests that the large deposits of the recent sediments within the Menai Strait (opposite Caernarfon town) and just outside the Belan inlet may be related to sediments supplied by Beaumaris Bay. Boitier (1982) reported that the waters of the Menai Strait are quite turbid through out the year and undoubtedly carry a considerable annual load of sediment in suspension, by saltation and traction. He suggests that just beyond Port Dinorwic, the Menai Strait increases in width abruptly and as a result the tidal current velocity decreases considerably thus depositing the recent sediments in

the shape of large inter and sub-tidal sand banks and sand ridges. Large deposits of recent sand which are present outside the Belan inlet can perhaps be linked to the subsequent transport of sediments from inside the Strait.

The greatest thickness of these sediments has been encountered south of Llanddwyn Island where they reach up to 8m. The increased thickness in this area may be attributed to two causes: i) the main channel passes through this area and perhaps brings relatively larger amounts of sediment, ii) from this area onwards (further offshore) the current velocity decreases dramatically thus resulting in the deposition of the sediment load.

Just beyond the outer limits of the ebb-tidal delta in Caernarfon Bay, the thickness of the recent sediments decreases dramatically and rarely exceeds more than a metre. The recent sediments usually occur in the form of sand patches covered by sand ribbons and small scale megaripples. Similar types of sand patches have also been reported by Dobson et al (1971) from the deeper parts of Caernarfon Bay. Decreasing amounts of recent sediments further offshore suggest that the recent sediment activity is mainly taking place in areas characterised by the strong tidal currents i.e. in the vicinity of the Belan tidal inlet and within the Menai Strait.

7.2 Distribution and morphology of the recent sand deposits.

The resulting distribution and morphology of the recent sand deposits in the study area can best be understood in the context of the Quaternary depositional history of the area. As described previously, the deposition of the recent sediments within the Menai Strait and Caernarfon Bay is a direct result of the late Quaternary changes which occurred in the area. However, the diverse morphologic characteristics within the resulting recent sand deposits may be attributed to the present hydrodynamic conditions such as wave and tidal activity.

Hayes (1975), after several years of studying the coastal deposits controlled by different tidal ranges, tidal currents, wave conditions, and coastal storms, concluded that the morphology of such deposits is largely a function of the tidal regimes and waves. Of these two, he believes that the tidal regime has the major effect over the distribution and morphologic development of coastal deposits. During the present study, owing to the unfortunate lack of available wave data and proper wave monitoring equipment, the effect of the waves on recent sediments in the area could not be taken into account. It may be quite reasonable to speculate that the narrowness of the Belan inlet largely prohibits southwesterly waves from entering the Menai Strait; as such the only area exposed to the waves is just outside the Belan inlet. Considering the above and Hayes's (1975) statement that "although some of the ebb-tidal deltas are exposed to great variations in open-ocean wave intensity, they are strikingly consistent in morphology", it can be said with fair confidence that the absence of the wave data does not invalidate the results obtained.

Various results described and discussed in Chapters 4, 5, and 6 strongly suggest that the morphology of the recent sand deposits in the study area is a function of the prevailing flood and ebb tidal currents flowing through the Strait. According to Hayes's (1975) terminology of sand bodies associated with narrow inlets, the sand deposits in and outside the inlet are referred to as flood and ebb-tidal deltas respectively.

7.2.1 Comparison of the present tidal inlet and the associated flood and ebb ebb-tidal deltas with the standard models suggested by Hayes (1980).

Although the general morphology and the processes associated with the Belan tidal inlet agree to a certain extent with typical tidal inlets affiliated with barrier island and estuaries, discussed by Oertal (1972), Hayes (1969, 1975, 1979,

1980), and Hine (1975), some diversities in the details of the morphology of the flood and ebb-tidal deltas do occur. These diversities are understandable since the general setup of the Belan inlet is considerably different to other inlets. The main differences between the Belan inlet and typical tidal inlets associated with barrier islands and estuaries are listed below.

1) Almost equal amounts of water during ebb and flood tides must flow through inlets associated with barrier islands. In the case of the Belan inlet, due to the southwesterly residual flow of water through the Strait, considerably higher amounts of water flow during ebb tides.

2) The sediment supply to the flood and ebb-tidal deltas associated with inlets found between barrier islands is mostly from offshore areas. In the case of the Belan tidal inlet the sediments are transported into the system from the far end of the Strait i.e. the NE side.

3) As with the Belan inlet, the inlets associated with estuaries may be characterised by higher ebb flows. However, in the case of estuaries the higher water flow during the ebb results from fresh water input by rivers. Because of the seasonal nature of the rivers, the amount of incoming fresh water varies according to the seasons. In the case of the Menai Strait the additional ebb flow is caused by the addition of the sea water from the NE end which, except for tidal variations, remains steady all the year.

4) In the case of estuaries, depending on the size of the river and nature of the sediments in the related onshore areas, a considerable amount of sediment is usually added to the system. In the case of the Belan inlet system the supply of the sediment is entirely from the coastal and offshore areas.

Comparison of the Belan inlet with other inlets therefore suggests that whilst it shows some resemblance to the typical

inlets discussed in the literature, it deviates considerably in some of the processes. In the following section the effects of these variations over the general morphology of the flood and ebb-tidal deltas will be discussed.

Flood-tidal delta.

Generally, the flood tidal currents on passing through an inlet are characterised by a radial flow as they reach the flood-tidal delta (Byrne et al, 1975). Hine (1975) reported that the flood tidal currents at Chatham Harbour estuary, Massachusetts flow in three different directions swinging through an arc of approximately 70 degrees. Certainly this is not happening in the case of the present flood-tidal delta associated with the Belan inlet where the tidal currents during the flood tide flow mainly in one direction and rarely swing more than 20 degrees. This is understandable since the elongated shape of the Menai Strait dictates the pattern of tidal flow. Owing to the relative narrowness of the Strait in comparison to other systems, the flood tidal currents, instead of spreading radially over the flood-tidal delta follow a straight course along the main channel upstream. Whilst the standard model of a flood-tidal delta suggested by Hayes (1980) represents a localised sand body which is restricted to the areas around the inlet, the Menai Strait/Caernarfon Bay flood-tidal delta elongates in its shape and includes an area up to 6km upstream.

Hayes (1980) suggests that sand waves and megaripples with a dominant flood orientation are the principal bedforms associated with flood-tidal deltas. The present studies have indicated a wide occurrence of such bedforms in many parts of the flood-tidal delta, but, in contrast to Hayes model, the bedforms are mainly ebb oriented or symmetrical during most of the tidal states (ebb oriented sand waves on the flood-tidal delta are clearly shown in photograph C which appears on Plate 1). Flood orientation only occurs in some parts during the spring tides. The above discussion suggests that the flood-tidal delta appears

to be unique in its distribution and processes and hardly shows any resemblance to the standard model of a flood-tidal delta suggested by Hayes (1980).

Ebb-tidal delta.

In contrast to the non-standard form of the Menai Strait/Caernarfon Bay flood-tidal delta, the ebb-tidal delta is strikingly consistent with the standard model suggested by Hayes (1980). It exhibits all the major features of a typical ebb-tidal delta such as a main ebb channel, marginal flood channels, terminal lobe, etc. However, it appears that the size of the ebb-tidal delta is, to a certain extent, a function of the setting of the area. Llanddwyn Island in the north of the delta plays a major role in controlling the tidal currents and subsequent sediment movement in the area.

The overall morphology of a typical ebb-tidal delta is usually characterised by the interaction of the ebb-tidal currents and prevailing longshore currents (Hine, 1975). In the present case it appears that LLanddwyn Island, to a large extent, shelters the main ebb-tidal delta from the influence of longshore currents on its northern side. However, on its southern side the delta is relatively more exposed to the prevailing northwesterly residual currents. Therefore the northwesterly curve in the terminal lobe of the delta may be related to the above effect (Fig: 4.14). It may be speculated that as the ebb-tidal delta started to develop after the evolution of the present tidal conditions, the prevailing northwesterly residual currents around station C2 and C3 continuously pushed the sand body towards the northwest.

Another important feature of the ebb-tidal delta is the presence of large sand waves (as seen on satellite images) over the terminal lobe. These sand waves are entirely consistent with the point above and suggest that these sand waves result from the southwesterly and then northwesterly movement of the sediments

above the terminal lobe under the influence of ebb-tidal currents and regional northwesterly residual currents respectively. Thus they restrict the seaward extension of the ebb-tidal delta.

Within the ebb-tidal delta sand body the main ebb channel serves as the major outlet for ebb currents coming out of the Belan inlet. Surrounding the main ebb channel, in the vicinity of the inlet, are two marginal flood channels (Fig: 4.14). Photograph F (shown in Plate 2) shows a part of the northern marginal flood channel where the large flood oriented megaripples can be seen. It appears that these marginal flood channels are active during the early parts of the flood tide when an ebb lag is still flowing through the main ebb channel. However, with the increasing flood tide the water must enter the inlet in an unconfined manner, with water flowing through both the marginal flood channels and the main ebb channel.

The floor of the main ebb channel is largely characterised by the presence of ebb oriented megaripples. The megaripples range in height from 0.6 to 1m and have wavelengths of 6 to 10m. The size of the bedforms on the ebb-tidal delta appear to be decreasing away from Belan inlet suggesting the decreasing intensity of the tidal currents going offshore. Hine (1975) reported that because much of the surface of an ebb-tidal delta sand bodies is topographically high and very shallow, it is not significantly influenced by ebb currents. Perhaps because of this factor the ebb oriented bedforms are generally restricted to the floor of the main channel and flanks of the sand banks. In addition to the main ebb channel, the other areas which also show ebb oriented bedforms are the spill over lobes (Hine, 1975). The spill over lobes of the present ebb-tidal delta appear to be in full agreement with Hines's findings and show some ebb oriented bedforms.

The above discussion suggests that while the flood-tidal delta in the present study area hardly shows any resemblance to the

standard model of Hayes (1980), the ebb-tidal delta is strikingly consistent with the typical ebb-tidal delta discussed by Hayes (1980).

7.3 Model of sediment transport pathways.

Based mainly on the bedform characteristics, grain size analysis, and to some extent on the sediment transport calculations, a model for sediment transport pathways prevailing in the study area is proposed and is shown in Fig: 7.1. Extra care and much effort has been devoted to preparing a model which closely represents the prevailing sediment transport paths in the area. However, because of the complex nature of the sedimentary processes related to the Menai Strait it would be reasonable to suggest that the proposed model may be treated as at best, an approximation to the actual sediment transport paths.

The model suggests that sediment mainly enters the study area from the northeast side of the Menai Strait. However, some sand is also transported from the offshore areas of Caernarfon Bay. The model appears to indicate three distinct areas of sand transport patterns which are markedly different from one another. For example, the transport pattern prevailing inside the Menai Strait is fairly straight forward and indicates a net sediment transport towards the southwest i.e. towards the Belan inlet. On the other hand, the sediment transport patterns representing the sediment movement in the offshore areas of Caernarfon Bay indicate a northeasterly direction with an increasing northerly component as they reach nearer to the ebb-tidal delta. The model suggests a relatively smaller net sediment transport in deeper parts of the study area. Some of the sediment, transported from the offshore area enters the ebb-tidal delta system through the southern marginal flood channel, while the rest is probably transported in a northwesterly direction along the distal portions of the ebb-tidal delta and ultimately, passing west of the LLanddwyn

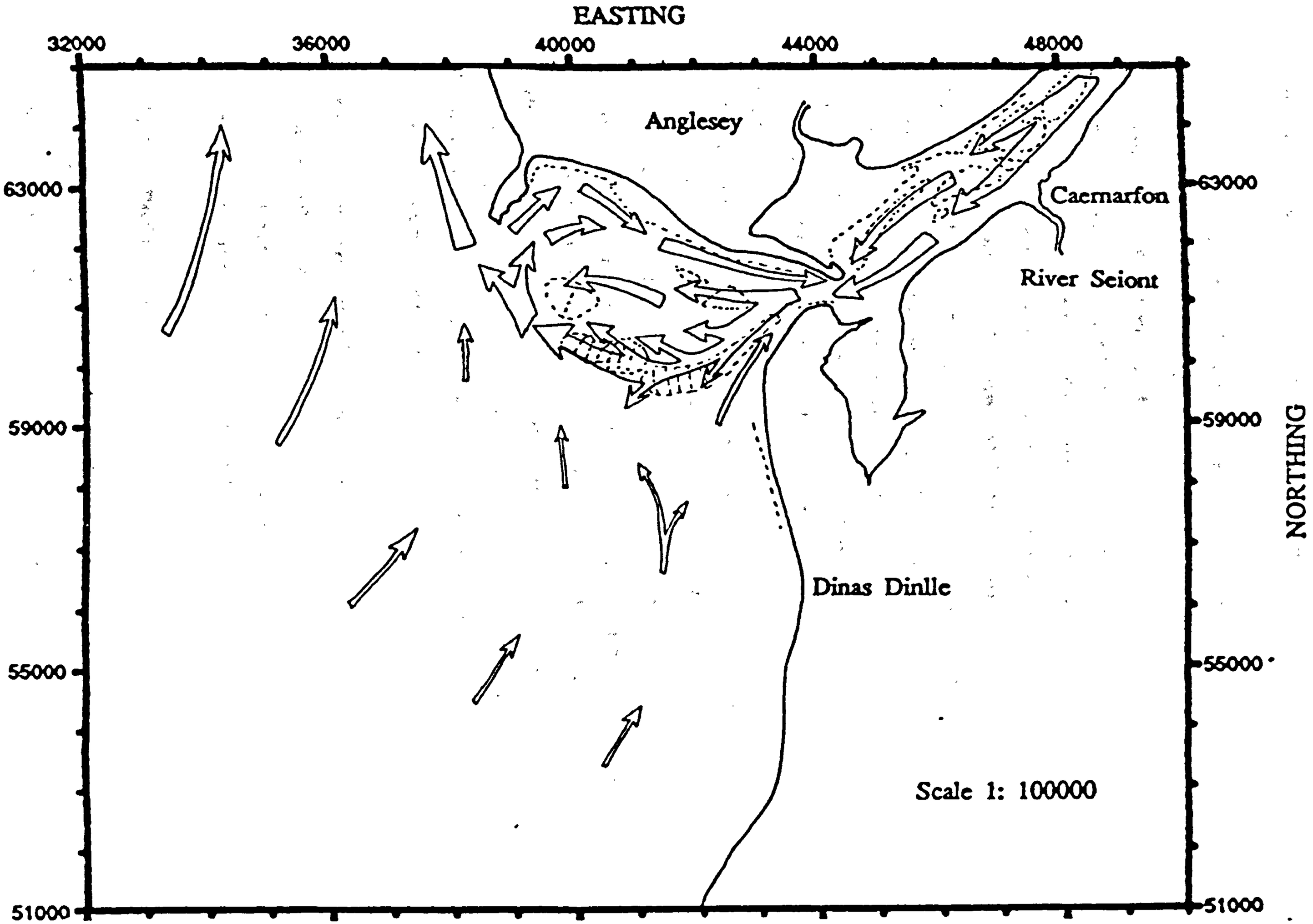

Fig: 7.1 proposed model of the sediment transport pathways in the study area.

Sand bodies

Island, is carried towards the north.

The third area, which represents the ebb-tidal delta, is a zone of complex sediment transport patterns resulting from the influence of strong tidal currents (associated with the Belan inlet) and regional tidal currents. The proposed model suggests that the sand in this area is transported in and out the inlet through a main ebb channel and neighbouring marginal flood tidal channels. Most of the offshore sediment entering the ebb-tidal delta system through the southern marginal flood channel is carried into the main ebb channel and transported seaward to the distal portions of the ebb-tidal delta i.e. towards the offshore sides of the terminal lobe. The sediment transported by the main ebb channel, under the influence of northwesterly residual currents, is carried northwards (i.e. to the area south of the LLanddwyn Island) and subsequently is transported landwards by the collective action of the flood tidal currents and the typical southwesterly waves prevailing in the area. When the sediments reach nearer to Newborough beach, some of the sediments are carried away by wind erosion and deposited as sand dunes on land, and some sediments are transported back towards the Belan inlet by flood currents in the northern marginal flood channel. Some sediments, from the south of LLanddwyn Island, also travel towards the north.

In order to further explain the sediment transport pathways in the study area, a discussion of the proposed model in the light of bedform and grain size results and sediment transport calculations will be given below.

7.3.1 Bedforms.

The presence of the various bedforms on the seabed reflects the bottom sediment transport, where bedload transport is assumed to be perpendicular to the crestlines of sand waves and parallel to the trend of sand ribbons (Knebel, 1989). The extensive occurrence of bedforms in the study area, ranging from small

scale megaripples (wavelength 1-5m) to huge sand waves (wavelength up to 45m), indicates a large scale sediment activity.

The area of most intense sediment transport activity appears to be inside the Menai Strait where a number of sand wave fields can be seen (Fig: 4.19). In addition to sand waves the other dominant bedforms recognised within the Strait are large scale megaripples. The distribution of megaripples within the Menai Strait suggests that bottom sediments are transported mainly within the tidal channels and along the flanks of the inter and sub-tidal sand bodies. Similar types of bedform patterns have been extensively reported in the literature (for examples see Hine (1975), Knebel (1989), Sha (1989)) and are related to the relatively extended flow of tidal currents (because of the rising and falling tide) in these areas. Within the Menai Strait sediment transport can occur either to the northeast (by flood currents) or to the southwest (by ebb currents). Side-scan sonar surveys and repeated echo-sounding surveys over neap/spring tidal cycles, conducted over a three year period in Caernarfon Bay/Menai Strait, reveal that within the Menai Strait the vast majority of the bedforms are most usually ebb oriented and/or symmetrical. This strongly implies that the net sediment transport within the Menai Strait is towards the southwest. These results support those who previously advocated ebb dominated sediment transport in the area (Deeming (1972), Jones (1984), and Nyandwi (1988)).

Jones' (1984) conclusions were predominantly made on the basis of direct measurements of megaripple migration over a period of 34 days. He reported a net megaripple movement of 12.07m during the entire study period (34 days) i.e. 0.35m/tidal day. The minimum or near zero movement of the megaripple over neap tides reported by Jones appears to be understandable in the light of the repeated echo-sounding surveys carried out for this project which suggest that neap tides are characterised by a relatively higher bedform steepness index. The maximum and near zero or

zero migration rates of bedforms during spring and neap tides, respectively, have been reported by several workers (Boothroyd and Hubbard (1975), Boersma and Terwindt (1981), Terwindt and Brouwer (1986)). The present studies also suggest similar trends for the spring and neap tides and therefore support the previous findings.

In the area occupied by the ebb-tidal delta, no previous studies related to sediment movement have been conducted, as such the prevailing bedform characteristics have been interpreted in the light of the conclusions drawn from the study of the bedforms within the Menai Strait and obtained tidal current results. On the basis of large sand waves and megaripple features present on the terminal lobe and on the floor of the main ebb channel respectively, it can be suggested that the net sediment transport patterns in this area are relatively complicated. The large sand waves present on the main terminal lobe indicate a permanent trend of sediment transport on the ebb-tidal delta and appear to be little affected by waves and flood tidal currents.

In the areas of the marginal flood tidal channels (Fig: 4.14), as expected, the flood oriented megaripples clearly visible near the Aber Menai point in photograph F (Plate 2) suggest sediment transport in the direction of flood tidal currents. The above type of flood tidal current pattern agrees remarkably well with the sediment transport patterns suggested for the typical ebb-tidal delta (Hayes (1975), Hine (1975)), and also with the present proposed model of the sediment transport pathways. Megaripples in the ebb-tidal delta area have a maximum wavelength of 10m and there is a trend of decreasing megaripple size going seaward, which most probably occurs under the influence of diminishing current speed.

Further away from the ebb-tidal delta, the deeper parts of the study area are characterised by the wide occurrence of sand ribbons. Karcz (1967) states that sand ribbons are formed on a fixed bed under conditions of limited sand supply. Dobson et al

(1971), on the basis of sand wave asymmetry, sand ribbon and sand ridge alignments, suggested paths and directions of sediment movement in the Irish Sea. Their results indicated that in the deeper parts of Caernarfon Bay (near to the present study area) sand ribbons occur widely with a northeasterly dominant direction of net sediment transport. The alignment of the sand ribbons reported by Dobson are generally similar to the ones mapped during the present study. However, Dobson et al's results indicate that the net sediment transport paths in Caernarfon Bay tend to curve strongly towards the north and quite far away from the present study area. Present evidence suggests that northeasterly net sediment transport reaches very close to the ebb-tidal delta and then partially turns towards the north. This diversity shown by Dobson et al's transport paths may perhaps be related to the lack of detailed bedform data within Caernarfon Bay. The alignment of these sand ribbons suggests that they are most probably related to the NE-SW regional tidal current pattern which prevails in that part of the study area (Fig: 4.13). On the basis of superimposed megaripples present on the surface of these sand ribbons and Dobson et al's (1971) results it can be concluded that these sand ribbons transport offshore sediments towards the ebb-tidal delta where some sand enters into the delta system while the rest of it is carried northward along the distal portion of the ebb-tidal delta. Hence this strongly supports the proposed model.

The above discussion, while on the one hand strongly supports the proposed model of sediment transport pathways in the study area, on the other provides firm evidence in support of the use of bedform characteristics to determine sediment transport pathways in areas similar to the Menai Strait and Caernarfon Bay.

7.3.2 Grain size distributions.

Progressive changes in grain size distributions (mean, mode, sorting etc.) within an area are thought to reflect the trends

of net sediment transport paths and directions. First of all, Krumbein (1938) reported such changes occurring in grain size distributions from source to final deposits. Since then a number of workers have recognised and supported the use of progressive changes to interpret sediment transport pathways (McCave (1978), Mclaren (1981), Mclaren and Bowles (1985), Dyer (1986)). Within the present studies, progressive changes in grain size distributions have been identified in some parts of the study area, particularly in those lying outside the Belan inlet, and may indicate some systematic changes occurring in the movement of sediments in the area.

Within the Menai Strait, owing to the intense topographic variations, there appears to be little systematic change taking place in the grain size parameters which might reflect some potential trends. Nevertheless, ignoring the topographic effects, some trends occurring over relatively small areas and some other features of interest can be identified. For example, relatively coarse sediments are predominantly found on the floor of the main channel, whereas, relatively fine sediments occur around the large sand deposits thus suggesting that the grain size within the Strait appears to be a function of water depth and is in full agreement with the comments previously made regarding the occurrence of bedforms on the sides and floors of the sand banks and main channel respectively. The sediments on the floors of the main channel are largely negatively skewed whereas the sorting of these sediments varies randomly along the channel. Since, within the main channel, the tidal currents are relatively fast and flow for extended periods of time, the negative skewness is understandable in terms of the winnowing of fine sediments by strong tidal currents. The randomly decreasing and increasing sorting of the sediments along the whole stretch of the main channel may indicate the variable nature of the tidal currents.

The sorting contour map (Fig: 5.17), although suggesting mainly random changes within the Strait, do show some interesting

trends over relatively small areas. For example, just before Belan inlet and starting from the contour values of 0.4 (Folk) and 0.3 (moments) the sediments become progressively more sorted towards the inlet. Some other small scale trends can also be seen at the NE extreme of the study area and westward off the 0.5 contour value (opposite Caernarfon town). All these trends, when considered individually, suggest that the sediments become better sorted towards Belan inlet. The proposed model of sediment transport suggest that the sediments are transported from the Menai Strait towards ebb-tidal delta then the sediments along the Strait represent a relative source. According to Mclaren (1981) if a source sediment undergoes erosion, the lag remaining must therefore be coarser, better sorted and more positively skewed (case II). As such, within the Strait, the relative increase in the sorting towards the Belan inlet supports both the proposed model of sediment transport paths and Mclaren's (1981) model. The skewness within most parts of the Strait however, appears to be a function of local variations and therefore comparisons to the Mclaren's model can not be made except in the case of the main channel which in contrast to the Mclaren's model, indicates negative skewness. Hence the present studies reject the other half of Mclaren's case II.

The mean grain size contour map (Fig: 5.14) suggests that the grain size tends to decrease away from Belan inlet, and roughly around the offshore boundary of the ebb-tidal delta reaches a minimum before starting to increase again moving offshore. The sorting (Fig: 5.17), mode (Fig: 5.16), and skewness (Fig: 5.19) contour diagrams, representing the above mentioned area also indicate some systematic changes. Superimposed on these systematic changes are some effects of topographic variations, particularly in the area of the ebb-tidal delta. The grain size results suggest that as the strong ebb tidal currents emerge out of Belan inlet, the decreasing current speed results in the deposition of sand on the ebb-tidal delta. This is inferred from the fact that whilst the coarse grained sediments are found on the sand ridge nearer to the inlet the finest sediments in the

area occur further away from the inlet. The decreasing current speed and shallow water depth (because of the sand ridge) facilitates the quick deposition of the coarse grained material at the mouth of the inlet. While it could be argued that the presence of coarser material in that area may be a result of the erosion of finer sediments by flood tidal currents and/or waves, the positive skewness of the sediments seems to be against any such argument. With the seaward decrease in current velocity and under the influence of the shape of the terminal lobe, most of the sediments are deposited around the terminal lobe area and some are carried away further seaward.

According to Mclaren (1981) and Mclaren and Bowles (1985), if sediment in transport undergoes selective deposition, the resultant deposit may either be finer and negative skewed (case IIIA) or coarser and positively skewed (case IIIB), but, the sorting will always be better. The results presented in this thesis also suggest a somewhat similar trend since the sediments in the area of the ebb-tidal delta are largely positively skewed and well sorted suggesting deposition in that area and supporting the proposed model of sediment transport pathways in the study area. The resulting negative skewness in the area around the northern flood marginal channel and in some parts of the main ebb channel may be related to the strong winnowing action of the flood tidal and ebb tidal currents respectively.

The zone along the distal portions of the ebb-tidal delta, which is characterised by the finest sediments encountered in the whole study area, represents the zone where the tidal current velocities are lowest during any tidal state. The sediments of this area are relatively poorly sorted and negatively skewed which perhaps results from the bimodal nature of some sediment distributions occurring in that area. This suggests that sediment distributions obtained from this zone are perhaps a mixture of the two types of sediments i.e. those coming from the Menai Strait and those from the offshore areas.

7.3.3 Sediment Transport calculations.

Heathershaw (1981), on the basis of studies conducted on the British continental shelf, concluded that while existing sediment transport equations may give widely differing estimates of the sediment transport rates, the directions of net sediment transport in the study area agree remarkably well with those inferred from sedimentological studies (eg. sand wave asymmetry, and orientation, and sand ribbon alignment). In the current study, whilst the net sediment transport directions estimated at station C2 and C3 fit very well in the proposed model of sediment transport paths (which is largely based upon the bedform and grain size results) for the area, the results obtained at station C1 are in total contrast to the present and previous studies. According to previous studies (Deeming (1972), Jones (1984), Nyandwi (1988) and recently acquired side-scan sonar and repeated echo-sounding data, it was expected that a net sediment transport towards the southwest should occur at station C1. But the sediment transport calculations based on the new data suggest a northwesterly net sediment transport. To explain this discrepancy two reasons can be sought

1) The discrepancy could be a result of previously described error in the current meter data acquired for the station C1 which was introduced by the tilting of the current meter. Earlier it was thought that the error in the data occurred during a number of flood tides only and the current meter recovered to its normal position during subsequent ebb tides, but now considering the discrepancy in the results it would be reasonable to suggest that the current meter perhaps did not record the data correctly for much of time of the deployment.

2) The northeasterly net sediment transport may have arisen from the use of the Hardisty's (1983) equation which is basically calibrated for velocities up to 55cm/s and according to Mahamod (1989) would over estimate the sediment transport at higher velocities. Such velocities are a common feature at

station C1.

At stations C2 and C3 there appears to be some sediment transport during spring tides while during neap tides the amount of residual sediment transport is relatively small. Relating this to the fact these two stations are located roughly in the zone of finest sediments in the area, the resulting small amount of residual sediment transport is hardly surprising.

Considering the bedform and grain size results and subsequent proposed model of sediment transport pathways which suggests a net residual sediment transport in the vicinity of station C2 and C3, Miller et al's (1971) threshold values which suggest nearly zero or very small net sediment transport values appear to be far from real as far as the present study area is concerned. Mahammod's (1989) threshold curve, which is based on Guy et al's (1961) data, seems to more closely represent the present area.

CHAPTER 8

CONCLUSIONS

On the basis of results described and discussed in the previous chapters some conclusions can be drawn. However, because of the nature of the complex geomorphology and hydrodynamic processes prevailing in the area the conclusions, in particular those related to the present sedimentary processes, may be treated as tentative.

1) Quaternary deposits in the study area are basically composed of three depositional sequences i.e. glacial, postglacial, and recent. The oldest sequence (glacial sequence) lies unconformably on the bedrock.
3) Deposition of the glacial sequence was controlled by the prevailing bedrock topography. Thus the greatest thickness of 68m occurs in the U-shaped valleys.
4) Before deposition of postglacial sediments in the study area, the top of glacial sequence was severely eroded and channelised by glacio-fluvial action.
5) The evolution of the morpho-hydrodynamic system prevailing in the Menai Strait and Caernarfon Bay area resulted from the late Quaternary changes and the completion of the system in its present form most probably took place c. 5000 years B.P.
6) The deposition and present morphologies of the recent sediments in the Menai Strait and Caernarfon Bay are linked to the flood and ebb tidal currents operating in the area. Within the study area ebb tidal currents flow for relatively longer periods of time and there is a southwesterly residual flow of water through the Strait.
7) Whilst the flood-tidal delta morphology and processes do not show similarity to the standard model given by Hayes (1980), the ebb-tidal delta is strikingly consistent with the standard model and exhibits all the major features.
8) The bedform studies suggest that most of the recent sediment

activity, under the influence of local geomorphology (especially the Belan inlet), is restricted to the areas occupied by the tidal deltas. The presence of Llanddwyn Island in the north plays a major role in the development of a well developed ebb-tidal delta, since it protects the delta from the erosive effects of longshore regional currents.

9) The change of environment takes place along the distal portion of the ebb-tidal delta where locally-influenced and regional tidal currents interact. This area marks the zone of weakest tidal current velocities and finest grained seabed sediment.
10) The net sediment transport in the Menai Strait occurs from northeast to southwest, whereas in the deeper parts of the Caernarfon Bay the net sediment transport takes place from southwest to northeast. The area occupied by the ebb-tidal delta marks a zone of complex sediment transport patterns and is largely a function of a combination of locally influenced and regional tidal currents. Bedform and grain size studies suggest that the sediment supply to the study area largely takes place from the NE side of the Strait, some sediments are also transported from the offshore areas.

Suggestions for further work

The multidisciplinary nature of the research described in this thesis will provide a strong base for any future geophysical, sedimentological, and oceanographic studies of the area. Various suggestions are made below.

1) A high resolution digital seismic survey of Caernarfon Bay may help in overcoming the multiple reflection problem and also in defining the detailed internal layering within the glacial and postglacial sequence and that could provide even better understanding of Quaternary depositional environments in the area.
2) Repeated sub-bottom profiling on a selected line over a

neap/spring tidal cycle may provide interesting results regarding the temporal variations in the thickness of unconsolidated surficial sediments, provided position fixing problems are overcome (perhaps, by using automatic trisponder position fixing system).

3) In order to study more vigorously the prevailing current patterns in the Menai Strait and Caernarfon Bay, more current meters should be deployed at various places, particularly just inside the Strait and in the area of the ebb-tidal delta.

4) Studies of the wave activity, particularly in the area occupied by the ebb-tidal delta, would help in further defining the sediment movement taking place in the study area.

5) Box coring of the bedforms over the tidal deltas and analysis of the internal sedimentary structures would provide better understanding of the net sediment transport directions.

REFERENCES

Admirality chart, (1975) Menai Strait.

Allen, J.R.L. (1965) The Sedimentation and palaeogeography of the Old Red Sand stone of Anglesey, North Wales.
Proc. Yorks. Geol. Soc., 35, 139-185.

Allen, J.R.L. (1965) Sedimentation to the lee of small under water sand waves.
Jour. Geol., 73, 95-116.

Allen, J.R.L. (1968) Current ripples: their relation to patterns of water and sediment motion.
Amsterdam: North-Holland Publishing Company. 433pp.

Allen, J.R.L. and Friend, P.F. (1976) Changes in intertidal dunes. during two spring-neap cycles, Lifeboat station Bank, Wells-next-the Sea, Norfolk (England).
Sedimentology, 23, 329-346.

Al-Shaikh, D. (1970) Geophysical investigations in the northern part of the Cardigan Bay (including a part of the central Irish Sea).
PhD Thesis, University of Wales.

Amos, C.L. and King, E.L. (1984) Bedforms of the Canadian eastern seaboard: a comparison with global occurrences.
Mar. Geol., 57, 167-208.

Ashmore, S. and Leatherman, S.P. (1984) Holocene sedimentation in Port Royal Bay, Bermuda.
Mar. Geol., 56, 289-298.

Baba, J. and Komar, P.D. (1981) Settling velocities of irregular grains at low Reynolds numbers.
Jour. Sediment. Petrol., 51, 121-128.

Bagnold, R.A. (1956) The flow of cohesionless grains in fluids.
Phil. Trans. Royal Soc., A249: 235.

Bagnold, R.A. (1963) Mechanics of marine sedimentation.
In: Hill, M.N. (Editor) The Sea, 3 , 507-582.

Bagnold, R.A. (1966) An approach to the sediment transport problems from general physics.
U.S. Geological Survey Prof. Paper, 422-I, 1-37.

Barber, A.J. and Max, M.D. (1979) A new look at the Mona Complex (Anglesey, North Wales).
Jour. Geol. Soc. London, 136, 407-432.

Bates, D.E.B. (1968) The lower Paleozoic Brachiopod and trilobite faunas of Anglesey.
Bull. Brit. Mus (Nat. Hist). Geol., 16, 127-199.

Bates, D.E.B. (1972) The stratigraphy of the Ordovician rocks of Anglesey.
Geol. Jour., 8, 29-58.

Bates, D.E.B. (1974) The structure of the Lower Paleozoic rocks of Anglesey, with special reference to faulting.
Geol. Jour., 9, 39-60.

Bates, D.E.B. and Davies, J.R. (1981) The geology of Anglesey.
In: Capewell, J.G. and Raine, G.T. (Editors) Field guide No. 40, The Geologists Association, London, pp1-31.

Belderson, R.H., Kenyon, N.H., Stride, A.H. and Stubbs, A.R. (1972).
Sonographs of the sea floor.
Elsevier, Amsterdam, 185 pp.

Belderson, R.H. and Stride, A.H. (1966) Tidal current fashioning of a basal bed.
Mar. Geol., 4, 237-257.

Blundell, J., Davey, F.J. and Graves, L.J. (1971) Geophysical surveys over the South Irish Sea and Nymphe Bank.
Jour. Geol. Soc. London, 127, 339-375.

Blundell, J., Griffiths, D.H. and King, R.F. (1969) Geophysical investigations of buried river valleys around Cardigan Bay.
Geol. Jour., 6, 161-180.

Boersma, J.R. and Terwindt, J.H.J. (1981) Neap-spring tide sequences of internal shoal deposits in a mesotidal estuary.
Sedimentology, 28, 151-170.

Boitier, D. (1982) A sub-bottom and seabed investigation of the Menai Strait off the Britania Bridge.
Msc Thesis, University of Wales.

Boothroyd, J.C. and Hubbard, D.K. (1975) Genesis of bedforms in mesotidal estuaries. In: L.E. Cronin (Editor) Estuarine Research, 5, II. Geology and Engineering.
Academic Press, New York, N.Y., pp. 113-158.

Bott, M.P.H. and Young, D.G.G. (1971) Gravity measurements in the north Irish Sea.
Quar. Jour. Geol. Soc. London, 128.

Bowen, D.Q. (1973) The Pleistocene history of Wales and the borderlands.
Geol. Jour., 8, 207-224.

Bowen, D.Q. (1974) The Quaternary of Wales. In: Owen, T.R. (Editor) The upper Paleozoic and post-Paleozoic rocks of Wales. Cardiff, 373-426.

Bowen, D.Q. (1977) The coasts of Wales. In: Kidson, C., Tooley, M.G. and Newall, G. (Editors) The Quaternary history of the Irish Sea, 223-256.

Bryne, R.J., Bullock, P. and Tyler, D.G. (1975) Response characteristics of a tidal inlet: A case study.
In: L.E. Cronin (Editor) Estuarine Research, 5, II. Geology and Engineering.
Academic Press, New York, N.Y.,

Buller, A.T. and McManus. J. (1979) Sediment sampling and analysis. In: Dyer. K.R. (Editor) Estuarine hydrography and sedimentation.

Campbell, S. (1990) Quaternary sequence at Dinas Dinlle. In: Addison, K., Edge, M.E. and Watkins, R. (Editors) North Wales field guide, Quaternary Research Association, 61-64.

Carlson, P.R. (1989) Seismic reflection characteristics of glacial and glacimarine sediment in the Gulf of Alaska and adjacent Fijords.
Mar. Geol., 85, 391-416.

Caston, V.N.D. (1965) Localised sediment transport and subsequent erosion in Tremadoc Bay, North Wales.
Mar. Geol., 3, 401-410.

Chin, J.L., Clifton, H.E. and Mullins, H.T. (1988) Seismic stratigraphy and Late Quaternary shelf history, South central Monterey Bay, California.
Mar. Geol., 81, 137-157.

Dalrymple, R.W., Knight, R.J. and Lambiase, J.J. (1978) Bedforms and their hydraulic stability relationships in a tidal environment, Bay of Fundy, Canada.
Nature, 275, 100-104.

Dalrymple, R.W. (1984) Morphology and internal structure of sand waves in the Bay of Fundy.
Sedimentology, 31, 365-382.

Davies, J.L. (1964) A morphogenetic approach to world shorelines.
In: Zeitchrift fur geomorphologie, Sonderheft Zum 70. Geburstag Prof H. Mortensen: 127-142.

Deeming, K.R. (1972) Sands of Traeth Gwyllt.
MSc Thesis, University of Wales.

Dobrin, M.B. (1976) Introduction to geophysical prospecting, 3rd edition. New York, McGraw-Hill.

Dobson, M.R., Evans, W.E. and James, K.H. (1971) The sediment on the floor of the Southern Irish Sea.
Mar. Geol., 11, 27-69.

Doeglas, D.J. (1946) Interpretation of the results of mechanical analyses.
Jour. Sediment. Petrol., 16, 19-40.

Duane, D.B. (1964) Significance of skewness in recent sediments, Western Pamlico sound, North Carolina.
Jour. Sediment. Petrol., 34, 864-874.

Dyer, K.R. (1970) Current velocity profiles in a tidal channel.
Geoph. Jour. Royal Astron. Soc., 22, 153-161.

Dyer, K.R. (1986) Coastal and Estuarine sediment dynamics.
Wiley Interscience, New York.

Edgerton, H.E. (1963) Sub-bottom penetrations in Boston Harbour.
Jour. Geophys. Res., 68, 2753-2760.

Edwards, W. (1905) The glacial geology of Anglesey.
Proc. Liverpool Geol. Soc., 1904-1905, pp26-37.

Embleton, C. (1964) The deglaciation of Arfon and southern Anglesey and the origin of the Menai Straits.
Proc. Geo. Ass., 75 (4), 407-430.

Emery, K.O. (1938) Rapid method of mechanical analysis of sands.
Jour. Sediment. Petrol., 8, 105-111.

Emerson, D.W. and Phipps, C.V.G. (1969) The deliniation of the bedrock configuration of part of Port Jackson, New South Wales, with a boomer system.
Geophys. Prosp., 17, 219-230.

Engelund, F. and Hansen, E. (1967) A monograph on sediment transport in alluvial streams. Technisk Vorlag, Copenhagen, 62pp.

Fairbridge, R.W. (1961) Eustatic changes in sea level. In: Ahrene, L.H (Editor) Physics and chemistry of the earth, 99-185. Pergamon, London.

Finely, R.J. (1975) Hydrodynamics and tidal deltas of North Inlet, South Carolina.
In: L.E Cronin (Editor) Estuarine Research, 5, II. Geology and Engineering.
Academic Press, New York, N.Y., pp. 113-158.

Finely, R.J. (1978) Ebb-tidal delta morphology and sediment supply in relation to seasonal wave energy flux, North Inlet, South Carolina.
Jour. Sediment. Petrol, 48 (1), 227-238.

Fitzgerald, D.M. (1977) Hydraulics, morphology and sediment transport at price inlet, South Carolina.
PhD Thesis, University of South Carolina.

Flemming, B.W. (1976) Side scan sonar: a practical guide.
The International Hydrographic Review, 53.

Flood, R.D. (1983) Classification of sedimentary furrows and a model for furrow intiation and evolution.
Geol. Soc. Am. Bull., 94, 630-639.

Folk, R.L. and Ward, W.C. (1957) Brazos river bar, a study in the significance of grain size parameters.
Jour. Sediment. Petrol., 27, 3-27.

Folk, R.L. (1966) A review of grain size parameters.
Sedimentology, 6, 73-93.

Folk, R.L. (1968) Petrology of sedimentary rocks.
Hemphills, Austin, Texas. 170pp.

Folk, R.L. (1974) Petrology of sedimentary rocks.
Hemphills, Austin, Texas.

Forbes, A.M.C. (1969) Electromagnetic monitoring of currents in the Menai Strait.
MSc Thesis, University of Wales.

Foster (1968) The glaciation of the Harlech Dome.
PhD Thesis, University of London.

Fouere, J.F. (1966) Sediments in the Menai Strait.
MSc Thesis, University of Wales.

Friedman, G.M. (1961) Distinction between dune, beach, and river sands from their textural charateristics.
Jour. Sediment. Petrol., 31, 514-529.

Friedman, G.M. (1967) Dynamic processes and statistical parameters comapred for size frequency distributions of beach and river sands.
Jour. Sediment. Petrol., 37, 327-354.

Fuller, A.O. (1961) Size distribution characteristics of shallow marine sands from the Cape of Good Hope, South Africa.
Jour. Sediment. Petrol., 31, 256-261.

Gadd, P.E., Lavelle, J.W. and Swift, D.J.P (1978) Estimates of the sand transport on the New York shelf using near bottom current meter observations.
Jour. Sediment. Petrol., 48, 239-252.

Gibbs, R.J., Mathews, M.D. and Link, D.A. (1971) The relationship between sphere size and settling velocity.
Jour. Sediment. Petrol., 41, 7-18.

Gilbert, G.K. (1914) The transportation of debris by running water.
U.S. Geol. Surv. prof. papers, 86, 263 pp.

Greenly, E. (1919) The geology of Anglesey.
Mem. Geol. Survey., 2 vols.

Griffiths, J.C. (1967) Scientific method in the analysis of sediments. McGraw-Hill, 508pp.

Guy, H.P., Simmons, D.B. and Richardson, E.V. (1966) Summary of alluvial channel data from flume experiments 1956-1961.
U.S. Geol. Survey Prof. Paper 462-I, 1-96.

Hagedoorn, J.G. (1959) The plus-minus method of interpreting seismic refraction sections.
Geophys. Prosp., 7, 158-182.

Hallermier, R.J. (1981) Terminal settling velocity of commonly ocurring sand grains.
Sedimentology, 31, 51-62.

Hamilton E.L. and Bachman, R.T. (1982) Sound velocity and related properties of marine sediments.
Jour. Acoust. Soc. Am., 72, 1891-1904.

Haner, B.E. (1984) Santa Ana River: An example of a sandy braided flood plain system showing sediment source area imprintation and selective sediment modification.
Sediment. Geol., 38, 247-261.

Hardisty, J. (1983) An assesment and calibration of formulations for Bagnold's bedload equation.
Jour. Sediment. Petrol., 53, 1007-1010.

Harris, S.A. (1958) Probability curves and the recognition of adjustment to depositional environment.
Jour. Sediment. Petrol., 28, 151-163.

Harris, P.T. (1982) The distribution and dynamics of sedimentary bedforms in the central and inner Bristol channel.
MSc Thesis, University of wales.

Harris, P.T. and Collins, M.B. (1985) Bedload distributions and sediment transport paths in the Bristol channel and Severn estuary, U.K.
Mar. Geol., 62, 153-166.

Harvey, J.G. (1967) The effect of weather on water level in the Menai Straits.
Deutsch. Hydrogr. Zeits., 20 (2), 54-58.

Harvey, J.G. (1968) The flow of water through the Menai Straits.
Geophys. Jour. Royal Astr. Soc., 15, 517-528.

Hayes, M.O. (1969) Coastal environments: NE Massachusetts and New Hampshire. Guidebook, field trip for eastern section of SEPM, May 9-11, 1969, 462pp.

Hayes, M.O. (1975) Morphology of sand accumulation in Estuaries: An introduction to the Symposium. In: Cronin, L.E. (Editor) Estuarine research, 5, II, Geology and Engineering.
Academic press, New York, N.Y., pp3-23.

Hayes M.O. (1979) Barrier island morphology as a function of tidal and wave regime. In: Leatherman, S. (Editor) Proceedings of the coastal symposium on Barrier islands, Academic Press.

Hayes, M.O. (1980) General morphology and sediment patterns in tidal inlet.
Sediment. Geol, 26, 139-156

Heathershaw, A.D. (1981) Comparisons of measured and predicted sediment transport rates in tidal currents.
Mar. Geol., 42, 75-104.

Helm, D.G. (1971) Succession and sedimentation of glacigenic deposits at Hendre, Anglesey.
Geol. Jour., 7, 271-298.

Hersey, J.B. (1963) Continuous Reflection Profiling.
In: Hill, M.N. (Editor) The Sea, 3, 47-72.

Hine, A.C. (1975) Bedform distribution and migration patterns on tidal deltas in the Chatham Harbour estuary, Cape Cod, Mass. In: L.E Cronin (Editor) Estuarine Research, 5, II. Geology and Engineering.
Academic Press, New York, N.Y., pp. 113-158.

Hjulstrom, F. (1939) Transportation of Detritus by moving water.
In: Trask, P.D. (Editor) Recent marine sediments.
Am. Ass. Petrol. Geol., Tulsa, 5-31.

Hjulstrom, F. (1935) Studies of the morphological activity of rivers as illustrated by the River Fyris.
Bull. Geol. Inst. Univ. of Upsala, 25, 221-528.

Hough, J.L. (1942) Sediments of Cape Cod Bay, Mass.
Jour. Sediment. Petrol., 12, 10-30.

Hubbard, D.K. (1975) Morphology and the Hydrodynamics of the Merrimack river ebb-tidal delta. In: L.E Cronin (Editor) Estuarine Research, 5, II. Geology and Engineering.
Academic Press, New York, N.Y, pp. 113-158..

Hubbbard, D.K. (1977) Variations in tidal inlet processes and the morphology in the Georgia embayment.
Coast. Res. Div. Geol. Dep. Univ. S.C., Tech. Rep, 14-CRD: 79pp.

Hulsey, J.D. (1961) Relations of settling velocity of sand-sized spheres and sample weight.
Jour. Sediment. Petrol., 31, 101-112.

Humphries, S.M. (1977) Morphologic equilibrium of a natural tidal inlet, Coastal sediments '77, Proc. of 5th Symp., WPCO Div. ASCE, Eng., Charleston, S.C., Nov. 2-4, 1977, 734-753.

Imperto, D.P., Sexton, W.J. and Hayes, M.O. (1988) Stratigraphy and sediment characteristics of a mesotidal ebb-tidal delta, North Edisto Inlet, South Carolina.
Jour. Sediment. Petrol., 58, 950-958.

Inman, D.L. (1952) Measures for describing the size distribution of sediments.
Jour. Sediment. Petrol., 22, 125-145.

Inman, D.L. (1949) Sorting of sediments in the light of fluid mechanics.
Jour. Sediment. Petrol., 19, 15-70.

Jago, C.F. (1981) Sediment response to waves and currents, North Yorkshire Shelf, North Sea.
Spec. Publs. Int. Ass. Sediment., 5, 283-301.

Jehu, T.J. (1909) The glacial deposits of western Caernarvonshire
Trans. Royal Soc. Edinb., 47, 17.

Jelgersma, S. (1966) Sea level changes in the last 10000 years.
In: International Symposium on World Climate from 8000-0 B.C.
Royal. Met. Soc., pp54-69.

Jelgersma, S. (1979) Sea level changes in the North sea Basin.
In: Oele, E. (Editors) The Quaternary. history of the North sea.
Acta. Univ. Ups. Symp. Univ. Ups. Annum Quingentesimum Celebrantis, 2, 253-248.

Jones, M.E. (1984) Megaripple stability in the southwest Menai Strait.
MSc Thesis, University of Wales.

Jones, P.G.W. and Haq, S.M. (1963) The distribution of phaeocystis in the eastern Irish Sea.
Jour. Cons. Perm. int. explor. mer, 28 (1), 8-20

Kachel, N.B. and Stenberg, R.W. (1971) Transport of bedload as ripples during an ebb current.
Mar. Geol., 10, 229-244.

Karcz, I. (1967) Harrow marks, current aligned sedimentary structures.
Jour. Geol., 75,113-121.

Kelland, N.C. (1975) Submarine geology of Start Bay determined by continuous seismic profiling and core sampling.
Jour. Geol. Soc. London, 131, 7-18.

Kenyon, N.H. (1970) Sand ribbons of European tidal seas.
Mar. Geol., 9, 25-39.

Kenyon, N.H. and Stride, A.H. (1970) The tide-swept continental shelf sediments between the Shetland Isles and France.
Sedimentology, 14, 159-173.

King, C.A.M. (1972) Beaches and Coast: Edward Arnold, London, 2nd ed., 570 pp.

Klein, G.De V. (1970) Depositional and dispersal dynamics of intertidal sand bars.
Jour. Sediment. Petrol., 40, 1095-1127.

Klovan, J.E. (1966) The use of factor analysis in determining environments from grain size distributions.
Jour. Sediment. Petrol., 36, 115-125.

Knebel, H.J. (1989) Modern sedimentary environments in a large tidal estuary, Delaware Bay.
Mar. Geol., 86, 119-136.

knot, S.T. and Hersey, J.B. (1956) Interpretation of high resolution echo-sounding techniques and their use in bathymetry, marine geophysics, and biology.
Deep sea Res., 4, 36-44.

Kohsiek, L.H.M. and Terwindt, J.H.J. (1981) Characteristics of forset and topset bedding in megaripples related hydrodynamic conditions on an interdtidal shoal.
In: Nio, S.D. et al (Editors) Holocene marine sedimentation in the North Sea Basin. Spec..

Krumbein, W.C. (1934) Size frequency distribution of sediments.
Jour. Sediment. Petrol., 4, 65-77.

Krumbein, W.C. (1936) Application of logarithmic moments to size frequency distributions of sediments.
Jour. Sediment. Petrol., 6, 35-47.

Krumbein, W.C. and Aberdeen, E. (1937) The sediments of Barataria Bay.
Jour. Sediment. Petrol., 7 (1), 3-17.

Krumbein, W.C. (1938) Size frequency distribution of the sediments and the normal phi curve.
Jour. Sediment. Petrol., 8, 84-90.

Krumbein, W.C. and Pettijohn, F.J. (1938) Manual of sedimentary petrography. Appleton-Centuary, New York, 549pp.

Lane, E. (1955) Design of stable channels.
Trans. Am. Soc. Civ. Engrs., 120, 1234-1260.

Langhorne, D.N. (1981) An evaluation of Bagnold's dimension-less coefficient of proportionality using measurements of sand wave movement.
Mar. Geol., 43, 49-64.

Larcombe, P. (1991) The post-glacial evolution and present-day processes of the Mawddach estuary.
Ph.D Thesis, University of Wales.

Leenhardt, O. (1963) Un sondage sismique Continu sur le plateau continental pres de planier (Marseille), C. R. Acad. Sci. Paris, 257, 6, 1541-1544.

Leenhardt, O. (1967) Topics on seismic research at the Monaco Oceanographic Museum.
Geophys. Pros., 15, 516-526.

Leenhardt, O. (1974) Side scanning sonar - A theoretical study.
Int. Hydrgr. Rev., 51 (1), 61-80.

Mahamod, Y.B. (1989) Sedimentary processes in the Dwyryd Estuary.
PhD Thesis, University of Wales.

Maltman, A.J. (1975) Ultramafic rocks in Anglesey - Their non-tectonic emplacement.
Jour. Geol. Soc. London, 131, 593-606.

Mason, C.C. and Folk, R.L. (1958) Differentiation of beach dune and aeolian flat environments by size analysis, Mustang island, Texas.
Jour. Sediment. Petrol., 28, 211-226.

McCammon, R.B. (1962) Efficiencies of percentiles for describing the mean size and sorting of sedimentary particles.
Jour. Geol., 70, 453-465.

McCave, I.N. (1978) Grain size trends and transport along Beaches: example from eastern England.
Mar. Geol., 28, M43-M51.

McLaren, P. (1981) An interpretation of trends in grain size measures.
Jour. Sediment. Petrol., 51, 611-624.

McLaren, P. and Bowles, D. (1985) The effect of sediment transport on grain size distributions.
Jour. Sediment. Petrol., 55, 457-470.

Migniot, C. (1977) Action des courants, de la houle et du vent sur les sediments.
Houille Blanche, 1, 9-47.

Miller, M.C., McCave, I.N. and Komar, P.D. (1977) Threshold of sediment motion under unidirectional currents.
Sedimentology, 24, 507-527.

Mitchum, R.M.Jr. and Vail, P.R. (1977) Seismic stratigraphic interpretation procedure. In: Payton, C.E. (Editor) Seismic stratigraphy - Application to hydrocorbon exploration.
AAPG Memoir, 26, 135-144.

Moore, D.G. and Shumway, G. (1959) Sediment thickness and physical properties: Pigeon Point Shelf, California.
Jour. Geophys. Res., 64, 367-374.

Morton, R.A. and Donaldson, A.C. (1973) Sediment distribution and evolution of tidal deltas along a tide-dominated shoreline, Wachapreague, Virginia.
Sediment. Geol., 10, 285-299.

Moss, A. (1962) The physical nature of common sandy and pebbly deposits, Part 1.
Am. Jour. Sci., 260, 337-373.

Nummedal, D.N., Oertal, G.F., Hubbard, D.K. and Hine, A.C. (1977) Tidal inlet variability - Cape Hatteras to Cape Canavral. Coastal sediments. 77, Proc. 5th Symp., WPCO Div. ASCE, Charleston, S.C., Nov. 2-4, 1977, pp. 543-562.

Nyandwi, N. (1988) Tidal flow and suspended sediment transport over a spring-neap-spring cycle on an intertidal sand bank in the southwestern Menai Strait.
M.Sc Thesis, University of Wales.

Oertal, G.F. (1972) Sediment transport on estuary entrance shoals and the formation of the swash platforms.
Jour. Sedment. Petrol., 42, 857-863.

Otto, G.H. (1939) A modified logarithmic probability graph for the interpretation of the mechanical analysis of sediments.
Jour. Sediment. Petrol., 9, 62-76.

Park, S.C., Kim, Y.S. and Hong, S.K. (1991) Shallow seismic stratigraphy and distribution pattern of Late Quaternary sediments in a macrotidal Bay: Gunhung Bay, west coast of Korea.
Mar. Geol., 98, 135-144.

Passega, R., (1957) Texture as a characteristics of clastic deposition.
Am. Ass. Petrol. Geol., 41, 1942-1984.

Pettijohn, F.J. (1957) Sedimentary rocks.
Harper, New York, N.Y., 718pp.

Postma, H. (1967) Sediment transport and sedimentation in the estuarine environment. In: Lauff, G.H. (Editor) Estuaries, Am. Ass. Adv. Sci. Publ., 83, 158-179.

Ramsay, A.C. (1860) The old glaciers of Switzerland and North Wales.
Longman, London.

Raudkivi, A.J. (1976) Loose boundary hydraulics.
Pergamon, Oxford.

Rigler, J.k., Collins, M.B. and Williams, S.J. (1981) A high precision digital recording sedimentation tower for sands.
Jour. Sediment. Petrol., 51, 642-644.

Rittenhouse, G. (1943) A visual method of estimating two-dimensional spherecity.
Jour. Sediment. Petrol., 13, 79-81.

Rogers, J.J.W. (1959) Detection of lognormal size distributions in clastic sediments.
Jour. Sediment. Petrol., 29, 402-407.

Sagoe, K.M.O. and Visher, G.S. (1977) Population breaks in grain size distributions of sand - a theoretical model.
Jour. Sediment. Petrol., 47, 285-310.

Sahu, (1964) Depositional mechanisms from the size analysis of clastic sediments.
Jour. Sediment. Petrol., 34, 73-83.

Salge, U. and Wong, H.K. (1988) Seismic stratigraphy and Quaternary sedimentation in the Skagerrak (Northeastern North Sea).
Mar. Geol., 81, 159-174.

Saunders, G.E. (1968) A fabric analysis of the ground moraine deposits of the Lleyn Peninsula of SW Caernarvonshire.
Jour. Geol., 6, 105-118.

Schlee, J. (1973) Atlantic continental shelf and slope of the United States: sediment textures of the northeastern part.
U.S. Geol. Surv., Prof. Pap., 529L: 64pp.

Sha, L.P. (1989) Sand transport patterns in the ebb-tidal delta off Texel inlet, Wadden Sea, The Netherlands.
Mar. Geol., 86, 137-154.

Shackleton, R.M. (1969) The Pre-Cambrian of North Wales In: A. Wood (Editor). The Pre-Cambrian and lower Paleozoic rocks of Wales. University of Wales Press.

Shennan, I., Tooley, M.J., Davis, M.J. and Haggart, B.A. (1983) The analysis and interpretation of Holocene sea level data.
Nature, 302, 404-406.

Sheriff, R.E. and Geldart, L.P. (1982) Exploration seismology Volume 2: Data processing and interpretation. Cambridge University Press. Cambridge, 221 pp.

Sheriff R.E. (1980) Seismic stratigraphy.
Boston: International Human Resources Development Corporation.

Sherwin, T.J. (1985) Co-phase chart of Menai Strait. Unit for coastal and Estuarine Studies (UCES), Univ. of Wales, Bangor, Project No. UCES 46.

Shields, A. (1936) Anwendung der Ahnlichkeits Mechanik und der Turbulenzforshung auf die Geschiebe Bewegung Preussesche Versuchanstalt fur Wasser bau und Schiffbau Berlin.

Simons, D.B. and Richardson, E.V. (1961) Forms of bed roughness in alluvial channels. Proc. Am. Ass. Civ. Eng.,
Jour. Hydraul. Div., 86 (2485), 73-99.

Slot, R.E. (1984) Terminal velocity formula for objects in a viscous fluid.
Jour. Hydraul. Res., 22, 235-243.

Slot, R.E. and Geldof, H.J. (1986) An improved settling tube system for sand. Delft University of Technology, department Department of Civil Engineering, Report No. 86-4, The Netherlands.

Sorby, H.C. (1852) On the oscillation of the currents drifting the sand stone beds of the southeast of Northumberland, and on the general direction in the coalfield in the neighbourhood of Edinburgh.
Proc. Yorkshire Geol. Soc. 3, 232-240.

Sorby, H.C. (1857) On the physical geography of the Tertiary estuary of the Isle of Wight.
Edinburgh New Phil. Jour., New ser., 5, 275-298.

Sorby, H.C. (1859) On the structures produced by the currents present during the deposition of stratfied rocks.
Geologist, 2, 137-140.

Sorby, H.C. (1908) On the application of quantitative methods to the study of the structure and history of rocks.
Quart. Jour. Geol. Soc. London, 64, 171-232.

Southard, J.B. (1971) Representation of bed configurations in depth-velocity diagrams.
Jour. Sediment. Petrol., 41, 903-915.

Spencer, D.W. (1963) The interpretation of grain size distribution curves of clastic sediments.
Jour. Sediment. Petrol., 33, 180-190.

Stein, R. (1985) Rapid grain size analyses of clay and silt fraction by Sedigraph 5000D: comparison with.Coulter counter and Atterberg methods.
Jour. Sediment. Petrol., 55, 590-593.

Sternberg, R.W. (1972) Predicting initial motion and bedload transport of sediment particles in the shallow marine environments. In: Swift, D.J.P. et al (Editors) Shelf sediment transport: Processes and patterns. Dowden, Hutchinson and Ross, Inc. Chapt3 3, 61-82.

Stokes, G.G. (1851) Trans. Cambridge Philos. Soc., Math. Phys. Sci., 9, 8-27.

Sundborg, A. (1956) The River Klaralven: a study in fluvial processes.
Geog. Ann. Stockholm, 38, 125-316.

Swift, D.J.P. (1969) Outer shelf sedimentation: processes and products. In: Stanley, D.J (Editor) The new concepts of continental margin sedimentation. Am. Geol. Ins. Washington, D.C., pp.5/1-5/26.

Synge, F.M. (1964). The glacial succession in west Carnarvonshire.
Proc. Geol. Ass. London, 75, 431.

Telford, W.M., Geldart, L.P., Sheriff, R.E. and Keys, D.A. (1976) Applied Geophysics. Cambridge University Press.

Terwindt, J.H.J. (1971) Sand waves in the southern bight of the North Sea.
Mar. Geol., 10, 51-67.

Terwindt, J.H.J. and Brouwer, M.J.N. (1986) The behavior of intertidal sand waves during neap-spring tide cycles and the relevance for paleoflow reconstructions.
Sedimentology, 33, 1-31.

Tooley, M.J. (1969) Sea level changes and the development of coastal plant communities during the Flandrian in Lancashire and adjacent areas.
PhD Thesis, University of Lancaster.

Tooley, M.J. (1974) Sea level changes during the last 9000 years in North-west England.
Geog. Jour. 140, 18-42.

Trabant, P.K. (1984) Applied high resolution geophysical methods.
Int. Hum. Resour. Dev. Corp., Boston, Mass., 265 pp.

Trask, P.D. (1930) Mechanical analysis of sediments by centrifuge.
Econ. Geol., 25, 581-599.

Trask, P.D. (1932) Origin and environment of source sediments of petroleum, Gulf. Publ. Co., Houston, 68-76 pp.

Udden, J.A. (1898) Mechanical composition of wind deposits:
Augustana Library Publ. No. 1.

Vail, P.R. (1987) Seismic stratigraphy interpretation utilising sequence stratigraphy. Part 1: Seismic stratigraphy interpretation procedure. In: Bally, A.W. (Editor) Atlas of seismic stratigraphy.
AAPG, Studies in geology series, 27.

Vail, P.R., Mitchum, R.M.Jr. and Thompson, S. (1977) Relative changes of sea level from coastal onlap. In: Payton, C.E (Editor) Seismic stratigraphy - applications to hydrocorbon exploration.
AAPG Memoir, 26, 63-82.

Vail, P.R., Todd, R.G. and Sangree, J.B. (1977) Chronostratigraphic significance of seismic reflections. In: Payton, C.E. (Editor) seismic stratigraphy - applications to hydrocorbon exploration.
AAPG Memoir, 26, 99-116.

Van Orstrand, C.E. (1925) Note on the representation of the distribution of grains in sands. Committee on Sedimentation: Research in sedimentation in 1924-Natl. Res. Council, 63-67.

Van veen, J. (1950) Ebb-en vloedschaar sytemen in de Nederlandse getijwateren. In Wadden Sea Symp. K. Ned. Aardrijk. Genoot. Tijdschr., Mei 1950. Sticht. Mar. Geol. off print pp.43-65.

Vincent, C.E., Young, R.A. and Swift, D.J.P. (1981) Bed-load transport under waves and currents.
Mar. Geol., 39, 71-80.

Visher, G.S. (1969) Grain size distributions and depositional processes.
Jour. Sediment. Petrol., 39, 1074-1106.

Vittori, J., Got, H., Le Quellec, P., Mascle, J. and Mirabile, L. (1981) Emplacement of the recent sedimentary cover and processes of deposition of the Matapan trench margin (Hellenic Arc).
Mar. Geol., 41, 113-135.

Vitturi, L.M. and Rabitti, S. (1980) Automatic particle size analysis of sediment fine fraction by Sedigraph 5000D:
Geologia applicata e Idrogeologia, 15, 101-108.

Van Weering, T. (1975) Late Quaternary history of the Skagerrak; An interpretation of acoustical profiles.
Geologie en Mijnbouw, 54 (3-4), 130-145.

Van Weering, T., Jansen, J.H.F. and Eisma, D. (1973) Acoustic reflection profiling of the Norwegian channel between Oslo and Bergen.
Neth. Jour. Sea Res., 6, 241-263.

Wentworth, C.K. (1922) A scale of grade and class terms for clastic sediments.
Jour. Geol., 30, 377-392.

Wentworth, C.K. (1929) Method of computing mechanical composition types in sediments.
Bull. Geol. Soc. Am., 40, 771-790.

Werner, F. and Newton, R.S. (1975) The pattern of large scale bedforms in the Langeland Belt (Baltic Sea).
Mar. Geol., 19, 29-59.

Wilks, P.J. (1977) Flandrian sea level change in the Cardigan Bay area.
PhD Thesis, University of Wales.

Williams, G.P. (1967) Flume experiments on the transport of coarse sand.
U.S. Geol. Survey Prof. Paper 562-B.

Wyrobek, S.M. (1956) Application of delay and intercept times in the interpretation of multilayer refraction time distance curves.
Geophys. Prosp., 4, 112-130

Yalin, M.S. (1963) An expression for bedload transportation.
Am. Soc. Civ. Eng. Proc., 89 (HY3), 221-250.

Yalin, M.S.(1972) Mechanics of sediment transport.
Pergamon, Oxford.

Yalin, M.S. (1977) Mechanics of sediment transport.
Pergamon, Oxford.

Yang, C.S. (1986) Estimates of sand transport in the Oosterschelde tidal basin using current velocity measurements.
Mar. Geol., 72, 143-170.

Zarillo, G.A. (1982) Stability of bedforms in a tidal environment.
Mar. Geol., 48, 337-351.

Zeigler, J.M., Whitney, G.G. and Hayes, C.R. (1960) Woods Hole rapid sediment analyser.
Jour. Sediment. Petrol., 30, 490-495.

ABEM TERRALOC® Mark 3

Powerful digital seismograph for shallow applications

Atlas Copco

Appendix II

3.0 SPECIFICATIONS

3.1 TRANSMITTER SECTION

Power Output	10 kw RMS during key pulse.
Output Impedence	50, 75, 100, 125, 150, 200, 250, 300, 400, 500, 600 ohms.
Frequency	Continuously adjustable 1 - 12 kHz. Other frequencies available.
Output Power Adjustment	Continuously adjustable from 0 to 10 kw at any of the above impedences.
Duty Cycle	.75 per cent at 10 kw, proportionately higher at lower power settings.
Pulse Length	(Controlled by auxiliary equipment; i. e., recorder, etc.) Internal pulse length control optional (maximum pulse length 2 ms for 10 per cent voltage droop at 10 kw); optional external capacitor available for longer pulse length.
Keying Signal	DTL/TTL compatible pulse, positive or negative going. (Compatible with most recorders.)

Internal Rep Rate and Pulse Length Controls	Available as an option. (See Section 7)

3.2 TRANSMITTER

Protective Circuits	Duty cycle automatically limited to less than 100 watts average transmitted power. Short circuit protected output stage. Overload protection AC power interruption protection.

Internal switch provided to separate transmitter output terminal from receiver input.

3.3 RECEIVER SECTION

Input Impedence	10K
Frequency	Adjustable 1 - 12 kHz. Other frequencies available.
Bandpass Filter	Center frequency continuously variable 1-12 kHz. Bandwidth adjustable from 1 kHz up to essentially flat.
Output Impedence	Less than 100 ohms.
Maximum Output Voltage	4 V p-p minimum.
Sensitivity	30 microvolts RMS input (for 20 db signal-to-noise ratio) produce 1 v RMS output.

3.4 TVG SECTION

TVG Dynamic Range	30 db
TVG Rate	Adjustable for normal water spreading loss (-20 log R) to (-40 log R).
TVG Delay	Adjustable from 1 ms to 1 sec.
TVG Finder	Front panel push buttom used to locate beginning of TVG ramp by adding "blip" to receiver output which appears on recorder paper.
TVG Bottom Tracker	Using bottom tracker mode, TVG ramp automatically starts when first bottom return is received.
TVG Delay	1 ms to 1 second.

3.5 SPECIAL FEATURES

(1) Transmitter and receiver frequencies independently adjustable.

(2) Receiver frequency is matched to transmitter frequency by depressing "Receiver Test" switch and tuning for maximum indication on "VU" meter. The "Receiver Test" switch produces a calibrated signal at receiver input, thus, also checking receiver sensitivity and bandwidth.

(3) "VU" meter is useful by itself for listening to sound sources (i. e., pingers, etc.) Transmitter can then be set to receive frequency by procedure similar to (2) above.

3.6 POWER REQUIREMENTS

Primary Voltage	105-125 VAC 57-63 Hz. (50 Hz and 230 V adapters available.)
Power Consumption	200 watts

3.7 CONSTRUCTION

Design Guide	MIL-E-16400
Electronics	All modular silicon solid state construction with maximum utilization of digital and linear intergrated circuits. Each circuit board contains up to eight test points accessible from top of card file.
Chassis	Bench/Rack chassis fully enclosed and fan cooled.
Power Supplies	Regulated, short circuit proof supplies used throughout.
Size	.17 inches wide by 17 inches deep by 7 inches high -- standard rack or bench mounting.
Weight	50 pounds.

Appendix III

Third Party Material excluded from digitised copy.
Please refer to original text to see this material.

Appendix IV

Third Party material excluded from digitised copy.
Please refer to original text to see this material.

Appendix V

Third Party Material excluded from digitised copy.
Please refer to original text to see this material.

Appendix VI

Current data from station E and F

Hours		Directions of streams (degrees)	Rates at spring tides (knots) / Rates at neap tides (knots)	E 53°07'·5N 4 19·7W		F 53°07'·3N 4 25·2W		
Before High Water	6			068	0 4 0 2	110	0 2 0·1	−6
	5			083	1·6 0 8	040	0 5 0·3	−5
	4			079	4·2 2·1	010	0 9 0·4	−4
	3			082	5·1 2·5	001	0·9 0·5	−3
	2			090	4·6 2·3	357	0 9 0·5	−2
	1			095	2·0 1·0	353	0·7 0·3	−1
High Water				267	3 5 1·7	307	0·2 0·1	0
After High Water	1			267	4·3 2 1	196	0·5 0·3	+1
	2			262	3·9 1·9	190	0 8 0·4	+2
	3			259	3 2 1·6	189	0·9 0 5	+3
	4			262	2·3 1·1	185	0·8 0·4	+4
	5			280	1·0 0 5	182	0·7 0·4	+5
	6				0 0 0 0	140	0 3 0·1	+6

(Admiralty chart of Menai Strait, 1975)

Tidal Streams referred to HW at HOLYHEAD

Appendix VII

Appendix VIII

Appendix IX

Fall Tower details

Fall Tower photograph

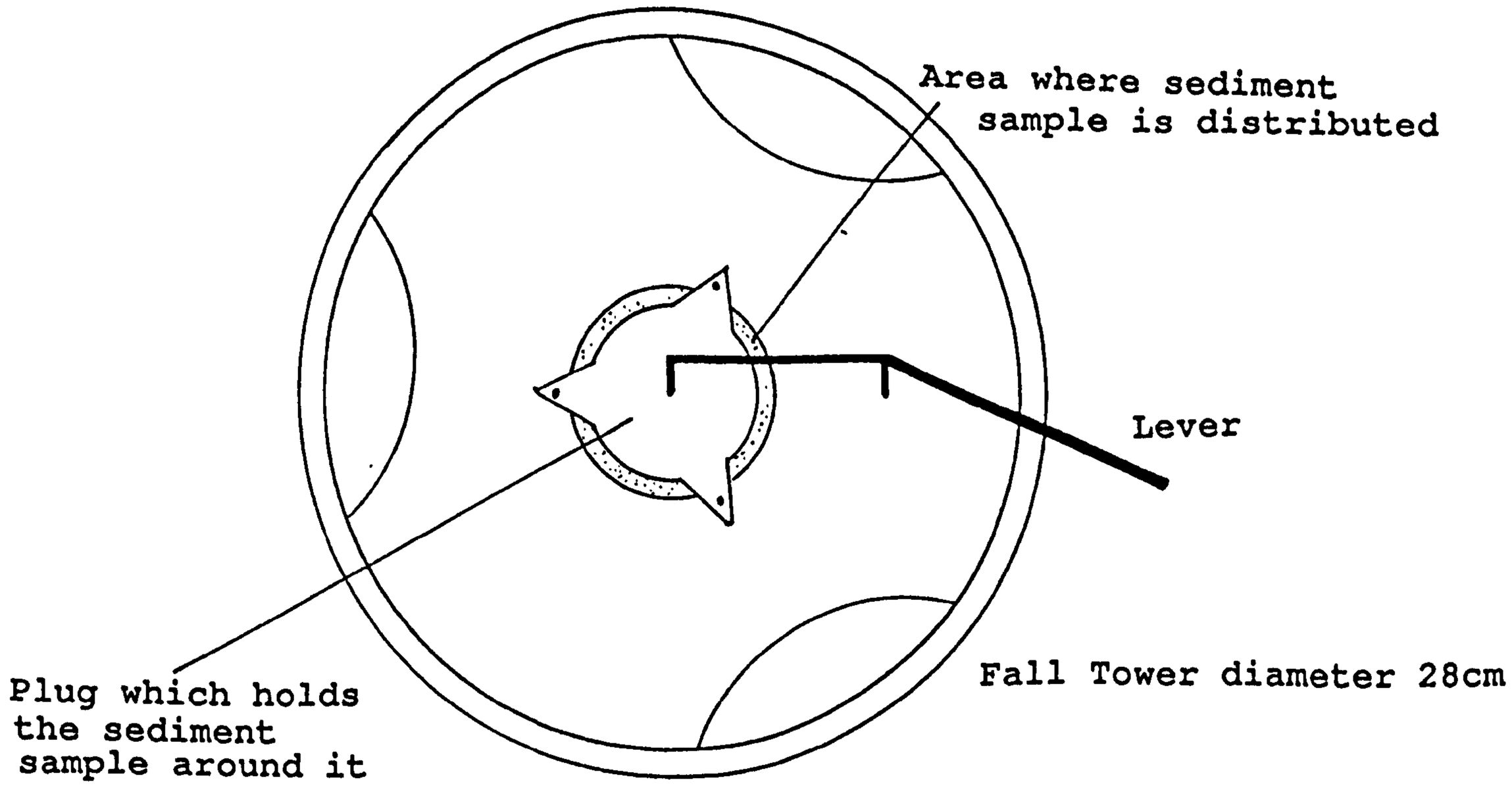

Overhead view of the sampling releasing system

Appendix X

Grain size results from Area 1

Sed. Sample No.	Mode	Mean		Sorting		Skewness	
		Moments	Folk	Moments	Folk	Moments	Folk
1	2.08	2.089	2.092	0.241	0.228	0.756	0.024
2	2.12	2.153	2.167	0.231	0.222	0.556	0.089
3	2.14	1.901	1.928	0.520	0.475	-1.339	-0.490
4	2.18	2.221	2.234	0.231	0.219	0.673	0.101
5	2.12	2.106	2.112	0.296	0.257	-0.363	-0.006
6	2.38	2.361	2.370	0.275	0.265	0.291	0.012
7	2.24	2.283	2.290	0.247	0.231	0.335	0.036
8	2.16	2.024	2.060	0.677	0.673	-0.720	-0.210
9	2.40	2.396	2.408	0.208	0.193	0.861	0.026
10	2.34	2.376	2.390	0.259	0.257	0.299	0.015
11	2.50	2.502	2.522	0.231	0.226	0.421	0.033
12	2.60	2.517	2.546	0.366	0.286	-2.242	-0.240
13	1.58	1.503	1.500	0.435	0.415	0.126	-0.060
14	1.82	1.895	1.898	0.358	0.338	0.378	0.125
15	2.12	2.127	2.148	0.274	0.274	0.507	0.052
16	2.64	2.642	2.707	0.338	0.345	0.198	0.039
17	2.56	2.537	2.580	0.221	0.211	-0.326	-0.086
18	2.14	2.122	2.131	0.206	0.195	0.853	0.018
19	2.22	2.250	2.264	0.243	0.238	0.455	0.102
20	2.42	2.382	2.428	0.212	0.208	0.125	-0.061
21	2.34	2.287	2.332	0.229	0.237	0.546	0.008
22	2.02	2.002	2.057	0.446	0.417	-1.216	-0.092
23	2.14	2.190	2.201	0.395	0.269	-3.180	0.108
24	2.02	1.934	1.973	0.457	0.359	-2.039	-0.175
25	2.02	1.931	1.993	0.354	0.213	-3.856	-0.018
26	2.26	2.210	2.237	0.539	0.343	-2.612	-0.232
27	2.22	2.004	2.142	0.535	0.403	-2.131	-0.134
28	2.26	2.161	2.223	0.527	0.292	-3.107	-0.105
29	2.26	2.376	2.313	0.514	0.234	-3.548	0.058
31	2.60	2.576	2.601	0.236	0.232	0.064	0.001
33	2.48	2.524	2.545	0.247	0.234	-0.267	0.069
34	2.12	2.189	2.186	0.205	0.192	1.111	0.215
36	2.54	2.567	2.593	0.250	0.241	-0.392	0.044
37	2.04	2.031	2.036	0.216	0.193	-0.071	-0.006
38	2.30	2.272	2.276	0.281	0.281	0.239	0.051
39	2.04	1.949	1.984	0.407	0.352	-1.373	-0.156
40	2.16	2.111	2.125	0.280	0.255	-0.650	-0.111
41	2.16	2.165	2.177	0.249	0.246	0.305	-0.004
42	2.28	2.295	2.296	0.220	0.214	0.594	0.093
43	2.12	2.095	2.135	0.212	0.215	0.496	0.014
44	2.02	1.937	1.950	0.306	0.292	-0.427	-0.148
45	1.86	1.880	1.893	0.328	0.322	0.609	0.072
46	2.18	2.155	2.177	0.259	0.248	0.547	-0.019
47	2.56	2.629	2.636	0.241	0.222	0.686	0.149
48	2.58	2.617	2.646	0.212	0.205	1.393	0.216
49	2.36	2.388	2.396	0.221	0.208	0.536	0.011
50	2.12	2.213	2.219	0.332	0.248	-2.485	0.115
53	2.22	2.270	2.213	0.318	0.214	-3.226	0.017
54	2.34	2.478	2.364	0.371	0.213	-3.291	0.124
55	2.48	2.537	2.499	0.367	0.211	-4.055	0.152
56	2.66	2.696	2.727	0.237	0.224	0.649	0.247
57	2.32	2.365	2.392	0.209	0.208	0.721	0.166
58	1.92	1.800	1.828	0.457	0.422	-1.005	-0.137
59	2.00	1.951	1.970	0.332	0.321	-0.218	-0.036
60	2.20	2.191	2.215	0.216	0.217	0.879	0.089

61	2.26	2.295	2.307	0.219	0.207	-0,120	0.092
62	2.32	2.322	2.331	0.244	0.230	-0.091	-0.011
63	2.38	2.427	2.439	0.301	0.281	0.423	0.103
64	2.58	2.619	2.664	0.259	0.261	0.747	0.053
65	2.56	2.595	2.643	0.217	0.216	1.175	0.191
66	2.32	2.307	2.362	0.221	0.227	0.544	0.025
69	2.40	2.401	2.418	0.211	0.209	0.407	0.010
70	2.42	2.365	2.430	0.178	0.174	1.005	0.133
72	2.22	2.252	2.285	0.242	0.248	0.437	0.098
73	2.60	2.578	2.602	0.181	0.182	0.594	0.056
74	2.50	2.508	2.510	0.234	0.222	-0.447	-0.004
76	2.52	2.511	2.538	0.206	0.206	0.584	0.088
75	2.54	2.513	2.551	0.228	0.218	-0.205	0.020

Grain size results from Area 2

Sed. Sample No.	Mode	Mean		Sorting		Skewness	
		Moments	Folk	Moments	Folk	Moments	Folk
75B	2.44	2.263	2.316	0.456	0.406	-1.663	-0.482
76B	2.26	2.246	2.268	0.236	0.213	-0.479	-0.055
82	2.22	2.188	2.209	0.250	0.240	-0.499	-0.138
83	2.38	2.352	2.370	0.213	0.202	0.762	0.009
84	1.82	1.800	1.837	0.424	0.375	-0.880	-0.040
86	2.32	2.258	2.272	0.220	0.204	0.161	-0.096
87	2.32	2.355	2.363	0.221	0.197	-0.595	0.087
91	2.50	2.537	2.556	0.184	0.159	0.212	0.103
92	1.92	2.058	2.074	0.329	0.328	0.130	0.086
93	2.32	2.318	2.324	0.165	0.141	0.463	0.017
95	2.02	1.952	1.960	0.369	0.369	-0.003	-0.092
96	2.40	2.264	2.302	0.412	0.382	-1.345	-0.368
97	2.48	2.458	2.500	0.338	0.264	-1.953	-0.087
100	2.52	2.496	2.499	0.228	0.210	-0.231	0.039
101	2.54	2.514	2.558	0.301	0.272	-1.079	-0.135
102	2.60	2.444	2.466	0.332	0.341	-0.006	-0.122
105	2.40	2.437	2.442	0.272	0.257	-0.205	0.032
106	2.56	2.559	2.598	0.256	0.224	-0.750	-0.064
107	2.38	2.380	2.392	0.228	0.217	0.527	-0.024
110	2.60	3.046	2.670	2.024	0.453	5.321	0.499
111	2.28	2.033	2.071	0.576	0.523	-1.734	-0.605
112	2.46	2.417	2.443	0.269	0.234	-1.136	-0.172
114	2.64	2.530	2.592	0.398	0.328	-2.096	-0.319
116	2.64	2.688	2.726	0.219	0.177	-1.319	0.171
118	2.72	2.528	2.587	0.688	0.602	-1.891	-0.550
120	2.68	2.691	2.710	0.189	0.169	0.311	0.138
121	2.62	2.621	2.691	0.167	0.153	0.755	0.119
122	2.58	2.625	2.649	0.190	0.169	-0.149	0.074
123	2.54	2.559	2.607	0.224	0.189	-0.718	0.085
124	2.54	2.519	2.553	0.284	0.237	-1.270	-0.136
125	2.40	2.388	2.425	0.251	0.218	-1.185	-0.115
126	2.28	2.192	2.204	0.270	0.268	-0.133	-0.135
128	2.30	2.180	2.203	0.328	0.315	-0.650	-0.141
129	2.46	2.423	2.441	0.213	0.206	0.451	0.003
130	2.44	2.472	2.477	0.215	0.189	-0.381	0.022
131	2.48	2.524	2.535	0.165	0.197	15.033	0.037

135	2.54	2.564	2.592	0.232	0.212	-0.437	-0.031
136	2.50	2.487	2.515	0.230	0.225	-0.041	-0.090
137	2.54	2.512	2.541	0.247	0.200	-1.632	-0.056
140	2.32	2.353	2.311	0.747	0.217	9.095	-0.036
142	2.08	1.876	1.906	0.485	0.475	-0.580	-0.109
144	2.42	2.450	2.472	0.198	0.179	0.520	0.202
146	2.60	2.643	2.690	0.249	0.202	-1.373	0.138
149	2.68	2.679	2.737	0.202	0.166	-0.658	0.139
151	2.68	2.691	2.713	0.239	0.191	-1.145	0.067
152	2.70	2.670	2.729	0.303	0.252	-1.514	-0.105
154	2.76	2.817	2.854	0.213	0.185	-0.050	0.204
155	2.68	2.652	2.709	0.346	0.288	-1.680	-0.121
156	2.56	2.556	2.581	0.212	0.211	0.916	0.048
157	2.46	2.499	2.527	0.195	0.185	1.479	0.221
158	2.38	2.421	2.429	0.226	0.169	-2.070	0.120
159	2.52	2.479	2.508	0.242	0.218	-0.624	-0.116
161	2.62	2.628	2.647	0.248	0.185	-2.269	-0.045
162	2.66	2.697	2.730	0.238	0.189	-1.476	0.079
163	2.54	2.547	2.574	0.210	0.189	-0.370	0.028
164	2.58	2.638	2.657	0.181	0.173	0.743	0.197
165	2.64	2.632	2.670	0.289	0.227	-1.972	-0.079
166	2.64	2.835	2.750	1.072	0.560	5.016	0.456
168	2.74	2.803	2.641	1.186	0.444	4.924	-0.286
169	2.70	2.698	2.735	0.635	0.343	6.886	-0.215
171	2.74	2.805	2.819	0.235	0.184	-1.428	0.144
175	2.48	1.411	1.399	1.003	1.030	-0.004	0.045
176	2.64	2.499	2.528	0.551	0.534	-1.296	-0.433
177	2.36	2.381	2.391	0.489	0.487	-0.537	-0.095
179	2.74	2.747	2.689	0.804	0.396	6.481	-0.254
181	2.74	2.528	2.574	0.477	0.438	-1.208	-0.222
182	2.36	1.961	1.923	1.012	1.060	-0.847	-0.527
183	2.56	2.671	2.659	0.743	0.331	7.297	0.067
184	2.68	2.785	2.751	0.754	0.271	7.696	0.087
186	2.58	2.575	2.623	0.359	0.267	-2.583	-0.124
188	2.64	2.452	2.461	0.534	0.526	-1.114	-0.534
190	2.68	2.700	2.705	0.924	0.444	5.110	-0.138
191	2.54	2.543	2.472	0.991	0.459	5.256	-0.070
194	2.50	2.547	2.547	0.727	0.434	5.743	0.013
195	2.52	2.602	2.585	0.784	0.451	6.000	-0.046
197	2.16	2.045	2.073	0.573	0.575	-0.325	-0.047
199	2.76	2.593	2.621	0.479	0.460	-1.220	-0.413
201	2.54	2.492	2.520	0.470	0.449	-1.010	-0.199
202	2.16	2.047	1.983	0.926	0.564	5.431	-0.134
203	2.08	2.148	2.145	0.408	0.406	0.335	0.067
204	2.64	2.640	2.627	0.835	0.480	5.037	-0.094
205	2.32	2.322	2.330	0.364	0.370	0.294	0.044
206	2.58	2.462	2.516	0.478	0.480	-0.513	-0.175
207	2.70	2.589	2.612	0.373	0.364	-0.398	-0.098
208	2.72	2.675	2.678	0.655	0.424	6.153	-0.236
209	2.70	2.616	2.562	1.030	0.523	5.380	-0.205

Grain size results from Area 3

Sed. Sample No.	Mode	Mean		Sorting		Skewness	
		Moments	Folk	Moments	Folk	Moments	Folk
210	2.80	2.477	2.490	0.564	0.509	-0.948	-0.342
211	2.85	2.478	2.519	0.699	0.526	-2.088	-0.215
212	2.40	2.417	2.426	0.525	0.483	-0.592	-0.006
213	2.35	2.320	2.339	0.494	0.436	-0.940	0.058
214	2.35	2.381	2.410	0.506	0.469	-1.051	0.019
215	2.90	2.419	2.465	0.663	0.585	-1.359	-0.229
216	2.40	2.386	2.436	0.604	0.527	-1.473	-0.099
218	2.40	2.290	2.331	0.571	0.471	-1.597	-0.090
219	1.85	0.589	0.488	2.066	2.084	-0.864	-0.730
220	2.35	2.223	2.247	0.493	0.404	-1.166	-0.030
221	2.35	2.412	2.432	0.544	0.486	-0.831	0.027
222	2.35	2.430	2.434	0.528	0.471	-0.848	-0.033
223	-2.15	-1.717	-1.833	1.702	1.673	0.487	0.036
224	2.35	2.353	2.425	0.685	0.607	-1.650	-0.252
225	-2.20	-1.442	-1.446	2.172	2.206	0.521	0.426
226	-3.10	-1.813	-1.810	1.760	1.761	0.731	0.460
227	1.80	1.681	1.705	0.479	0.434	-0.717	-0.179
228	1.90	2.037	2.056	0.374	0.308	-0.494	0.173
229	1.85	1.856	1.891	0.535	0.491	-0.947	-0.151
230	2.40	2.281	2.299	0.470	0.419	-0.903	-0.098
231	1.85	1.908	1.941	0.444	0.400	-0.903	0.051
232	2.35	0.437	0.602	1.868	1.744	-0.140	-0.369
233	1.90	1.908	1.951	0.602	0.555	-1.001	-0.174
234	-1.50	-1.097	-1.130	1.642	1.673	0.443	0.255
235	-3.05	-1.793	-1.691	2.020	2.063	1.102	0.590
236	2.25	2.193	2.211	0.404	0.333	-1.226	-0.027
237	1.90	0.233	0.364	2.586	2.467	-0.729	-0.743
238	1.75	-1.433	-1.499	2.697	2.684	0.001	0.199
239	1.65	1.740	1.748	0.410	0.378	-0.054	0.102
240	-1.40	-1.115	-0.996	2.117	2.208	0.525	0.359
241	-2.15	-0.976	-0.939	1.642	1.637	0.129	0.239
242	-3.00	-1.859	-2.028	1.741	1.657	1.107	0.274
243	1.85	1.813	1.966	0.866	0.546	-3.052	-0.152
244	2.00	1.926	2.198	1.139	0.827	-2.561	-0.321
245	-1.40	-1.518	-1.448	1.093	0.955	-0.764	-0.225
246	-0.60	-0.449	-0.323	1.538	1.254	-1.758	-0.040
247	1.80	0.270	0.305	2.013	1.984	-0.785	-0.546
248	1.85	1.896	1.923	0.427	0.372	-1.101	-0.005
249	1.60	1.492	1.756	1.142	0.916	-1.944	-0.323
250	2.50	2.435	2.465	0.411	0.318	-2.087	-0.125
251	1.95	2.089	2.124	0.395	0.278	-2.156	0.073
252	2.35	0.357	0.469	1.867	1.819	-0.217	-0.363
255	2.04	1.687	1.920	1.979	1.095	-0.288	-0.443
256	0.82	-1.383	-1.641	2.889	2.527	1.152	0.207
257	2.38	2.292	2.310	0.356	0.307	-0.670	-0.156
258	2.10	0.264	0.186	2.499	2.281	0.187	-0.577
259	1.72	1.718	1.725	0.380	0.357	0.155	-0.007
260	-2.84	-1.894	-1.865	2.469	2.388	0.805	0.186
261	1.64	1.576	1.592	0.333	0.303	-0.021	-0.151
262	2.32	2.315	2.319	0.286	0.251	0.148	0.087
263	2.28	2.367	2.283	1.016	0.338	6.511	0.002
264	2.40	2.396	2.410	0.341	0.323	0.007	0.000
265	2.26	2.276	2.281	0.296	0.242	-1.453	0.056

266	1.76	1.692	1.722	0.330	0.321	-0.240	-0.012
267	2.60	2.711	2.630	1.186	0.372	5.464	-0.159
268	2.66	2.729	2.734	0.671	0.215	9.680	0.023
269	2.08	2.180	2.180	0.321	0.303	0.540	0.202
270	1.54	1.706	1.665	0.709	0.335	8.819	0.254
271	2.28	2.368	2.302	0.852	0.345	7.481	0.022
272	2.20	2.168	2.185	0.293	0.259	-0.456	-0.023
273	2.46	2.496	2.450	0.946	0.317	6.702	-0.006
274	2.24	2.206	2.227	0.349	0.325	-0.425	-0.063
275	2.16	2.208	2.237	0.282	0.236	-1.068	0.065
276	1.62	0.609	0.692	1.346	1.126	0.044	-0.382
277	1.62	1.574	1.466	1.192	0.590	5.181	-0.064
278	1.84	1.808	1.815	0.342	0.329	-0.029	-0.076
279	2.02	0.942	0.505	3.051	2.969	0.480	-0.341
280	1.98	1.782	1.800	0.475	0.468	-0.575	-0.263
281	2.26	2.038	2.108	0.689	0.672	-0.718	-0.271
282	2.26	2.166	2.109	1.113	0.673	4.128	-0.270
283	2.24	2.358	2.215	1.088	0.350	6.255	0.199
284	1.96	2.166	1.989	1.318	0.390	5.620	0.240
285	-4.52	-2.422	-2.651	3.237	2.603	1.835	0.434
286	1.16	1.155	1.047	1.941	1.043	2.880	-0.134
287	-4.26	-2.727	-2.800	2.971	2.384	2.215	0.488
290	2.12	2.160	2.149	0.267	0.235	1.470	0.158
291	2.34	2.483	2.361	1.173	0.353	5.846	0.132
292	2.32	2.412	2.291	1.144	0.357	6.009	0.103
293	2.28	2.234	2.243	0.277	0.258	-0.278	-0.087
294	1.86	2.142	1.894	1.525	0.437	4.847	0.176
295	2.26	2.352	2.244	0.745	0.492	3.276	0.137
296	2.24	2.166	2.187	0.413	0.329	-1.480	-0.201
297	2.12	2.249	2.138	0.973	0.303	7.036	0.083
300	1.92	1.661	1.689	0.554	0.528	-0.973	-0.354
301	1.18	-1.525	-1.366	2.895	2.782	-0.511	-0.358
302	1.72	1.683	1.681	0.434	0.421	0.140	-0.046
303	1.72	1.407	1.517	2.379	1.792	0.299	-0.274